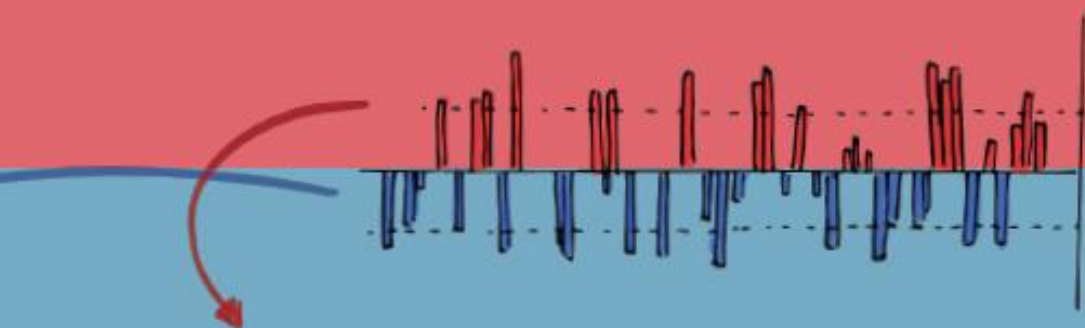# Floods, droughts and climate variability

From early warning to early action

Gabriela Guimarães Nobre

VRIJE UNIVERSITEIT

Floods, droughts and climate variability: From early warning to early action

ACADEMISCH PROEFSCHRIFT

ter verkrijging van de graad Doctor
aan de Vrije Universiteit Amsterdam,
op gezag van de rector magnificus
prof.dr. V. Subramaniam,
in het openbaar te verdedigen
ten overstaan van de promotiecommissie
van de Faculteit der Bètawetenschappen
op vrijdag 15 november 2019 om 11.45 uur
in de aula van de universiteit,
De Boelelaan 1105

door

Gabriela Guimarães Nobre

geboren te Recife, Brazilië

promotoren: prof.dr. J.C.J.H. Aerts

prof.dr. P.J. Ward

Summary in Dutch (Samenvatting)

Klimaatvariabiliteit, zoals de El Niño-Southern Oscillation, zorgt voor jaarlijkse fluctuaties in hydro-meteorologische en klimatologische extremen. Elk jaar veroorzaken zulke extremen, zoals overstromingen of droogtes, wereldwijd voor hoge economische schades. Ondanks dat een aantal studies suggereren dat de kwetsbaarheid en financiële verliezen van overstromingen de laatste paar decennia afnemen, vergt rampenrisicovermindering (disaster risk reduction; DRR) nog steeds een substantiële verandering van het managen van rampen naar het managen van risico's. Om DRR te bereiken is het daarom belangrijk om te begrijpen hoe klimaatvariabiliteit kan resulteren in impacts van overstromingen en droogtes.

De impact van rampen kan worden verminderd wanneer betrouwbare, voorspelde risico informatie beschikbaar is om preventieve risicoverminderingsmaatregelen aan te sturen. De afgelopen jaren hebben deze systemen de kwaliteit van voorspellingen over hydro-meteorologische en klimatologische variabelen verbeterd, door voorspellingen over de omvang van overstromingen en droogtes met hogere precisie op langere tijdschalen dan voorheen te produceren. Er is echter nog steeds een gat in het vertalen van extreme gebeurtenissen naar impact informatie, zoals de schade van weer-gerelateerde gebeurtenissen. Eén van de grootste uitdagingen is daarom de overgang van "wat voor een weer wordt het?" naar "wat zal het weer doen?". Voorspellingen die zijn ontworpen om de verwachte impact uit te drukken, worden "impact-based forecasting" genoemd. Recente literatuur beschrijft manieren om automatisch preventieve maatregelen, gebaseerd op vroege waarschuwingssystemen, te activeren om zo de impact van weer-gerelateerde gebeurtenissen te verminderen. In zulke systemen kunnen vroege acties worden geactiveerd wanneer een voorspelling een bepaalde drempelwaarde overstijgt. Boeren kunnen bijvoorbeeld van tevoren financieel gecompenseerd worden wanneer neerslagtekorten onder een bepaalde drempelwaarde voorspeld worden, gebruik makende van indicatoren van neerslaganomalieën. Echter, ondanks vooruitgang in overstromings- en droogtevoorspellingen, blijven bijbehorende onzekerheden van de voorspellingsinformatie groot, en is wetenschappelijk bewijs voor de gunstige impact van vroeg handelen gebaseerd op voorspellingen nog beperkt. Doordat men niet precies weet hoe hydro-meteorologische gebeurtenissen een impact kunnen hebben op mens hun leven, levensonderhoud en op de economie, treffen stakeholders vaak niet de juiste maatregelen. Als gevolg hiervan wordt het grote deel van vroege waarschuwingen niet routinematig gebruikt als een basis voor het financieren en activeren van preventieve maatregelen tegen weer-gerelateerde gebeurtenissen.

Het hoofddoel van deze scriptie is om het begrip van de verbanden tussen klimaatvariabiliteit en weer-gerelateerde impacts van zowel overstromingen als droogtes te verbeteren. Dit verband wordt onderzocht van globale tot regionale schaal en op verschillende tijdschalen, met als doel om een impact-based forecast te bereiken die effectief de implementatie van vroege handelingen kan leiden voordat een potentiele droogte of overstroming plaatsvindt.

Als eerste worden de ruimtelijke en temporele invloeden van klimaatvariabiliteit op extreme meteorologische- en overstromingsgebeurtenissen op pan-Europese schaal geanalyseerd. Dit wordt gedaan door de El Niño Southern Oscillation (ENSO), de North Atlantic Oscillation (NAO) en de East Atlantic pattern (EA) te onderzoeken tijdens hun neutrale, positieve en negatieve fases, om zo hun relatie tot vier overstromingsindicatoren te begrijpen: het voorkomen van extreme neerslag, de intensiteit van extreme neerslag, het voorkomen van overstromingen en schade van overstromingen. Resultaten laten zien dat klimaatvariabiliteit sterke connecties heeft met de vier overstromingsindicatoren. Zowel de positieve als de negatieve fase van de NAO en EA worden in verband gebracht met meer frequente en intensere extreme neerslag over grote gebieden in Europa, terwijl de effecten van ENSO op de intensiteit en frequentie van extreme neerslag in Europa veel kleiner is. Voor de eerste keer wordt aangetoond dat de schade van overstromingen en het voorkomen van overstromingen in Europa sterk geassocieerd worden met klimaatvariabiliteit, met name in Zuid- en Oost-Europa, waarbij de sterkste link geobserveerd wordt voor de NAO.

Vervolgens wordt de rol van seizoensgebonden vertragingen en gelijktijdige indices van klimaatvariabiliteit op overstromingsverliezen op sub-regionale Europese schaal onderzocht. Speciale aandacht wordt gegeven aan het onderzoeken van de waarschijnlijkheid van seizoensgebonden overstromingsverliezen gebaseerd op indices van klimaatvariabiliteit, en om te detecteren of sommige van deze verliezen een seizoen eerder voorspeld kunnen worden. Resultaten laten zien dat de indices van klimaatvariabiliteit gebruikt kunnen worden om classificaties van schadelijke, laag schadelijke en medium schadelijke overstromingsgebeurtenissen te voorspelling, veelal in op zijn minst twee van de vier seizoenen in alle Europese deelregio's. Bovendien wordt aangetoond dat de classificaties van overstromingsverliezen een seizoen eerder voorspeld kunnen worden omdat er een vertraagde relatie kan bestaan tussen de indices van klimaatvariabiliteit en de overstromingsverliezen in alle Europese deelregio's. We zien dat de waarschijnlijkheid van het voorkomen van overstromingsverliezen kan toe- of afnemen met tot wel ±100% in vergelijking met historische kansen. De resultaten bieden een beter begrip van het gecombineerde effect van klimaatvariabiliteit op overstromingsverliezen, en reflecteren op hoe zulke op impact gebaseerde informatie kan worden gebruikt om overstromingsrisicomanagement te verbeteren.

Bovendien identificeert deze scriptie regio's waarin anomalieën in Europese gewassenproductie kunnen worden voorspeld aan de hand van de indices van klimaatvariabiliteit, gebruik makend van een Machine Learning techniek genaamd "Fast-and-Frugal Trees". Resultaten laten zien dat door Fast-and-Frugal Trees toe te passen, hoge/lage klassen van suikerbietenproductie in 77% van de onderzochte regio's kunnen worden voorspeld, overeenkomend met 81% van de totale Europese suikerbietenproductie. Voor bijna de helft van deze regio's is zulke op impact gebaseerde informatie zes of vijf maanden voor het begin van het suikerbietenoogst beschikbaar, wanneer ongeveer 44% van de gemiddelde jaarlijkse suikerbieten worden geproduceerd. Gebruikmakend van deze resultaten bediscussieert deze scriptie hoe impact-based forecasting het management van de agrarische sector in Europa sterk kan verbeteren. Om verdere inzichten in de sterke en zwakke punten van deze aanpak te verschaffen, wordt de voorgestelde methode vervolgens getest op andere datasets van gewassenproducties en typen gewassen.

De Fast-and-Frugal Trees aanpak wordt ook toegepast op een case in Kenia (gebaseerd op indices van klimaatvariabiliteit en vegetatie dekking) om maïsoogsten te voorspellen. Dit vroege waarschuwingssysteem van lage maïsoogsten wordt gebruikt om de kostenefficiëntie te analyseren van het van tevoren uitbetalen van boeren in plaats van het compenseren van gederfde inkomsten na een droogte. Resultaten laten zien dat de Fast-and-Frugal Trees modellen vaardig zijn in het voorspellen van lage maïsoogsten in alle vijf Keniaanse districten. In de meeste gevallen hebben de modellen al zes maanden voor het begin van het oogstseizoen een voorspellende vaardigheid. Ondanks dat het niet perfect is, voorspelt het model 85% van de tijd correct de "lagere oogst drempelwaarde", over verschillende percentielen, districten en looptijden van de opbrengsten. De modelprestaties verbeteren richting het einde van het groeiseizoen, gedreven door een afname van 29% in de kans op een False Alarm. Wanneer we een perfecte voorspelling aannemen (Hits=100% en False Alarms=0%), zijn geldtransacties zes maanden van tevoren het meest kosteneffectief. Bovenal, wanneer gebruik gemaakt wordt van de daadwerkelijke voorspellingen gebaseerd op de Fast-and-Frugal Trees voorspellingen, laten resultaten zien dat geldtransacties vooraf vaak meer kosteneffectief zijn dan geldtransacties achteraf, in het bijzonder voor de meer extreme oogsttekorten. Meerdere uitdagingen voor het operationaliseren van geldtransacties gebaseerd op indicatoren van droogtes worden geïdentificeerd. Zo heeft het ondernemen van gepaste maatregelen naar aanleiding van vroege waarschuwingen van droogte-risico's gebaseerd op indices van klimaatvariabiliteit bijvoorbeeld een diepgaand begrip nodig van de potentiele impact en timing van een extreme gebeurtenis.

Ondanks zulke uitdagingen, biedt deze scriptie beleidsaanbevelingen waarin we kansen laten zien om het risico op rampen te verminderen, door te reageren op voorspellingen van klimaatvariabiliteit, en door het bijbehorende risico beter te begrijpen. Het laat voorbeelden zien van organisaties die al gebruik maken van ENSO-voorspellingen om risico's te verminderen, maar erkent ook dat een aantal

beperkingen voor vroeg handelen met betrekking tot de ENSO-voorspellingen nog bestaan. Ondanks dit concluderen we dat vooraf bekende informatie over de ruimtelijke configuratie van risico, bevorderd door impact-based forecasting met lange looptijden zoals degene ontworpen in deze scriptie, een verschuiving richting een meer anticiperende en preventieve risicomanagement kan ondersteunen.

Deze scriptie laat een aantal belangrijke uitdagingen en onderwerpen zien die in de toekomst verder onderzocht moeten worden. Zo wordt gesuggereerd dat onderzoek naar de dynamiek van klimaatvariabiliteit nodig is om het begrip van de impacts van klimaatvariabiliteit te verbeteren. Verder wordt ook voorgesteld om dit begrip van de impacts van klimaatvariabiliteit te verbeteren, betere data en een onderzoek naar de relatie tussen mensen en natuurlijke systemen nodig is. Bovendien laat deze scriptie zien dat toekomstig onderzoek naar impact-based forecasting verbeterd kan worden door de voorspellingsvaardigheden en looptijden van indices van klimaatvariabiliteit te verbeteren, en door de voorspelling van de indices van klimaatvariabiliteit met de socio-economische impact van overstromingen en droogtes te combineren. Als laatste kan toekomstig onderzoek worden uitgevoerd om de onderliggende interesses en motieven die belangrijk zijn voor stakeholders om DRR te integreren in overstromings- en droogterisicomanagement te identificeren, in combinatie met het verkennen van de voordelen van vroeg handelen. Deze scriptie biedt vooruitgang in het begrip van de connecties van klimaatvariabiliteit en weer-gerelateerde impacts van zowel overstromingen als droogtes, die gebruikt kunnen worden om impact-based forecasts te maken en vroegtijdige handelingen te activeren.

Summary

Climate variability, such as El Niño-Southern Oscillation, drives year-to-year fluctuations in hydro-meteorological and climatological extremes. Every year, such extremes (e.g. floods and droughts) account for high economic losses around the globe. Despite some studies suggesting progress in reducing vulnerability and the financial losses of floods in recent decades, disaster risk reduction (DRR) still requires a substantial shift from managing disasters to managing risks. Therefore, an important step for achieving DRR lies in understanding how climate variability may result in flood and drought impacts.

The impact of disasters can be reduced when reliable forecasted risk information is available to steer preventative risk reduction measures. In recent years, these systems have improved the capability of forecasting hydrometeorological and climatological variables, producing predictions of flood and drought magnitudes with higher accuracy at longer lead times than before. However, there is still a gap in translating hazard events into impact information, such as damages from weather events. Hence, one of the biggest research challenges is the transition from "what will the weather be?" to "what will the weather do?". Forecast information that is designed to express the expected impacts is known as "impact-based forecasting". Recently, there has been an emerging literature describing ways to automatically trigger preventative actions to reduce the impacts of weather events based on early warning systems. In such a system, early actions can be triggered when a forecast surpasses a certain threshold. For example, farmers could receive ex-ante cash compensation when a forecast projects rainfall deficits below a certain threshold using an indicator of rainfall anomalies. However, despite advances in flood and drought forecasting systems, associated uncertainties with the forecast information remain large, and scientific evidence of the beneficial impacts of acting early based on forecast information is still limited. Hence, not knowing precisely how hydrometeorological hazards might have an impact on people's lives, livelihoods and on the economy, stakeholders often do not take appropriate action. As a consequence, the vast majority of early warnings are not routinely used as a basis for financing and triggering preventative actions against weather events.

The main objective of this thesis is to improve the understanding on links between climate variability and weather-related impacts of both floods and droughts. This relationship is investigated from global to regional scales, and at different lead times, with the purpose of achieving an impact-based forecast that can guide the implementation of early actions effectively before a potential drought or flood materializes.

First, the spatial and temporal influence of climate variability on extreme meteorological and flood events at the pan-European scale is analysed. This is done by investigating the El Niño Southern Oscillation (ENSO), the North Atlantic Oscillation (NAO), and the East Atlantic pattern (EA) during their neutral, positive, and negative phases, to understand their relationships with four flood indicators: Occurrence of Extreme Rainfall, Intensity of Extreme Rainfall, Flood Occurrence, and Flood Damage. The results show that climate variability has strong links with the four flood indicators. Both positive and negative phases of NAO and EA are associated with more frequent and intense extreme rainfall over large areas of Europe, whereas the effect of ENSO on the intensity and frequency of extreme rainfall in Europe is much smaller. It is shown for the first time that Flood Damage and Flood Occurrence in Europe are strongly associated with climate variability, especially in southern and eastern Europe with the strongest link being observed for NAO.

Subsequently, the role of seasonally lagged and synchronous indices of climate variability on flood losses at the sub-regional European scale is examined. Special attention is given to investigating the likelihood of seasonal flood losses based on indices of climate variability, and to detect whether some of these losses can be predicted one season ahead. Results show that the indices of climate variability can be used to predict classes of Damaging, Low Damaging and Medium Damaging flood events, mostly in at least 2 out of 4 seasons in all European sub-regions. Furthermore, it is shown that some of the classes of flood losses can be predicted one season ahead because a lagged relationship may exist between the indices of climate variability and the flood losses in all European sub-regions. It is observed that the likelihood of flood losses occurring may increase or decrease by up to ±100% in comparison to historical probabilities. The results provide a better understanding of the combined effect of climate variability on flood losses, and reflect on how such impact-based information can be used to improve flood risk management practices.

Furthermore, this thesis identifies regions where anomalies in European crop production can be forecasted based the indices of climate variability using a Machine Learning technique called "Fast-and-Frugal Trees". Results show that by applying the Fast-and-Frugal Trees, high/low classes of sugar beet production can be predicted in 77% of the investigated regions, corresponding to 81% of total European sugar beet production. For nearly half of these regions, such impact-based information is available six or five months before the start of the sugar beet harvesting season, where approximately 44% of the mean annual sugar beet is produced. Based on such findings, this thesis discusses how impact-based forecasting information can widely improve the management of the agricultural sector in Europe. To provide further insights into the strengths and limitations of

the approach, the proposed method is subsequently tested on other crop production database and crop type.

The Fast-and-Frugal trees approach is also applied to a case in Kenya (based on indices of climate variability and vegetation coverage) for predicting maize yields. This early warning information of low maize yields are used to assess the cost-effectiveness of providing farmers with ex-ante cash transfers, instead of compensating yield losses after a drought. Results show that the Fast-and-Frugal Trees models have skill to forecast low maize yields in all five Kenyan districts. In most cases, models have predictive skill already six months before the start of the harvesting season. While not perfect, the model correctly forecasts "below yield threshold" 85% of the time, across different low yield percentiles, districts, and lead times. The models' performance improves towards the end of the growing season driven by a decrease of 29% in the probability of False Alarms. When assuming a perfect forecast (Hits = 100% and False Alarms = 0%), cash transfers can be most cost-effective ex-ante at a lead time of 6 months. Moreover, when using actual forecasts based on the Fast-and-Frugal trees predictions, results demonstrate that ex-ante cash transfers can often be more cost-effective than ex-post cash transfers, especially for the more extreme yield deficits. Multiple challenges for operationalizing cash transfers based on indicators of droughts are identified. For instance, taking adequate actions in response to early warnings of drought risks based on indices of climate variability requires an in-depth understanding of the potential impact and timing of a hazard.

Despite such challenges, this thesis provides policy recommendations showcasing opportunities to reduce the risk of disasters by responding to forecasts of climate variability, and by better understanding risks associated with it. It shows examples of organizations that already use ENSO forecasts for reducing risks, but also acknowledges that some constraints to early action still exist to respond to ENSO forecasts. Nevertheless, it concludes that ex-ante information regarding the spatial configuration of risk leveraged by impact-based forecasts with long lead times, such as the ones developed in this thesis, can support a shift towards a more anticipatory and preventative risk management.

This thesis highlights some key challenges and topics that require further investigation in future research. For instance, it suggests that in order to improve the understanding of the impacts of climate variability, research is required regarding the dynamics of climate variability. It also proposes that for improving the understanding on the impacts of climate variability, better data and an investigation on the relationships between human and natural systems is needed. Moreover, this thesis indicates that future studies can enhance impact-based forecasting by improving the forecasting skill and lead-time of indices of climate variability, and by combining the forecast of indices of climate variability with

socioeconomic impacts of floods and droughts. Lastly, further research can be performed to identify the underlying interests and incentives that are relevant to stakeholders for mainstreaming DRR into flood and drought risk management and policies, in combination with exploring the benefits of acting early. This thesis advances the understanding on links between climate variability and weather-related impacts of both floods and droughts, which can be used for generating impact-based forecasting and triggering early action.

Contents

Chapter 1

Introduction

1.1 Context: from disaster to risk management

In January 2017, the Famine Early Warning System Network (FEWS NET) forecasted an unprecedented global food security crisis. Indeed, in 2018, a global food security crisis occurred, especially across southern, eastern and western Africa, where 1.0 – 4.9 million people were in need of humanitarian assistance (FEWS NET, 2018a). However, despite the availability of the forecast information, the droughts and food shortages further pushed several countries into deeper humanitarian crises. Food insecurity is a recurrent crisis in large areas in Africa (Coughlan de Perez et al., 2019), where droughts have high socio-economic impacts, such as crop failures and the widespread death of livestock, high food prices and inflation, and increased levels of malnutrition and displacement (ReliefWeb, 2018). The chain of impacts often begins when rainfall is significantly lower or higher than average. Therefore, droughts and food insecurity have strong links with the variability in the climate.

Climate variability, such as El Niño-Southern Oscillation (ENSO) events, drive year-to-year fluctuations in hydrometeorological and climatological extremes such as floods and droughts. However, the severity of these disasters and their consequent losses – either to the economy or to well-being – not only depend on the intensity and frequency of an event, but deeply on "who" and "what" is susceptible to it. These two "Ws" are known as vulnerability and exposure (UNISDR, 2009). Developing countries are relatively vulnerable and have a high exposure to natural hazards: they often lack resources to invest in risk-reducing measures and 'build-back-better' strategies, their populations often live in hazard-prone areas, and people work in sectors highly susceptible to weather events, such as (rainfed) agriculture (D'Alessandro et al., 2015). However, developed countries face similar challenges, and increasingly strive for disaster resilience. European countries, for instance, have experienced increases in exposed population, economic wealth, and urbanization of hazard-prone areas (Paprotny et al., 2018). Consequently, every year disasters account for billions of Euros of economic losses across the continent. Despite studies suggesting some progress in reducing vulnerability (Jongman et al., 2015) and the financial losses of floods in recent decades (Paprotny et al., 2018), disaster risk reduction (DRR) still requires a substantial shift from managing disasters to managing risks. Such an anticipatory and preventative approach is urged in several international frameworks such as the Sendai Framework for Disaster Risk Reduction and the Agenda for Humanity (UNISDR, 2015b; UNOCHA, 2016a).

An important step for achieving DRR lies in understanding how climate variability may drive flood and drought impacts. The impact of disasters can be reduced when reliable forecasted risk information is available to steer

preventative risk reduction measures. To this end, several continental-scale flood and drought forecasting systems have been developed, such as the Africa Flood and Drought Monitor of Princeton University (Sheffield et al., 2014), and the European Flood Awareness System of the European Commission (Bartholmes et al., 2009). Other examples of global-scale forecasting systems are FEWS NET of the US Agency for International Development (Funk et al., 2019), and the Global Flood Awareness System (GloFAS) of the European Centre for Medium-Range Weather Forecasts (Alfieri et al., 2013). In recent years, these systems have improved the capability of forecasting hydrometeorological and climatological variables, producing predictions of flood and drought magnitudes with higher accuracy at longer lead times than before. For instance, GloFAS has been producing probabilistic flood forecasts with up to 2 weeks lead time in a semi-operational fashion since 2011 (Emerton et al., 2016). From April 2018 onwards, GloFAS has been running operationally to produce global probabilistic forecasts of river discharge up to 30 days ahead. In addition, it provides seasonal hydrological outlooks on emerging high/low flow anomalies up to four months ahead (ECMWF, 2018, 2019). However, these systems focus on forecasting the physical hazard, and there is still a gap in translating this information into socioeconomic impacts such as damages from weather events (Dottori et al., 2017). Hence, one of the biggest research challenges is the transition from "what will the weather be?" to "what will the weather do?". Forecast information that is designed to express the expected impacts is known as "impact-based forecast"(WMO, 2015).

Recently, there has been an emerging literature describing ways to automatically trigger preventative actions against weather events based on early warning systems (Coughlan De Perez et al., 2016, 2015; Suarez & Tall, 2010). For instance, in 2015 the first pilot of the "Forecast-based Financing" (FbF) project from the Red Cross Red Crescent was initiated, inspired by the idea that humanitarian financing could be made automatically available based on forecasts of extreme events. In such a system, early actions can be triggered when a forecast surpasses a certain threshold. For example, farmers could receive ex-ante cash compensation when a forecast projects rainfall deficits below a certain threshold using an indicator of rainfall anomalies. However, despite advances in flood and drought forecasting systems, associated uncertainties with the forecast information remain large. Hence, not knowing precisely how hydrometeorological hazards might impact on people's lives, livelihoods and on the economy often leads governments, economic sectors and the public to not take appropriate action. In addition, insufficient funding and the lack of measured benefits of early actions undermines the integration of forecast-based actions in disaster risk management strategies. As a

consequence, the vast majority of early warnings are not routinely used as a basis for financing and triggering preventative actions against weather events.

The main objective of this thesis is to improve the understanding on links between climate variability and weather-related impacts of both floods and droughts. In this thesis, this relationship is investigated from global to regional scales, and at different lead times, with the purpose of achieving an impact-based forecast that could guide the implementation of early actions effectively before a potential drought or flood materializes.

1.2 Definitions: elements of disaster risk assessment

There is a growing understanding that disasters are far from "natural", because disasters only occur when hazard meets vulnerability and exposure (Cannon, 1994). This thesis adopts the definition of "disaster risk as used by the United Nations Office for Disaster Risk Reduction (UNDRR). Thus, the risk of a disaster is defined as the probability and magnitude of harm to a society or a community in a specific period of time, as a function of hazard, exposure and vulnerability (illustrated in Figure 1.1.). Natural hazards are predominantly associated with natural processes and phenomena that pose a level of threat to life, property or the environment (UNISDR, 2009), which is addressed as "weather and climate events" in Figure 1.1. Exposure refers to "people, infrastructure, housing, production capacities and other tangible socio-economic assets located in hazard-prone areas" (ibid). Lastly, vulnerability is defined as "the conditions determined by physical, social, economic and environmental factors or processes, which increase the susceptibility of an individual, a community, assets or systems" to suffer adverse impacts when interacting with a hazard (ibid).

Hydrometeorological hazards are of atmospheric, hydrological or oceanographic origin (UNISDR, 2009), which may lead to different types of flood and drought events. For instance, floods most frequently occur due to heavy rainfall when (natural) watercourses are unable to accommodate excess water, which can result in riverine floods, flash floods and urban floods (UNISDR, 2017). Furthermore, floods can also initiate from other phenomena, especially in low-lying coastal zones, such a storm surge, tsunami or a high tide, which is also known as coastal flooding (ibid). Droughts come in four different types (Wilhite & Glantz, 1985): (1) meteorological drought, which refers to precipitation deficits; (2) hydrological drought, which reflects reduced water availability from surface water or groundwater, not including human demand; (3) agricultural drought, which links characteristics of meteorological and hydrological droughts to agricultural impacts; and (4) socio-economic drought, which associates the supply and demand of economic goods with elements of

all three types of droughts described. In this thesis, special attention is placed on agricultural droughts.
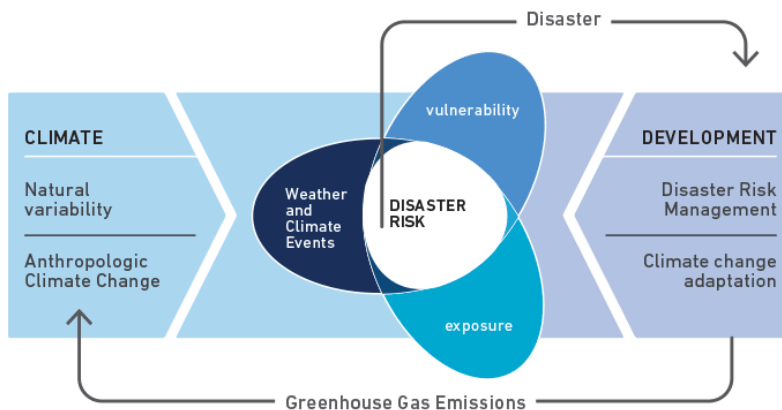
Figure 1.1 Framework for defining the term "disaster risk". Source: Field et al., (2012).

To estimate flood and drought risk, risk assessment models require data on characteristics of the event (hazard) with information on the assets (exposure) and the susceptibility of what or who is exposed (vulnerability) in the hazard-prone zone (Vogt et al., 2018; Ward, De Moel, & Aerts, 2011). More specifically, flood risk is often expressed in terms of the "expected annual damage" (EAD) with an economic figure attached to it (e.g. US$/year). Commonly, the first step towards calculating the EAD is to produce hazard-maps, where specific characteristics of the flood event are highlighted, such as inundation depth, extent, duration, and flow velocity in the case of river floods (Ward et al., 2011). Secondly, such hazard maps are then combined with exposure data, such as land use maps (Meyer, Haase, & Scheuer, 2009) or detailed building-level data (Aerts et al., 2013). Lastly, this information is combined with information on vulnerability. For example, depth-damage functions are often used, which show the physical vulnerability of buildings or land use classes to flood waters of different depths (Romali et al., 2015). In summary, flood risk includes both the probability of an event and its potential socioeconomic impact.

In contrast to floods, drought risk assessment is often carried out for a specific sector of interest. Consequently, droughts are monitored using indicators that are typically derived from hydroclimatic variables (e.g. precipitation, soil moisture), but that can express drought impacts over a specific sector (Vogt et al., 2018). For instance, indicators of rainfall anomalies and soil moisture such as the Standardized Precipitation-Evapotranspiration Index (SPEI, Vicente-

Serrano, Beguería, and López-Moreno 2010), and the Soil Moisture-based Drought Severity Index (Cammalleri, Micale, & Vogt, 2016) can be used to assess the risk of droughts to the agricultural sector, whereas hydrological indicators, such as flow percentiles or the Standardized Stream Flow Index can be used to quantify low flow volumes in reservoirs, which is relevant to the hydropower sector. In addition, remote sensing-based indicators such the Normalized-Difference Vegetation Index (NDVI) are also used to monitor drought impacts on vegetation cover (Vogt et al., 2018).

Databases of historical events that capture information on actual losses of disasters are often used to evaluate the performance of such models. An example of such disaster loss database is the Emergency Events Database (EM-DAT). This open access global database registers the impact of floods and other disasters from 1900 onwards, such as the number of people killed, injured or affected, the disaster-related economic damage, and disaster-specific international aid contributions (Guha-Sapir, Vos, & Below, 2014). This database is compiled from various sources, including UN agencies, non-governmental organisations, insurance companies, research institutes and press agencies. Furthermore, other private databases exist, such as the NatCatSERVICE database managed by the re-insurance company Munich Re. Munich Re's NatCatSERVICE is one of the largest databases for flood loss events worldwide, and has been reporting flood events since 1980 (Munich Re, 2016a). Despite the fact that global disaster databases face limitations, such as reporting errors and underreporting of small flood events (Kron et al., 2012; Paprotny et al., 2018), systematic data collection on costs and impact of disasters can support both short and long-term strategies to address flood risks. For droughts, global- and regional databases exist for monitoring and reporting statistics on food, agriculture and agricultural drought losses data. Examples of global scale initiatives are the EM-DAT and the FEWS NET, while the European Statistical Office (EUROSTAT) of the European Union provides information at the continental scale. Crop production and yield are particularly sensitive to weather conditions at key periods of the growing season. Therefore, comprehensive statistics on crop production and yield could support the better understanding of the relationship between weather variability and agricultural drought impacts, which may assist several programs designed to strengthen agricultural climate resilience.

1.3 From climate variability to impacts
As illustrated in Figure 1, anthropogenic climate change and natural climate variability are key drivers of disaster risk. Short- and long-term changes in the climate system can increase disaster risk in several ways, including the change

in frequency and intensity of hazard events (Field et al., 2012). While climate tends to change at a slow pace over decades, there are seasonal to annual fluctuations of hydrometeorological variables compared to climatic means. This phenomenon is called "climate variability", which refers to the climatic fluctuations on seasonal to multi-seasonal time-scales of natural processes that affect the atmosphere (Kimball, 2008). Climate change refers to alterations in the global atmosphere over longer periods – decadal to millennia – due to natural internal processes or external forcing (e.g. modulations of the solar cycles, volcanic eruption) and by human activity (IPCC, 2018).

Globally, the El Niño Southern Oscillation (ENSO) is the most dominant mode of climate variability, and has been linked with changes in hydrometeorological extremes in past studies at different scales (Emerton et al., 2017; Ionita, Boroneanţ, & Chelcea, 2015; Villafuerte et al., 2014). Extreme phases of ENSO are known as El Niño and La Niña. El Niño is a phenomenon that occurs when there are unusually warm oceanic and atmospheric conditions in the tropical Pacific. This can cause the trade winds, which usually blow towards Indonesia and Australia, to slow down or even reverse direction, allowing the warmer water to spread east towards the South American coast. As opposed to El Niño, the so-called La Niña emerges when unusually cold oceanic and atmospheric conditions are observed in the eastern tropical Pacific. Typically, ENSO events are identified monitoring seas surface temperatures anomalies in a region called Niño 3.4. However, it is now widely recognized that ENSO can occur in many different "flavors" (Johnson, 2013). Moreover, ENSO's impact is not constant throughout the year, nor are all continents of the globe equally affected by El Niño and/or La Niña. ENSO's phases occur irregularly every two to seven years, and their signal tends to peak during boreal winter months, affecting mostly African, Asian and Latin American countries (Trenberth, 1997).

ENSO's phases cause large variability in hydrometeorological and climatological systems over different parts of the world. For instance, El Niño or La Niña intensify extreme rainfall mostly in boreal winter, and least during summer seasons (Sun et al., 2015). Extremes are more severe in the boreal winter during El Niño, mainly in central and southern North America, southeast and northeast China, and southeast South America, and during La Niña in western Pacific areas (Sun et al., 2015). In addition, El Niño and La Niña exert a significant influence on annual floods in river basins covering over a third of the world's land surface (Ward et al., 2014), and about one-fifth of the global land surface is more likely to experience abnormally high river flows during El Niño conditions, especially in the tropics (Emerton et al., 2017). These anomalies in precipitation and river flow compared to normal conditions are often asymmetric between ENSO

phases (Lee, Ward, & Block, 2018). Connections between El Niño or La Niña and low river flows also exist in many parts of the world (Chiew et al., 1998; Lü et al., 2011; Richard et al., 2001; Ryu et al., 2010). Furthermore, globally, disasters triggered by droughts occur twice as often during the second year of an El Niño event than during other years, especially in Southern Africa and Southeast Asia (Richard et al., 2001). Regions where rainfall and hydrological extremes are influenced by ENSO (Dai & Wigley, 2000; Dettinger & Diaz, 2000) also show a connection between ENSO and annual total water availability or water scarcity conditions. In these areas, rainfall deficits during an ENSO event enhance droughts, which can result in water scarcity events if consumptive demands outweigh the available water resources (Dilley & Heyman, 1995). As a result, regional water scarcity conditions become more extreme under El Niño and La Niña phases for almost one-third of the global land area (Veldkamp et al., 2015). Lastly, El Niño and La Niña conditions are also related with changes of mean sea level of ± 20-30 cm (Becker et al., 2012), and are strongly associated with extreme storm surges (Muis et al., 2018). ENSO events can induce changes in tropical cyclone activity in the Atlantic basins (Saunders et al., 2000), as well as extra-tropical cyclone activity (Eichler & Higgins, 2006).

The Euro-Atlantic region is less influenced by ENSO (Casanueva et al., 2014), and is mainly dominated by four northern hemisphere modes of climate variability. The North Atlantic Oscillation (NAO) is the main mode of low-frequency variability over the North Atlantic, and consists of a north-south dipole of anomaly in surface pressure between Greenland and the central latitudes of the North Atlantic between 35°N and 40°N. The East Atlantic Pattern (EA) is the second prominent mode of low-frequency variability over the North Atlantic, consisting of a north-south dipole of anomaly centres that extends across the entire region from the East to the West. The East Atlantic/West Russian pattern (EAWR) represents four main anomalies, centred over Europe and northern China, the central North Atlantic and north of the Caspian Sea. Lastly, the Scandinavian Pattern (SCA) captures anomalies primarily over the Scandinavian Peninsula, with centres of action over the north eastern Atlantic and central Siberia (Barnston & Livezey, 1987; Bueh & Nakamura, 2007). These four types of atmospheric circulation are often represented using indices based on sea surface pressure averages at different geopotential heights, which are then standardized based on their climatological mean. When such anomalies are above or below zero, the indices are classified as being in "positive" or "negative" phase, respectively.

Positive and negative phases of the four northern hemisphere modes of climate variability can also cause large variability in hydrometeorological variables in

Europe. Previous studies have found links between anomalies in seasonal mean and extreme rainfall in Europe with phases of the NAO, EA, EAWR and SCA (Álvarez-García et al., 2018; Bueh & Nakamura, 2007; Casanueva et al., 2014; Comas-Bru & McDermott, 2014; Vicente-Serrano et al., 2009). In addition, these modes of climate variability have been found to influence annual maximum and mean river discharges across the continent (Bouwer, Vermaat, & Aerts, 2008; Kingston et al., 2006; Steirou et al., 2019). A recent study suggests that NAO in winter exerts a strong influence on streamflow extremes in large parts of Europe (46% of the stations investigated; Steirou et al. 2019). Furthermore, past studies have shown that different indices of climate variability may play a role in explaining European drought variability and severity (van der Schrier et al., 2006; Vicente-Serrano et al., 2016, 2011). The NAO and SCA were found to influence droughts strongly in southern Europe (Sousa et al., 2011), whereas the EAWR affects droughts in western and central Europe (Kingston et al., 2015). Furthermore, other studies show some predictive capacity for drought conditions based on indices of climate variability. For instance, Ionita (2014) suggests that spring drought conditions can be predicted based on EAWR over extended European regions.

Scientific evidence on the relationship between climate variability and the socioeconomic impacts of floods and droughts is still limited, especially in relation to the four northern hemisphere modes of climate variability, and at several lead times before observing such impacts. At the global level, an initial study assessed links between ENSO and the reported frequency of drought and flood disasters (Dilley & Heyman, 1995). Subsequently, Bouma et al. (1997) investigated links between El Niño and the burden on human health, while a recent study by Anyamba et al. (2019) suggests that the 2015–2016 El Niño event may have triggered a series of global disease outbreaks in areas affected by ENSO teleconnections. These studies were followed by Goddard and Dilley (2005), where they analysed whether phases of ENSO could be associated with an increase in reported climate-related disasters. More recently, global flood risk models were used to examine ENSO's relationship with river flood risk at the global scale (Ward et al., 2014), and the number of people potentially exposed to global coastal flooding (Muis et al., 2018). A recent study has also found connections between NAO and flood losses in Europe (Zanardo et al., 2019). Furthermore, previous studies have investigated relationships between modes of climate variability and agricultural impacts worldwide. For example, Heino et al. (2018) investigated the role of ENSO, NAO and the Indian Ocean Dipole, concluding that two-thirds of global cropland is significantly affected by one of these large-scale climate oscillations. Furthermore, ENSO was found to either negatively or positively to affect crop productivity in 28% of global

cropland area, inhabited by 1.5 billion people, while other studies found significant connections between major European crops and NAO, EA, EAWR and SCA (Ceglar et al., 2017). Recent studies suggest that ENSO can affect food security and agricultural production, with cascading effects on livelihoods. For instance, the rapid shift between El Niño and La Niña conditions in 2016 intensified the shortage of rainfall, driving major hydrological crises over Eastern and Southern Africa, where 29 million people were faced with food insecurity due to the combination of drought exacerbated conditions (Funk et al., 2019), while contributing to severe flooding in the northwest of Latin America, forcing the evacuation of more than 150,000 people (BBC News, 2015).

1.4 From weather to impact-based forecasts

Weather forecasting refers to predictions of atmospheric variables and how they are expected to change on a timescale of days or less, while climate forecasting refers to these expected changes on a timescale of at least a month (WMO, 2015). Translating climate forecasts into socioeconomic impacts is referred to as "impact-based forecasting" (ibid). Over the past years, new drought and flood forecasting systems have emerged, while others have greatly improved their capability of forecasting flood and drought events at longer lead times than before. Despite such advancements, there is still a gap in translating forecasts for flood and drought events into societal impacts. Several ways exist to forecast flood and drought impacts, for example by using a modelling chain that combines climatological-, hydrological- and hydrodynamic processes with exposure and vulnerability information. Other approaches employ statistical methods describing relationships between weather variables and actual flood and drought impacts (Carisi et al., 2018; Devia, Ganasri, & Dwarakish, 2015). Statistical models may neglect or simplify some of the underlying physical and socio-economic processes, assuming that past interactions between risk drivers may propagate similarly in the future. However, such models are simple and can provide a first rapid estimation of the impacts of floods and droughts.

One example of an impact-based flood forecasting systems that runs operationally using a chain of dynamical models is the European Flood Awareness System (EFAS), which provides information on expected flood impacts for the continent with a lead time up to 10 days (Dottori et al., 2017). In addition to dynamic modelling predictions, scenario development methodologies are used to assist in forecasting future impacts. For instance, to describe the forecasted levels of acute food insecurity, FEWS NET (Funk et al., 2019) translates numerous drivers (e.g. rainfall, staple food price, migration patterns and others) into one indicator: integrated Food Security Phase

Classification (IPC). This indicator is intended to help actors on the ground to readily understand the level of food insecurity, and the urgency to take action. However, forecasting the expected impact (e.g. famine and displacement) given a certain drought/flood event is surrounded with much uncertainty.

One advantage of producing impact-based forecasts using indices that represent climate variability is that some of them can be predicted with longer lead times than hydrometeorological variables such as rainfall and streamflow (Ceglar et al., 2017). For instance, with an improvement of stratosphere–troposphere coupling and atmospheric initial conditions, high skill has been observed in predicting an important mode of circulation in the northern hemisphere winter circulation (Ceglar et al., 2017; Stockdale, Molteni, & Ferranti, 2015). Furthermore, increased horizontal and vertical resolution of climate models, and a greater availability of forecast ensembles in combination with improved understanding of potential sources of NAO's predictability, have allowed skilful predictions of the winter NAO more than a year in advance (Dunstone et al., 2016). Also ENSO forecasting is highly developed, and most prediction systems have some skill in detecting events with lead-times of 12–14 months (Gonzalez & Goddard, 2016). EA summer and autumn anomalies have been forecasted with a lead-time of 1 to 2 months (Iglesias, Lorenzo, & Taboada, 2014). In comparison, GloFAS produces global probabilistic forecasts of 10-day rainfall up to 10 days ahead and daily river discharge up to 30 days ahead. Further value could be added to the forecasts of indices of climate variability by combining them with information on the resulting socioeconomic impacts (e.g. flood and drought risk), thereby enabling the seasonal forecasting of those socioeconomic impacts. Such forecasts may support risk management, enable the prioritization of adaptation efforts, and allow for improved early warning and action by local-to-national governments and non-governmental organizations. Thus, understanding the effects of climate variability on flood and drought impacts will support disaster resilience from global to regional scales.

Some organizations are starting to use climate information, such as the predictions of ENSO, to estimate the seasonal impacts of floods and droughts, and to trigger early actions and risk transfer mechanisms such as insurance products. For instance, an El Niño contingent insurance product was developed for the region of Piura (Peru) to compensate firms for lost profits or possibly occurring extra costs as a result of floods (Cavanaugh, Collier, & Skees, 2010; Coughlan De Perez et al., 2015). Furthermore, in 2015, based on an El Niño forecast, funds were released through the World Food Program's Food Security Climate Resilience Facility for Zimbabwe and Guatemala (World Food

Programme, 2016) to help both countries to face their consequent droughts. Despite these advances, associated uncertainties in forecast systems remain large, and the vast majority of forecast information is not routinely used as a basis for financing early action for drought and flood risk reduction. One of the reasons for such insufficient funding is the lack of evidence regarding the beneficial impacts of acting upon uncertain early warning information.

1.5 From financing post-disaster recovery to financing risks

In 2019, the FEWS NET estimated that there were 85 million people in need of emergency food assistance, 80% more than in 2015 (FEWS NET, 2019). Between 1991 and 2010, the international financing community heavily funded emergency responses to humanitarian crises, while financing for disaster risk reduction was a low priority in development aid (Kellett & Caravani, 2013). During this period, over US$3 trillion was spent in aid, of which US$106.7 billion was allocated to disasters induced by natural hazards. Of this amount, 13% was spent on ex-ante risk reduction measures, compared to 87% spent on ex-post activities - 22% on reconstruction and rehabilitation and 65% on emergency response (ibid). Furthermore, for some middle-income countries, flood prevention and control has accounted for a very high proportion of overall ex-ante disaster risk reduction funding. It is estimated that over the period from 1991 to 2001, investments in flood prevention and control made up 90% of all ex-ante disaster risk reduction financing (ibid). On the other hand, drought-affected low-income countries have received negligible international financing for drought risk reduction (ibid). Apart from protection measures (e.g. levees to reduce flood impacts or developing reservoirs to store water for a period of drought), there is always a residual risk, which can be addressed through risk transfer mechanisms. An example is insurance, which shifts the financial burden of risks from one party to another (Bouwer et al., 2007). A well-known example is index-based insurance, which correlates crop losses with weather parameters (Clement et al., 2018). The coverage of a risk is obtained from an insurer in exchange for ongoing premiums paid by farmers to the insurer (Dick et al., 2011).

However, at present, the insurance penetration rates in developing countries are low (Linnerooth-Bayer et al., 2009), and other mechanisms are needed to reduce residual risks. Furthermore, when a disaster hits a country, and governments appeal for international financial support, the aid often arrives too late, and can involve highly bureaucratic processes. Acting ex-ante to a crisis could enable governments to be more proactive in achieving short- and long-term goals of disaster risk reduction, while alleviating the weight of natural hazards on the most vulnerable. Therefore, a debate has started as to whether

aid should be given directly to people in the form of cash as an alternative to traditional in-kind food aid and food vouchers (Harvey, 2007). Such cash transfers are typically less expensive to administer and have the advantage of transferring the purchasing power to the recipients. They can therefore be effective for disaster risk financing (Kenya Red Cross, 2017; UNDP, 2015). However, among the numerous cash transfer programmes (Garcia & Moore, 2012), only a handful focus on transfers before an event occurs; the majority focus on transfers after an event occurs. Therefore, cash transfer programmes for disaster responses are typically based on observations after an event has taken place (Pulwarty & Sivakumar, 2014), which may result in ineffective delayed assistance.

Given the recent improvement of forecasting systems, combined with an emerging understanding on ways to automatically trigger action based on early warning systems (Coughlan De Perez et al., 2015; Stephens et al., 2015; Suarez & Tall, 2010), there is a growing recognition that there may exist a window of opportunity to take actions to reduce risks based on a forecast, rather than taking actions after a disaster has occurred. Timely ex-ante action has the potential to be more cost-effective than ex-post disaster relief when leveraged by a credible plan, pre-agreed triggers for action, and pre-arranged financing. One way to leverage investments for ex-ante action is improving the understanding of the beneficial impacts of acting early. A key research question is whether early action can be efficiently managed based on improvements in the forecastability of natural hazard and new automated funding allocation methods. Currently, there is an increasing interest in the use of Big Data in combination with Machine Learning algorithms for improving impact-based forecasts and designing more accurate triggers for parametric financial products and humanitarian aid (Meier, 2015). Such emerging technologies may offer decision-makers with skilful impact-based predictions, providing insights on how to deliver effective disaster risk mitigation efforts that maximize benefits and reduce human impact and losses. However, given the fact that there is no system with a "perfect forecast" skill, predictions of future impacts always remain susceptible to errors and uncertainties. In order to create guidelines for ex-ante aid and risk transfer mechanisms, a comprehensive understanding of the costs and likelihood of "acting in vain" due to false alarms is needed.

1.6 Research objectives and questions

In response to the limited understanding on links between climate variability and weather-related impacts of both floods and droughts, and the current gap

in translating such relationships into impact-based information that can be used as a basis for triggering early action, the main objective of this thesis is:

To assess the link between climate variability and weather-related impacts (flood and drought) at the global and regional levels, and to develop impact-based forecast methods that can potentially reduce these impacts through early action.

In order to fulfil this objective, the following five research questions are formulated:

1. What are the links between large-scale climate variability, the occurrence and intensity of extreme rainfall, and anomalies in flood occurrence and damage?

2. Can large-scale climate variability be used to forecast flood losses?

3. Can large-scale climate variability be used to forecast agricultural production and support agricultural management and decision-making?

4. How can information about climate variability be used to increase the cost-effectiveness of ex-ante risk financing programmes?

5. How can the reduction of disaster risks be achieved by improving our understanding and prediction of the impacts associated with large-scale climate variability?

1.7 Reading guide

This thesis contains 7 chapters, in which chapters 2-6 address the research questions presented above, as illustrated in Figure 1.2. Chapters 2-7 are outlined as follow:

*   Chapter 2 analyses the El Niño Southern Oscillation, the North Atlantic Oscillation, and the East Atlantic pattern during their neutral, positive, and negative phases, to understand their relationships with four flood indicators: Occurrence of Extreme Rainfall, Intensity of Extreme Rainfall, Flood Occurrence, and Flood Damage. This chapter investigates the spatial and temporal influence of climate variability in extreme meteorological and flood events at the pan-European scale. This chapter pays special attention to assessing relationships between multiple indices of climate variability and flood losses;
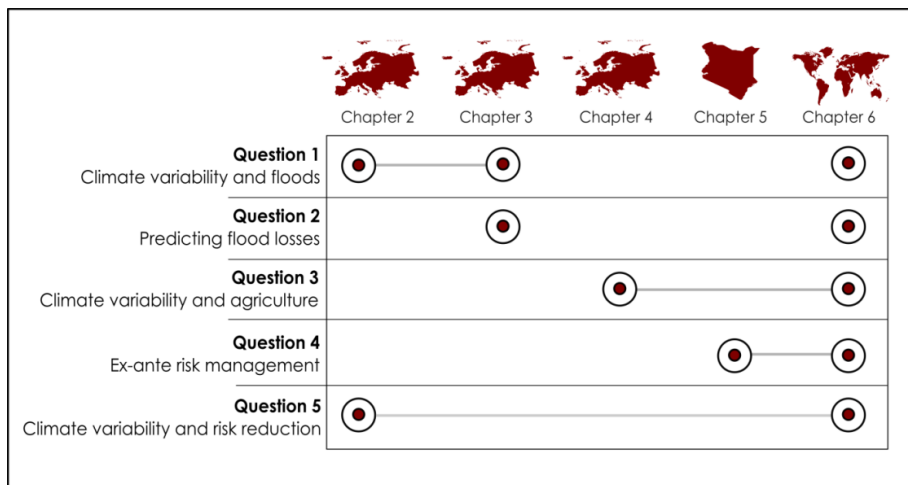
Figure 1.2 Thesis' reading guide.

- Building upon findings from Chapter 2, Chapter 3 examines the role of seasonally lagged and synchronous indices of climate variability on flood losses at the sub-regional European scale. Furthermore, this chapter investigates the likelihood of seasonal flood losses based on indices of climate variability, and whether some of these losses can be predicted one season ahead. It aims at providing a better understanding of the combined effect of climate variability on flood losses, and how such information could be used to improve flood risk management practices;

- Chapter 4 analyses multiple time-scale relationships between large-scale indices of climate variability and anomalies in crop production at the pan-European scale. It aims at identifying regions where anomalies in crop production can be forecasted based on the indices of climate variability. It also discusses how this information potentially improves the management of the agricultural sector;

- Chapter 5 evaluates the cost-effectiveness of ex-ante cash transfers during the growing season of maize, prompted by the expected probabilities of low maize yield obtained from a predictive model. It compares the costs of ex-ante cash transfers with the costs of ex-post cash transfers after harvesting. This chapter provides novel early warning information that can be useful for reducing the costs and increasing the effectiveness of existing cash transfer programmes for drought risk management. The approach is tested in five districts in Kenya;

- Chapter 6 reviews the global effects of El Niño Southern Oscillation on disaster risks, including water scarcity and agricultural droughts, extreme rainfall, and river- and coastal flooding. It provides policy recommendations by showcasing opportunities to reduce the risk of disasters by responding to El Niño Southern Oscillation forecasts;
- Chapter 7 concludes and summarises the thesis, providing answers to the research questions and discussing future avenues of research.

Chapter 2

The role of climate variability in extreme floods in Europe

Abstract

Climate variability is shown to be an important driver of spatial and temporal changes in hydrometereological variables in Europe. However, the influence of climate variability on flood damage has received little attention. We investigated the El Niño Southern Oscillation (ENSO), the North Atlantic Oscillation (NAO), and the East Atlantic pattern (EA) during their neutral, positive, and negative phases, to understand their relationships with four flood indicators: Occurrence of Extreme Rainfall, Intensity of Extreme Rainfall, Flood Occurrence, and Flood Damage. We found that positive and negative phases of NAO and EA are associated with more (or less) frequent and intense seasonal extreme rainfall over large areas of Europe. The relationship between ENSO and the Occurrence of Extreme Rainfall and Intensity of Extreme Rainfall in Europe is much smaller than the relationship with NAO or EA, but still significant in some regions. We show that Flood Damage and Flood Occurrence have strong links with climate variability, especially in southern and eastern Europe. Therefore, when investigating flooding across Europe, all three indices of climate variability should be considered. Future research should focus on their joint influence on flood risk. The potential inclusion of seasonal forecasts of indices of climate variability could be effective in forecasting flood damage.

2.1 Introduction

Between 1980 and 2015, Europe experienced 18% of worldwide weather-related loss events, which accounted for over US$500 billion (bn) in damage (Munich Re, 2016b). Consequently, it is urgent to further develop adaptation strategies to mitigate the consequences of weather-related disasters, such as floods (Jongman et al., 2014). Europe's capability to prepare for such disasters is challenged by a large range of uncertainties and a limited understanding of the driving forces of hydrometeorological hazards (Apel et al., 2004). One of the major sources of uncertainty is the relationship between climate variability and weather-related losses (Merz et al., 2014).

Climate variability refers to natural fluctuations of the climate system around the long-term trend (Stocker et al., 2013). Such variability is caused by coupled interactions between atmospheric and oceanic components, measured by an index. Globally, ENSO is the most important mode of climate variability, and has been linked with changes in hydrometeorological extremes in past studies at different scales, including national (Rios-Cornejo et al., 2015; Sun et al., 2014; Villafuerte et al., 2014), continental (Cannon, 2015; Casanueva et al., 2014; Ionita et al., 2015), and global (Sun et al., 2015; Veldkamp et al., 2015; Ward et al., 2010, 2014).

In addition to ENSO, hydrometeorological variables across Europe show relationships with other indices of climate variability, such as the NAO and EA. NAO measures anomalies in sea level pressure over the subpolar and the subtropical region of the North Atlantic (Hurrell et al., 2003), while the EA measures these anomalies across the entire North Atlantic region from east to west (Barnston & Livezey 1987;NOAA 2017). ENSO, NAO, and EA have positive, negative, and neutral phases, and can be related with variations in the European climate. For instance, an NAO$^+$ phase links with increased westerlies over the middle latitudes, and intense weather systems over the North Atlantic. On the other hand, NAO$^-$ phase shows an opposite pattern over these regions (Hurrell et al., 2003). Therefore, different phases of ENSO, NAO and EA can be associated with increases or decreases in disaster burden (Goddard & Dilley, 2005; Mitchell et al., 2017; Pinto et al., 2009) .

Whilst several studies have assessed the regional influence of ENSO, NAO, and EA on precipitation (Goddard & Dilley, 2005; Gregersen et al., 2013; Lopez-Bustins, Martin-Vide, & Sanchez-Lorenzo, 2008; Lorenzo, Taboada, & Gimeno, 2008; Mariotti, Zeng, & Lau, 2002; Rodó, Baert, & Comin, 1997) and discharge (Markovic & Koch, 2014; Struglia, Mariotti, & Filograsso, 2004), less research has been carried out at Pan-European scale. Fewer still have examined peak discharge. An exception is an investigation of observed European peak river

discharge relationships with NAO, Arctic Oscillation (AO), frequency of west circulation (FWC), and north to south sea level pressure difference (SLPD) (Bouwer et al., 2008). Some studies have examined climate variability's influence on extreme precipitation (Casanueva et al., 2014). However, these studies do not address differences in the frequency and intensity of extreme precipitation during positive and negative phases compared to neutral phases.

Only few studies specifically addressed relationships between climate variability and the socioeconomic impacts of flood disasters. At the global level, an initial study (Dilley & Heyman, 1995) assessed links between ENSO and the reported frequency of drought and flood disasters. Subsequently, others (Bouma et al., 1997) investigated links between El Niño and the burden on human health. These studies were followed up by research (Goddard & Dilley, 2005) that analysed whether phases of ENSO could be associated with an increase in reported climate-related disasters. Recently, a global flood risk model was used to examine ENSO's relationship with flood risk at the global scale (Ward et al., 2014), while other studies have assessed relationships between NAO and EA and agriculture risks e.g. (Brown, 2013; Cantelaube, Terres, & Doblas-Reyes, 2004; Fuhrer et al., 2006; Hernández-Barrera & Rodríguez-Puebla, 2017; Irannezhad, Chen, & Kløve, 2016).

To the best of our knowledge, no studies have examined the impacts on flood damage of multiple indices of climate variability. Therefore, we analyse ENSO, NAO, and EA indices during their neutral, positive and negative phases, to answer the following research questions:

- Are there differences in the frequency and intensity of extreme rainfall between the different phases of the indices of climate variability?
- Are there anomalies in flood occurrence and damage between the different phases of the indices of climate variability?

In section 2.2 we describe the climate and flood indicators, and the statistical methods, followed by the presentation and discussion of the results in sections 2.3 and 2.4. We conclude with section 2.5.

2.2 Methods: climate and flood indicators and statistical approach

We use statistical methods to analyse relationships between ENSO, NAO, and EA indices and four indicators of flooding, namely: (1) Occurrence of Extreme Rainfall (OER); (2) Intensity of Extreme Rainfall (IER); (3) Flood Occurrence; and (4) Flood Damage. These indicators were derived from two datasets: a database of flood disasters and losses in Europe (Munich Re, 2016a) and a gridded dataset of daily precipitation (Haylock et al., 2008). An overview of the

methodological framework is displayed in Figure 2.1. The methods and datasets are described in more detail in the following subsections.
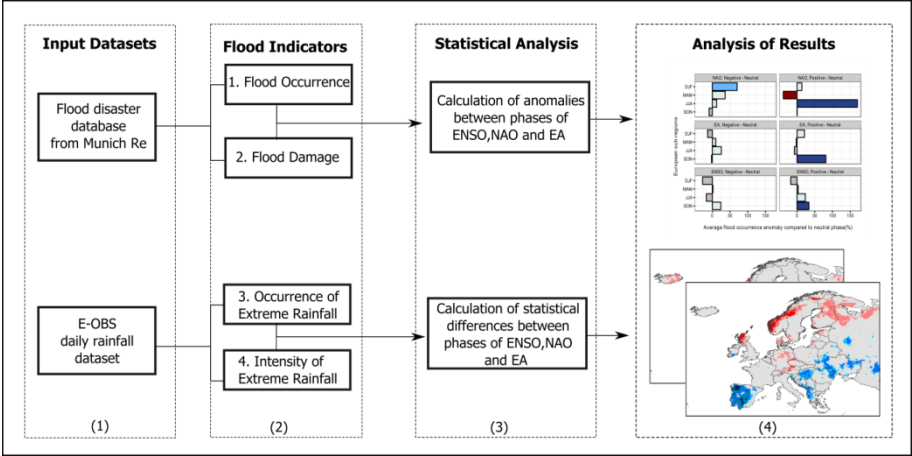
Figure 2.1 Flowchart representing the methodological framework applied in this study, handled in four steps: (1) collection of two input datasets; (2) extraction of four flood indicators based on input datasets; (3) application of statistical methodology; (4) analysis of results.

2.2.1 Indices of climate variability

In this study, we represent climate variability using the ENSO, NAO and EA indices, whose phases were divided into negative, positive and neutral.

For ENSO, we used the Oceanic Niño Index (ONI) from 1950-2014 (http://www.cpc.ncep.noaa.gov). ONI is a three-months running mean of sea surface temperature (SST) anomalies in the Niño 3.4 region. We used the data for December-February (DJF), March-May (MAM), June-August (JJA), and September-November (SON). ENSO's phase classification was established by the National Oceanic and Atmospheric Administration (NOAA), which compares the running mean value to a 30-year average to derive periods of below or above normal SSTs. ENSO$^-$ (ENSO$^+$) phases are classified when the threshold of $-$ (+) 0.5°C is met for a minimum of five consecutive overlapping 3-month periods.

For NAO, we used the Hurrell NAO index (station-based) from the Climate Data Guide (https://climatedataguide.ucar.edu/climate-data). We obtained the seasonal index from 1950-2014 for DJF, MAM, JJA, and SON. For EA, we used the monthly standardized index from NOAA. Again, we averaged the EA series for the same period as for NAO. Both the NAO and EA indices follow a Gaussian distribution, therefore, the three phases were classified using a ± 1σ (Jeong &

Ho, 2005). An overview of the indices and their classification is shown in the appendix Figure A1.

2.2.2 Flood indicators and European sub-regions

We assess flood by means of four indicators: OER, IER, Flood Occurrence and Flood Damage. Because Flood Occurrence and Flood Damage records were not sufficient to establish comparison at the country level, we grouped the records into four sub-regions. For the European sub-regions (appendix Figure A2), we used the classification established by the United Nations Statistics Division. We extracted all four indicators seasonally: winter (DJF), spring (MAM), summer (JJA), and autumn (SON).

2.2.2.1 Occurrence of Extreme Rainfall and Intensity of Extreme Rainfall

We obtained the OER and IER from the E-OBS rainfall dataset (http://www.ecad.eu/). This dataset contains daily gridded precipitation for 1950-2014, with a horizontal resolution of 0.25 degree. We extracted the OER events per season and year, and the intensity of those events. We define extreme rainfall using Partial Duration Series (Coles et al., 2001), where the n largest rainfall events are extracted per year, relative to the length of the daily series (Prudhomme & Genevier, 2011). The extreme series contain an average of three high rainfall events per season (n = 3×65 years). We applied an inter-event time criterion of 24 hours to fulfil the independence of the series, and calculated the OER by counting the number of extremes per season/year; the indicator of IER is the ratio of the sum of the intensity of these respective events (per season/year) and the OER indicator.

2.2.2.2 Flood Occurrence and Flood Damage

We used the NatCatSERVICE dataset of Munich Re (Munich Re, 2016a) to derive time-series of Flood Occurrence and Flood Damage. This dataset registers flood events in Europe, and their respective period, timing, location and damages (US$) between 1980-2012. To calculate Flood Occurrence we extracted the initial date of the floods, and then counted and sorted these events into a specific season of the year. For the Flood Damage indicator, we deflated the nominal flood damage recorded from 1980-2012 into 2010 US$ values, and converted these into Purchasing Power Parity (PPP) equivalent (further description in the Appendix A3). The distribution of reported flood events and damage recorded in the Munich Re database per sub-region and season is available in Figure A3.

2.2.3 Statistical approach

For the OER and IER indicators, we applied a two-tailed T-Test (each tail α=5%). The test identifies whether the mean occurrence and intensity of extreme rainfall found in positive or negative phases are significantly different from the one found during the neutral phase. Field significance of the gridded results was assessed using the binomial distribution (Livezey & Chen, 1983).

For the Flood Occurrence and Flood Damage indicators, we used a methodology proposed in previous research (Iizumi, Luo, et al., 2014). Following this approach, we investigated anomalies in Flood Occurrence and Flood Damage within phases of ENSO, NAO and EA by calculating the percentage anomaly that deviates from a normal value (defined as 5-years running mean) for the time interval (t in years) $t - 2$ to $t + 2$. We applied a 5-years running mean to minimize possible pitfalls regarding reporting issues in the Munich Re dataset. Often, an issue with disaster databases is that the frequency count of damaging floods includes increased reporting of disasters towards more recent years (Merz et al., 2012). In addition, we tested the long-term average (1982-2010) as a normal value, however results did not greatly differ between the two methodologies (appendix A4). The percentage anomaly (F') for a respective season (S) and sub-region (R) is obtained by:

$$F'_{S,R} = \frac{F_{S,R} - \overline{F}_{S,R}}{\overline{F}_{S,R}} \times 100$$

Equation 2.1

$F_{S,R}$ indicates the value of the Flood Occurrence or Flood Damage, and $\overline{F}_{S,R}$ is the normal value for the indicator. The calculation of the percentage flood anomaly aims to detect the major changes in these two indicators induced by short-term climate factors, although other factors like exposure and vulnerability may also contribute to yearly variations. The second step is to obtain an average flood anomaly (%) for each phase of the climate indicator (I) for 1982-2010:

$$F'_{R,\,I^+} = \frac{1}{n_{I^+,\,R}} \sum_{1982}^{2010} F'_{S,R} \; if \, I_S \geq u$$

Equation 2.2

$$F'_{R,\,I^-} = \frac{1}{n_{I^-,\,R}} \sum_{1982}^{2010} F'_{S,R} \; if \, I_S \leq \text{-}u$$

Equation 2.3

$$F'_{R,\,I^N} = \frac{1}{n_{I^N,\,R}} \sum_{1982}^{2010} F'_{S,R} \; if \; \text{-}u < I_S < u$$

Equation 2.4

$n_{I^+,R}, n_{I^-,R}$ and $n_{I^N,R}$ are the numbers of positive, negative and neutral phases of indices of climate variability, respectively, and threshold u is $\pm 1\sigma$ or $\pm 0.5°C$ depending on the climate indicator. Next, we compared the difference between average percentage flood anomalies in positive or negative seasons to the values in neutral seasons:

$$\Delta F'_{R,I^+} = F'_{R,I^+} - F'_{R,I^N} \qquad\qquad \text{Equation 2.5}$$

$$\Delta F'_{R,I^-} = F'_{R,I^-} - F'_{R,I^N} \qquad\qquad \text{Equation 2.6}$$

A negative (positive) value of $\Delta F'_{R,I^+}$ and $\Delta F'_{R,I^-}$, suggests, on average, a lower (higher) impact of the index of climate variability I^+ and I^-, compared to the average in flood anomaly for the indicators in neutral phases. We tested the statistical significance of the difference by bootstrapping the values of the percentage flood anomaly for a sub-region using 10,000 iterations. The two-sided test considers significance level of 5% (strong significance) and 10% (weak significance) in each tail, adopting the null hypothesis that the difference between the average percentage flood anomaly in I^+ or I^- and I^N are equal to zero (details in the Appendix A5).

2.3 Results

In this section, we firstly describe the differences in OER and IER indicators within ENSO, NAO and EA phases, followed by outcomes regarding anomalies in Flood Occurrence and Flood Damage.

2.3.1 Differences in the Occurrence and Intensity of Extreme Rainfall

In Figure 2.2, we display the seasonal differences in the OER indicator between the I$^+$ and I$^-$ phases compared to the I^N phases in percentage terms. The strongest link can be seen for NAO and EA. The mean OER per season and phase is displayed in Figure A6.1 in the appendix.

Extreme rainfall in winter occurs more frequently in southern and eastern Europe, and less frequently in northern countries during NAO$^-$; the opposite pattern is seen during NAO$^+$. In spring, during NAO$^-$ we observe more frequent extreme rainfall in large portions of eastern Europe. The main signal in summer and autumn is less frequent extreme rainfall, particularly in southern and eastern Europe during NAO$^+$. Extreme rainfall is less frequent in large part of Europe during EA$^-$, although more frequent extremes are seen in south-eastern regions. In winter and spring, we observe a higher OER in sparse areas of

northern Europe during EA^+, and opposite pattern in southern and western Europe in all seasons.

In general, the influence of ENSO on the OER in Europe appears to be much smaller than the influence of NAO or EA. In winter, less frequent extreme rainfall is seen during $ENSO^-$ in sparse areas, particularly in the east. During spring, we observe positive differences in parts of northern Spain and southern France during $ENSO^-$, and over Sweden during $ENSO^+$. In autumn, we observe more frequent extreme rainfall in large areas of Europe within both phases of ENSO, especially in Iceland during $ENSO^+$.

In Figure 2.3, we show the significant differences in the IER for the I^+ and I^- phases compared to the I^N phases for each season in percentage terms. Again, NAO and EA show the strongest relationships. The mean IER per season and phase is displayed in Figure A6.2 in the appendix.

In winter during NAO^-, we observe higher IER in eastern Europe, and lower IER in northern and western Europe. The reverse pattern is observed during NAO^+. Except in winter during NAO^+, IER is lower in large areas of Europe. However, the opposite is observed in southeastern and northeastern Europe in summer during a NAO^-.

During EA^-, extreme rainfall is less intense over the year in northern and western Europe. In all seasons, we observe lower IER during EA^+ in large areas of the continent, except in summer and autumn in parts of northern and eastern Europe, where extreme rainfalls are on average 25% more intense.

In general, the influence of ENSO on the IER in Europe is limited and rather local. During $ENSO^-$, we observe lower IER in all seasons in scattered areas of western and eastern Europe, and higher IER over Spain during $ENSO^+$, except in autumn.

2.3.2 Anomalies in Flood Occurrence and Flood Damage at the pan-European scale

At the pan-European scale, all three indices of climate variability show significant relationships with Flood Occurrence in one or more phase and/or season (Figure 2.4a). The strongest link is observed for NAO. In summer, during NAO^+, anomalies in Flood Occurrence are 170% higher than during NAO^N. In winter, during NAO^-, anomalies in Flood Occurrence are on average 70% higher than during NAO^N. We also found that Flood Occurrence in spring is significantly lower during NAO^+, and higher (81% and 33%) during EA^+ and $ENSO^+$ but we find no significant anomalies during their negative phases.
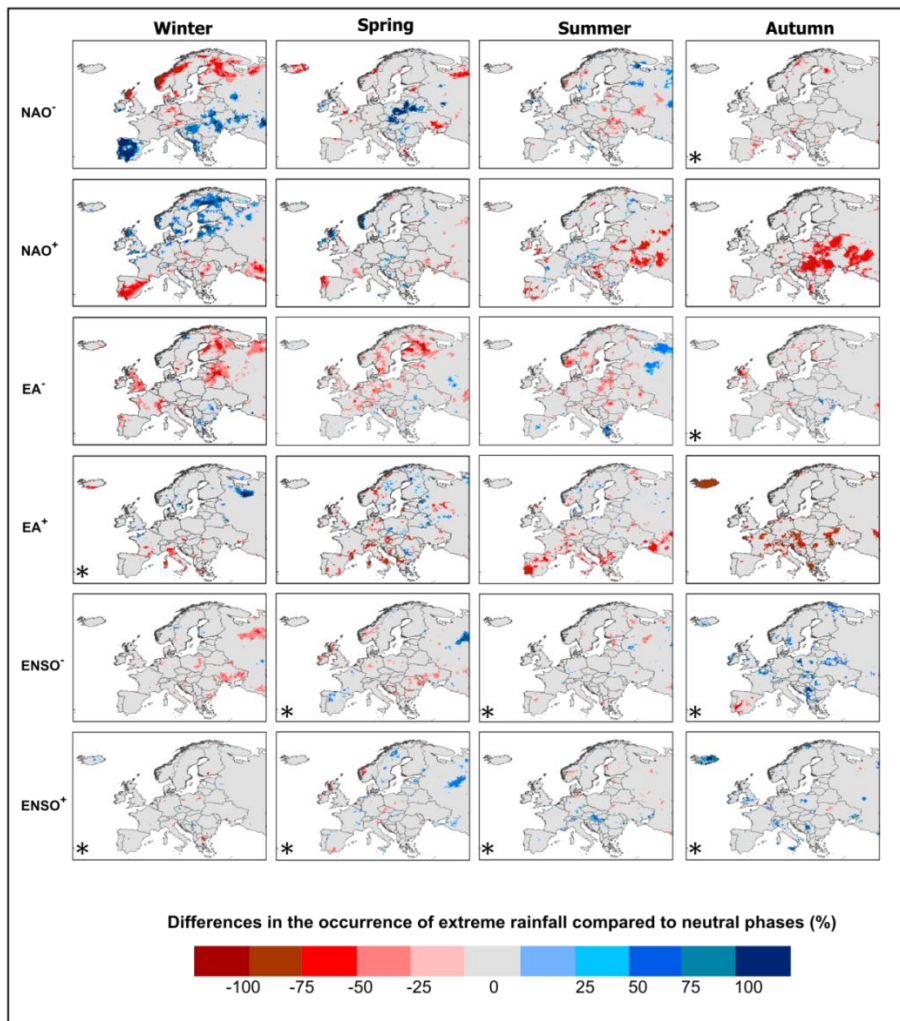
Figure 2.2 Mean percentage difference in the seasonal occurrence of extreme rainfall (OER) (number of events/season) between negative phase and positive phase of the indices of climate variability, compared to the neutral phase. Blue (red) colours symbolize a significantly higher (lower) number of extreme events compared to the neutral phase (each tail α= 5%). Field significance of the gridded results was assessed using the binomial distribution and found to be highly significant (P < 0.001). Seasons/phases of the indices of climate variability that were found to be significant only due to T-Test are indicated with an asterisk (*).

We find significant anomalies in Flood Damage (compared to I^N phases) linked to all three indices of climate variability, with the strongest anomalies again for NAO (Figure 2.4b). Anomalies in winter Flood Damage are on average 222% higher during NAO⁻, and 104% lower in spring during NAO⁺. Still in spring, Flood Damage is 137% higher during EA⁻. We observe positive anomalies in summer
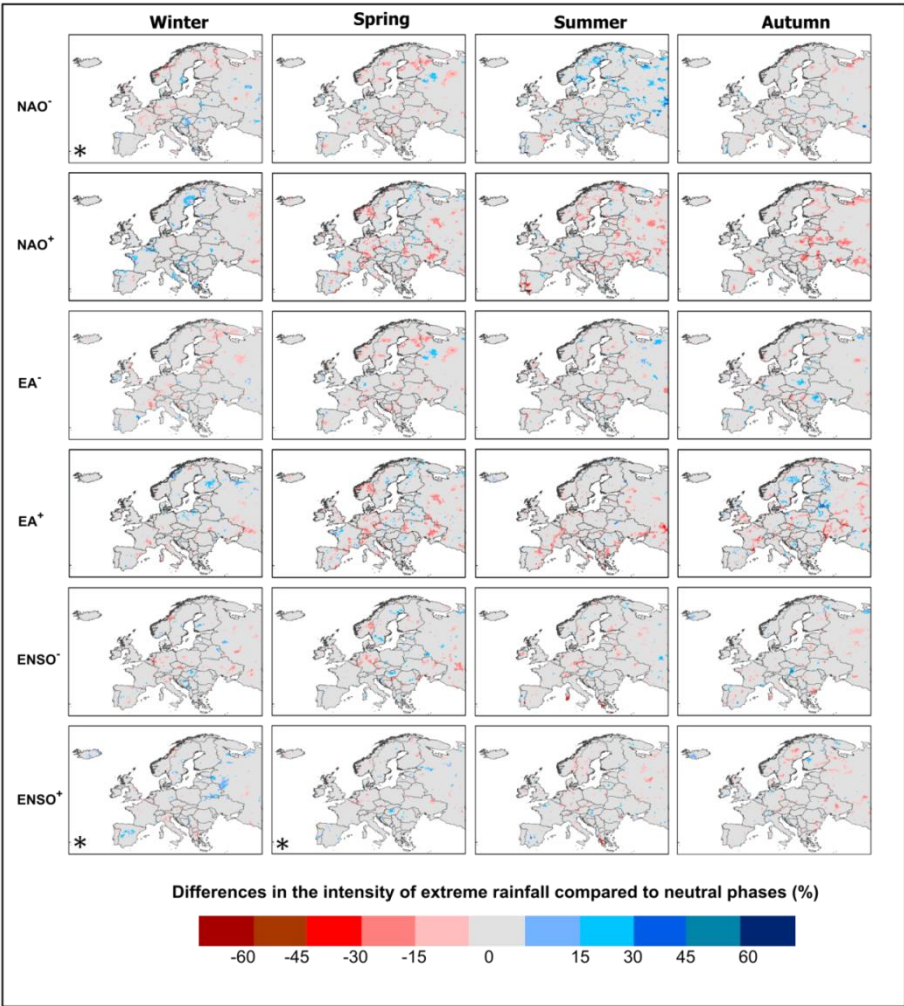
Figure 2.3 Mean difference in the intensity of extreme rainfall (IER) (mm/event) between negative phases and positive phases of the indices of climate variability, compared to neutral phases. Blue (red) colours symbolize significantly higher (lower) intensity of extremes events compared to a neutral phase (each tail α= 5%). Field significance of the gridded results was assessed using the binomial distribution and found to be highly significant (P < 0.001). Seasons/phases of the indices of climate variability that were found to be significant only due to T-Test are indicated with an asterisk (*).

during the positive phase of the NAO and ENSO, with the highest anomalies (374%) during NAO$^+$.
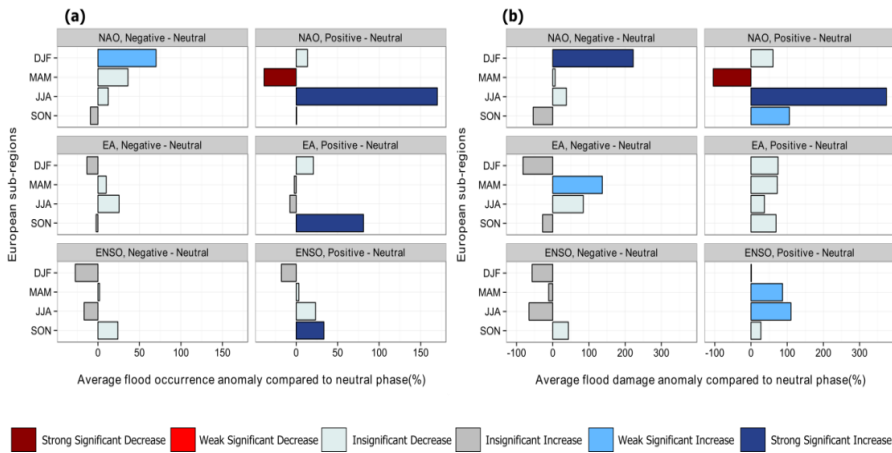
Figure 2.4 Pan-European analysis of the average percentage anomalies in (a) Flood Occurrence and (b) Flood Damage per season, during the positive and negatives phases of the different climate indices (compared to neutral). For strong significance, we use α= 5%, while for a weak significance α= 10% at each tail.

2.3.3 Anomalies in Flood Occurrence and Flood Damage at the sub-regional scale

In Figure 2.5, we show the anomalies in Flood Occurrence per season for the four European sub-regions. In southern Europe (Figure 2.5a), Flood Occurrence anomalies during winter are 181% higher during NAO⁻, and 40% lower in spring during ENSO⁻. In summer seasons Flood Occurrence anomalies are 111% higher during NAO⁺, and 48% lower during EA⁺ phases. However, anomalies in Flood Occurrence are 164% and 80% higher in autumn during EA⁺ and ENSO⁺, respectively.

For eastern Europe (Figure 2.5b), Flood Occurrence anomalies in winter are 89% and 59% higher during NAO⁺ and EA⁺, respectively. However, during NAO⁺ in spring, Flood Occurrence is 47% lower compared to neutral, and 110% higher in summer. We found positive anomalies in Flood Occurrence in spring for NAO⁻, and in autumn for ENSO⁻.

In western Europe (Figure 2.5c), during NAO⁺ in summer, Flood Occurrence is much higher (247%) compared to neutral. In addition, anomalies in Flood Occurrence in summer and autumn are on average 53% and 69% higher during EA⁻ and EA⁺.

In northern Europe (Figure 2.5d), in spring and summer, anomalies in Flood Occurrence are on average 47% and 62% lower during NAO⁺ and ENSO⁺,

respectively. In addition, significant positive anomalies are seen in autumn during positive phases of ENSO and EA.
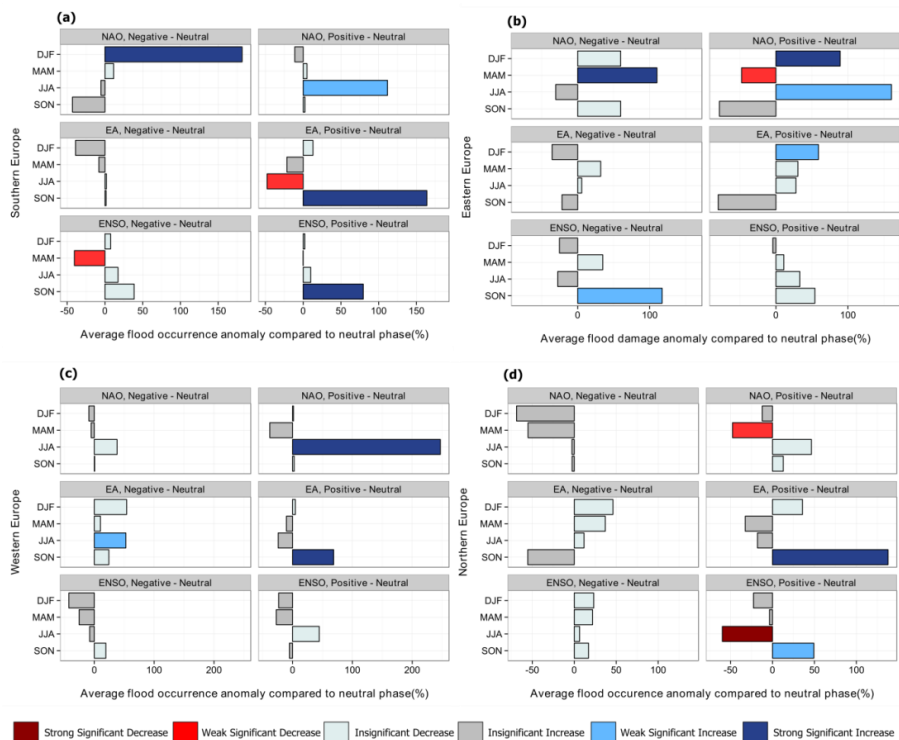
Figure 2.5 Average percentage anomalies in flood occurrence per season, within the positive and negative phases of the different climate indices (compared to neutral). Results are shown for: (a) southern Europe; (b) eastern Europe; (c) western Europe; (d) northern Europe. For strong significance, we use α= 5%, while for a weak significance α= 10% at each tail.

In terms of Flood Damage for southern Europe (Figure 2.6a), we find significant anomalies (compared to neutral) during several phases and/or seasons of the indices of climate variability. Anomalies in Flood Damage are positive (373%) in winter during NAO$^+$, and in summer (389%, 129% and 230%) for NAO$^-$ (389%), EA$^-$ (129%) and ENSO$^-$ (230%), respectively. Flood damages are lower during ENSO$^+$ in spring.

In eastern Europe (Figure 2.6b), we found significant anomalies in Flood Damage for one or more seasons or phases for all of the indicators of climate variability. Anomalies in Flood Damage are 120% in winter during EA$^+$, and 125% (277%) lower (higher) in spring during NAO$^+$ (EA$^-$). Flood Damages are 293% higher in summer during NAO$^+$, and −125% and 140% in autumn during the negative phases of ENSO and EA.

In western Europe (Figure 2.6c), we observe significant anomalies in Flood Damage during several phases and/or seasons of NAO and ENSO. In winter and summer, anomalies in Flood Damage are 107% and 400% higher during NAO$^+$, respectively. In summer and autumn, we find higher Flood Damage (121% and 157%) during ENSO$^+$ and ENSO$^-$.

In northern Europe (Figure 2.6d), spring and summer seasons are associated with negative anomalies in Flood Damage during the positive phases of the indices of climate variability. Anomalies in Flood Damage are higher in autumn (95% and 126%) during ENSO$^+$ and EA$^+$, respectively.
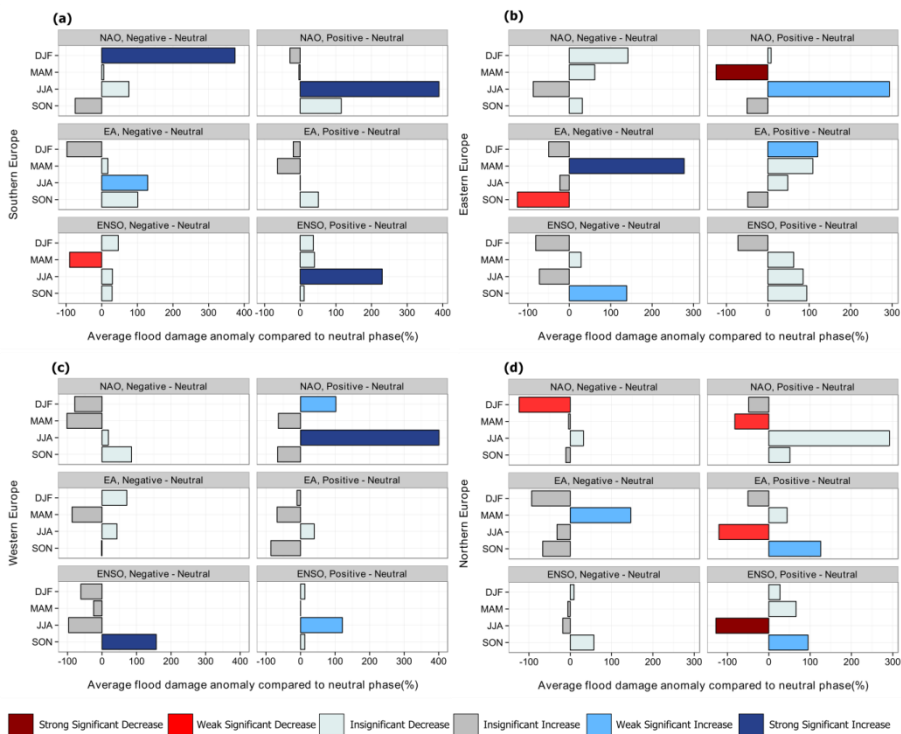
Figure 2.6 Average percentage anomalies in flood damage per season, within the positive and negative phases of the different climate indices (compared to neutral). Results are shown for: (a) southern Europe; (b) eastern Europe; (c) western Europe; (d) northern Europe. For strong significance, we use α= 5%, while for a weak significance α= 10% at each tail.

2.4 Discussion

2.4.1 Similarities and differences between the four flood indicators

We observe major similarities in the overall patterns among the four flood indicators. Large differences in OER and IER (Figures 2.2-2.3) often coincide with large anomalies in Flood Occurrence and Flood Damage (Figures 2.4-2.6 and appendix Table A7). For example, in winter southern- and eastern Europe receive more frequent and intense extreme rainfall during NAO⁻. This may be causing the high anomalies in Flood Occurrence and Flood Damage at the pan-European scale. Floods, especially in summer, are greatly anomalous in eastern and western Europe, where more frequent events coincide with higher costs (appendix A3). Summer and autumn major floods in Europe are mostly driven by river and flash floods, which are triggered by regional heavy rainfall followed by consecutive wet days (Figure A5.2) (Barredo, 2007; Kundzewicz et al., 2005). For instance, in western and eastern Europe, regions where major European river basins are located, three of their most destructive floods occurred in summer caused by such weather conditions (Kundzewicz et al., 2005).

However, there are also some differences between the indicators. For example, for some regions/phases, floods events are not more frequent, but they are more damaging; this is the case in winter in western Europe during NAO⁺. However, we note that this sub-region also shows more intense extreme precipitation in winter during NAO⁺, which could result in larger floods and damages, even though the frequency of floods may not increase. Flood frequency can only partly explain anomalies in flood damage, and other drivers such as changes in exposure, vulnerability and intensity of extreme may also play a significant role. In addition, in some areas extreme rainfall is not more frequent, but more intense, as is the case in Scandinavian countries during NAO⁻ in summer. Additionally, some of the significant anomalies in Flood Damage may be influenced by a few exceptionally high damage events. For example, anomalies in Flood Damage during summer in southern Europe were heavily influenced by one single event in Italy in 2002, with an estimated US$ 5.5 bn in damages (35% of the total summer Flood Damage for the southern sub-region). Moreover, some high anomalies in Flood Occurrence may be related to other hydrometereological variables than IER and OER, such as snow melt and storm surge, which needs further study (Hall et al., 2014; Muis et al., 2016).

2.4.2 Comparison to previous research

We provide a detailed comparison between our results and those of past studies in Europe in A8 of the appendix. In brief, the following points can be summarised: (*i*) occurrence of winter extreme rainfall in southern regions is greatly related to NAO⁻, while NAO⁺ is linked to more frequent and intense extreme precipitation over northeastern areas, which agrees with previous studies e.g. (Lopez-Bustins et al., 2008; Quadrelli, Pavan, & Molteni, 2001; Rodó

et al., 1997; Uvo, 2003); (*ii*) ENSO's influence on the European climate is not clear, and changes in the intensity and frequency of extreme precipitation are minor (Brönnimann, 2007; Frias et al., 2010; Rocha, 1999; Sun et al., 2015); (*iii*) in summer, we observe that NAO exerts great influence on rainfall patterns, but with an opposite sign to that observed in winter (Barnston & Livezey, 1987; Casanueva et al., 2014; Lorenzo et al., 2008); (*iv*) in autumn, extreme precipitations are less frequent and intense during NAO$^+$, which are associated with drier conditions over southern and eastern regions, as highlighted by others (Casanueva et al., 2014).

Another aspect that affects susceptibly to climate-related disasters is the level of flood protection. According to a modelling study (Scussolini et al., 2015), large portions of southern and eastern Europe are protected against floods up to about a 20-year return period. Consequently, many locations are not well adapted to deal with extreme flood events. This has been the case in Italy and Spain, which have previously suffered major flash floods and river flood disasters (Barredo, 2007). The high levels of flood protection in northern Europe (Scussolini et al., 2015), may reduce the influence of climate variability on Flood Occurrence and Flood Damage.

Socioeconomic development also plays a role in flood risk, and may alter the relationship between hydrometeorological extremes and resulting losses (Jongman et al., 2015). Only few studies analyzed changes in vulnerability, flood damage and risk due to the lack of reliable and long flood damage data (Merz et al., 2012). However, some studies found that changes in exposure and socioeconomic development are a key drivers of increasing flood losses in Europe (Barredo, 2009; Llasat et al., 2008). Others have suggested that increased flood damage is also associated with increased precipitation (Pielke Jr & Downton, 2000). Therefore, understanding trends in flood frequency and damage can only be partially explained by estimating meteorological changes.

2.4.3 Applications, limitations and recommendations

The indices of climate variability assessed in this study can be forecast with varying levels of skill and lead-times. Hindcasts of winter-mean NAO show that there is skill for predicting this index with lead-times of at least a month (Scaife et al., 2014; Smith et al., 2016). EA summer and autumn anomalies can be properly forecast with a lead-time of 1 to 2 months (Iglesias et al., 2014). ENSO forecasting is more developed, and most prediction systems have some skill to detect events with lead-times of 12–14 months (Gonzalez & Goddard, 2016). In those regions of Europe where ENSO, NAO and EA show strong relationships with precipitation and flood indicators, seasonal risk outlooks could potentially

be developed based on predicted values of the indices of climate variability. Such outlooks could provide information on whether flood impacts in upcoming seasons are likely to be higher or lower than average, which could be useful for flood disaster preparedness. For example, the European Union's Solidarity Fund, holding 500 million Euros per year to help member states finance disaster losses, is greatly affected by large-scale correlations in flood losses (Jongman et al., 2014). Taking into account some of the long term climate variability anomalies in the design and budgetary planning of international finance mechanisms could reduce the chance of such a fund facing unexpected pay-outs across large regions in Europe, and reduce the chance of fund depletion.

The primary limitation of this investigation is that we analyse the impact of ENSO, NAO and EA separately. Globally, ENSO is the main driver of interannual climate variability, but interactions between ENSO and both NAO and EA have been identified in several studies e.g. (Greatbatch, 2004; Iglesias et al., 2014; Rodríguez-Fonseca et al., 2016). Future work should assess the joint impacts of ENSO, NAO and EA on floods. Future work would also benefit from using different methods to classify the different phases of climate variability, and examining time lags between the indices of climate variability on the flood indicators. For instance, ENSO's impact on climate may vary throughout its developing, mature or decaying phases (Huang et al., 2012; Ronghui & Yifang, 1989; Wang & Gu, 2016; Zhang, Sumi, & Kimoto, 1999). Moreover, some of the significant results may had occurred by random chance on season/phases of the indices of climate variability marked with an asterisk on Figures 2.2 and 2.3, where results would improve with a local analysis. Furthermore, global disaster databases, such as the one used in this study, are also know to face major limitations, such as reporting errors (Kron et al., 2012). Lastly, extreme rainfall frequency and intensity, and large-scale climate variability can only partly explain anomalies in flood risk (Barredo, 2009; Pielke Jr & Downton, 2000). Other aspects such as changes in exposure and vulnerability (Jongman et al., 2015; Scussolini et al., 2015) were not included in this study.

2.5 Conclusions

In this paper, we examined relationships between the different phases of ENSO, NAO and EA, and differences and anomalies in the OER, IER, Flood Occurrence, and Flood Damage. We show that:

- Positive and negative phases of NAO and EA are associated with more frequent extreme rainfall over large areas of Europe. The NAO^+ and EA^+ phases are associated with less frequent extreme rainfall, especially during summer and autumn.

- Positive and negative phases of NAO and EA are associated with significant differences in the intensity of extreme rainfall compared to the neutral phase.
- The effect of ENSO on the intensity and frequency of extreme rainfall in Europe is much smaller than the influence of NAO or EA.
- At the aggregated pan-European scale, NAO, EA and ENSO show significant relationships with Flood Occurrence and Flood Damage in one or more phases and/or season. In summer during NAO$^+$, these anomalies are on average 170% and 136% higher.
- Anomalies in Flood Damage in spring and summer are on average 110% lower in northern Europe during NAO$^+$, EA$^+$ and ENSO$^+$.
- Flood Damage and Flood Occurrence are strongly related with climate variability, especially in southern and eastern Europe.

Therefore, when investigating at the Pan-European scale, all three indices of climate variability should be taken into account. Future work should focus on their mutual relations to flood risk. Consequently, the inclusion of seasonal forecasts of the indices of climate variability could be used to develop flood risk outlooks for the continent.

Chapter 4

Translating large-scale climate variability into crop production forecast in Europe

Abstract

Studies show that climate variability drives interannual changes in meteorological variables in Europe, which directly or indirectly impacts crop production. However, there is no climate-based decision model that uses indices of atmospheric oscillation to predict agricultural production risks in Europe on multiple time-scales during the growing season. We used Fast-and-Frugal trees to predict sugar beet production, applying five large-scale indices of atmospheric oscillation: El Niño Southern Oscillation, North Atlantic Oscillation, Scandinavian Pattern, East Atlantic Pattern, and East Atlantic/West Russian pattern. We found that Fast-and-Frugal trees predicted high/low sugar beet production events in 77% of the investigated regions, corresponding to 81% of total European sugar beet production. For nearly half of these regions, high/low production could be predicted six or five months before the start of the sugar beet harvesting season, which represents approximately 44% of the mean annual sugar beet produced in all investigated areas. Providing early warning of crop production shortages/excess allows decision makers to prepare in advance. Therefore, the use of the indices of climate variability to forecast crop production is a promising tool to strengthen European agricultural climate resilience.

4.1 Introduction

By 2050, the global demand for agricultural goods is expected to grow sharply, driven by the projected demands from an expanding world population, dietary shifts, and increasing biofuel consumption (Godfray et al., 2010; Pingali, 2007; Ray et al., 2013). At the same time, there are several major obstacles to boosting crop yields, including a decrease in the area of arable land per person (FAO, 2000), and variability in global climate. Creating a resilient agricultural system requires the incorporation of preparedness measures against weather-related events that can trigger disruptive risks such as droughts.

The use of climate information with long lead times, such as the seasonal predictions of the El Niño Southern Oscillation (ENSO), has allowed farmers to anticipate risks and to improve their management in several parts of the world (Bussay et al., 2015; Haigh et al., 2015; Iizumi, Luo, et al., 2014; Meinke & Stone, 2005; Motha & Baier, 2005; Nnaji, 2001). ENSO influences global agriculture in several ways, including through changes in hydrometeorological extremes (Casanueva et al., 2014; Sun et al., 2015; UNMGCY, 2017; Veldkamp et al., 2015;Ward et al., 2010;Ward et al., 2014) and climate extremes (Barlow, Nigam, & Berbery, 2001; Dilley & Heyman, 1995; Donat et al., 2014; Trenberth & Fasullo, 2012), which directly or indirectly impact crop yield, production and prices (Ferreyra et al., 2001; Iizumi, Luo, et al., 2014; Ray et al., 2015; Rowhani et al., 2011). However, ENSO only slightly modulates the European climate (Brönnimann, 2007; Guimarães Nobre et al., 2017), where the interannual anomalies in common atmospheric variables such as temperature and precipitation are driven mostly by other atmospheric oscillations (Casanueva et al., 2014). For instance, the North Atlantic Oscillation (NAO), the East Atlantic/West Russian pattern (EA/WR) and the East Atlantic Pattern (EA) are known to be related with precipitation patterns in Europe, especially in the Iberian Peninsula (Casanueva et al., 2014; Lopez-Bustins et al., 2008; Mariotti et al., 2002; Markovic & Koch, 2014; Rios-Cornejo et al., 2015; Rodó et al., 1997; Struglia et al., 2004), and the Scandinavian Pattern (SCA) influences rainfall in northeastern Europe (Bueh & Nakamura, 2007).

Whilst several studies have found connections between these indices of climate variability and common atmospheric variables, few have addressed the role of large-scale atmospheric oscillations on the variability of agricultural production, especially at the pan-European level. Initial studies (Cantelaube et al., 2004; Kettlewell et al., 2003) investigating the relationship between modes of climate variability and winter wheat anomalies concluded that NAO and EA patterns are strong indicators of yearly wheat deviations, and other studies found significant connection between major European crops and indices of large-scale climate

variability (Ceglar et al., 2017; Gimeno et al., 2002; Gouveia & Trigo, 2008; Lorenzo et al., 2013; Marta, Grifoni, & Mancini, 2011).

Agricultural producers make decisions regularly throughout the year, including tactical ones (actions to be taken within weeks or months) and strategic ones (actions to be taken within future seasons or years) (Haigh et al., 2015; Hollinger, 1991). Introducing climate forecasting into producer management depends on the availability of relevant information during the decision-making process, which requires an understanding of the relationship between European climate variability and crop production at several lead times (LD) (Calanca et al., 2011; Easterling & Mjelde, 1987; Haigh et al., 2015; Mase & Prokopy, 2014). To the best of our knowledge, there is no climate-based decision model that uses indices of atmospheric oscillation to predict agricultural production risks in Europe at different lead times.

In this paper, we develop such a model for multiple time-scales by exploring the relationship between large-scale indices of climate variability and anomalies in sugar beet production. Therefore, we aim at identifying those regions where a robust model can be established based on the indices of atmospheric oscillation investigated. For this, we applied a supervised Machine Learning decision tree-based algorithm (Phillips, Woike, & Gaissmaier, 2017), using predictors (in this case the ENSO, NAO, SCA, EA and EA/WR) recorded within the growing season to establish a prediction between high and low values of the predictands (sugar beet production). Based on the accuracy and predictive skill of the model, we also discuss how this information potentially improves the management of the agricultural sector by combining the findings with a seasonal forecasting system of crop production.

4.2 Methods

We use Fast-and-Frugal Trees (FFT) (Phillips et al., 2017) to predict impacts on agricultural production applying five large-scale indices of climate variability: ENSO, NAO, SCA, EA and EA/WR. The FFT models identify which indices of climate variability are capable of classifying production in given years into high or low production classes. From a database of historical sugar beet production of the European statistical office (EUROSTAT), we derived a yearly agricultural production indicator from 1975-2013, namely high/low production based on observed anomalies. For the same period, we obtained 3-month average values for the indices of climate variability from January to March, February to April, March to May, April to June, May to July and June to August, further referred to as LD6, LD5, LD4, LD3, LD2 and LD1, respectively. An overview of the methodological framework is displayed in Figure 4.1. The methods and datasets are described in detail in the following subsections.
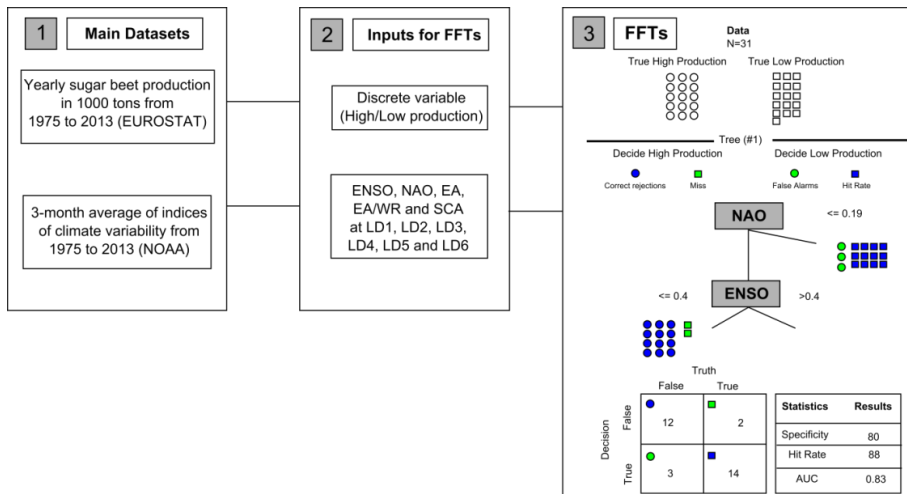
Figure 4.1 Flowchart representing the methodological framework applied in this study, handled in three steps: (1) collection of two main datasets; (2) extraction of five climate indicators at six lead times, and a discrete variable based on sugar beet climatological anomalies; and (3) example of an FFT output model containing standard classification statistics for a specific NUTS2 region and LD3.

4.2.1 Indices of climate variability

In this study, we represent climate variability using a 3-month average of the ENSO, NAO, EA, EA/WR and SCA indices from the National Oceanic and Atmospheric Administration Climate Prediction Center (http://www.cpc.ncep.noaa.gov). We extracted 3-month average values from 1975-2013, corresponding to the months of January to March, February to April, March to May, April to June, May to July and June to August. These values represent six different LD before the start of the sugar beet harvesting season (September) in Europe (Sacks, Deryng, & Foley, 2010). For instance indices of climate variability at LD6 represent a 3-month average between January to March, therefore six months before the start of the sugar beet harvesting season (September).

We used the standardized Southern Oscillation Index (SOI) from 1951-2016, calculated from observed sea level pressure differences between Tahiti and Darwin (Australia), as a continuous measure of ENSO strength(NOAA, 2005). The time series of the four Northern Hemisphere teleconnection patterns from 1950-2016 represent monthly mean standardized 500-mb height anomalies at 20°N-90°N (Barnston & Livezey, 1987). The NAO is the main mode of low-frequency variability over the North Atlantic, and consists of a north-south

dipole of anomaly in surface pressure between Greenland and the central latitudes of the North Atlantic between 35°N and 40°N (Barnston & Livezey, 1987). The EA pattern is the second prominent mode of low-frequency variability over the North Atlantic, consisting of a north-south dipole of anomaly centers that extends across the entire region from the East to the West. The EA/WR represents four main anomalies, centred over Europe and northern China, central North Atlantic and north of the Caspian Sea, while the SCA shows anomalies mainly in Scandinavia and western Russia (Barnston & Livezey, 1987). The Euro-Atlantic region is mainly dominated by these four Northern Hemisphere teleconnections (Casanueva et al., 2014; Ceglar et al., 2017).

4.2.2 Index of agricultural impact

We obtained annual historical records of sugar beet production (in 1000 ton of fresh weight) from 1975 to 2013 for 232 NUTS2 from EUROSTAT. We examined sugar beet records for three major reasons: the European Union (EU) is the world's leading producer of sugar beet (EUROSTAT, 2016); sugar beet production is wide-spread within the EU territory; and generally, this crop is not extensively irrigated, thus having a strong dependency on rainfall (EUROSTAT, 2010). We performed the analysis on historical records of sugar beet production instead of sugar beet yield (tons/hectare) due to the large unavailability of datasets of the latter in the vast majority of NUTS2 regions.

Years without sugar beet production records (M_{N2}) at the NUTS2 level were filled according to the following method. First, we compared sugar beet production data registered at the national level (P_N) by EUROSTAT (if available) with the sum registered at the NUTS2 level (P_{N2}) for a given country (c) and year (t).

$$M_{N2,t,c} = P_{N,t,c} - \sum P_{N2,t,c} \qquad \qquad \text{Equation 4.1}$$

If there was a positive difference between both datasets ($P_{N,t,c} > \sum P_{N2,t,c}$) and more than one NUTS2 region without a record, the missing production record at the NUTS2 (M_{PN2}) region was filled proportionally with respect to the sum of its sugar beet harvesting area (HA_{N2}) :

$$M_{PN2,t,c} = M_{N2,t,c} \Big/ \frac{100}{\sum HA_{N2}} \qquad \qquad \text{Equation 4.2}$$

We assumed a positive and direct relationship between harvesting area and production: the larger the harvesting area, the higher the production, even

though other factors, such as agricultural management, could affect production. Estimates of sugar beet harvesting areas are obtained from MIRCA 2000 and described in Sack et al. 2010 (Sacks et al., 2010) (available in the appendix Figure C1). In case of missing records in the NUTS2 region but no difference in the overall production ($P_{N,t,c} = \sum P_{N2,t}$), we assigned $M_{PN2,t,c} = 0$. Last, in the case of a negative difference ($P_{N,t,c} < \sum P_{N2,t}$), the missing sugar beet production remained unaltered.

For each NUTS2 region, we calculated sugar beet production anomalies (observed value minus the multiyear mean) after removal of the linear trend (if the p-value is less than or equal to 0.1). We classified below zero anomalies as "low production", and above zero anomalies as "high production", creating a discrete agricultural impact indicator. Only NUTS2 regions with time series longer than 20 years were further investigated (NUTS2 areas that fit the criteria, and their respective summary of statistics are displayed in appendix Figure C2 and Table C3, consecutively). In total, we were able to fit a FFT model in 207 NUTS2 regions.

4.2.3 Statistical approach: Fast-and-Frugal Decision Tree (FFT)

In this study, we used FFT to predict sugar beet production as a function of indices of climate variability. In heuristic decision-making, FFT are simple decision trees for classifying cases (e.g. sugar beet production) into one of two classes (e.g. low production vs. high production) based on a particular predictor, or *cue*. FFT models establish simple rules for making decisions based on fast-and-frugal heuristics approach (Gigerenzer, Czerlinski, & Martignon, 1999; Raab & Gigerenzer, 2015), and offer simple and transparent search rules for practical decision problems (Phillips et al., 2017) as a competitive alternative for more complex Machine Learning and regression methods (Guimarães Nobre et al., 2019).

As displayed in Figure 4.1 step 3, the structure of an FFT determines the exact number, sequence and threshold of predictors that are applied to reach a final classification (Gigerenzer et al., 1999; Gigerenzer & Todd, 1999). The FFTs algorithm applied in this study is limited to maximum five cues (Phillips et al., 2017). Consequently, a five-cue decision tree is based on the best five performing indices of climate variability. However, FFTs can be based on 1 to 5 cues since it uses non-compensatory decision rules, which apply a limited subset of all predictors for establishing a binary classification (Guimarães Nobre et al., 2019). Non-compensatory algorithms ignore information, once a decision is completed, and therefore, no additional predictors can change such decision (Phillips et al., 2017). This aspect is often perceived to have both practical and

statistical advantages over compensatory algorithms, such as regression models (Guimarães Nobre et al., 2019). First, because by only using a partial subset of predictors, FFTs are relatively simple, and can perform better in predicting new data, thus they tend to avoid overfitting (Phillips et al., 2017). Second, FFT algorithms uses search rules that specify where to look for information and when to end search, which can guide decision makers in gathering information and assist in supporting decision tasks (Phillips et al., 2017; Raab & Gigerenzer, 2015).

The FFT algorithm is designed to learn from and make predictions on data. FFTs are fitted to a training dataset, which is used for learning the model, and deriving its parameter. In summary, the FFT's algorithm is constructed as instructed: a) select predictors; b) determine a decision threshold for each predictor; c) determine the order of predictors; and d) determine the exit for each predictor (Guimarães Nobre et al., 2019; Phillips et al., 2017). By definition, FFTs must have either a negative or a positive exit (or both in the case of the final node of a decision tree) (Phillips et al., 2017).

The accuracy of the FFT is measured by the Balanced Accuracy (BACC) Index, which is calculated based on the amount of correct decisions (Table 4.1) obtained from the ifan decision algorithm, which is described in detail in previous research (Phillips et al., 2017). In summary, the ifan decision algorithm tests several different thresholds of the investigated indices of climate variability to find one that maximizes the predictor's accuracy. Consequently, once the set of multiple FFTs has been created, ifan selects the decision tree with the highest balanced accuracy.

In order to avoid overfitting, we cross-validated the FFTs using the train-test split method. For this, we partitioned 70% of all data for training the FFT models, and the other 30% for testing the models. We chose this validation method to assess the FFT potential success (if applied in a practical case), and its hindcast skill in predicting past sugar beet production events. In addition, this method takes less computation power than other cross validation techniques such as k-fold. A more detailed explanation of the train-test split method is available in the appendix C4. For each FFT, we assessed the skill of the model to predict classes of "low production" and "high production" using the Area Under the Curve (AUC) index (Metz, 1978). AUC measures how well the FFT can distinguish binary classes (low/high) (Zweig & Campbell, 1993), displayed in appendix Figure C5. The AUC index was calculated using the trapezoidal rule, and values can vary between 0 and 1, where a perfect prediction has an AUC=1.0, and predictions that are randomly drawn are presumed to provide an AUC=0.5 (Hamill & Juras, 2006). We tested the statistical significance of the AUC

by bootstrapping the values of the high and low sugar beet production events at the NUTS2 level using 1000 iterations (more details in the appendix C6). Field significance of the results was assessed using the binomial distribution (Livezey & Chen, 1983).

For NUTS2 regions with an AUC>0.7, we display standard classification statistics such as Hit Rate (HR), False Alarm Rate (FAR), Correct Rejections Rate (CR), Miss Rate (MS), Positive Predictive Value (PPV) and Negative Predictive Value (NPV). Their definition and formula are given in Table 4.1. We obtained FFT for each particular lead time and NUTS2 region through the following steps:

1. Calculating the pruning parameter of the model, meaning that we assessed the ideal size of decision trees by cross-validating the FFT models using train-test split method (see appendix C4);
2. Selecting the pruning parameter and decision tree that maximizes the BACC index of the tested model;
3. Calculating the AUC index for each best performing decision tree;
4. Assessing the statistical significance of the AUC obtained in step 3 by bootstrapping and calculating field significance (see appendix C6);
5. Analysing the performance of the significant FFT model by calculating standard classification statistics (Table 4.1).

After following such steps, we built a new FFT after recombining the two samples (training and testing) and adopting the pruning parameter that was found to maximize the BACC index. Hence, this procedure enables us to find the set of predictors which are most important for each NUTS2 region and lead time (Figure 4.1 step 3). Since we aim at identifying regions where a robust model can be established based on the indices of atmospheric oscillation, we focus our results in regions with AUC>0.7.

4.3 Results

4.3.1 General performance of the FFT models

In this section, we analyse the performance of the FFT in predicting high/low sugar beet production events. The best performing indices of climate variability for each NUTS2 (Nomenclature of territorial units for statistics) region are shown in the appendix (Table C7.1-C7.6 and Figure C8).

In total, the cross-validated FFT models distinguished between sugar beet high/low production events in 160 out of 207 NUTS2 regions, covering nearly 77% of investigated areas (Figure 4.2G); 81% of the mean annual sugar beet production is harvested in these regions (Figure 4.3). An overview of the mean sugar beet production in all NUTS2 regions investigated is available in Figure C9.

In some locations, the FFT models have skill to predict high/low production for more than one LD, and already at LD6 (March) before the start of the sugar beet harvesting season.

Table 4.1 Definition of Standard Classification Statistics

Standard Classification Statistics	Definition	Abbreviation	Formula
Hit Rate	Probability of a "True Low Production" (TL) over the total samples of "Low production" (LP)	HR	$\left(\frac{TL}{LP}\right) \times 100$
Correct Rejections Rate	Probability of a "True High Production" (TH) over the total samples of "High Production" (HP)	CR	$\left(\frac{TH}{HP}\right) \times 100$
False Alarm Rate	Probability of a false "Low Production"	FAR	1 - CR
Miss Rate	Probability of a false "High Production"	MS	1 - HR
Positive Predictive Value	Probability of a "True Low Production" over all "Low Production"	PPV	$\dfrac{HR}{HR + FAR}$
Negative Predictive Value	Probability of a "True High Production" over all "High Production"	NPV	$\dfrac{CR}{CR + MS}$
Balanced Accuracy	Average of Hit Rate and Correct Rejection	BACC	$HR \times 0,5 + CR \times 0,5$
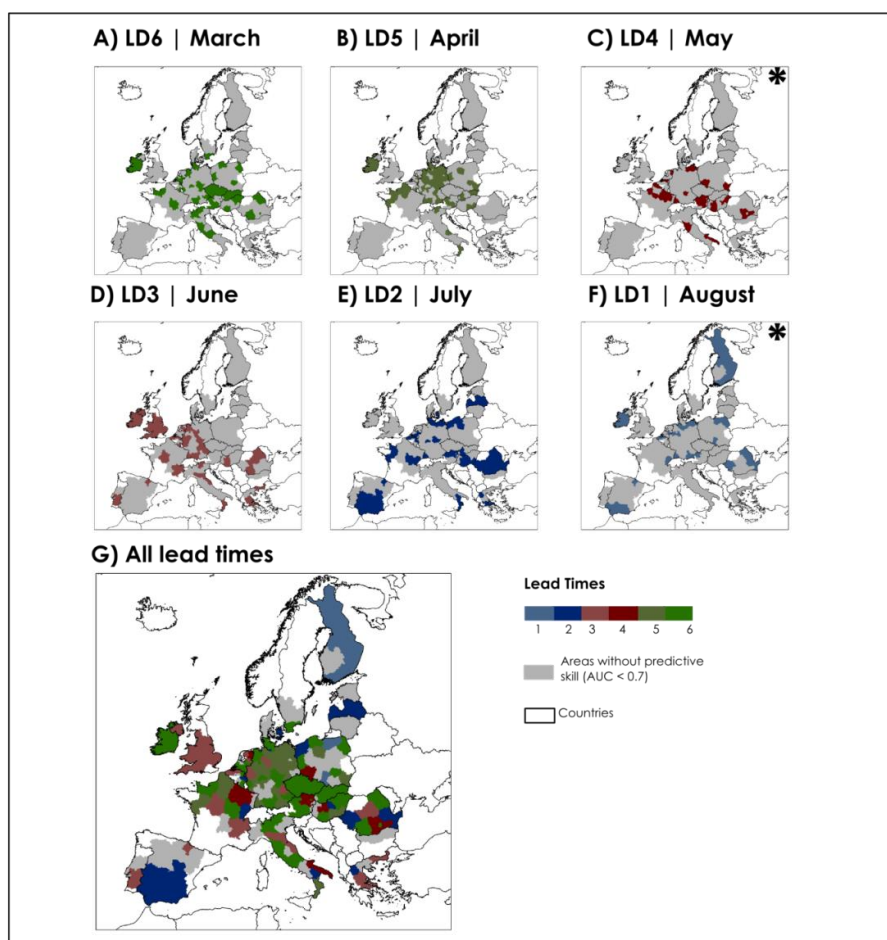
Figure 4.2 Regions where the FFT models have predictive skill (Area Under the Curve index or AUC>0.7): a) six months (March) to f) one month (August) before the beginning of the harvesting season. In g) the maps were overlaid in descending order from longest to shortest lead time. Regions without predictive skill (AUC<0.7) are shown in grey. Field significance of the results was assessed using the binomial distribution and found to be highly significant (P<0.001). Lead times that were found to be significant only due to bootstrapping (P<0.1) are indicated with an asterisk.

4.3.2 Predicting sugar beet high/low production events

In March and April, six (LD6) and five (LD5) months before sugar beet harvesting in Europe respectively, we found that the FFT models have predictive skill in a total of 79 out of 207 NUTS2 regions, with an Area Under the Curve (AUC) index ranging from 0.70 to 1.00 (Appendix Table C7.1 and C7.2). Western and eastern Europe have the highest number of NUTS2 regions with AUC>0.7. In 56% and 55% of the NUTS2 regions located in western and eastern Europe respectively, significant predictions (P<0. 1) are already observed in these lead times. For

LD6 and LD5, the overall balanced accuracy (BACC), which represents the skill of the FFT in correctly predicting high/low production events, is on average, 79% for both lead times. Approximately 44% of the mean annual sugar beet is produced in these 79 NUTS2 regions. The HR, thus the probability of a predicting a true low sugar beet production event in these regions is, on average, 74% and 84% at LD6 and LD5, respectively.
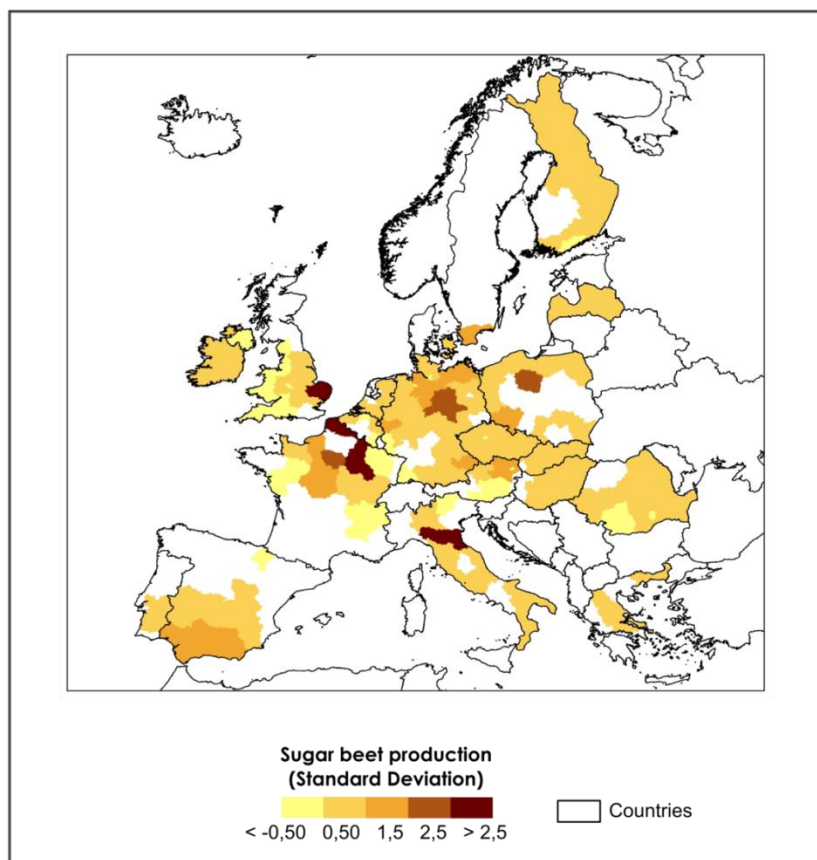
Figure 4.3 Standard deviation of the mean sugar beet production in NUTS2 regions where the FFT models have predictive skill (AUC>0.7) in all lead times.

The spatial distribution of the HR, FAR and PPV are shown in Figure 4.4. The HR values are especially high (above 90%) in central Europe, particularly over large areas in Germany. On average, the probability of predicting a false low sugar beet production event (FAR) is 17% and 26% at LD6 and LD5, respectively. The probability of a true low production (hereafter referred to as PPV) over all low production events predictions represents the trade-off between HR and FAR.

PPV values are, on average, 90% and 83% at LD6 and LD5, respectively. In Figure 4.5, the results are presented for predicting high sugar beet production events. We found that the probability of predicting a true high sugar beet production event in these regions (defined as CR) is, on average, 83% and 74% at LD6 and LD5 respectively (Figure 4.5A and 4.5B). The probability of predicting a false high sugar beet production event (defined as MS) is, on average, 26% and 16% at LD6 and LD5, respectively. The average NPV, which represents the probability of a true high production (CR) over all high production events predictions, is 74% and 81% at LD6 and LD5 respectively. In the appendix Figure C8, we display the respective large-scale indices of climate variability that were used by the FFT models as a predictor of high/low production events; results are shown for areas with significant predictive skill (AUC>0.7 and P<0. 1). In March and April, during the early growing stages of sowing and emergence, sugar beet is sensitive to water deficits and frost, and winter and early spring weather conditions in Europe are strongly associated with EAWR, NAO and EA (Casanueva et al., 2014; Ceglar et al., 2017; Guimarães Nobre et al., 2017; Hurrell & Deser, 2010; Ionita, 2014). Relationships between sugar beet production and mean EAWR, EA and NAO from January to March, and mean EA and NAO from February to April were found in this study, and also by others when assessing the relationship between these atmospheric oscillations and other crop types, productivity and vegetation dynamics (Ceglar et al., 2017; Gouveia et al., 2008; Heino et al., 2018; Kim & Mccarl, 2005). In addition, we observed that in most of the regions, multiple indices of atmospheric oscillations were used simultaneously as a predictor of sugar beet production instead of a single index (appendix Figure C8 and Figure C10). We observed that winter and early spring NAO influences summer crop production in large areas in Europe, especially in Germany (LD5), as previously found by others (Ceglar et al., 2017; Gonsamo & Chen, 2015), where positive NAO in January and February drives more intense precipitation in northern and north western Europe and the opposite in the south of the continent (Casanueva et al., 2014; Guimarães Nobre et al., 2017), which might affect the early growing season. However, we neither find a north-south dipole impact of the NAO at these lead times, as often is observed for rainfall, nor a large influence of NAO in southern Europe, as found by others (Gimeno et al., 2002; Kim & Mccarl, 2005). Other important predictors of sugar beet high/low production events are EA and EA/WR patterns, especially in regions in western and eastern Europe. Since precipitation and temperature variability in Europe are more strongly modulated by winter and spring oscillation regimes, the relevance of winter and spring atmospheric oscillations may be twofold: (a) winters and early spring modes of climate variability provide soil moisture for crop development in summer, as also suggested by others (Gonsamo & Chen, 2015; Kettlewell et al.,

2006; Wang, Dolman, & Alessandri, 2011); (b) winter and spring weather conditions affect sowing and early growing stage, as found by previous research (Ceglar et al., 2017; Petkeviciene et al., 2009).

In May and June, four and three months before the start of the sugar beet harvesting season, the FFT models have predictive skill in a total of 92 out of 207 NUTS2 regions, as displayed in Figure 4.2C and 4.2D. Within the investigated areas, approximately 47% of the mean annual sugar beet is produced in these 92 NUTS2 regions. Comparing all lead times investigated, LD3 was found to be the one with the most regions with predictive skill (74 out of 207). In May and June, western and northern Europe have the highest number of NUTS2 regions with AUC>0.7. In 54% and 67% of the NUTS2 located in western and northern Europe respectively, significant predictions (P<0. 1) are found in these lead times. In addition to LD6 and LD5, the FFT models extend the predictive skill to some western and southern European regions and the United Kingdom. The AUC index ranges from 0.70 to 1.00 (appendix Table SC7.3 and C7.4). On average, the mean BACC is 78% (LD4) and 83% (LD3). In these areas, HR, PPV and FAR are, on average, 78%, 86% and 22% (LD4) and 89%, 82% and 27% (LD3) respectively. The CR and NPV are, on average, 78% and 74% (LD4), and 72% and 88% (LD3) respectively. The mean MS at LD4 and LD3 is 22% and 11% respectively (Fig. 4.5c and 4.5d). In June, sugar beet root has reached its vegetative growth, and beet leaves are subjected to both heat and water stress (Clarke et al. 1993). FFT models primarily used EA/WR and ENSO averages from spring and late spring (Figure C8 LD3) as the main predictors of sugar beet production in western and eastern Europe. These indices have also been found to have links with maize grain and wheat yield in other studies (Ceglar et al. 2017; Iizumi, Luo, et al. 2014). Spring/late spring weather in Europe are associated with a range of atmospheric oscillations including EA/WR and EA (Gao et al. 2017), and less influenced by NAO (Casanueva et al. 2014). The EA/WR pattern influences mainly western and eastern Europe, where a positive (negative) EA/WR phase is related to high temperature anomalies (Ceglar et al. 2017) and drier (wetter) conditions. ENSO was previously found to have significant associations with changes in precipitation in spring, especially over western and northern Europe (Shaman 2014;Casanueva et al. 2014). However, in Spain, where we would expect a larger spatial link between SCA, EA and ENSO patterns on precipitation (Casanueva et al. 2014) and consequently on crop production (Ceglar et al. 2017), the effect of these climate patterns may be weaker than elsewhere, probably due to common irrigation practices in some areas, especially in southern and north western Spain (EUROSTAT 2010; Wriedt et al. 2008; Wriedt et al. 2009).

In July and August, the FFT models predict sugar beet high/low production events in 62 of the 207 NUTS2 regions (Figure 4.2E and 4.2F), with an AUC index ranging from 0.70 to 1.00 (appendix Table C7.5 and C7.6). In July and August, western and eastern Europe have the highest number of NUTS2 regions with AUC > 0.7. In 35% and 41% of the NUTS2 located in western and eastern Europe respectively, significant predictions (P<0. 1) are found in LD2 and LD1. In addition to models at LD6 to LD3, the FFT models extend the predictive skill to several regions in Europe, especially in large areas of Spain and Finland. On average, the mean BACC for LD2 and LD1 is 80%. Within the investigated areas, approximately 22% of the mean annual sugar beet is produced in these 62 NUTS2 regions. The average HR, FAR and PPV is 81%, 22% and 82% for LD2, and 83%, 22% and 84% for LD1 (Figure 4.4E and 4.4F). We found that the CR, MS and NPV is, on average, 78%, 19% and 83% for LD2, and 78%, 16% and 81% for LD1. (Figure 4.5E and 4.5F). In July and August, when the sugar beet has reached its late development stage, reduced water availability has a small impact on the yield. EA/WR from May to July in addition to EA and NAO averages in June to August are most used as sugar beet production predictors in large areas of Europe. In summer, the EA/WR pattern was found in previous research (Ceglar et al., 2017) to have strong links with positive temperature anomalies and below-average rainfall in western and south eastern Europe, which is beneficial for harvesting. However, our results also suggest that multiple indices of atmospheric oscillation show links with sugar beet production in scattered areas in Europe, especially at LD2 (Figure C8). In addition, previous investigations found that the precipitation, temperature, vegetation dynamics and maize yield in Europe have links with these atmospheric oscillations in summer (Casanueva et al., 2014; Ceglar et al., 2017; Gouveia et al., 2008). Large-scale atmospheric oscillation indices may have less predictive skill for production in early summer than winter and spring for two reasons: (a) due to the higher importance of regional-to-local atmospheric phenomena during summer, also highlighted by others (Ceglar et al., 2017). This means that sugar beet production estimates might be more efficiently captured by the regional crop model forced by observed surface climate variables locally; and (b) in July and August, when the sugar beet has reached its late development stage, reduced water availability has a small impact on the crop (FAO, 2015).
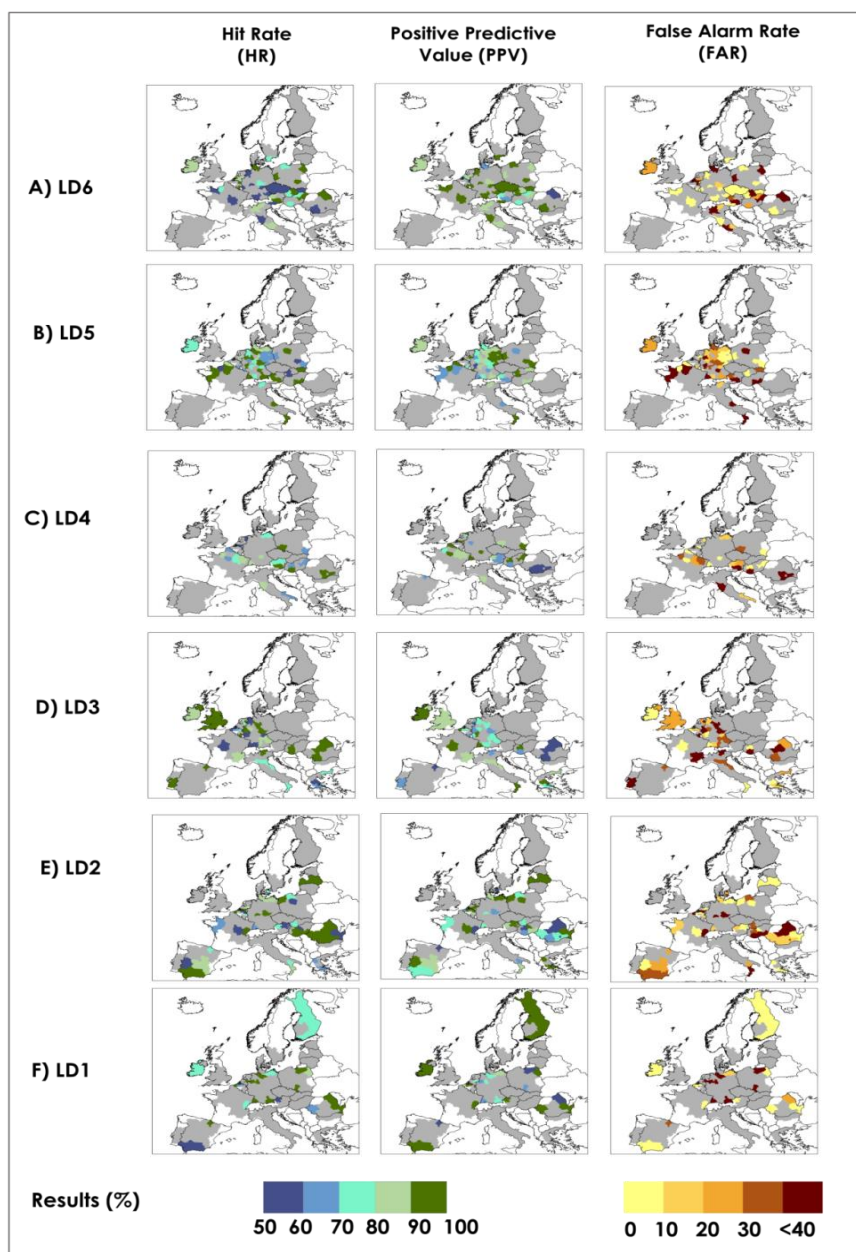
Figure 4.4 Performance metrics for predicting low production sugar beet events for areas with AUC>0.7 at six lead times. Hit Rate (HR) is the probability of low production occurrences that were correctly predicted; Positive Predictive Value (PPV) index represents the probability of FFT to detect true low production sugar beet events over all low production (including False Alarms); False Alarm Rate (FAR) is the probability of a false low production occurrence. Regions without predictive skill (AUC<0.7) are shown in grey. The FAR is cut off at <40% because in more than 90% of the NUTS2 regions the results are below this threshold.
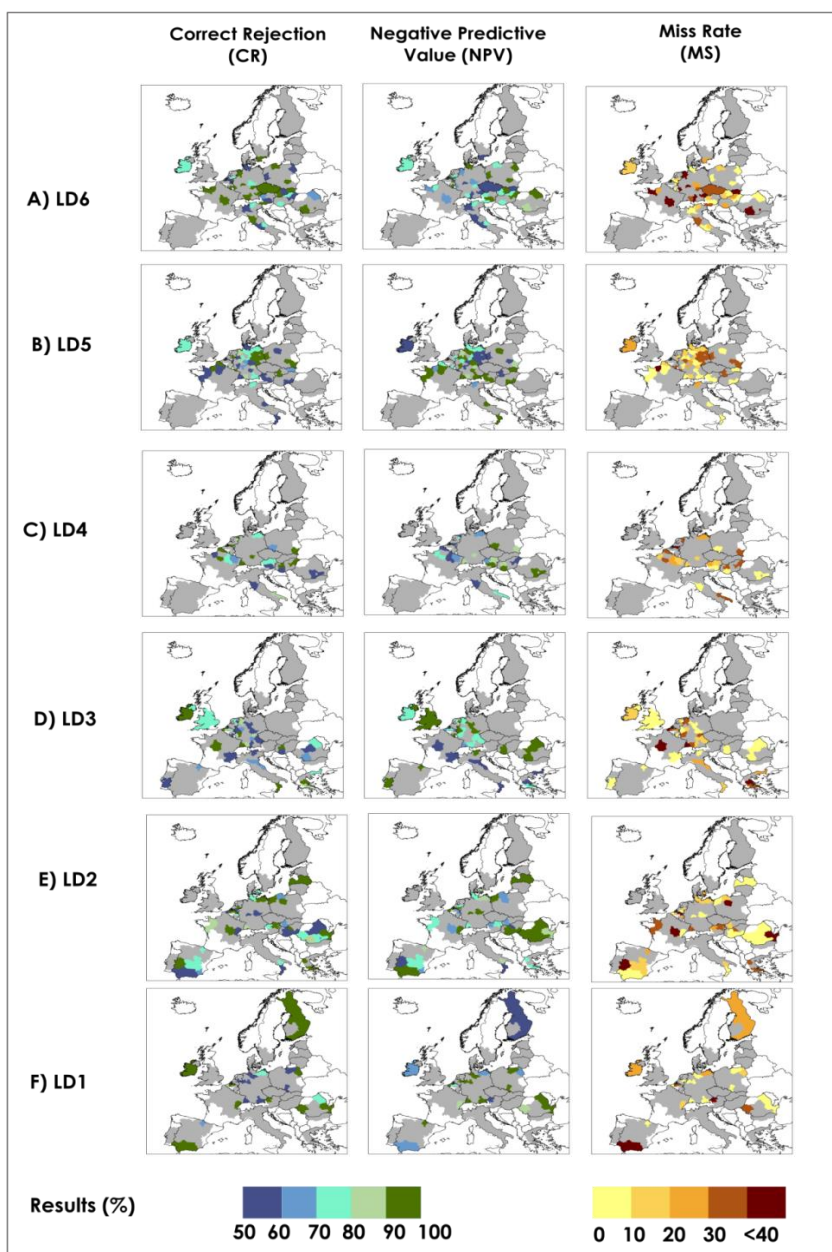
Figure 4.5 Display of standard classification statistics for predicting high production sugar beet events for areas with AUC>0.7 at six lead times. Correct Rejection Rate (CR) shows the probability of high production occurrences that were correctly predicted; Negative Predictive Value (NPV) index represents the probability of the FFT detecting a true high production sugar beet event over all high production (including Misses); Miss Rate (MS) is the probability of a false high production occurrence. Regions without predictive skill (AUC<0.7) are shown in grey. The MS is a cut off at <40% because in more than 90% of the NUTS2 regions the results are below this threshold.

4.4 Discussion and Conclusions

In this section we discuss how our findings could be used to support agricultural management and decision-making processes in Europe, followed by recommendations, limitations and conclusions of the study.

Currently, the Joint Research Centre (JRC) MARS crop yield forecasting system (M-CYFS) forecasts national sugar beet yields for the current growing season based on a scenario technique and trend analysis (Baruth et al., 2008), which substantially differs from the method applied in this study, which also targets production. The M-CYFS is a decision support system with the purpose of providing evidence-based information on the status of annual crops in the EU and neighbouring countries by monitoring crop growth and forecasting crop yields along the season (Bussay et al., 2015; Lecerf et al., 2018; van der Velde et al., 2019). It uses agro-meteorological indicators derived from observed meteorological data as well as crop growth models and remote sensing information, which are applied together to build a statistical yield forecast using best-fit criterion to explain a cause-effect relationship with historical yield statistics at national level. Sugar beet forecasts early in the season are purely based on observed trends, but could potentially gain predictive skill if indices of climate variability, such the ones investigated in this study, are integrated in M-CYFS based on the outcomes of this study. In general, agro-meteorological and remote sensing indicators start to demonstrate a certain reliability for the regression forecasts (r-squared value > 0.5 if de-trended data are used) from the end of June or beginning of July depending on the country. Furthermore, since large-scale indices of climate variability can be predicted with higher lead times than weather variables and related crop growth variables, the M-CYFS could further extend its lead time if predictions of the large-scale indices of climate variability were used from dynamic climate models (Ceglar et al., 2017).

Anomalies in temperature and precipitation driven by climate variability do not always explain crop production, and regions without predictive skill, may have been masked by a number of local agro-management activities. For instance, irrigation practices, which are observed in Spain and Bulgaria, may have lowered the negative impacts of unfavourable weather conditions and the skill of the FFT models in detecting high and low production. Overall, the decision-model performed more consistently in eastern and western Europe. These regions also have low shares of irrigated areas, which may have influenced the model performance (EUROSTAT, 2010). Additionally, in some regions, limitations in data availability on crop production were encountered during this investigation (described in the methods section), and this may have affected the extraction of the high/low sugar beet production indicator per NUTS2 region.

For instance, we disaggregated national crop production statistics data in several NUTS2 regions (available in appendix C3), and our downscaling method adds uncertainty to the model predictions. Therefore, the FFT models may not be performing satisfactorily in some regions for three reasons: (a) presence of irrigation practices, which may inhibit the impacts of unfavourable weather conditions; (b) lack of underlying physical relationship between sugar beet production and the investigated indices of climate variability; and (c) due to limitations in the sugar beet production downscaling method.

In Europe, the growing period of sugar beet is normally between 140 and 160 days (FAO, 2015), mostly in the northern half of Europe, where the climate is more suited to growing beet (European Comission, 2017). Sugar beet is planted in early spring and harvested in late September, before the cold season starts. In March, beet producers make strategic decisions regarding the amount of sowing for the year and planning tactical actions for the germination and early plant development stages, which comprise the most sensitive periods of the crop (FAO, 2015). Due to strict regulations of the EU sugar market, the 2007 Sugar Reform limited total EU production to 14.7 million tonnes of raw sugar until the marketing year 2016/2017 (European Comission, 2017). If climatic conditions indicate a probable "high production" scenario at this early stage, the EU could better plan "out-of-quota" measures, such as: exporting the excess of sugar beet production to the EU's annual World Trade Organisation quota, which is limited to 1.374 million tonnes; disposing excess on the EU market for industrial purposes; or counting against the following year's sugar "quota" (European Comission, 2017). In addition, each year the EU market must decide by March 16th for a first "preventive" withdrawal to allow producers to reduce their beet sowings. However, the quota management ended as of 30 September 2017. On the other hand, if climatic conditions show signs of shortage in production, tactical measures can be taken to increase supplies as follows: (1) better preparation or further investment in responsive irrigation schemes as sugar beet is particularly sensitive to water deficits in early spring (Clarke et al., 1993; Romano et al., 2012); (2) taking measures to prevent freeze damage to crops such as active methods (e.g. adding heat and covering crops) and passive methods (e.g. proper scheduling of planting within the safe freeze-free period) as night frost in spring can damage sugar beet and delay seed germination (Pidgeon et al., 2001; Snyder & de Melo-Abreu, 2005); and (3) before planting, producers could decide to reduce their financial losses by purchasing appropriate crop insurance products against deviations from their long-term yields. Prior information about the spatial configuration of risk would support insurance companies to better allocate resources to comply with the EU solvency requirements, which demands that insurers have adequate

reserves for 99.5% of potential loss events (European Parliament and Council, 2009).

By June, sugar beet root has reached its vegetative growth, and its leaves are subjected to both heat and water stress (Clarke et al., 1993). Temperatures greater than 30°C greatly decrease sugar yields (FAO, 2015), and water stress is considered the major limitation to crop productivity and yield stability (Romano et al., 2012). In central and western Europe, drought stress can reduce sugar beet yields by 10-30% compared to the long-term average (Ober, 2001; Van Swaaij, Heijbroek, & Basting, 2001). Beet water requirements are moderate, and if low production is predicted, adequate water should be available to allow the sugar beet to develop a good root system for extracting water from the soil. Predictions of low or high production, mainly needed on a regional scale for industries and policy makers (Vandendriessche, 1995), supports the sugar industry in adapting normative plans for optimizing processing campaigns (Kenter, Hoffmann, & Märländer, 2006), such as factory operations concerning delivery schedules and storage capacity, transport logistics and export sales. Sugar beet production forecasts could also be a useful aid for marketing operations, where prices fluctuate based on the supply and demand of the product (Vandendriessche, 1995).

In August, when the sugar beet has reached its late development stage, reduced water availability has a small impact on the yield (FAO, 2015). Forecasts of low production could support sugar beet producers to better prepare against cold and wet days, which often lead to deterioration of harvesting conditions and increase the probability of fungal infections, increasing the risk of late harvesting in autumn (JRC MARS Bulletin, 2016). Moreover, forecasts of high production may indicate favourable conditions to the harvesting period, when certain levels of soil moisture and rain-free days are preferred (JRC MARS Bulletin, 2016).

Our study did not aim to produce quantitative prognostic information about crop production; instead, we focused on identifying those regions where a robust model can be established based on the indices of atmospheric oscillation investigated, and used as an early warning indicator for crop impacts. This is a primary step towards the adoption and use of climate-related forecasts in agricultural decision-making: if there were no climate variability influence on crop production, it is unlikely that agricultural stakeholders and markets would benefit from long lead time climate information. In addition, the observed indices of climate variability assessed in this study can be forecast with varying levels of skill and lead times. Skilful predictions of NAO have been extended to more than a year ahead (Ceglar et al., 2017; Dunstone et al., 2016). EA summer

and autumn anomalies can be properly hindcast with a lead time of 1 to 2 months (Guimarães Nobre et al., 2017; Iglesias et al., 2014), while ENSO forecasting is more developed, and most prediction systems have some skill for predicting events up to 14 months lead times (Gonzalez & Goddard, 2016). Given that the seasonal predictability of large-scale climate variability is generally higher than that of surface weather variables in Europe (Ceglar et al., 2017), empirical seasonal risk outlooks could potentially be developed based on predicted values of the indices of climate variability (Ossó et al., 2017).

The current study is a statistical analysis of the effect of climate variability on sugar beet production, and resulted in the selection of related predictors for each region in Europe out of a total of five indices of climate variability. Future work could benefit from using different methods to classify the different "low/high production", and examining time-lags between the indices of climate variability on the agricultural impact indicators. Moreover, some of the significant results may had occurred by random chance (LD4 and LD1 Figure 1), and results may be interpreted with caution. Further insights into relationship between climate variability and crop production can be obtained by applying compensatory models since a more complex model can reveal important features that are not being captured by a simple model. In addition, this study can benefit from testing different decision algorithms, since the ifan algorithm, which was adopted in this study, assumes independence between predictors. Furthermore, crop production databases, such as the one used in this study, are also known to face limitations, such as reporting errors. Testing the proposed method on other crop production databases and crop types could provide further insight in the strengths and limitations of the approach. Lastly, climate can only partly explain sugar beet production. Other important aspects such as changes in farm-level management, economy, agronomy and quality of the land were not included in this study.

Chapter 5

Financing agricultural drought risk through ex-ante cash transfers

Abstract

Despite advances in drought early warning systems, forecast information is rarely used for triggering and financing early actions, such as cash transfer. Scaling up cash transfer pay-outs, and overcoming the barriers to actions based on forecasts, requires an understanding of costs resulting from False Alarms, and the potential benefits associated with appropriate early interventions. On this study, we evaluate the potential cost-effectiveness of cash transfer responses, comparing the relative costs of ex-ante cash transfers during the maize growing season to ex-post cash transfers after harvesting in Kenya. For that, we developed a forecast model using Fast-and Frugal Trees that unravels early warning relationships between climate variability, vegetation coverage, and maize yields at multiple lead times. Results indicate that our models correctly forecast low maize yield events 85% of the time across the districts studied, some already six months before harvesting. The models' performance improves towards the end of the growing season driven by a decrease of 39% in the probability of False Alarms. Overall, we show that timely cash transfers ex-ante to a disaster can often be more cost-effective than investing in ex-post expenditures. Our findings suggest that early response can yield significant cost savings, and can potentially increase the effectiveness of existing cash transfer systems.

5.1 Introduction

In February 2018 the government of Kenya declared a national drought emergency, identifying 2.7 million people as food insecure (ReliefWeb, 2018). This emergency occurred due to a prolonged drought, leading to a cascade of events that affected the access to, and consumption of, food (FEWS NET, 2018b; ReliefWeb, 2018). Droughts can have high socio-economic impacts in Kenya, such as crop failures (Omoyo, Wakhungu, & Oteng'i, 2015; ReliefWeb, 2018), high food prices and inflation (The World Bank, 2009), and increased levels of malnutrition (Alinovi et al., 2010). One of the most vulnerable groups is smallholder farmers, who rely on rainfall for the cultivation of staple crops, and on maize production for income generation (D'Alessandro et al., 2015). Among important crops, maize is considered the main staple food of the Kenyan diet, accounting for about 65% of total staple food calorific intake (Mohajan, 2014). Therefore, increasing maize productivity and climate resilience of smallholder farming systems, and enabling them to better prepare for climate extremes, is a an important issue. This critical challenge will largely determine whether Kenya succeeds in achieving the Kenya Vision 2030 development agenda (Harvey et al., 2014), and the Sendai Framework goal of substantially reducing disaster risk.

A potential way to compensate smallholder farmers' production losses and increase their climate resilience is through weather index insurance programs, which correlate crop losses with weather parameters (Dick et al., 2011). While there has been an increased interest in such insurance products, most of these programs have failed to reach significant scale in Kenya (World Bank, 2015). Humanitarian assistance, such as the distribution of goods, food vouchers, and cash transfer (Bailey, 2012), is still an important instrument for enabling the poorest to achieve short-term goals of drought preparedness and recovery. Recently, there has been an increasing debate as to whether aid should be given to people directly in the form of cash as an alternative to traditional in-kind food aid and food vouchers (Harvey, 2007). Such cash transfers are typically less expensive to administer, and have the advantage of transferring the purchasing power to the recipients. They can therefore be effective for disaster risk financing (Kenya Red Cross, 2017; UNDP, 2015).

Among the numerous cash transfer programmes (Garcia & Moore, 2012), only a handful focus on transfers before an event occurs (ex-ante); the majority focus on transfers after an event occurs (ex-post). Therefore, cash transfer programmes for drought responses are typically based on observations after an event has taken place (Pulwarty & Sivakumar, 2014), which may result in the assistance not being in place in a timely manner. An example of ex-post cash transfers is the Kenya Hunger Safety Net Programme, which releases cash

based on an observed Vegetation Condition Index that serves as a rough proxy for drought conditions (National Drought Management Authority, 2016).

Over the past decades, new drought forecasting systems have emerged, which could pave the way towards ex-ante cash transfers. Examples are the Africa Flood and Drought Monitor (Sheffield et al., 2014), and the Famine Early Warning System (FEWS NET). Recently, there has been an emerging literature on ways to automatically trigger action based on early warning systems (Coughlan De Perez et al., 2016; Stephens et al., 2015; Suarez & Tall, 2010). For instance in 2015, based on an El Niño forecast, funds were released through the World Food Program's Food Security Climate Resilience Facility for Zimbabwe and Guatemala (World Food Programme, 2016) to help both countries to face its consequent droughts. Despite these advances, associated uncertainties in forecast systems remain large, and the vast majority of forecast information is not routinely used as a basis for financing early action for drought risk reduction (Kellett & Caravani, 2013). Improving the understanding between the full costs of ex-ante and ex-post assistance associated with uncertainties of forecast information may influence more cost-effective ex-ante humanitarian aid. Furthermore, since agriculture employs the majority of the population in Kenya, adopting forecasting information into farmers' decision-making may result in better forecast-based monetary policies (Anand et al., 2011), since agricultural production, prices and rainfall play an important role on inflation (Durevall, Loening, & Ayalew, 2013; Mawejje et al., 2016).

Timely finance prior to a disaster can be more cost-effective than investing in post-disaster expenditures (The World Bank, 2016a). However, assessments of the cost-effectiveness of ex-ante and ex-post cash transfers are still missing. Creating better guides to cash transfer pay-outs, while overcoming the challenges to actions based on forecasts, greatly relies on a comprehensive understanding of the costs of 'acting in vain' due to false alarms and model uncertainty. The overall objective of this research is therefore to compare the potential cost-effectiveness of forecast-based ex-ante cash transfers during the maize growing cycle with ex-post cash transfers made after harvesting. To the best of our knowledge, no previous studies have examined the cost-effectiveness of ex-ante and ex-post cash transfers. By doing this, we provide novel early warning information that can be useful for reducing cost and increasing the effectiveness of existing cash transfer programmes. We do this with a case study for five districts in Kenya. First, we set a forecast model using Fast-and-Frugal Tree (FFT) that unravels early warning relationships between climate variability, vegetation coverage, and maize yields at multiple lead times before the maize harvesting. We then evaluate the cost-effectiveness of ex-ante

cash transfers during the growing season prompted by the expected probabilities of low maize yield that are obtained from the FFT models, and compare these with the costs of ex-post cash transfers after harvesting.

5.2 Methods

The methodological framework used in this study involves three main steps (Figure 5.1). First, we extract monthly indicators of climate variability and vegetation coverage, to be used as predictors; and annual indicators of maize yield, to be used as predictands. The two indicators used to represent climate variability are: Net Precipitation (Np) and Oceanic Niño Index (ONI). Vegetation coverage is represented by the Normalized Difference Vegetation Index (NDVI). These three indices are obtained for each month of the maize growing season during the long-rain season (March to August). For Np, we use the cumulative sum over the growing period (one to six months prior to harvest) and for NDVI we use cumulative mean of the monthly NDVI maximum through the same period. Maize yields are obtained from an annual database produced by the Kenyan Ministry of Agriculture, Livestock and Fisheries for the period 1983-2014 (Figure 5.1, Step1). Second, we apply the Fast-and-Frugal Tree Machine Learning algorithm (Phillips et al., 2017) to predict high/low maize yield events for each month within the growing season. FFT uses the predictors (in this case the indices of climate variability and vegetation coverage) to establish a classification between high or low values of the predictands (in this case high and low yield years) (Figure 5.1, Step 2). In summary, FFT models adopt non-compensatory algorithms that apply simple rules for making decisions based on few pieces of information (Gigerenzer et al., 1999), and offer transparent guides for practical decision problems (Phillips et al., 2017) as a competitive alternative for more complex Machine Learning methods. Third, we evaluate the cost-effectiveness of ex-ante cash transfers during the growing season prompted by the expected probabilities of low maize yield that are obtained from the FFT models, and compare these with the costs of ex-post cash transfers after harvesting (Figure 5.1, Step 3). The study area, datasets, and methods are described in more detail in the following subsections.

5.2.1 Step 1: Extract indicators from datasets

5.2.1.1Maize yield data and study area

Annual historical maize yields (in ton/hectare) from 1983 to 2014 are based on collated reports from the Kenyan Ministry of Agriculture, Livestock and Fisheries. These yield data have been used in prior studies examining agricultural drought simulations (Davenport, Husak, & Jayanthi, 2015) and climate/development scenarios (Davenport, Funk, & Galu, 2018).
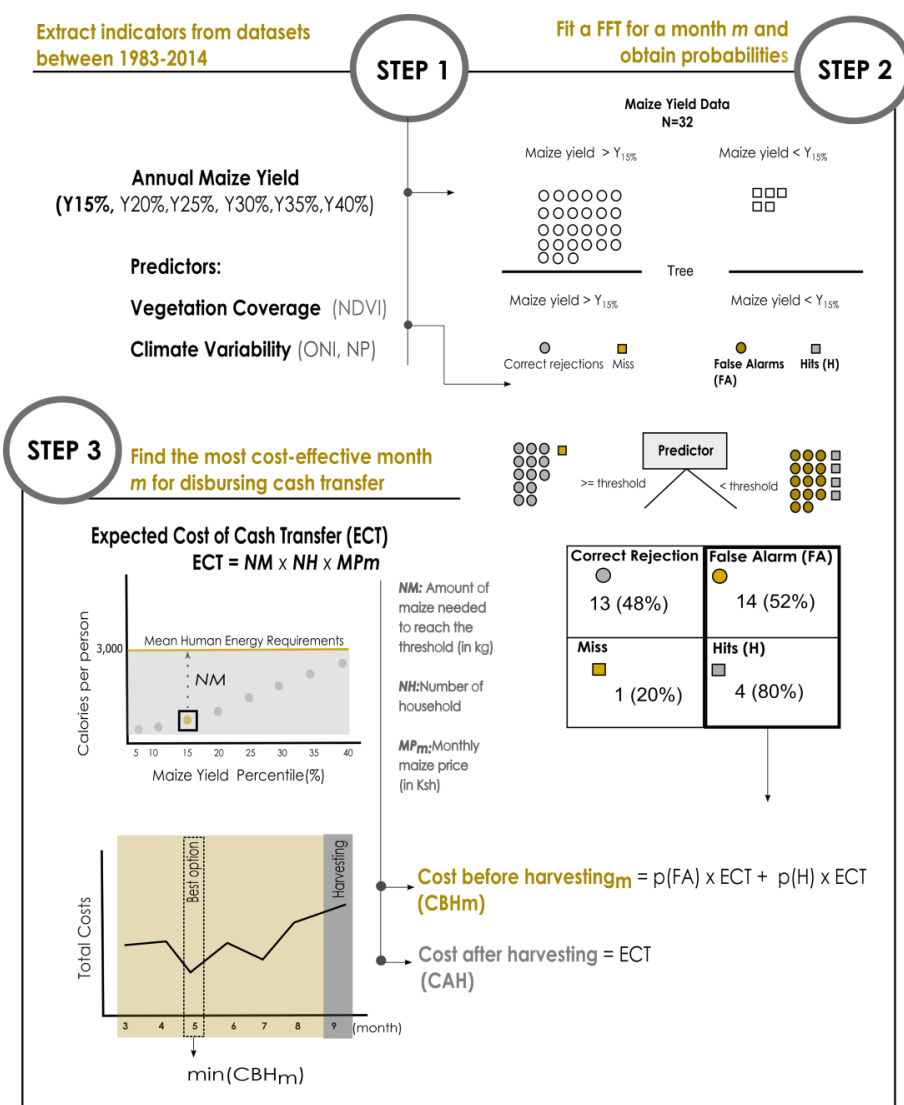
Figure 5.1 Flowchart of the methodological framework applied in this study, handled in three steps: (1) extraction of monthly indicators of climate variability, vegetation coverage and annual indicators of maize yield; (2) predictions of low maize yield years for each month within the growing season and district using Fast-and-Frugal Tree; (3) evaluation of the cost-effectiveness of ex-ante cash transfers at each month of the growing season compared with ex-post cash transfer after harvesting. Ex-ante cash transfers are considered to be more cost-effective than ex-post cash transfers in months when $CBH_m < CAH$.

In this paper we focus on five districts (Figure 5.2), where the primary growing season occurs during the long-rains season, therefore planting generally occurs in early March and harvest in September (FEWS NET, 2017). In addition, these

areas are chosen because critically low annual maize yields events are often observed, as displayed in appendix Figure D1. While harvests occur in September, peak rains typically occur much earlier, in April.

From the annual data, we derive six percentiles of annual yield (Y), namely $Y_{15\%}$ representing the lowest 15% of annual maize yields, and $Y_{20\%}$, $Y_{25\%}$, $Y_{30\%}$, $Y_{35\%}$ and $Y_{40\%}$. For each percentile, we classify annual maize yields as "below yield threshold" (when they are below the defined percentile) and "above yield threshold" (when they are above the defined percentile). An overview of the annual maize yields and the six percentiles per district is shown in appendix Figure D1.
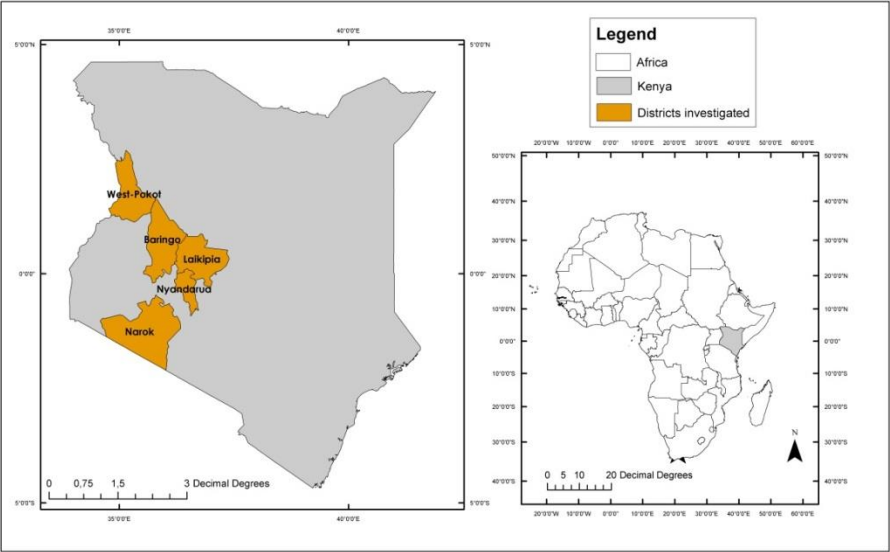
Figure 5.2 Map of Kenya and districts examined in this study.

5.2.1.2 Climate variability and vegetation coverage indicators

In this study, we represent climate variability using ONI and cumulative Np indicators, and vegetation coverage using NDVI.

5.2.1.2.1 El Niño Southern Oscillation

We use the Oceanic Niño Index (ONI) from 1983–2014 (NOAA, 2017a) to represent the El Niño Southern Oscillation (ENSO). ONI is a three-month running mean of sea surface temperature anomalies in the Niño 3.4 region using centred 30-year base periods updated every 5 years. This index is calculated based on a moving average of three-months. The ONI record in March, for instance, is the mean value observed in February, March and April.

While some authors have suggested weak links between Kenyan boreal spring rains and ENSO (Lyon, 2014), FEWS NET studies have shown that a predictable La Niña drought impact has arisen due to human induced warming in the Western Pacific (Funk et al., 2014; Funk et al., 2018; Shukla, Funk, & Hoell, 2014).

5.2.1.2.2 Cumulative Net Precipitation

We use the difference between monthly precipitation (P) estimates from the Climate Hazards group Infrared Precipitation with Stations (CHIRPS), and the reference evapotranspiration (E) to calculate the Net Precipitation (Np) indicator for 1983-2014. CHIRPS is a quasi-global (50°S-50°N), high resolution (0.05°), daily, pentad (five-day rainfall), and monthly precipitation dataset, which was created to support the drought early warning system FEWS NET (Funk et al., 2015). The CHIRPS dataset is freely available online at the CHIRPS website. The reference evapotranspiration product is a multi-scalar measure of anomalous atmospheric evaporative demand, which captures signals of water stress (in mm) at weekly to monthly timescales. This product can be used as a tool for preparedness planning for both flash droughts and ongoing. The cumulative Np indicator (Equation 5.1) is calculated at the district level *d*, and within each month of the maize growing season *m* (from March to August):

$$Np_{i,m,d} = \sum_{i=1}^{6} P_{i,m,d} - \sum_{i=1}^{6} E_{i,m,d} \qquad \text{Equation 5.1}$$

where *i* represents a time window accumulation that varies from 1 to 6 months. For instance, an $Np_{6,August,Laikipia}$ represents the 6 month cumulative Net Precipitation observed from March until August at the district of Laikipia.

5.2.1.2.3 Cumulative Normalized Difference Vegetation Index (NDVI)

For the same period (1983-2014), we use cumulative mean of NDVI maximum values over the growing season (Equation 5.2), as a proxy to measure the physiologically functioning surface greenness level of a region (Myneni et al., 1995). The NDVI dataset generated from NOAA's Advanced Very High Resolution Radiometer has an 8 kilometre resolution, and can be used to monitor vegetation changes at different spatial scales (Pinzon, Jorge E and Tucker, 2014). We use the version termed NDVI3g, and obtained data from https://ecocast.arc.nasa.gov/data/pub/gimms/.

$$\sum_{i=1}^{6} NDVI_{i,m,d}$$ Equation 5.2

The monthly mean of NDVI maximum indicator is accumulated at the district level d, within each month of the maize growing season m, where i represents a time window applied for accumulation, similarly as described for the Np indicator.

5.2.2 Step 2: Fit Fast-and-Frugal Tree (FFT) for a month m and obtain probabilities

FFT model is a simple algorithm that establish rules for making efficient and accurate decisions based on limited information (Gigerenzer et al., 1999; Phillips et al., 2017). Such models seldom over-fit data (Phillips et al., 2017), and are easier to interpret and psychologically more plausible to internalise (Keller et al., 2010) than other Machine Learning methods (Luan, Schooler, & Gigerenzer, 2011). We use FFT to predict classes of maize yields as a function of the indices of climate variability and vegetation coverage (Np, ONI, NDVI described in 'Climate variability and vegetation coverage indicators' section). In heuristic decision-making, FFT is a supervised learning algorithm that is used for classifying cases (e.g. maize yield) into two classes (in this case below or above yield threshold) based on particular predictors.

As displayed in appendix Figure D2, the structure of an FFT model determines the exact number and sequence of predictors that are applied to reach a final classification (Gigerenzer et al., 1999; Gigerenzer & Todd, 1999). FFT uses a maximum of five cues, meaning that a five-cue decision tree is based on the best five performing indices out of the total number of climate variability and vegetation coverage indicators accumulated for each respective month, as displayed in Table 5.1. The selection of the five best performing indices for each particular month, district and maize yield percentile is based on their marginal weighted accuracy (WACC), which is further described in the paragraph below. Therefore, FFT uses non-compensatory algorithms, which include only a limited subset of all predictors for establishing a binary decision. Non-compensatory algorithms are designed to ignore information, because once a decision is completed based on the selected predictors, no additional predictors can change the decision (Phillips et al., 2017). This characteristic is considered to have both practical and statistical advantages over compensatory algorithms, such as regression models. First, given that FFT models use a subset of predictors, the decision trees can perform better in predicting unseen data,

thus they tend to be robust against overfitting. Second, FFT algorithms use information in specific and sequential order, which can guide decision makers in collecting information and assist in decision tasks (Phillips et al., 2017).

The FFT algorithm is designed to learn from, and make predictions on, data. FFT is fitted to a training dataset, which is used derive the parameters of the model. The FFT algorithm is constructed as follows: a) select predictors; b) determine a decision threshold for each predictor; c) determine the order of predictors; and d) determine the exit for each predictor, which by definition, FFT must have either a negative or a positive exit (or both in the case of the final decision node) (Phillips et al., 2017). The FFT models are then tested using an independent testing dataset. In order to select trees that identify "below yield threshold" rather than "above yield threshold" cases, we set the Sensitivity Weighting Parameter w to w=0.75, using the *ifan* algorithm, which is described in detail by Phillips et al. (2017). Sensitivity Weighting Parameter determines the overall value of WACC of the FFT, and the WACC measures how well the algorithm balances correct decisions. In summary, the *ifan* decision algorithm tests several different thresholds of the predictors to identify the one that maximizes the predictor's accuracy. Consequently, once the set of FFT is created, *ifan* selects the tree with the highest weighted accuracy. For clarification, it is important to notice that the value of w parameter does not change how the set of FFT is constructed, but rather, it changes which specific tree in the set of FFT is selected (Phillips et al., 2017). We performed an additional sensitivity analysis on the WACC index by assigning similar weight when identifying below yield threshold and above yield threshold cases, thus setting w=0.5.

We analyse the performance of the FFT models to predict classes of "below yield threshold" and "above yield threshold" using Receiver Operating Characteristic (ROC) (Metz, 1978). ROC is a graphical plot (appendix Figure D3) that illustrates the performance of a binary classifier system (Zweig & Campbell, 1993). The ROC index varies between 0 and 1, where perfect and random predictions have values of ROC=1.0 and ROC=0.5, respectively (Hamill & Juras, 2006). We calculate the ROC index using the trapezoidal rule, and test the predictive skill of the FFT models using leave-one out cross validation, further described in appendix D4. We use this cross validation method since: a) it is highly recommended for small sets of training data; and b) it can be used with any kind of predictive modelling, including discriminant analysis such as decision trees (James et al., 2013).

Table 5.1 Description of accumulation periods for each variable and total number of predictors considered in each month. From April onwards, we included predictors of current and previous months. Therefore, FFT models in April take information from March if any predictor registered in the latter had a higher marginal weighted accuracy WACC value than predictors observed in April. FFTs use a maximum of five predictors.

Month	March	April	May	June	July	August
Np_1	M	A	M	J	J	A
Np_2	FM	MA	AM	MJ	JJ	JA
Np_3	JFM	FMA	MAM	AMJ	MJJ	JJA
Np_4	DJFM	JFMA	FMAM	MAMJ	AMJJ	MJJA
Np_5	NDJFM	DJFMA	JFMAM	FMAMJ	MAMJJ	AMJJA
Np_6	ONDJFM	NDJFMA	DJFMAM	JFMAMJ	FMAMJJ	MAMJJA
$NDVI_1$	M	A	M	J	J	A
$NDVI_2$	FM	MA	AM	MJ	JJ	JA
$NDVI_3$	JFM	FMA	MAM	AMJ	MJJ	JJA
$NDVI_4$	DJFM	JFMA	FMAM	MAMJ	AMJJ	MJJA
$NDVI_5$	NDJFM	DJFMA	JFMAM	FMAMJ	MAMJJ	AMJJA
$NDVI_6$	ONDJFM	NDJFMA	DJFMAM	JFMAMJ	FMAMJJ	MAMJJA
ONI	FMA	MAM	AMJ	MJJ	JJA	JAS
Total number of predictors	13	26	39	52	65	78

For each FFT model where the ROC is higher than 0.5, we analyse standard classification statistics such as probabilities of Hits (H), False Alarms (FA), Correct Rejections (CR), and Misses (MS). Their definitions and formulae are given in appendix Table D5. In summary, we obtain FFT model for each particular month within the growing season, each district, and each percentile level of annual yield, through the following steps:

1. Ranking and selecting 5 best predictors based on their marginal WACC, for each district, maize yield percentile, and month;

2. Pruning decision trees by cross-validating the FFT model using leave-one out cross validation, further described in appendix D4;
3. Calculation of the ROC index;
4. Analysis of the performance of the cross-validated FFT model by calculating standard classification statistics, as displayed in appendix Table D5.

From April onwards, we include maize predictors of the current and previous months. For instance, when fitting FFT model in April, information from March was also taken into consideration if any predictor registered in March had a higher marginal WACC value than predictors observed in April. After following these steps, we build a new FFT using all the dataset and adopting the pruning parameter that maximizes the WACC index. Hence, this procedure enables us to suggest the set of predictors which are most important for each district, lead time and yield percentile.

5.2.3 Step 3: Cost-effectiveness analysis

We use a simple methodology to assess the cost-effectiveness of cash transfers. In humanitarian response, early action aims to provide short-term resources for emergency situations. Therefore, the aim of this cash transfers is to prevent populations from becoming undernourished, from slipping below the limit of the mean Human Energy Requirement (HER) in seasons with low yields. HER is defined as "the amount of food energy needed to balance energy expenditure in order to maintain body size, body composition and a level of necessary and desirable physical activity consistent with long-term good health"(Pacetti, Caporali, & Cristina, 2017). The HER depends on individual characteristics such as age, sex, body weight and lifestyle, and according to FAO a mean HER is approximately 3,000 kcal/cap/day (Pacetti et al., 2017; World Health Organization, 2004).

We define a household energy loss value by the difference between the predicted low maize yield transformed into calories, and the HER mean per capita. Therefore, the expected cost of cash transfer (hereafter ECT) is defined by the amount of calories (multiplied by price levels, see Figure 5.1 step 3 and appendix Figure D1) needed to supply a household calorific deficit in comparison to the HER mean threshold. The expected total cost of cash transfer determines the least costly (hence most cost-effective) month for initiating cash transfer. The expected cost of cash transfer before harvesting (hereafter CBH_m) takes into account the probability of Hits and False Alarms in a month m (equation 5.3), while the expected cost of cash transfer after harvesting (hereafter CAH) considers 100% and 0% probabilities of Hits and False Alarms, respectively (equation 5.4). Therefore, CAH is defined as the total expected cost

of the cash transfers only. A cash transfer is considered to be cost-effective before harvesting in months when $CBH_m < CAH$.

$$CBH_m = P(Hits_m) \times ECT_m + P(False\ Alarms_m) \times ECT_m \qquad \text{Equation 5.3}$$

$$CAH = ECT \qquad \text{Equation 5.4}$$

In more detail, we set the cash transfers as the total costs involved in compensating low maize yields (in monetary values) to fulfil the calorific deficit of a group of smallholder farmers (equation 5.5). In this study, the total costs of the cash transfer depend on: a) total number of households that the cash transfer aims to support (NH); b) total amount of maize per household needed to reach the HER mean threshold (NM); and c) monthly maize price (MP_m). For simplicity, we do not take into consideration administrative costs of ex-ante and ex-post cash transfers. Occasionally funding can be spent to "act in vain", as the result of a false alarm. To compute the total expected costs of this action, cash transfers are considered to be irreversible once disbursed, and therefore the costs associated with False Alarms are equal to those associated with Hits.

$$ECT_m = NH \times NM \times MP_m \qquad \text{Equation 5.5}$$

We use wholesale monthly price records from Nairobi between 2000 and 2017 from the FEWS NET data warehouse to calculate monthly mean maize prices between March and August. Prices are deflated to February 2009 values using a consumer price index generated by the Kenyan National Bank. We fit a linear model between deflated annual Nairobi prices in September and annual maize yields. When this relationship is significant (p-value<0.05), we use this model to determine maize prices based on yields. When not significant, we assume that prices in September (P_s or MP_9) vary proportionally to the low maize yield percentile (Y_p) being investigated (appendix Figure D6.2) and described in equation 5.6. Lastly, we consider that maize prices within the growing season (P_i) follow their observed respective monthly mean ($\bar{P}_i$), as described in equation 5.7

$$P_s = -1 \times Y_p + 100 \qquad \text{Equation 5.6}$$

$$\bar{P}_i = \frac{\sum P_i}{N} \qquad \text{Equation 5.7}$$

Where i represent months 3 (March or MP_3) to 8 (August or MP_8), and N represents the length of the price time series in years. In addition, we assess the sensitivity of the cost-effectiveness analysis by adopting four different rates of variations in September prices for the districts where prices at harvesting are assumed to be conditioned to maize supply (appendix D7).

In order to calculate the amount of calories available per household per year, we consider that: 100g of maize has 365 kcal (United States Department of Agriculture, 2016); the mean size of a household in the Rift Valley in Kenya is 4.6 persons (Munene, 2003); each household owns one hectare of land for farming; and the total number of households granted with cash transfer is 1000 per district. Therefore, for each of the six investigated percentiles of maize yield, we transform tonnes/hectare/year into kcal/household/year. In addition, we also assume that cash transfers do not create a disincentive to work, and beneficiaries do not cease maize production. This assumption was previously suggested by the Food and Agriculture Organization of the United Nations, where an investigation (Food and Agriculture Organization, 2016) concluded that cash transfer programmes were linked to increased livelihood activities of farmers. An illustration of the cost-effectiveness analysis is found in Figure 5.1 (step 3).

5.3 Results

5.3.1 Obtaining probabilities using FFT models

In Figure 5.3, we present the performance of the tested FFT models in predicting true low maize yield events (Hits probabilities are highlighted in blue), and false low maize yield events (False Alarms probabilities are highlighted in yellow) per district, for the six low maize yield percentiles and the different lead times before harvesting. We predict high/low maize yield events for each month within the growing season (March to August), which represent six lead times. The spatial distribution of the probabilities of Hits and False Alarms are available in appendix D8. Overall, the performance of the FFT models improve with shorter lead times as a result of reduced probability of False Alarms, and consequently increased probability of Correct Rejections. The FFT models have skill (ROC>0.5) in predicting annual high/low maize yield in all districts. For most models some skill already exists six months before the harvesting season (on average ROC=0.63) despite the high probabilities of False Alarms at this lead time. The WACC index, which measures how well the algorithm balances correct decisions, exhibits the highest value among districts and yield percentile levels in July (lead time 2 months), and the lowest in March (lead time 6 months). Among all models with predictive skill, lead times, and yield percentiles, the district of West Pokot has, on average, the highest WACC and ROC (0.81 and 0.73, respectively) driven specially by the high probabilities of Hits in this district; and on average the district of Nyandarua has the lowest WACC (0.72), as shown in appendix Figure D9. Across different yield percentiles, districts, and lead times, the mean probability of Hits is 85%. Results of the sensitivity analysis are available in appendix Figure D10.1. When adopting a

different weight parameter (w=0.5 instead of w=0.75), the performance of the FFT models improves with shorter lead times as a result of reduced probability of False Alarms. Among lead times, percentiles and districts, the probability of Hits is, on average, 66%. Overall, the probabilities of False Alarms and Hits are, on average, lower compared to those obtained when w=0.75. The best performing predictors of maize yield per district, and their respective thresholds, are shown in the appendix Table D11.

In March and April, six and five months before the maize harvesting season in Kenya, the FFT models have predictive skill (ROC>0.5) for most districts and yield percentiles (Y). Exceptions are for percentiles $Y_{15\%}$ and $Y_{25\%}$ in Baringo, $Y_{20\%}$ in Narok, and $Y_{40\%}$ in Nyandarua during lead time 6, and for $Y_{20\%}$ in Baringo, $Y_{30\%}$ and $Y_{35\%}$ in Nyandarua during lead time 5 (Figure 5.3). On average, the probability of Hits for the different maize yield percentiles is 84% and 86% for lead times of 6 and 5 months, respectively, while the probability of False Alarms is 56% for both of these lead times. The mean probability of Misses for the different maize yield percentiles is 16% and 14% for lead times of 6 and 5 months respectively, while the mean probability of Correct Rejection is 44% for both of these lead times. The most important predictor for FFT models in these two lead times is Net Precipitation five in March ($Np_{5,March}$). In other words, the FFT models mostly use the difference between cumulative five months precipitation and reference evapotranspiration observed in months previous to sowing (March) for classifying between above and below yield threshold. Such results demonstrate that initial soil conditions play an important role during the emergence and establishment of maize growth, and in the vegetative development (approximately 60 days after sowing (Barron et al., 2003)), when higher moisture levels benefit yields (FAO, 2017; Mati, 2000).

In May and June, four and three months before the maize harvesting season in Kenya, the FFT models also have predictive skill for most districts and percentiles. Exceptions are for $Y_{30\%}$, $Y_{35\%}$ and $Y_{40\%}$ in Narok, $Y_{30\%}$ and $Y_{35\%}$ in Nyandarua during lead time 4, for $Y_{30\%}$ in Laikipia, and $Y_{15\%}$ in Narok during lead time 3 (Figure 5.3). Compared to the two antecedent months (March and April), the probability of False Alarms remains high on average in May (56%), and lower in June (47%). The probability of Hits, on average, remains high (86% and 83%) in May and June, respectively. In May and June, the FFT models predict maize percentiles $Y_{15\%}$, $Y_{20\%}$ and $Y_{25\%}$ using the Net Precipitation variability accumulated from previous and post maize planting date, such as $Np_{5,March}$, $Np_{6,April}$, and $Np_{4,May}$. Other predictor that is often used is the Normalized Difference Vegetation Index (NDVI) such as $NDVI_{3,April}$ and $NDVI_{5,June}$. Next to the climatic predictors of maize yield also suggested by others (Estes et al., 2014;

Funk & Verdin, 2010; Shi & Tao, 2014), the NDVI index was also found to be a predictor for maize yields in previous studies (Lewis, Rowland, & Nadeau, 1998; Rojas, 2007). For predicting below yield threshold/ above yield threshold maize percentiles $Y_{30\%}$, $Y_{35\%}$ and $Y_{40\%}$, FFT models mostly used $Np_{5,March}$ in combination with other intra-seasonal indices of climate variability and vegetation coverage, such as the Oceanic Niño Index (ONI) in April and $NDVI_{5,June}$; Both El Niño and NDVI indicators have also been highlighted as predictors of maize yield in other studies (Amissah-Arthur, Jagtap, & Rosenzweig, 2002; Lewis et al., 1998; Rojas, 2007). The most damaging crop water deficits arise during these lead times (maize reproductive stage), when the cereal plants switch from growing leaves to growing grains (Funk & Verdin, 2010), and midseason water deficits can drastically reduce maize yields (Senay & Verdin, 2003). Even though the climatological conditions during the vegetative growth period are relevant, conditions during the reproductive growth period influence yields more directly (Iizumi, Yokozawa, et al., 2014). This may explain the improved performance of FFT models during lead time 3 months (maize reproductive growth stage), which uses intra-seasonal information of indices of climate variability and vegetation coverage observed in June to predict maize yield percentiles.

In July and August, the FFT models have predictive skill in all districts and percentiles, except for $Y_{15\%}$ in Narok (Figure 5.3, lead time 2). Compared to the previous two months of May and June, the performance of the FFT models improves slightly. On average, the mean probability of False Alarms is lower (44% and 40% in July and August, respectively), and Hits, on average, remains high (87% and 83%). For predicting below yield threshold/above yield threshold maize percentiles $Y_{15\%}$, $Y_{20\%}$ and $Y_{25\%}$, the FFT models mostly use indicators that include observations from June and July such as $NDVI_{5,June}$, and $Np_{2,July}$ and $Np_{6,July}$, while FFT models mostly predict below yield threshold/above yield threshold maize percentiles $Y_{30\%}$, $Y_{35\%}$ and $Y_{40\%}$, using $Np_{5,March}$, $NDVI_{5,June}$ and $Np_{2,July}$. At these lead times, maize reaches its grain filling and drying stages (Barron et al., 2003), and late season soil water deficits after the grain biomass accumulation is complete may lead to higher yields (Funk & Verdin, 2010). Very high accumulated levels of precipitation in June and July may cause maize yields to decline due to the high likelihood of diseases, insects, and mould infestation, which are favourable when such conditions are observed (Funk & Verdin, 2010). Furthermore, maize yield in the investigated districts is linked to other seasonal indices of climate variability and vegetation coverage and to accumulated rainfall and soil moisture conditions prior to the maize-planting season.
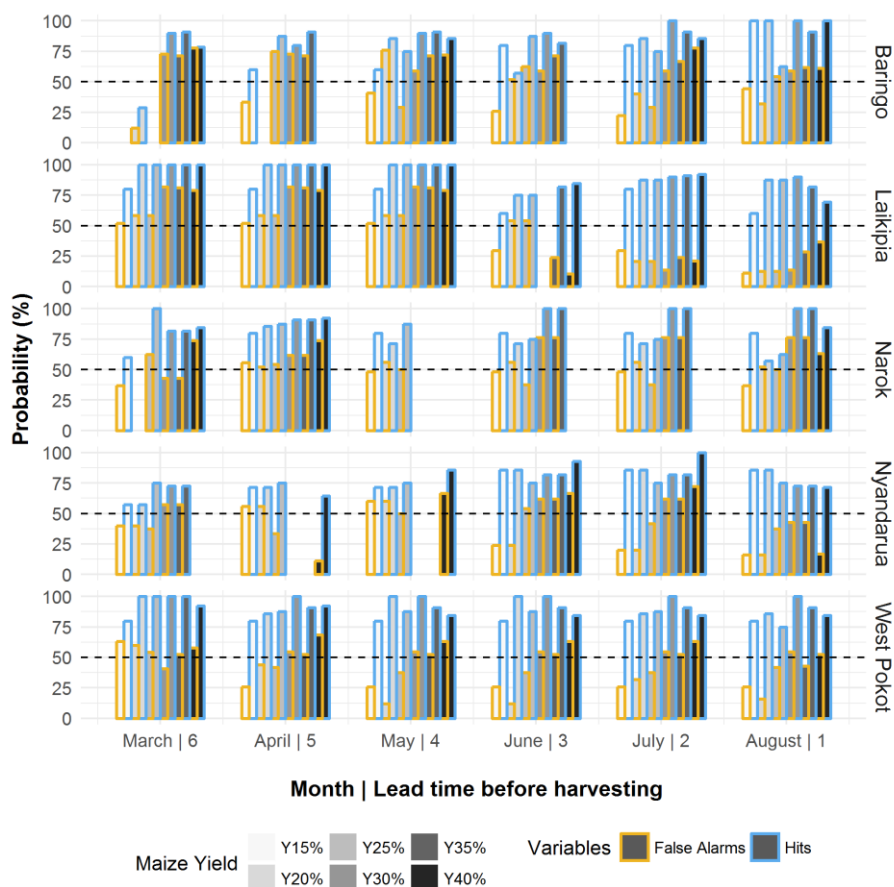
Figure 5.3 Performance of the tested FFT models in predicting true low maize yield events (Hits), and false low maize yield events (False Alarms) per district, for different maize yield percentiles (shades of grey) and lead times (x-axis). Yellow bars represent the probabilities of False Alarms, and blue bars probabilities of Hits. The six levels of low maize yield percentiles are highlighted in shades of grey. Dashed black line is drawn at the 50% probability. Sensitivity weighting parameter is w=0.75.

3.2 Cost-effectiveness of cash transfers

3.2.1 Cost-effectiveness of cash transfer assuming a perfect forecast

In Figure 5.4, we display the cost-effectiveness analysis of cash transfers assuming a perfect forecast skill within the growing season from March to August. Therefore, for this analysis we assume that the probability of Hits and False Alarms is 100% and 0%, respectively. (H=100% and FA=0%). Thus, in this case the cost-effectiveness is solely based on maize price variations. We only carried out a cost-effectiveness analysis for districts and maize yield percentiles

for which the calories/household/year fall below the Human Energy Requirement mean threshold (section Methods section and appendix Figure D1) (boxes in Figure 5.4 that are not blank). For all of the 17 cases for which this is the case, we find that cash transfers assuming a perfect forecast skill are most cost-effective at a lead time of 6 months. This is due to lower mean maize price in March compared to September. In the appendix Figure D6.1 and D6.2, we display the pricing models used in the districts for the month of September, and average monthly maize prices adopted for months between March and August. This shows that during the growing season, mean prices are relatively low in March, and highest in June.

3.2.2 Cost-effectiveness of cash transfer using probabilities from FFT models

In Figure 5.5, we present the results of the cost-effectiveness analysis using the probabilities of Hits and False Alarms obtained from the FFT models per district, lead time, and maize yield percentile. These probabilities are available in Figure 5.3. Overall, in 11 out of the 17 cases tested, cash transfers are cost-effective (CBH < CAH) for at least one of the lead times before harvesting.

In addition, in Figure5.5, we show that for $Y_{15\%}$, in all districts there is at least one lead time for which the expected cost of ex-ante cash transfers is lower than ex-post cash transfers, while for $Y_{20\%}$ ex-ante cash transfer is more cost effective in 3 out of 4 districts. Ex-ante cash transfers are often cost-effective when the probability of a False Alarms is below 50%, and when prices during the growing season are lower than prices in September. Cash transfer costs ex-ante for $Y_{15\%}$ and $Y_{20\%}$ can be, on average, 29% and 14% lower than ex-post cash transfers in September, respectively.

Ex-ante cash transfers during the growing season are also estimated to be more cost-effective for $Y_{25\%}$ and $Y_{30\%}$. In Laikipia and Nyandarua districts (Figure 5.5), the expected costs of ex-ante cash transfers are 5% and 2% lower than those associated with ex-post cash transfers, respectively. This is attributed to a combination of low probabilities of False Alarms (below 13%), and low mean prices during the growing season compared to September. However, the number of months with cost-effective ex-ante cash transfers decreases when comparing $Y_{25\%}$ and $Y_{30\%}$ to those found in $Y_{15\%}$ and $Y_{20\%}$. For $Y_{35\%}$ we found ex-post cash transfers to be more cost-effective than ex-ante. This is because the assumed price of maize in September, when a maize supply of $Y_{35\%}$, is below the monthly average from May and July (appendix Figure D6.2). Consequently, cost-effective ex-ante cash transfers would only be possible in March, April and August if there is a low probability of a False Alarms. However, the additional

costs driven by high probability of a False Alarms in March, April and August resulted in cash transfers being more cost-effective ex-post.
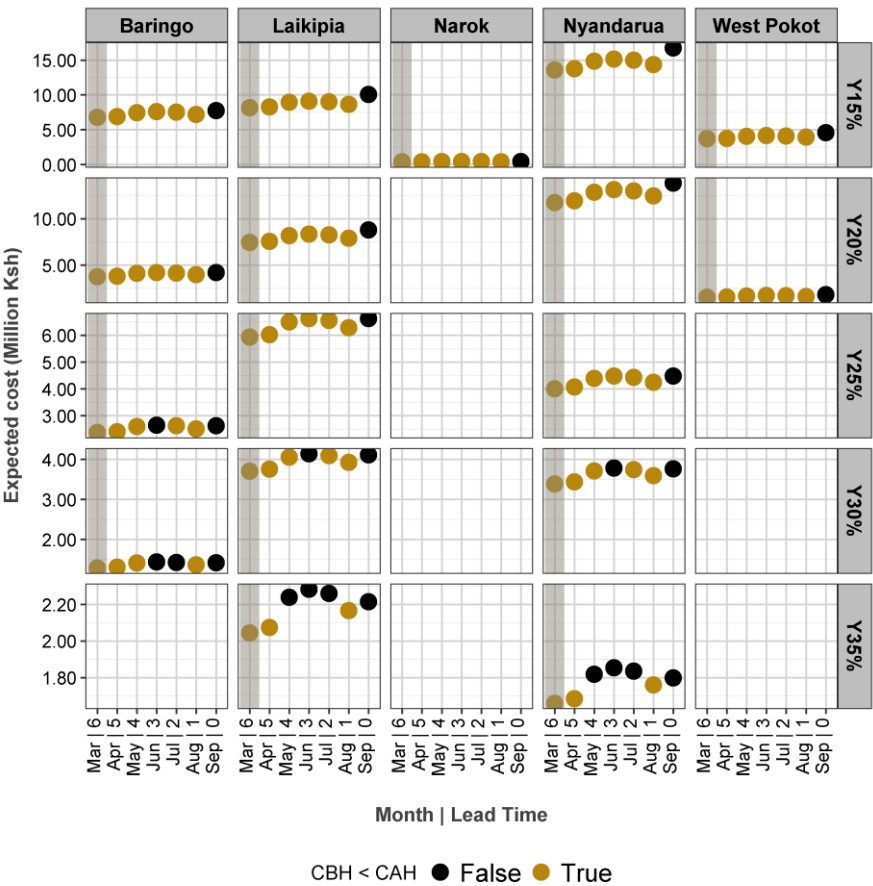
Figure 5.4 Total expected cost of cash transfer per district, for different lead times and maize yield percentiles, assuming a perfect forecast before harvesting from March to August. Therefore, the probabilities of Hits and False Alarms are 100% and 0%, respectively. Yellow dots show all lead times before harvesting (starts in September) for which expected cost of cash transfer is lower than the expected cost of cash transfer after harvesting (CBH$_m$ < CAH); black dots show the opposite. The most cost effective lead time is highlighted in grey. Boxes are blank when the maize yield percentile for the specific district is higher than the mean human energy requirement (3,000 kcal/day/person), and therefore no cash transfer is required.
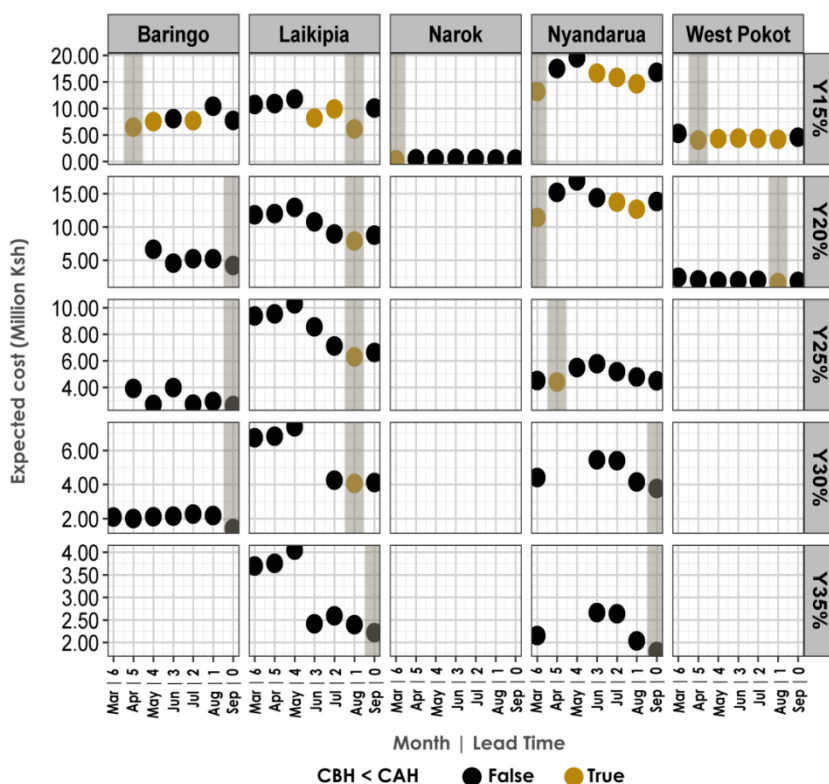
Figure 5.5 Total expected cost of cash transfer per district, lead time, and maize yield percentile calculated based on the probabilities of Hits and False Alarms obtained from the FFT models (using a weighting parameter of w=0.75). Yellow dots show all lead times before harvesting (starts in September) for which expected cost of cash transfer is lower than the expected cost of cash transfer after harvesting (CBH_m < CAH); black dots indicate the opposite. The most cost effective lead time is highlighted in grey. Boxes are blank when the maize yield percentile for the specific district is higher than the mean human energy requirement (3,000 kcal/day/person), and therefore cash transfer is not triggered. Results are shown only for models with ROC>0.5.

In addition, we assessed the sensitivity of the results using two moderate (Figure 5.6A an 5.6B) and two conservative (Figure 5.6C and 5.6D) scenarios of September prices for the districts where prices at harvesting are assumed to be conditioned to maize supply (Laikipia, Nyandarua, West Pokot). A more detailed illustration is available in appendix Figure D7.1 and D7.2. We show that when adopting price scenarios 1-3, there is at least one lead time for 17 out of the 36 tested cases (boxes that are not blank in Figure 5.6A-5.6C) for which cash transfers are more cost-effective ex-ante. When considering price scenario 4, we still find some lead times for which the ex-ante cash transfers are expected

to have lower costs than ex-post cash transfers. Therefore, despite prices variations, we show that ex-ante cash transfers can often be more cost-effective than ex-post cash transfers, especially for the more extreme yield deficits.
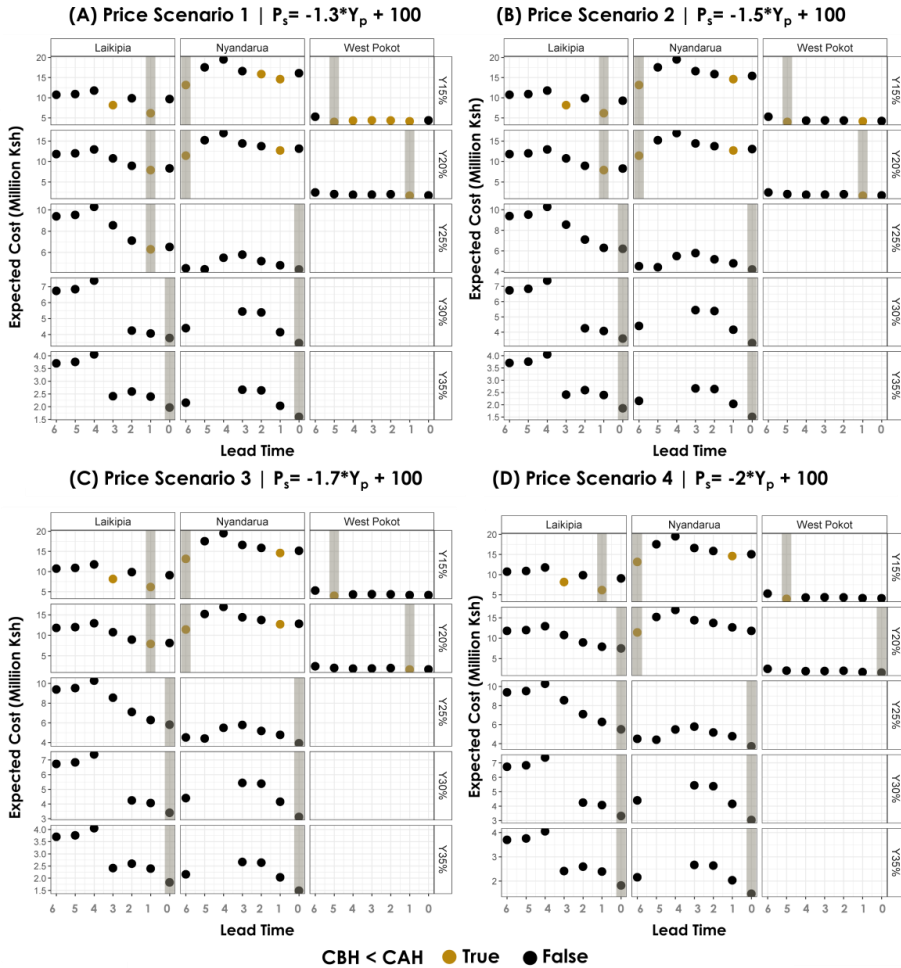
Figure 5.6 Sensitivity analysis of total expected cost of cash transfer testing four rates of change in P_s (price) for change in Y_p (maize yield), per district, lead time, and maize yield percentile. Yellow dots highlight all lead times before harvesting when expected ex-ante costs of cash transfer are lower than the expected ex-post costs of cash transfer (CBHm < CAH); black dots show the opposite. The most cost effective lead time is highlighted in grey. Boxes are blank when the maize yield percentile for the specific district is higher than the mean human energy requirement, and therefore cash transfer is not triggered. Results are shown only for models with ROC>0.5.

5.4 Discussion

5.4.1 Current practices and challenges of cash transfer operationalization

In our study, we show that despite model uncertainties and prices variations, ex-ante cash transfers can often be more cost-effective than ex-post cash transfers, especially for the more extreme yield deficits. Even though studies on the cost-effectiveness of early action are very limited, some suggest that early response can yield significant cost savings (Venton, 2018; Wilkinson et al., 2018). For instance, in 2015 a FoodSECuRE Cost Benefit Analysis (ex-ante) in Sudan and Niger suggested that early actions based on a forecast mechanism could reduce the cost of emergency response by approximately 50 percent compared to ex-post responses (World Food Programme, 2016).

Our results could potentially increase the efficacy and efficiency of existing cash transfer systems. Currently, the Kenya Hunger Safety Net Programme triggers two types of cash transfers (standard and emergency payments) based on a single satellite vegetation condition index (VCI). Neither of these cash transfer types depend on field assessment, and emergency payments are made monthly in any Sub-County when the VCI hits the scale up threshold (from moderate to extreme drought), and payments are suspended when the threshold is no longer reached for that month (National Drought Management Authority, 2016). The use of a single drought indicator may not provide a comprehensive assessment of drought impact, and can occasionally trigger payments in situations where drought conditions are not evolving (National Drought Management Authority, 2016). The National Drought Management Authority could potentially improve the reliability of cash transfers and anticipate pay-outs by including other drought early warning indicators, such as the ones adopted in this investigation.

Furthermore, when different drought severity levels are observed in pre-selected areas, fixed emergency cash transfers of 2,550 Ksh (approximately 25 US$) are payed in addition to standard payments that are given monthly to households. This emergency payment aims to support the increased needs that households may experience during a drought period. However, establishing a fixed amount of cash in order to respond to different drought severity levels does not fully account for different needs that may arise during a drought, especially the more severe ones. Establishing payments of cash that vary based on forecasts of different agricultural drought levels, such as proposed in this study, may be more efficient in achieving households' dietary diversity and reducing malnutrition rates.

In addition, the Kenyan National Drought Management Authority holds the National Drought Contingency Fund (NDCF), which receives contributions from the government of Kenya and multi-donors, with the capacity to disburse funds to drought-prone affected districts in a flexible way (National Drought

Management Authority, 2016). This fund enables fast drought early responses in all districts based on drought early warning information and contingency plans. To enable fast triggering and scalability, efficient budget allocation within lead times while avoiding fund depletions, a set of evidence-based mechanisms should be in place based on drought forecasts. Therefore, impact-based forecast information and cost-effectiveness analysis, such as developed in this study, could support a more timely pooling and distribution of resources, and consequently a more efficient management of the NDCF.

Multiple challenges can be observed for operationalizing cash transfers based on indicators of droughts. Taking actions in response to early warnings of drought risks based on indices requires an in-depth understanding of the potential impact, scale, aid-triggering thresholds, severity and timing of a disaster (Wilkinson et al., 2018). Operationally, cash transfer programs can be unconditional, meaning that they aim to reduce poverty by providing cash independent of the receiver's actions; or conditional, meaning that receivers must make pre-specified investments.

Most emergency drought response systems use unconditional cash transfers, which often have a lower cost per beneficiary compared to other interventions such as vouchers and in-kind food (Doocy & Tappis, 2017). However, cash transfer is not always a suitable option, especially when the local economy is isolated from other markets, in which case an inflow of cash can increase prices (Cunha, De Giorgi, & Jayachandran, 2019). Furthermore, beneficiaries of the program must be aware of the predicted drought threats in order to spend cash wisely (National Drought Management Authority, 2016). Therefore, cash transfer programs could benefit from information on individual preferences regarding the timing and expenditure of cash transfers when dealing with food insecurity. In addition, establishing a range of early warning drought indicators as triggers for payments may be beneficial since it can remove possible subjective analysis or political influence on decisions to disburse cash transfer (National Drought Management Authority, 2016). Lastly, initiatives that use forecast-based early action, such as cash transfer, have either provided support directly to beneficiaries, or have worked with national governments and partners through state institutions (Wilkinson et al., 2018). As such, a choice between these distribution alternatives must be made based on the capacity and coordination of government actors, on the country specific context, and on the mandates of agencies promoting forecast-based early action in order to ensure timely aid (Wilkinson et al., 2018).

5.4.2 Limitations and recommendations

The primary limitation of this investigation was that we assumed that prices are solely dependent on the supply of maize, when in reality price is associated with a combination of factors including supply and demand in neighbouring regions and global price shocks (Brinkman et al., 2010). We also assumed that prices during the growing season would follow their mean values, when in practice price levels and volatility can increase under a perceived or actual drought impact. Another important cost component of cash transfers which was not investigated in this study is operational costs. For instance, including transaction costs in the analysis would result in a more realistic estimation of costs. In addition, we considered only indicators of climate variability and vegetation coverage as drivers of maize yield while other aspects such as in-farm level management activities play an important role on yields. Regarding the applied methods, further insights into relationships between climate variability and maize yields can be obtained by applying compensatory models (e.g. Random Forest) since a more complex model can reveal important features that are not captured by a simple model such as the FFT. In addition, the accuracy of the results could potentially improve when testing different decision algorithms, since the *ifan* algorithm used in this study assumes independence between predictors. Furthermore, historical crop yield databases, such as the one used in this study, are also known to face limitations, such as reporting errors.

Future work could benefit from using other indices of climate variability at different time scales, and from including other aspects such as in-farm level management activities. More accurate results and predictions of maize yields can also be obtained if the threshold of skilfulness of the FFT model (ROC>0.5) is increased. However, this would inhibit large part of the analysis, especially at longer lead times, since the FFT models have, on average, ROC scores between 0.63 and 0.72. In addition, this study would substantially benefit from a more detailed analysis of supply and demand dynamics and drivers of maize price in Kenya. Furthermore, testing the proposed methods using different algorithms, crop databases, crop types, and early actions (such as vouchers or in-kind food aid) would provide further insights in the strengths and limitations of the approach. Lastly, in order to produce a robust economic estimation, which would potentially reflect the actual expected costs of ex-ante and -post cash transfer programmes, other information should be taken into account such as operational costs, the precise number of beneficiaries, and maize yield per household.

Providing timely finance prior to a disaster can be more cost-effective than investing in post-disaster expenditures, and may prevent farmers, especially small-scale ones, from falling into poverty. Increasing the productivity and

climate resilience of smallholder farming systems is a great challenge that will be important in determining whether the world succeeds in achieving the post-2015 development agenda, and the Sendai goal of substantially reducing disaster risk. In Kenya, and East Africa in general, yield growth has remained relatively stagnant as population continues to grow rapidly (Funk & Brown, 2009), as predictable droughts become more frequent (Davenport et al., 2018; Funk et al., 2014). As suggested here, developing more proactive disaster mitigation responses should help buffer the impacts of future crop yield deficits. A secondary, but important benefit of such actions might be the reduction of food price volatility. As seen in 2010/11, and to a smaller degree in 2016/17, these price spikes can affect even more fragile pastoral and marginal agro-pastoral households.

5.5 Conclusion

Our study developed a forecast model using FFT for multiple lead times for assessing early warnings of low maize yield based on predictors of climate variability and vegetation coverage. Using this model, we focused on assessing the relative costs of ex-ante and ex-post cash transfer in Kenya. This is a primary step towards the adoption and use of climate information in disaster risk financing and humanitarian early action. In this paper we showed that:

- Overall, FFT models have skill to forecast low maize yields in all five districts. In most cases, we identify some model skill already six months before the start of the harvesting season;
- Across different yield percentiles, districts, and lead times, the FFT models correctly forecast "below yield threshold" 85% of the time. On average, the probability of False Alarms is 49%, but this value decrease towards the end of the maize growing season;
- When assuming a perfect forecast (Hits=100% and False Alarms=0%), cash transfers can be most cost-effective ex-ante at a lead time of 6 months (March).
- Despite uncertainties associated with FFT predictions, we show that ex-ante cash transfers can often be more cost-effective than ex-post cash transfers, especially for the more extreme yield deficits.

Chapter 7

Synthesis and outlook

7.1 Introduction

In response to the limited understanding on links between climate variability and weather-related impacts of both floods and droughts, and the current gap in translating such relationships into impact-based information that can be used as a basis for triggering early action, the main objective of this thesis was:

- *To assess the link between climate variability and weather-related impacts (flood and drought) at the global and regional levels, and to develop impact-based forecast methods that can potentially reduce these impacts through early action.*

The thesis' main objective was achieved by investigating five research questions, previously defined in Chapter 1. In this final chapter, answers to the five research questions are provided. The chapter ends with a discussion of future challenges and avenues of research on the topic of climate variability, impact-based forecasting and early action.

7.2 Key research findings

Research question 1| *What are the links between large-scale climate variability, the occurrence and intensity of extreme rainfall, and anomalies in flood occurrence and damage?*

Using a pan-European case study, Chapter 2 analyses the spatial and temporal influence of climate variability on extreme meteorological and flood events. This is done by investigating the El Niño Southern Oscillation (ENSO), the North Atlantic Oscillation (NAO), and the East Atlantic pattern (EA) during their neutral, positive, and negative phases, to understand their relationships with four flood indicators: Occurrence of Extreme Rainfall, Intensity of Extreme Rainfall, Flood Occurrence, and Flood Damage. Statistical tests such as the T-Test, bootstrapping and field significance are applied to investigate the strengthen and significance of the relationship between the indices of climate variability and the four flood indicators. This chapter pays special attention to assessing relationships between multiple indices of climate variability and flood losses, an avenue of research that has not been widely investigated.

The results show that climate variability has strong links with the four flood indicators. Both positive and negative phases of NAO and EA are associated with more intense and frequent extreme rainfall over large areas of Europe, whereas the effect of ENSO is much smaller. Anomalies in the indicators of occurrence and intensity of extreme rainfall linked to the positive/negative phases of the indices of climate variability can be up to ±100% and ±60%, respectively. At the aggregated pan-European scale, all three indices of climate

variability show significant relationships with Flood Occurrence in one or more phase and/or season, with the strongest link being observed for NAO. Positive and negative phases of NAO are linked with high anomalies in Flood Occurrence in Europe during summer and winter, respectively. In summer, during positive phase of NAO, anomalies in Flood Occurrence are 170% higher than during the neutral phase of NAO. In winter, during the negative phase of NAO, anomalies in Flood Occurrence are on average 70% higher than during the neutral phase of NAO. Anomalies in Flood Damage are linked to all three indices of climate variability, with the strongest anomalies also found in connection with the NAO positive phase in summer (374% higher than during neutral phase). It is shown for the first time that Flood Damage and Flood Occurrence in Europe are strongly associated with climate variability, especially in southern and eastern Europe.

In this study, limitations are also identified. The first one emerges from assessing the impact of ENSO, NAO and EA individually, and not from a multivariate perspective. Past studies have suggested that the indices of climate variability may intensify or reduce each other's influence, and produce combined hydroclimatological effects (Heino et al., 2018; Seager et al., 2010). Therefore, analysing such indices individually may result in the underrepresentation of the relationship between climate variability and the four flood indicators. The second limitation emerges from not examining time-lags between the indices of climate variability and the flood indicators. Given the long memory of atmospheric anomalies, a delayed influence on extreme rainfall (Tabari & Willems, 2018) and on flooding is expected, and therefore, such lagged relationships should be examined. These limitations are addressed in Chapter 3, and in Chapter 4 when investigating the relationship between climate variability and agricultural impacts.

Research question 2| *Can large-scale climate variability be used to forecast flood losses?*

Building upon recommendations from Chapter 2, Chapter 3 examines the role of seasonally lagged and synchronous indices of climate variability on flood losses at the sub-regional European scale. This chapter investigates the relationship between five indices of climate variability - the El Niño Southern Oscillation, the North Atlantic Oscillation, the East Atlantic pattern, East Atlantic/West Russian pattern and the Scandinavian Pattern - and the probability of four classes of flood losses ocurring: Damaging, Low Damaging, Medium Damaging and High Damaging. As well as investigating the likelihood of such classes of flood losses occurring based on indices of climate variability, Chapter 3 assesses whether some of these losses can be predicted one season

ahead. To achieve this, a range of logistic models in combination with a Leave-one out cross validation technique are applied. This analysis aims at providing a better understanding of the combined effect of the indices of climate variability on flood losses while at the same time assessing the predictive skill of such models and indices.

Whilst in Chapter 3 the logistic regressions are unable to predict High Damaging floods based on synchronous indices of climate variability, it is shown that the indices can be used to predict classes of Damaging, Low Damaging and Medium Damaging flood events, mostly in at least 2 out of 4 seasons in all regions of Europe. This study also shows that some of the classes of flood losses can be predicted one season ahead because a lagged relationship may exist between the indices of climate variability and the flood losses in all European sub-regions. It is observed that the probability of classes of flood losses may increase or decrease by up to ±100% in comparison to historical probabilities depending on the phase of the index of climate variability. The negative (positive) phase of the best performing index is often related to an increase (decrease) in the probability of Damaging and Low Damaging floods in comparison with the historical probability in southern and western Europe, and that the opposite is found for northern and eastern Europe. Furthermore, most of the models show improved probability of flood losses when the indices of climate variability are combined and in their extreme phases. For instance, the probability of Low Damaging flood events in southern Europe during winter months can increase when negative EAWR (EAWR = -1) and positive SOI (SOI = +1) are combined and synchronous (92%) relative to probabilities obtained from a simple logistic regression using only EAWR (EAWR = -1; 81%).

In Chapter 3, some avenues for improvement are also suggested, such as exploring relationships between the five large-scale climate variability and impacts through techniques that primarily focus on predictions, such as supervised Machine Learning algorithms. This is further addressed in Chapter 4. Furthermore, to strengthen this analysis, it is suggested that elements of exposure, vulnerability and local weather variability should be included, which play an important role in the socio-economic impacts of floods and droughts. These recommendations are further explored in Chapters 4 and 5.

Research question 3| *Can large-scale climate variability be used to forecast agricultural production and support agricultural management and decision-making?*

Chapter 4 analyses the multiple time-scale relationships between large-scale indices of climate variability and anomalies in crop production at the pan-

European scale. This analysis is uses a supervised Machine Learning algorithm named "Fast-and-Frugal Trees" within each month of the growing season (during different vulnerable stages) of sugar beet. The role of five large-scale indices of climate variability - the El Niño Southern Oscillation, the North Atlantic Oscillation, the East Atlantic pattern, East Atlantic/West Russian pattern and the Scandinavian Pattern - are investigated, with the aim of identifying regions where anomalies in sugar beet production can be forecasted based on such indices. This chapter widely discusses how such impact-based forecasting information could potentially improve the management of the agricultural sector in Europe.

The results in is Chapter 4 shows that by applying the Fast-and-Frugal Trees, high/low classes of sugar beet production could be predicted in 77% of the investigated regions, corresponding to 81% of total European sugar beet production. For nearly half of these regions, such impact-based information is available six or five months before the start of the sugar beet harvesting season, where approximately 44% of the mean annual sugar beet is produced. Chapter 4 finds that winter and spring averages of the indices of atmospheric oscillation can be used as a first indicator of summer harvesting performance. The Fast-and-Frugal Trees models perform more consistently in eastern and western Europe. Chapter 4 also argues that the Fast-and-Frugal Trees may not perform satisfactorily in some regions due to: (a) management activities, such as presence of irrigation, which may inhibit the impacts of unfavourable weather conditions; (b) lack of underlying physical relationships between sugar beet production and the investigated indices of climate variability; and (c) due to limitations in the dataset.

It is suggested that testing the proposed method on other crop production databases and crop types can provide further insights into the strengths and limitations of the approach. Therefore in Chapter 5, these considerations are implemented further to explore the performance of Fast-and-Frugal trees (based on indices of climate variability and vegetation coverage) for predicting maize yields in Kenya.

Research question 4| *How can information about climate variability be used to increase the cost-effectiveness of ex-ante risk financing programmes?*

Chapter 5 evaluates the cost-effectiveness of ex-ante cash transfers during the growing season of maize leveraged by a novel impact-based forecasting model. It compares the costs of ex-ante cash transfers with the costs of ex-post cash transfers after harvesting in five districts in Kenya. First, a forecast model using Fast-and Frugal Trees is developed that unravels early warning relationships

between indices of climate variability (Net Precipitation and the El Niño Southern Oscillation), vegetation coverage (normalized difference vegetation index), and maize yields at multiple lead times before the maize harvesting season. The cost-effectiveness of ex-ante cash transfers during the growing season is evaluated prompted by the expected probabilities of low maize yield that are obtained from the Fast-and-Frugal trees models. These costs are compared with the costs of ex-post cash transfers after harvesting.

Results show that the Fast-and-Frugal Trees models have skill to forecast low maize yields in all five districts, and that in most cases, models have predictive skill already six months before the start of the harvesting season. The model correctly forecasts "below yield threshold" 85% of the time, across different low yield percentiles, districts, and lead times. The models' performance improves towards the end of the growing season driven by a decrease of 29% in the probability of False Alarms. The Fast-and-Frugal Trees models improve with shorter lead times because information concerning climate variability and vegetation coverage during the final months of the growing season is added to the model. When assuming a perfect forecast (Hits = 100% and False Alarms = 0%), cash transfers can be most cost-effective ex-ante at a lead time of 6 months. Moreover, when using actual forecasts based on the Fast-and-Frugal trees predictions, results demonstrate that ex-ante cash transfers can often be more cost-effective than ex-post cash transfers, especially for the more extreme yield deficits (yields that are equal or below the 15% or 20% percentile of the observed maize yield time series). The costs of ex-ante cash transfer for compensating farmers during years of extreme yield deficits can be, on average, 29% and 14% lower than ex-post cash transfers. Consequently, early response can yield significant cost savings.

Chapter 5 highlights that multiple challenges exist for operationalizing cash transfers based on indicators of droughts. For instance, taking adequate actions in response to early warnings of drought risk based on indices of climate variability requires an in-depth understanding of the potential impact and timing of a hazard. Further recommendations on how to reduce risks using impact-based forecasting and assessment are provided in Chapter 6.

Research question 5| *How can the reduction of disaster risks be achieved by improving our understanding and prediction of the impacts associated with large-scale climate variability?*

Globally, the El Niño Southern Oscillation (ENSO) is the most important mode of climate variability, and has been linked with changes in hydrometeorological extremes and corresponding socio-economic impacts at different scales. A good

understanding of risks during ENSO extremes is key for adequate response. Chapter 6 has shown that ENSO may increase the risk of water scarcity and low crop yields globally, and change the probabilities of extreme rainfall, and coastal and river flooding. Moreover, climate forecasts can predict the El Niño Southern Oscillation months in advance, enabling stakeholders to take disaster risk reducing actions. Chapter 6 discusses some examples of organizations that already use ENSO forecasts for reducing risks are provided. For instance, an El Niño contingent insurance product has been developed for the region of Piura (Peru) to compensate firms for lost profits or extra costs likely to occur as a result of floods. Moreover, Chapter 6 acknowledges that some constrains to action still exist to respond to ENSO forecasts such as the uncertainties surrounding ENSO's influence on the likelihood of droughts or floods. Nevertheless, this chapter concludes that ex-ante information regarding the spatial configuration of risk leveraged by impact-based forecasts with long lead times, such as the ones developed in Chapter 2-5, could support a shift towards a more anticipatory and preventative risk management.

This thesis demonstrates several opportunities to reduce the risk of disasters by responding to forecasts of the indices of climate variability. Chapter 2 highlights that the El Niño Southern Oscillation, the North Atlantic Oscillation, and the East Atlantic pattern can be forecasted with varying levels of skill and lead times, and that seasonal risk outlooks could potentially be developed based on forecasted values of the indices of climate variability. The findings of this study, in combination with such risk outlooks, could provide information on whether flood impacts in upcoming seasons are likely to be higher or lower than average, which could be useful for flood disaster preparedness. For example, the European Union's Solidarity Fund, holding €500 million per year to help member states finance disaster losses, is greatly affected by large-scale correlations in flood losses (Jongman et al., 2014). Taking into account some of the long-term forecasting of climate variability anomalies in the design and budgetary planning of international finance mechanisms could reduce the chance of such a fund facing unexpected pay-outs across large regions in Europe, and thereby reduce the chance of fund depletion.

Furthermore, Chapter 3 argues that major floods can be driven by large-scale atmospheric oscillations, and as result such flood events may increase the pressure on trans-national risk reduction and risk transfer mechanisms due to the high interdependencies of flood hazard across European regions. The spatial-temporal information of the probability of flood losses, in combination with average costs of flood events, may be useful for decision-makers to guide flood preparedness actions. Some of the models presented in Chapter 3 may be

transformed into an impact-based flood forecasting system when a relationship between the indices of atmospheric oscillations and flood losses are found either one season ahead, or when the indices of atmospheric oscillation can be predicted at a seasonal lead time or longer. For instance, the ex-ante information regarding the spatial configuration of risk could support insurance or reinsurance companies in allocating and managing portfolios more efficiently in order to comply with the EU solvency requirements, which demands that (re)insurers have adequate reserves for 99.5% of potential loss events (European Parliament and Council, 2009).

Findings of Chapter 4 could support agricultural stakeholders in implementing a large range of actions throughout the growing season based on the provided long lead time impact information. For instance, six months before harvesting, if climatic conditions indicate shortage in production, tactical measures can be taken to increase supplies as follows: (1) better preparation or further investment in responsive irrigation schemes as sugar beet is particularly sensitive to water deficits in early spring (Clarke et al., 1993; Romano et al., 2012); (2) taking measures to prevent freeze damage to crops such as active methods (e.g. adding heat and covering crops) and passive methods (e.g. proper scheduling of planting within the safe freeze-free period) as night frost in spring can damage sugar beet and delay seed germination (Pidgeon et al., 2001; Snyder & de Melo-Abreu, 2005); and (3) before planting, producers could decide to reduce their financial losses by purchasing appropriate crop insurance products against deviations from their long-term yields. Additional actions are proposed for shorter lead times that can strengthen the European agricultural climate resilience.

Chapter 5 provides recommendations on ways to potentially increase the efficiency of existing cash transfer systems. Currently, the Kenya Hunger Safety Net Programme triggers two types of cash transfers (standard and emergency payments) based on a single satellite Vegetation Condition Index (VCI). The cash transfer do not depend on field assessment, and emergency payments are made monthly in any sub-county when the VCI hits the scale up threshold (from moderate to extreme drought), and payments are suspended when the threshold is no longer reached for that month (National Drought Management Authority, 2016). The use of a single drought indicator may not provide a comprehensive assessment of drought impact, and can occasionally trigger payments in situations where drought conditions are not evolving (National Drought Management Authority, 2016). The National Drought Management Authority could potentially improve the reliability of cash transfers and

anticipate pay-outs by including other drought early warning indicators, such as the ones adopted in this investigation.

7.3 Future challenges and avenues of research

This thesis advances the understanding on links between climate variability and weather-related impacts of both floods and droughts, which can be used for generating impact-based forecasting and triggering early action. The outcomes of this thesis highlighted some key challenges and topics that require further investigation in future research.

7.3.1 Climate variability and impacts

Improving our understanding of the impacts of climate variability requires more investigation on the dynamics of climate variability

Despite an increased understanding of the dynamics and the improved "forecastability" of indices that represent climate variability, uncertainties regarding their physical mechanisms and expected outcomes still remain. Therefore, further research is required to enhance the understanding of the physical processes that cause climate variability, both for the current climate and under future climate scenarios. For instance, a recent study (Huang et al., 2018) investigated NAO variability under various climate forcings, and concluded that the effects of uniform sea surface temperature warming and direct CO_2 radiative forcing could enhance westerly winds at mid-high latitudes, which intensifies NAO variability. This study also suggests that changes in meridional temperature gradient and in westerly wind in response to changes in sea surface temperature patterns are not uniform among the models. This indicates that the responses of NAO to sea surface temperature alterations is still unclear (Huang et al., 2018). Furthermore, despite progress in understanding ENSO dynamics in the past decade, ENSO's characteristics have been changing during the last millennium (Cobb et al., 2003;Trenberth & Stepaniak, 2001), which may be due to the combination of its natural variability and anthropogenic forcing (Yeh et al., 2018). Moreover, some climate models suggest that ENSO teleconnections will change because of anthropogenic forcing, while other research suggests that changes in ENSO teleconnections in a warmer world are still unclear (Cai et al., 2014, 2015; Collins et al., 2010; Dommenget & Yu, 2017). Consequently, reducing uncertainties in the forecasts of indices of climate variability is intrinsically aligned with a better understanding of its physical processes.

Improving our understanding on the impacts of climate variability requires better data and a thorough investigation on the relationships between human and natural systems

Large-scale climate variability and hydrometeorological hazards only partly explain in flood and drought risk. This is because the severity of disasters and their consequent losses not only depends on the intensity and frequency of hazards but are strongly influenced by the mutual interactions between humans and the natural systems. Socioeconomic development plays a major role in flood and drought risk, and alters the relationship between hydrometeorological hazards and their resulting impacts (Jongman et al., 2015). While better and more granular flood and drought impact datasets are needed for better assessing links between climate variability and impacts, a more comprehensive understanding of the interactions between human responses to the natural system is also required for a more realistic representation of disaster risks. Recent studies have shown that flood and drought risks are shaped by a range of nonlinear and complex relationships between humans and the natural system, such as risk perception, adaptation decisions, trust in authorities and awareness (Aerts et al., 2018; Di Baldassarre et al., 2018; Veldkamp et al., 2017; Wens et al., 2019). Therefore, understanding trends in flood and drought impacts can only be partially explained by estimating hydrometeorological changes. Overcoming these limitations would enable a better understanding of how the variability in the climate may unfold into socioeconomic impacts, and therefore novel modelling approaches such Agent-Based Modelling that include human responses to risks should be further developed in the future.

7.3.2 Impact-based forecasting

Impact-based forecasting can be enhanced by improving the forecasting skill and lead time of indices of climate variability

Since seasonal forecasts only have moderate levels of skill in predicting hydrometeorological conditions, it is important to explore different approaches to use variables of seasonal forecasts with improved skill, such as those of large-scale climate variability (Ceglar et al., 2017). For instance, improvements in seasonal forecasting systems have allowed skilful predictions of the winter NAO and ENSO to be extended to more than a year ahead (Dunstone et al., 2016; Gonzalez & Goddard, 2016), while EA summer and autumn anomalies have been hindcasted with a lead time of 1 to 2 months (Iglesias et al., 2014). This is leveraged by a substantial progress in understanding potential sources of predictability coupled with model improvements. Yet, producing a reliable forecast of the indices of large-scale climate variability is still challenging. For instance, in 2014 the National Oceanic and Atmospheric Administration Climate Prediction Center issued a forecast in early July that indicated close to 80% chance of a strong El Niño forming in that year during the Northern Hemisphere

fall. However, sea surface temperature anomalies began to decay, and seasonal forecasts became increasingly uncertain by the end of 2014 (McPhaden, 2015). Furthermore, NAO seasonal predictability is limited to winter and spring months only (Dunstone et al., 2016; Li, 2010), while EA predictability is limited to summer and autumn months (Iglesias et al., 2014; Wulff et al., 2017). Seasonal predictions of the EAWR and SCA are currently unavailable. Therefore, generating and extending the predictability of the indices of climate variability would allow for seasonal predictions of teleconnections and impacts, which could potentially be developed into impact-based forecasting. Therefore, improving the forecasting skill of indices of climate variability and making it available at longer lead times it is an important step to achieve impact-based forecasting.

Impact-based forecasting can be harnessed by combining the forecast of indices of climate variability with socioeconomic impacts of floods and droughts

Further value could be added to the forecasts of indices of climate variability by combining them with information on the resulting flood and drought losses, thereby enabling the seasonal forecasting of those socioeconomic impacts. Such seasonal outlooks could provide information on emerging flood and drought seasonal impacts, which could be useful for flood and drought risk preparedness. Ex-ante information regarding the spatial configuration of risk could support a more efficient allocation of financial resources and actions, and the development of disaster financing schemes in developed and developing countries that could alleviate the abrupt financial burden of disasters. Therefore, future research should focus on further understanding the link between indices of large-scale climate variability and the socioeconomic impact of floods and droughts, which would allow combining such information with skilful forecasts to develop seasonal flood and drought risk outlooks. Risk information with long lead times can support a shift towards a more anticipatory and preventative risk management, as urged by the Sendai Framework for Disaster Risk Reduction (UNISDR, 2015b).

7.3.3 Early Action

Leveraging early action requires exploring the benefits of acting early

Despite advances in early warning systems, forecast information is rarely used for triggering and financing early actions. Scaling up early actions, and overcoming the institutional and financial barriers to actions based on forecasts, requires an understanding of the potential benefits associated with appropriate early interventions while avoiding impacts. Despite this need, assessments of the costs and benefits of ex-ante and ex-post actions are largely

missing in the literature. Therefore, more research should be performed to assess the incentives for early action, and to better guide the understanding of the benefits of acting upon emerging drought and flood risks in association with forecasting model uncertainties. Throughout this thesis, it was argued that providing timely finance prior to a disaster can be more cost-effective than investing in post-disaster expenditures. Such cost-effectiveness was shown despite model uncertainties and price variations in an exercise in which farmers could be compensated for expected failed yields during the growing season of maize. These findings suggest that early response could yield significant cost savings, and can potentially increase the effectiveness of existing early action systems. However, the primary limitation of this investigation was to assume that prices are solely dependent on the national supply of maize, when in reality prices are associated with a combination of factors including supply and demand in neighbouring regions and global price shocks (Brinkman et al., 2010). Therefore, the macro spatial scale dynamics of price variability, such as the risk of multiple breadbasket failures (Janetos et al., 2017), should be further investigated for a more realistic estimation of the cost-effectiveness of early actions. Furthermore, cost-effectiveness of early action analysis could be further performed for other (multi-)hazards. The relative importance of such investigations lies primarily in the fact that humanitarian needs are often heavily underfunded (UNOCHA, 2018), and therefore finding ways to improve the cost-effectiveness of existing early action budgets would allow for maximizing benefits while avoiding human suffering and losses. As suggested in this thesis, developing more proactive disaster preparedness and prevention could help buffer the impacts of future risks.

Leveraging early action requires mainstreaming disaster risk reduction into flood and drought risk management and policies

The indices of climate variability investigated in this thesis have been linked to socioeconomic impacts in large parts of the world, by increasing the likelihood of extreme events such as floods and droughts. Climate forecasts can predict some of these indices several months in advance, and therefore impact-based forecasts can be produced. Some governments and humanitarian organizations are increasingly taking precautionary measures to reduce the risk of disaster based on these forecasts. Consequently, there are more and more examples of good practices of actions taken to reduce the socioeconomic burden of extreme events based on impact-based forecasts, such as the pilots of the forecast-based financing projects established by the Red Cross Red Crescent (Coughlan De Perez et al., 2015) and the Food and Agricultural Organization (FAO, 2019). Consequently, an enhanced understanding of current and future (multi-)risks, at

all scales, is needed to foster improvement in the management of hazards driven by climate variability, and to mobilize innovation and finance that enables risk-informed sustainable development. Multiple challenges can be observed for operationalizing forecast-based early action for droughts and floods. Taking actions in response to early warnings of drought and flood risks based on indices of climate variability requires an in-depth understanding of the potential impact, scale, aid-triggering thresholds, severity and timing of a disaster (Wilkinson et al., 2018). Given these challenges, communicating and mobilizing funds to mitigate climate variability-related impacts remains difficult, which includes translating uncertain early warning information into multiple and flexible early actions. However, there has been a growing interest from development agencies, governments and the humanitarian community in mainstreaming disaster risk reduction actions for sustainable development by tackling underlying risk factors before a disaster, even at the cost of "acting in vain". The potential to act in vain based on forecasts, and the lack of measured benefits of early action, are important political disincentives to integrate forecast-based actions in international development financing and national DRR strategies (Wilkinson et al., 2018). Although "False Alarms" are often not appreciated, such early actions offer opportunity for building up risk awareness and can provide benefits even if a disaster does not materialise. Currently, there is a strong will to institutionalise predictable and faster early action in humanitarian responses and government risk-financing (Wilkinson et al., 2018). Developing standard operating procedures with an agreed set of actions, thresholds and funding will increase confidence and mainstream forecast-based actions. Therefore, further research should be carried out to identify and comprehend the underlying interests and incentives that are relevant to stakeholders if early warning early action is to become best practice.
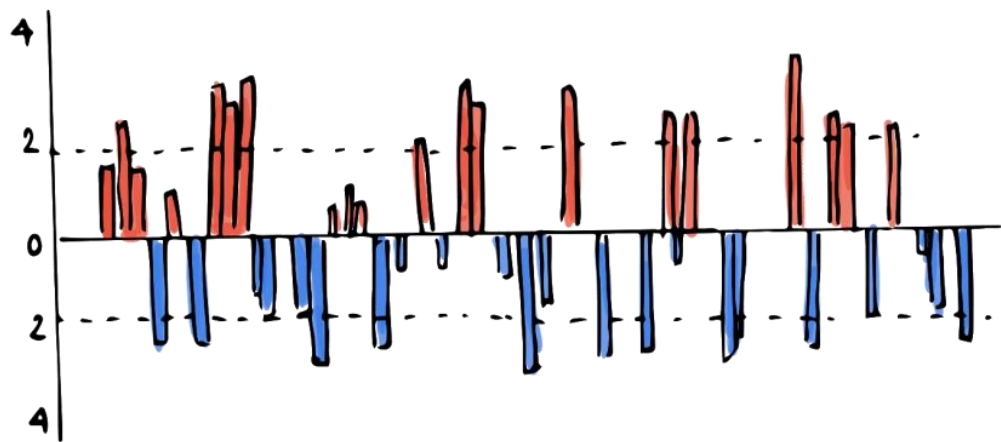
Chapter 6

Achieving the reduction of disaster risk by better predicting impacts of El Niño and La Niña

Abstract

Extreme phases of the El Niño Southern Oscillation (ENSO) show relationships with economic damages due to disasters worldwide. Climate forecasts can predict ENSO months in advance, enabling stakeholders to take disaster risk reducing actions. An understanding of risks during ENSO extremes is key for adequate response. Here, we review the effects of ENSO on disaster risks, including droughts and floods. We show that ENSO may increase the risk of water scarcity and low crop yields globally, and change the probabilities of extreme rainfall, and coastal and river flooding. We provide recommendations on how to reduce risks using ENSO forecasts.

6.1 Introduction

The recent 2015-16 El Niño event was one of the strongest ever recorded. El Niño conditions began to emerge in mid-2014 and intensified throughout 2015. El Niño conditions contributed to severe droughts and water shortages in Africa for two consecutive years, and increased food insecurity and famine (Funk et al., 2019; Heino et al., 2018). Donors, such as the European Union, raised funds to more than €500 million to address the impacts related to the ensuing drought and water shortage crisis in East Africa (Francis, 2017). Simultaneously, the 2015-16 El Niño contributed to severe flooding in the northwest of Latin America, forcing the evacuation of more than 150,000 people in Paraguay, Argentina, Brazil and Uruguay (BBC News, 2015).

El Niño conditions occur when there are unusually warm oceanic and atmospheric conditions in the tropical Pacific. This can cause the trade winds, that usually blow towards Indonesia and Australia, to slow down or even reverse direction, allowing the warmer water to spread east towards the South American coast (Funk et al., 2019). As opposed to El Niño, the so-called La Niña emerges when unusually cold oceanic and atmospheric conditions are observed in the eastern tropical Pacific. El Niño and La Niña events occur roughly every two to seven years. These oceanic and atmospheric variations are known as the El Niño Southern Oscillation (ENSO), which is the dominant driver of interannual variability in global climate conditions (McPhaden, 2015). ENSO can affect weather patterns worldwide through so-called "teleconnections" (Santoso, Mcphaden, & Cai, 2017). In turn, these changes in weather patterns can influence the frequency and severity of extreme hazards, including droughts and floods. The impacts of ENSO on floods and droughts are well-studied at local and regional scales, while increased attention has recently been placed on understanding of how ENSO impacts societies at the global scale (Emerton et al., 2017; Heino et al., 2018; Muis et al., 2018; Veldkamp et al., 2015; Ward et al., 2015).

Over the past decades, the skill of ENSO predictions has improved considerably. The 2015-2016 event was predicted months in advance (Bureau Of Meteorology, 2017). In general, ENSO events can now be predicted with reasonable skill at lead times up to 14 months (Gonzalez & Goddard, 2016). Reliable forecasts enable the prioritization of risk reduction efforts in the most affected regions ahead of extreme events, and allow for early warning and action by local governments and non-governmental organizations, such as the Red Cross and Red Crescent Climate (Coughlan De Perez et al., 2015), especially when there is a good understanding of the likelihood of societal impacts that may be influenced by ENSO.

Since such impact-based information with long lead times may also substantially support the shift towards more anticipatory and preventative risk management, as urged in several international frameworks such as the Sendai Framework for Disaster Risk Reduction (UNISDR, 2015b), in this article we summarize recent research on the global effects of ENSO on disaster risk. This is especially timely given that current forecasts give a 76% chance of El Niño conditions developing again in the boreal spring of 2019 (IRI, 2019).

6.2 Results: increased likelihood of disaster risk due to El Niño and La Niña events

6.2.1 Drought and water scarcity

The connection between ENSO events and rainfall deficits, droughts, and water scarcity is increasingly well understood (Dilley & Heyman, 1995). Connections between ENSO and low river flows exist in northern America (Ryu et al., 2010), Southeast Asia (Lü et al., 2011), Southern Africa (Richard et al., 2001), and Australia (Chiew et al., 1998). Worldwide, disasters triggered by droughts occur twice as often during the second year of an El Niño event than during other years, especially in Southern Africa and Southeast Asia (Richard et al., 2001). Regions where rainfall and hydrological extremes are influenced by ENSO (Dai & Wigley, 2000; Dettinger & Diaz, 2000) also show a connection between ENSO and annual total water availability or water scarcity conditions. In these areas, rainfall deficits during an ENSO event feed droughts, which can result in water scarcity events if consumptive demands outweigh the available water resources (Dilley & Heyman, 1995). In result, regional water scarcity conditions become more extreme under El Niño and La Niña phases for almost one-third of the global land area (Veldkamp et al., 2015).

6.2.2 Food security and agricultural production, with cascading effects on livelihoods

ENSO influences global agriculture in several ways, including changes in hydrometeorological conditions (Figure 6.1) (Guimarães Nobre et al., 2017; Ward et al., 2010) and climate extremes (Trenberth & Fasullo, 2012), which may affect crop yields (Heino et al., 2018) and export prices.

The global mean yields of major crops, such as maize, rice, and wheat, are likely to be below normal during both El Niño and La Niña conditions (-4.0 to -0.2%). However, El Niño events are linked to increased soybeans yields (+2.9 to +3.5%), especially in the United States of America and Brazil, where most of the global soybean is currently produced (Iizumi, Luo, et al., 2014). Furthermore, a

recent study has found that ENSO may affect both negatively and positively crop productivity in 28% of global cropland area, inhabited by 1.5 billion people (Heino et al., 2018).

ENSO can affect food security and agricultural production, with cascading effects on livelihoods and health. For instance, the rapid shift between El Niño and La Niña conditions in 2016 intensified the shortage of rainfall, driving major hydrological crises over Eastern and Southern Africa, where 29 million people were faced with food insecurity due to the combination of drought exacerbated conditions (Funk et al., 2019). Furthermore, recent work has shown that the 2015–2016 El Niño event may have triggered a series of global disease outbreaks in areas affected by ENSO teleconnections (Anyamba et al., 2019).

6.2.3 Extreme rainfall and river flooding

El Niño or La Niña intensify extreme rainfall mostly in boreal winter, and least during summer seasons (Sun et al., 2015). The deviations from normal conditions are often asymmetric, which means that most parts of the world experience higher or lower extremes for either El Niño or La Niña conditions. Extreme rainfall during ENSO conditions can be up to 50% higher compared to neutral conditions. Extremes are more severe in the boreal winter during El Niño, mainly in central and southern North America, southeast and northeast China, and southeast South America, and during La Niña in western Pacific areas (Sun et al., 2015).

ENSO exerts a significant influence on annual floods in river basins covering over a third of the world's land surface (Ward et al., 2014). While, about one-fifth of the global land surface is more likely to experience abnormally high river flow during El Niño conditions, especially in the tropics (Emerton et al., 2017). As with extreme precipitation, these deviations from normal conditions are often asymmetric between ENSO phases (Lee et al., 2018). ENSO also influences the duration of flooding, with flood duration appearing to be even more sensitive to ENSO than is the case for flood frequency (Ward, Kummu, & Lall, 2016). In terms of economic damage, El Niño years are associated with anomalies in expected annual urban damage in 29% of the Earth's land surface, with significantly higher urban damage for 10% and lower damage for 19%. During La Niña years, significant anomalies are simulated across 23% of the Earth's land surface, with higher damage for 10% and lower damage for 13% (Ward et al., 2014).
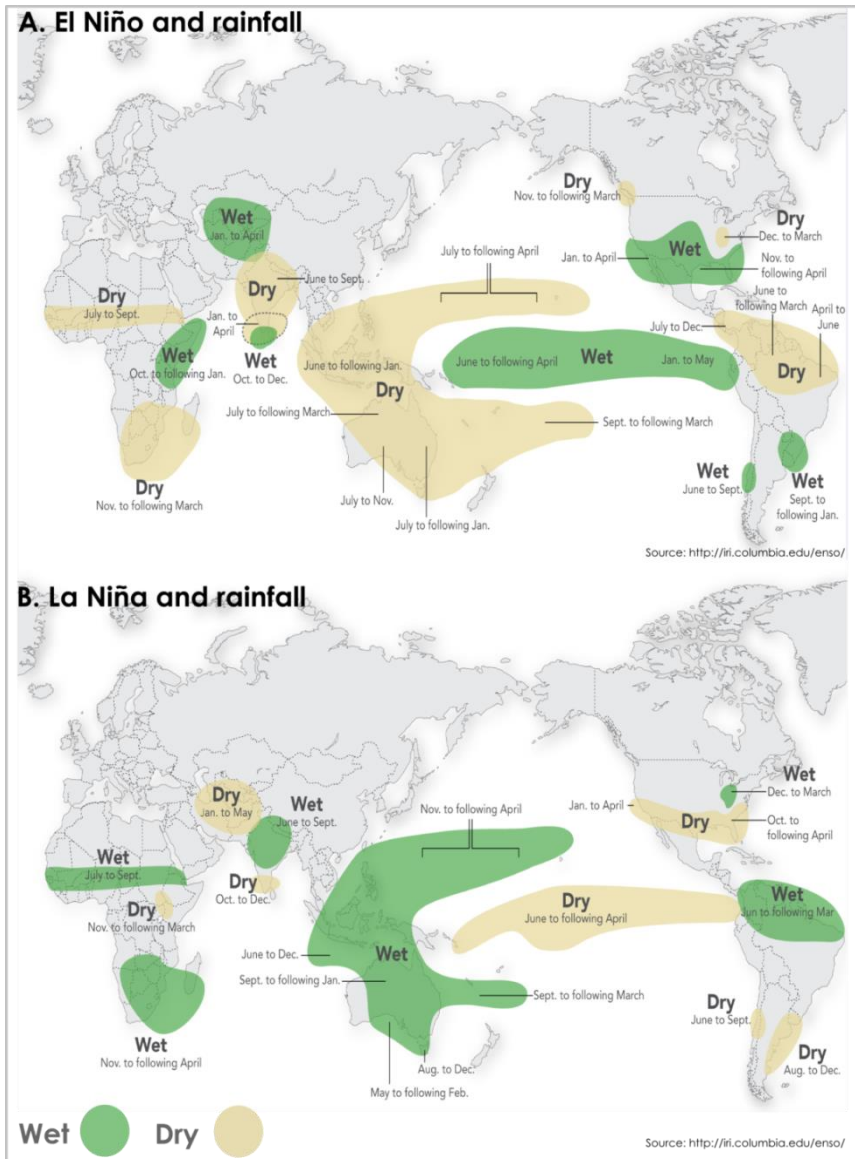
Figure 6.1 Typical changes in rainfall observed during (A) El Niño and (B) La Niña episodes. Areas in green or yellow are likely to become wetter or dryer than normal during the indicated months. Source: http://iri.columbia.edu/enso/

6.2.4 Coastal hazards

ENSO events have been linked with increased probabilities of beach erosion and coastal flooding around the world. Two mechanisms cause this (Muis et al., 2018): (1) warmer ocean temperatures and changes in ocean circulation can

induce an increase in mean sea level; and (2) perturbations of the tropical and subtropical atmospheric circulation influence storm activity around the world. Increases in mean sea level particularly affect the tropical Pacific (Muis et al., 2018). El Niño and La Niña conditions result in changes of mean sea level of ± 20-30 cm (Becker et al., 2012). During the five largest El Niño events between 1979 and 2012, mean sea levels along the North American west coast were on average 0.11 m higher (Barnard et al., 2015). In regions with a large change in mean sea-level and a small tidal range, these variations in mean sea level can have a significant influence on the occurrence of extremes (Muis et al., 2018). ENSO events can also induce changes in tropical cyclone activity (Saunders et al., 2000), as well as extra-tropical cyclone activity (Eichler & Higgins, 2006). Such changes in storm activity can have an impact on the occurrences of storm surge and waves. A recent study has shown that ENSO has a significant but small effect on the number of people potentially exposed to coastal flooding at the globally aggregated scale (Muis et al., 2018).

6.3 Policy implications and recommendations

6.3.1 Responding to ENSO forecasts

The likelihood of extreme hazards can vary from year to year due to ENSO. As ENSO can be predicted with reasonable skill, individuals, organizations, and governments can make use of such ENSO forecasts to take actions that reduce the impacts of extreme hazards. In Figure 6.2, we show the global probabilities of below- and above-normal precipitation for the 2019 boreal spring season based on ENSO forecasts.

Governments are increasingly interested in using seasonal forecasts of ENSO to reduce disaster risk. Peru provides a prime example. In the past, El Niño events have contributed to huge economic losses. For example, during the 1982-83 El Niño disaster losses exceeded 2 billion USD (Lagos & Buizer, 1992) and during the 1996-97 El Niño losses exceeded 3.5 billion USD (UNISDR, 2015a). This is because Peru's main economic activities (e.g. fishing, agriculture and tourism), are heavily exposed to the effects of El Niño. In response to the forecast of a strong ENSO in 2015, the Peruvian government declared a 60-day state of emergency, and spent around 20 million USD for flood and drought prevention. This included building reservoirs in areas predicted to be affected by drought, dredging and deepening rivers in flood-prone areas, and providing agricultural insurance for farmers (Hillier & Magrath, 2016). In addition, an El Niño contingent insurance product has been developed for the region of Piura to compensate firms for lost profits or extra costs likely to occur as a result of floods (Cavanaugh et al., 2010; Coughlan De Perez et al., 2015). Lastly, to reduce the impacts of heavy rains, the Peruvian Red Cross has defined a

comprehensive set of early actions based on ENSO forecasts,, which are triggered when an ENSO-based threshold is met (German Red Cross, 2016).
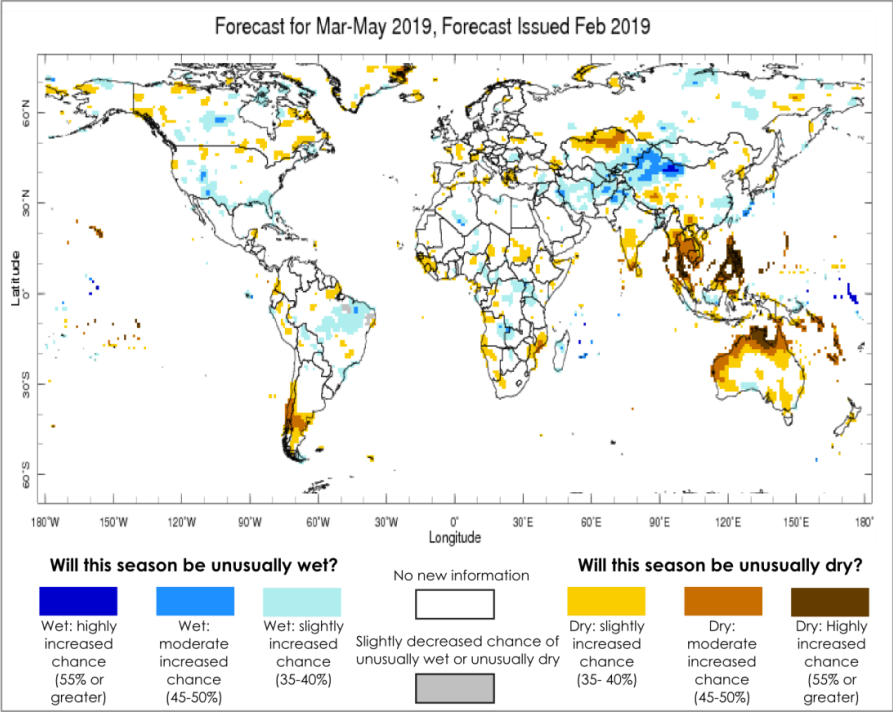
Figure 6.2 This map shows the likelihood that total 3-month precipitation will be unusually high or low between March and May 2019. Source: http://iri.columbia.edu/enso/

Similar strategies are being implemented in Africa, where ENSO forecasts are used to assist agricultural producers to select crops most likely to be successful in the coming growing season (Tall, Jay, & Hansen, 2012). At the same time, crop insurance systems based on ENSO forecasts are becoming more established. An example is the African Risk Capacity, an index-based insurance mechanism for infrequent, severe drought events (African Risk Capacity, 2019). Early warning systems, such as the Famine Early Warning System, are providing outlooks that help governments and non-governmental organizations to foresee humanitarian crises (Funk et al., 2019) and better plan for mitigating the upcoming risks.

6.3.2 Challenges

Despite an increased understanding of ENSO and improvements in ENSO forecast skill, its socioeconomic impacts continue to surprise the world (McPhaden, 2015). Several constrains to action still exist for those who wish to respond to ENSO forecasts. First, we need to improve our understanding of ENSO dynamics and likelihood. For instance, in 2014 the National Oceanic and Atmospheric Administration Climate Prediction Center issued a forecast in early July that indicated close to 80% chance of a strong El Niño forming in that year during the Northern Hemisphere fall. However, sea surface temperature anomalies began to decay, and seasonal forecasts became increasingly uncertain by the end of 2014 (McPhaden, 2015). Moreover, uncertainties surrounding ENSO's influence on the likelihood of droughts or floods are high. Each ENSO event is unique and can have a different signature. For instance, during the strong 2015-16 El Niño, several countries took preparedness measures for expected flooding. While Peru experienced severe flooding, no floods were registered in other locations with an elevate probability of flooding, such as Japan (Emerton et al., 2017). Second, we need to develop a better understanding of how ENSO extremes may unfold into socioeconomic impacts. This is due to the fact that the severity of these disasters and their consequent losses not only depends on the intensity and frequency of hazards, but on the mutual interactions between social and physical systems (Di Baldassarre et al., 2015). Third, we need to improve our understanding on the influence of climate change on ENSO dynamics given that the changing climate may also have an effect on the frequency and strength of ENSO events (Cai et al., 2014). Hence, it is important to enhance our knowledge of how ENSO may respond to climate change in the future.

Given these challenges, communicating and mobilizing funds to mitigate ENSO-related impacts remains difficult, which includes translating uncertain early warning information into multiple and flexible early actions. However, in response to the growing interest in forecasts from development agencies, governments and the humanitarian community (Tozier de la Poterie et al., 2018), there has been an emerging literature on ways to 'automatically' trigger early action based on forecast systems, using predetermined thresholds. For instance in 2015, based on an El Niño forecast, funds were released through the World Food Program for Zimbabwe and Guatemala to help both countries to reduce the negative consequences of droughts (World Food Programme, 2016). Furthermore, since mid-2015, the Central Emergency Response Fund has allocated 117.5 million USD to 19 countries for early action in response to disasters associated with El Niño. Reflecting recent pledges and new funding requests of a total of 5 billion USD by twenty-three countries, the funding gap in 2016 was almost 3.1 billion USD (UNOCHA, 2016b). Ex-ante information

regarding the spatial configuration of risk could support a more efficient allocation of financial resources and actions, and the development of disaster financing schemes that could alleviate the abrupt financial burden of disasters. For instance, a recent study showed that ex-ante cash transfers before a drought can be more cost-effective than ex-post compensations based on indicators of climate variability, including ENSO (Guimarães Nobre et al., 2019).

6.4 Conclusions

ENSO events have been linked to high economic damages in large parts of the world, by increasing the likelihood of extreme events such as floods and droughts. Climate forecasts can predict ENSO several months in advance, and some governments and humanitarian organizations are increasingly taking precautionary measures to reduce disaster risks based on these forecasts. To take adequate action requires an understanding of the hotspots of risks during El Niño and La Niña events. There are more and more examples of good practices of actions taken to reduce the socioeconomic burden of extreme events based on ENSO forecasts, such as the ones carried in Peru. Consequently, an enhanced understanding of current and future risks, at all scales, is needed to foster improvement in the management of ENSO-related hazards, and to mobilize innovation and finance that enable risk-informed sustainable development. However, several constrains to action still exist for those who wish to respond to ENSO forecasts, such as the limited understanding of ENSO dynamics; the relationship between ENSO extremes and socioeconomic impacts; and the influence of climate change on future ENSO extremes. Nevertheless, we believe that ex-ante information regarding the spatial configuration of risk leveraged by impact-based forecasts with long lead times can support a shift towards a more anticipatory and preventative risk management, as urged by the Sendai Framework for Disaster Risk Reduction.

References

Aerts, J. C. J. H., Botzen, W. J., Clarke, K. C., Cutter, S. L., Hall, J. W., Merz, B., … Kunreuther, H. (2018). Integrating human behaviour dynamics into flood disaster risk assessment. *Nature Climate Change*, *8*(3), 193–199. https://doi.org/10.1038/s41558-018-0085-1

Aerts, J. C. J. H., Lin, N., Botzen, W., Emanuel, K., & de Moel, H. (2013). Low-Probability Flood Risk Modeling for New York City. *Risk Analysis*, *33*(5), 772--788. https://doi.org/10.1111/risa.12008

African Risk Capacity. (2019). African Risk Capacity: Transforming disaster risk management & financing in Africa. Retrieved from http://www.africanriskcapacity.org/

Alfieri, L., Burek, P., Dutra, E., Krzeminski, B., Muraro, D., Thielen, J., & Pappenberger, F. (2013). GloFAS-global ensemble streamflow forecasting and flood early warning. *Hydrology and Earth System Sciences*, *17*(3), 1161. https://doi.org/10.5194/hess-17-1161-2013

Alinovi, L., D'Errico, M., Mane, E., & Romano, D. (2010). Livelihoods strategies and household resilience to food insecurity: An empirical analysis to Kenya. *Promoting Resilience through Social Protection in Sub-Saharan Africa*, 28–30.

Álvarez-García, F. J., OrtizBevia, M. J., Cabos, W., Tasambay-Salazar, M., & RuizdeElvira, A. (2018). Linear and nonlinear links of winter European precipitation to Northern Hemisphere circulation patterns. *Climate Dynamics*, 1–23. https://doi.org/https://doi.org/10.1007/s00382-018-4531-6

Amissah-Arthur, A., Jagtap, S., & Rosenzweig, C. (2002). Spatio-temporal effects of El Nino events on rainfall and maize yield in Kenya. *International Journal of Climatology*, *22*(15), 1849–1860. https://doi.org/10.1002/joc.858

Anand, S., Anderson, J., Guttmann, R., Lee, R., Sanford, C., & Yang, M. (2011). Moving Toward a Monetary Union and Forecast-Based Monetary Policy in East Africa. *Journal of Economic Statistics*, *23*(1), 6--7.

Anyamba, A., Chretien, J.-P., Britch, S. C., Soebiyanto, R. P., Small, J. L., Jepsen, R., … others. (2019). Global Disease Outbreaks Associated with the 2015--2016 El Niño Event. *Scientific Reports*, *9*(1), 1930. https://doi.org/https://doi.org/10.1038/s41598-018-38034-z

Apel, H., Thieken, a. H., Merz, B., & Blöschl, G. (2004). Flood risk assessment and associated uncertainty. *Natural Hazards and Earth System Science*,

4(2), 295–308. https://doi.org/10.5194/nhess-4-295-2004

Arnal, L., Cloke, H. L., Stephens, E., Wetterhall, F., Prudhomme, C., Neumann, J., … Pappenberger, F. (2018). Skilful seasonal forecasts of streamflow over Europe? *Hydrology and Earth System Sciences*, *22*(4), 2057--2072. https://doi.org/10.5194/hess-22-2057-2018

Bailey, R. (2012). *Famine early warning and early action: The cost of delay*. Chatham House London.

Barlow, M., Nigam, S., & Berbery, E. H. (2001). ENSO, Pacific decadal variability, and U.S. summertime precipitation, drought, and stream flow. *Journal of Climate*, *14*(9), 2105–2128. https://doi.org/https://doi.org/10.1175/1520-0442(2001)014<2105:EPDVAU>2.0.CO;2

Barnard, P. L., Short, A. D., Harley, M. D., Splinter, K. D., Vitousek, S., Turner, I. L., … Heathfield, D. K. (2015). Coastal vulnerability across the Pacific dominated by El Niño/Southern Oscillation. *Nature Geoscience*, *8*(10), 801–807. https://doi.org/10.1038/ngeo2539

Barnston, A. G., & Livezey, R. E. (1987). Classification, seasonality and persistence of low-frequency atmospheric circulation patterns. *Monthly Weather Review*, *115*(6), 1083–1126. https://doi.org/https://doi.org/10.1175/1520-0493(1987)115<1083:CSAPOL>2.0.CO;2

Barredo, J. I. (2007). Major flood disasters in Europe: 1950-2005. *Natural Hazards*, *42*(1), 125–148. https://doi.org/10.1007/s11069-006-9065-2

Barredo, J. I. (2009). Normalised flood losses in Europe: 1970–2006. *Natural Hazards and Earth System Science*, *9*(1), 97–104. https://doi.org/10.5194/nhess-9-97-2009

Barron, J., Rockström, J., Gichuki, F., & Hatibu, N. (2003). Dry spell analysis and maize yields for two semi-arid locations in east Africa. *Agricultural and Forest Meteorology*, *117*(1–2), 23–37. https://doi.org/10.1016/S0168-1923(03)00037-6

Bartholmes, J. C., Thielen, J., Ramos, M. H., & Gentilini, S. (2009). The european flood alert system EFAS - Part 2: Statistical skill assessment of probabilistic and deterministic operational forecasts. *Hydrology and Earth System Sciences*, *13*(2), 141--153. https://doi.org/10.5194/hess-13-141-2009

Baruth, B., Royer, A., Klisch, A., & Genovese, G. (2008). The use of remote sensing within the MARS crop yield monitoring system of the European

Commission. *Proceedings ISPRS*, *27*(January 2015), 935–940. Retrieved from http://www.isprs.org/proceedings/XXXVII/congress/8_pdf/10_WG-VIII-10/02.pdf

BBC News. (2015). Flooding 'Worst in 50 Years', as 150,000 Flee in Paraguay, Argentina, Brazil and Uruguay.". Retrieved from https://www.bbc.com/news/world-latin-america-35184793

Becker, M., Meyssignac, B., Letetrel, C., Llovel, W., Cazenave, A., & Delcroix, T. (2012). Sea level variations at tropical Pacific islands since 1950. *Global and Planetary Change*, *80–81*, 85–98. https://doi.org/10.1016/j.gloplacha.2011.09.004

Bischiniotis, K., Van Den Hurk, B., Jongman, B., Coughlan De Perez, E., Veldkamp, T., De Moel, H., & Aerts, J. (2018). The influence of antecedent conditions on flood risk in sub-Saharan Africa. *Natural Hazards and Earth System Sciences*, *18*(1), 271--285. https://doi.org/10.5194/nhess-18-271-2018

Bladé, I., Liebmann, B., Fortuny, D., & Oldenborgh, G. Van. (2012). *The summer North Atlantic Oscillation (SNAO) in CMIP3 models and related uncertainties in precipitation projections in the Euro-Mediterranean region*. *14*, 11846.

Blöschl, G., Hall, J., Parajka, J., Perdigão, R. A. P., Merz, B., Arheimer, B., ... others. (2017). Changing climate shifts timing of European floods. *Science*, *357*(6351), 588–590. https://doi.org/10.1126/science.aan2506

Bouma, M. J., Kovats, R. S., Goubet, S. A., Cox, J. S., & Haines, A. (1997). Global assessment of El Niño's disaster burden. *Lancet*, *350*(9089), 1435–1438. https://doi.org/10.1016/S0140-6736(97)04509-1

Bouwer, L. M., Crompton, R. P., Faust, E., Höppe, P., & Pielke, R. A. (2007). Confronting disaster losses. *Science*, *318*(5851), 753--753. https://doi.org/10.1126/science.1149628

Bouwer, L. M., Vermaat, J. E., & Aerts, J. C. J. H. (2006). Winter atmospheric circulation and river discharge in northwest Europe. *Geophysical Research Letters*, *33*(6), 2–5. https://doi.org/10.1029/2005GL025548

Bouwer, L. M., Vermaat, J. E., & Aerts, J. C. J. H. (2008). Regional sensitivities of mean and peak river discharge to climate variability in Europe. *Journal of Geophysical Research*, *113*(D19), D19103. https://doi.org/10.1029/2008JD010301

Brinkman, H.-J., de Pee, S., Sanogo, I., Subran, L., & Bloem, M. W. (2010). High Food Prices and the Global Financial Crisis Have Reduced Access to Nutritious Food and Worsened Nutritional Status and Health. *Journal of Nutrition*, *140*(1), 153S--161S. https://doi.org/10.3945/jn.109.110767

Brönnimann, S. (2007). Impact of El Niño-Southern Oscillation on European climate. *Rev. Geophys.*, *45*(3). https://doi.org/https://doi.org/10.1029/2006RG000199

Brown, I. (2013). Influence of seasonal weather and climate variability on crop yields in Scotland. *International Journal of Biometeorology*, *57*(4), 605–614. https://doi.org/https://doi.org/10.1007/s00484-012-0588-9

Brown, S. J. (2018). The drivers of variability in UK extreme rainfall. *International Journal of Climatology*, *38*, e119--e130. https://doi.org/10.1002/joc.5356

Bueh, C., & Nakamura, H. (2007). Scandinavian pattern and its climatic impact. *Quarterly Journal of the Royal Meteorological Society*, *133*(629), 2117–2131. https://doi.org/https://doi.org/10.1002/qj.173

Bureau Of Meteorology. (2017). ENSO Outlook 28 March 2017 - An Alert System for the El Niño–Southern Oscillation. Retrieved from http://www.bom.gov.au/climate/enso/outlook/

Bussay, A., van der Velde, M., Fumagalli, D., & Seguini, L. (2015). Improving operational maize yield forecasting in Hungary. *Agricultural Systems*, *141*(12), 94–106. https://doi.org/https://doi.org/10.1016/j.agsy.2015.10.001

Cai, W., Borlace, S., Lengaigne, M., van Rensch, P., Collins, M., Vecchi, G., … Jin, F.-F. (2014). Increasing frequency of extreme El Niño events due to greenhouse warming. *Nature Climate Change*, *5*(2), 1–6. https://doi.org/10.1038/nclimate2100

Cai, W., Santoso, A., Wang, G., Yeh, S. W., An, S. Il, Cobb, K. M., … Wu, L. (2015). ENSO and greenhouse warming. *Nature Climate Change*, *5*(9), 849. https://doi.org/10.1038/nclimate2743

Calanca, P., Bolius, D., Weigel, A. P., & Liniger, M. A. (2011). Application of long-range weather forecasts to agricultural decision problems in Europe. *The Journal of Agricultural Science*, *149*(01), 15–22. https://doi.org/https://doi.org/10.1017/S0021859610000729

Cammalleri, C., Micale, F., & Vogt, J. (2016). A novel soil moisture-based drought severity index (DSI) combining water deficit magnitude and

frequency. *Hydrological Processes*, *30*(2), 289--301. https://doi.org/10.1002/hyp.10578

Cannon, A. J. (2015). *Revisiting the nonlinear relationship between ENSO and winter extreme station precipitation in North America*. *4014*(January), 4001–4014. https://doi.org/10.1002/joc.4263

Cannon, T. (1994). Vulnerability analysis and the explanation of "natural" disasters. In *Disasters Development and Environment*.

Cantelaube, P., Terres, J., & Doblas-Reyes. (2004). Influence of climate variability on European agriculture- analysis of winter wheat production. *Climate Research*, *27*(2), 135–144. https://doi.org/10.3354/cr027135

Carisi, F., Schröter, K., Domeneghetti, A., Kreibich, H., & Castellarin, A. (2018). Development and assessment of uni- and multivariable flood loss models for Emilia-Romagna (Italy). *Natural Hazards and Earth System Sciences*, *18*, 2057--2079. https://doi.org/10.5194/nhess-18-2057-2018

Casanueva, A., Rodríguez-Puebla, C., Frías, M. D., & González-Reviriego, N. (2014). Variability of extreme precipitation over Europe and its relationships with teleconnection patterns. *Hydrology and Earth System Sciences*, *18*(2), 709–725. https://doi.org/10.5194/hess-18-709-2014

Cavanaugh, G., Collier, B., & Skees, J. (2010). Incorporating Weather Index Insurance with Territorial Approaches to Climate Change (TACC) in Northern Peru. *Unpublished, Working Paper*.

Ceglar, A., Turco, M., Toreti, A., & Doblas-Reyes, F. J. (2017). Linking crop yield anomalies to large-scale atmospheric circulation in Europe. *Agricultural and Forest Meteorology*, *240–241*, 35–45. https://doi.org/10.1016/j.agrformet.2017.03.019

Chiew, F. H. S., Piechota, T. C., Dracup, J. A., & Mcmahon, T. A. (1998). *Nino / Southern Oscillation and Australian rainfall , streamflow and drought : Links and potential for forecasting*. *204*(1–4), 138–149. https://doi.org/https://doi.org/10.1016/S0022-1694(97)00121-2

Clarke, N., Hetschkun, H., Jones, C., Boswell, E., & Marfaing, H. (1993). Identification of stress tolerance traits in sugar beet. In *Interacting stresses on plants in a changing climate* (pp. 511–524). Springer.

Clement, K. Y., Wouter Botzen, W. J., Brouwer, R., & Aerts, J. C. J. H. (2018). A global review of the impact of basis risk on the functioning of and demand for index insurance. *International Journal of Disaster Risk Reduction*, *28*,

845--853. https://doi.org/10.1016/j.ijdrr.2018.01.001

Cobb, K. M., Charles, C. D., Cheng, H., & Edwards, R. L. (2003). El Niño/Southern Oscillation and tropical Pacific climate during the last millennium. *Nature*, *424*(6946), 271. https://doi.org/10.1038/nature01779

Coles, S., Bawa, J., Trenner, L., & Dorazio, P. (2001). *An introduction to statistical modeling of extreme values* (Vol. 208). Springer.

Collins, M., An, S. Il, Cai, W., Ganachaud, A., Guilyardi, E., Jin, F. F., … Wittenberg, A. (2010). The impact of global warming on the tropical Pacific Ocean and El Niño. *Nature Geoscience*, *3*(6), 391. https://doi.org/10.1038/ngeo868

Comas-Bru, L., & McDermott, F. (2014). Impacts of the EA and SCA patterns on the European twentieth century NAO--winter climate relationship. *Quarterly Journal of the Royal Meteorological Society*, *140*(679), 354–363. https://doi.org/https://doi.org/10.1002/qj.2158

Coughlan de Perez, E., van Aalst, M., Choularton, R., van den Hurk, B., Mason, S., Nissan, H., & Schwager, S. (2019). From rain to famine: assessing the utility of rainfall observations and seasonal forecasts to anticipate food insecurity in East Africa. *Food Security*, *11*(1), 57--68. https://doi.org/10.1007/s12571-018-00885-9

Coughlan De Perez, E., Van Den Hurk, B., Van Aalst, M. K., Amuron, I., Bamanya, D., Hauser, T., … Zsoter, E. (2016). Action-based flood forecasting for triggering humanitarian action. *Hydrology and Earth System Sciences*, *20*(9), 3549–3560. https://doi.org/10.5194/hess-20-3549-2016

Coughlan De Perez, E., Van Den Hurk, B., Van Aalst, M. K., Jongman, B., Klose, T., & Suarez, P. (2015). Forecast-based financing: An approach for catalyzing humanitarian action based on extreme weather and climate forecasts. *Natural Hazards and Earth System Sciences*, *15*(4), 895–904. https://doi.org/10.5194/nhess-15-895-2015

Cunha, J. M., De Giorgi, G., & Jayachandran, S. (2019). The price effects of cash versus in-kind transfers. *The Review of Economic Studies*, *86*(1), 240--281. https://doi.org/https://doi.org/10.1093/restud/rdy018

Cusinato, E., Zanchettin, D., Sannino, G., & Rubino, A. (2019). Mediterranean thermohaline response to large-scale winter atmospheric forcing in a high-resolution ocean model simulation. In *Meteorology and Climatology of the Mediterranean and Black Seas* (pp. 363–390).

https://doi.org/https://doi.org/10.1007/s00024-018-1859-0

D'Alessandro, S. P., Caballero, J., Lichte, J., & Simpkin, S. (2015). *Kenya : Agricultural Sector Risk Assessment. Agriculture global practice technical assistance paper*. World Bank, Washington, DC.

Dai, A., & Wigley, T. M. L. (2000). Global patterns of ENSO-induced precipitation. *Geophysical Research Letters*, *27*(9), 1283–1286. https://doi.org/10.1029/1999GL011140

Davenport, F., Funk, C., & Galu, G. (2018). How will East African maize yields respond to climate change and can agricultural development mitigate this response? *Climatic Change*, *147*(3–4), 491--506. https://doi.org/10.1007/s10584-018-2149-7

Davenport, F., Husak, G., & Jayanthi, H. (2015). Simulating regional grain yield distributions to support agricultural drought risk assessment. *Applied Geography*, *63*, 136–145. https://doi.org/10.1016/j.apgeog.2015.06.010

Dettinger, M. D., & Diaz, H. F. (2000). Global Characteristics of Stream Flow Seasonality and Variability. *Journal of Hydrometeorology*, *1*(4), 289–310. https://doi.org/10.1175/1525-7541(2000)001<0289:GCOSFS>2.0.CO;2

Devia, G. K., Ganasri, B. P., & Dwarakish, G. S. (2015). A Review on Hydrological Models. *Aquatic Procedia*, *4*, 1001--1007. https://doi.org/10.1016/j.aqpro.2015.02.126

Di Baldassarre, G., Nohrstedt, D., Mård, J., Burchardt, S., Albin, C., Bondesson, S., … Parker, C. F. (2018). An Integrative Research Framework to Unravel the Interplay of Natural Hazards and Vulnerabilities. *Earth's Future*. https://doi.org/10.1002/2017EF000764

Di Baldassarre, G., Viglione, A., Carr, G., Kuil, L., Yan, K., Brandimarte, L., & Blöschl, G. (2015). Debates - Perspectives on socio-hydrology: Capturing feedbacks between physical and social processes. *Water Resources Research*, *51*(6), 4770--4781. https://doi.org/10.1002/2014WR016416

Dick, W., Stoppa, A., Anderson, J., Coleman, E., & Rispoli, F. (2011). Weather index-based insurance in agricultural development: A technical guide. *International Fund for Agricultural Development (IFAD)*.

Dilley, M., & Heyman, B. N. (1995). ENSO and disaster: droughts, floods and El Niño/Southern Oscillation warm events. *Disasters*, *19*(3), 181–193. https://doi.org/10.1111/j.1467-7717.1995.tb00338.x

Dommenget, D., & Yu, Y. (2017). The effects of remote SST forcings on ENSO dynamics, variability and diversity. *Climate Dynamics*, *49*(7–8), 2605--2624. https://doi.org/10.1007/s00382-016-3472-1

Donat, M. G., Peterson, T. C., Brunet, M., King, A. D., Almazroui, M., Kolli, R. K., … Al Shekaili, M. N. (2014). Changes in extreme temperature and precipitation in the Arab region: Long-term trends and variability related to ENSO and NAO. *International Journal of Climatology*, *34*(3), 581–592. https://doi.org/10.1002/joc.3707

Doocy, S., & Tappis, H. (2017). Cash-based approaches in humanitarian emergencies A systematic review. *3ie Systematic Review Report*, *28*.

Dottori, F., Kalas, M., Salamon, P., Bianchi, A., Alfieri, L., & Feyen, L. (2017). An operational procedure for rapid flood risk assessment in Europe. *Natural Hazards and Earth System Sciences*, *17*(7), 1111--1126. https://doi.org/10.5194/nhess-17-1111-2017

Dunstone, N., Smith, D., Scaife, A., Hermanson, L., Eade, R., Robinson, N., … Knight, J. (2016). Skilful predictions of the winter North Atlantic Oscillation one year ahead. *Nature Geoscience*, *9*(11), 809–814. https://doi.org/10.1038/ngeo2824

Dunstone, N., Smith, D., Scaife, A., Hermanson, L., Fereday, D., O'Reilly, C., … Belcher, S. (2018). Skilful Seasonal Predictions of Summer European Rainfall. *Geophysical Research Letters*. https://doi.org/10.1002/2017GL076337

Durevall, D., Loening, J. L., & Ayalew, Y. (2013). Inflation dynamics and food prices in Ethiopia. *Journal of Development Economics*, *104*(December 2012), 89–106. https://doi.org/10.1016/j.jdeveco.2013.05.002

Easterling, W. E., & Mjelde, J. W. (1987). The importance of seasonal climate prediction lead time in agricultural decision making. *Agricultural and Forest Meteorology*, *40*(1), 37–50. https://doi.org/https://doi.org/10.1016/0168-1923(87)90053-0Get

ECMWF. (2018). Major upgrade for Global Flood Awareness System. Retrieved from https://www.ecmwf.int/en/about/media-centre/news/2018/major-upgrade-global-flood-awareness-system

ECMWF. (2019). Seasonal Outlook. Retrieved May 8, 2019, from http://www.globalfloods.eu/technical-information/seasonal-outlook/

Eichler, T., & Higgins, W. (2006). Climatology and ENSO-related variability of

North American extratropical cyclone activity. *Journal of Climate*, *19*(10), 2076–2093. https://doi.org/10.1175/JCLI3725.1

Emerton, R. E., Cloke, H. L., Stephens, E. M., Zsoter, E., Woolnough, S. J., & Pappenberger, F. (2017). Complex picture for likelihood of ENSO-driven flood hazard. *Nature Communications*, *8*, 14796. https://doi.org/10.1038/ncomms14796

Emerton, R. E., Stephens, E., & Cloke, H. L. (2019). What is the most useful approach for forecasting hydrological extremes during El Niño? *Environmental Research Communications*, *1*(3). https://doi.org/https://doi.org/10.1088/2515-7620/ab114e

Emerton, R. E., Stephens, E. M., Pappenberger, F., Pagano, T., Weerts, A. H., Wood, A. W., … others. (2016). Continental and global scale flood forecasting systems. *Wiley Interdisciplinary Reviews: Water*, *3*(3), 391–418. https://doi.org/10.1002/wat2.1137

Estes, L. D., Chaney, N. W., Herrera-Estrada, J., Sheffield, J., Caylor, K. K., & Wood, E. F. (2014). Changing water availability during the African maize-growing season, 1979-2010. *Environmental Research Letters*, *9*(7). https://doi.org/10.1088/1748-9326/9/7/075005

European Comission. (2017). EU sugar policy. Retrieved March 7, 2017, from https://ec.europa.eu/agriculture/sugar_en

European Parliament and Council. (2009). *Directive on the taking-up and pursuit of the business of insurance and reinsurance (Solvency II) , Directive 2009/138/EC*. Retrieved from www.eur-lex.europa.eu

EUROSTAT. (2010). Agri-environmental indicator - irrigation. Retrieved February 12, 2017, from http://ec.europa.eu/eurostat/statistics-explained/index.php/File:Irrigated_area_of_intensive_crops_(potatoes_and_sugar_beet),_2010_(%25_of_total_area_of_each_crop).png

EUROSTAT. (2016). Agricultural production - crops. Retrieved February 12, 2017, from http://ec.europa.eu/eurostat/statistics-explained/index.php/Agricultural_production_-_crops#Sugar_beet

FAO. (2000). Achieving sustainable gains in agriculture. *FAO- South America*. Retrieved from http://www.fao.org/docrep/014/am859e/am859e01.pdf

FAO. (2015). Crop Water Information: Sugarbeet. Retrieved March 9, 2017, from http://web.archive.org/web/20160831112022/http://www.fao.org/nr/wa

ter/cropinfo_sugarbeet.html

FAO. (2017). GIEWS - Global Information and Early Warning System. Retrieved March 23, 2018, from http://www.fao.org/giews/countrybrief/country.jsp?code=KEN

FAO. (2019). *Saving livelihoods saves lives*. https://doi.org/CC BY-NC-SA 3.0 IGO

Ferreyra, R. A., Podestá, G. P., Messina, C. D., Letson, D., Dardanelli, J., Guevara, E., & Meira, S. (2001). A linked-modeling framework to estimate maize production risk associated with ENSO-related climate variability in Argentina. *Agricultural and Forest Meteorology*, *107*(3), 177–192. https://doi.org/https://doi.org/10.1016/S0168-1923(00)00240-9

FEWS NET. (2017). Kenya Food Security Outlook. Retrieved from https://www.fews.net/sites/default/files/documents/reports/KENYA Food Security Outlook_June 2017-January 2018_Final_0.pdf

FEWS NET. (2018a). Food assistance outlook brief. Retrieved May 3, 2019, from http://fews.net/sites/default/files/documents/reports/Oct_2018_FAOB_P ublic.pdf

FEWS NET. (2018b). Kenya Food Security Outlook, October 2017 to May 2018. Retrieved from https://reliefweb.int/report/kenya/kenya-food-security-outlook-october-2017-may-2018

FEWS NET. (2019). Hunger-related mortality likely as IPC phase 4 outcomes and large-scale assistance needs persist. Retrieved May 7, 2019, from https://fews.net/sites/default/files/Food_assistance_needs_Peak_Needs_ 2019.pdf

Field, C. B., Barros, V., Stocker, T., Qin, D., Dokken, D., Ebi, K., … others. (2012). IPCC, 2012: Managing the risks of extreme events and disasters to advance climate change adaptation. A special report of Working Groups I and II of the Intergovernmental Panel on Climate Change. *Cambridge University Press, Cambridge, UK, and New York, NY, USA*, *30*(11), 7575–7613.

Food and Agriculture Organization. (2016). *Cash transfers : their economic and productive impacts Evidence from programmes in sub-Saharan Africa*.

Francis, O. (2017). EU Gives $178 Million More to Combat East Africa Famine, Drought. Retrieved from https://www.bloomberg.com/news/articles/2017-03-20/eu-gives-178-million-more-to-combat-east-africa-famine-drought

Frias, M. D., Herrera, S., Cofino, A. S., & Gutierrez, J. M. (2010). Assessing the skill of precipitation and temperature seasonal forecasts in Spain: Windows of opportunity related to ENSO events. *Journal of Climate*, *23*(2), 209–220. https://doi.org/10.1175/2009JCLI2824.1

Fuhrer, J., Beniston, M., Fischlin, A., Frei, C., Goyette, S., Jasper, K., & Pfister, C. (2006). Climate risks and their impact on agriculture and forests in Switzerland. *Climatic Change*, *79*(1–2), 79–102. https://doi.org/10.1007/s10584-006-9106-6

Funk, C., & Brown, M. E. (2009). Declining global per capita agricultural production and warming oceans threaten food security. *Food Security*, *1*(3), 271–289. https://doi.org/10.1007/s12571-009-0026-y

Funk, C., Harrison, L., Shukla, S., Pomposi, C., Galu, G., Korecha, D., … Verdin, J. (2018). Examining the role of unusually warm Indo-Pacific sea surface temperatures in recent African droughts. *Quarterly Journal of the Royal Meterological Society*, *144*, 360–383. https://doi.org/10.1002/qj.3266

Funk, C., Hoell, A., Shukla, S., Bladé, I., Liebmann, B., Roberts, J. B., … Husak, G. (2014). Predicting East African spring droughts using Pacific and Indian Ocean sea surface temperature indices. *Hydrology and Earth System Sciences*, *18*(12), 4965–4978. https://doi.org/10.5194/hess-18-4965-2014

Funk, C., Peterson, P., Landsfeld, M., Pedreros, D., Verdin, J., Shukla, S., … Michaelsen, J. (2015). The climate hazards infrared precipitation with stations — a new environmental record for monitoring extremes. *Scientific Data*, *2*, 150066. https://doi.org/10.1038/sdata.2015.66

Funk, C., Shukla, S., Thiaw, W. M., Rowland, J., Hoell, A., McNally, A., … others. (2019). Recognizing the Famine Early Warning Systems Network (FEWS NET): Over 30 Years of Drought Early Warning Science Advances and Partnerships Promoting Global Food Security. *Bulletin of the American Meteorological Society*, (2019). https://doi.org/https://doi.org/10.1175/BAMS-D-17-0233.1

Funk, C., & Verdin, J. P. (2010). Real-time decision support systems: the famine early warning system network. In *Satellite rainfall applications for surface hydrology* (pp. 295–320). Springer.

Garcia, M., & Moore, C. M. T. (2012). The Cash Dividend - The Rise of Cash Transfer Programs in Sub-Saharan Africa. In *The World Bank*. https://doi.org/10.1596/978-0-8213-8897-6 Library

German Red Cross. (2016). Forecast-based Financing Peru. Retrieved from https://www.forecast-based-financing.org/projects/peru/

Gigerenzer, G., Czerlinski, J., & Martignon, L. (1999). How good are fast and frugal heuristics? *Decision Science and Technology*, 81–103.

Gigerenzer, G., & Todd, P. M. (1999). Fast and frugal heuristics: The adaptive toolbox. In *Simple heuristics that make us smart* (pp. 3–34). Oxford University Press.

Gimeno, L., Ribera, P., Iglesias, R., de la Torre, L., Garía, R., & Hernández, E. (2002). Identification of empirical relationships between indices of ENSO and NAO and agricultural yields in Spain. *Climate Research*, *21*(2), 165–172. https://doi.org/10.3354/cr021165

Goddard, L., & Dilley, M. (2005). El Niño: Catastrophe or opportunity. *Journal of Climate*, *18*(5), 651–665. https://doi.org/10.1175/JCLI-3277.1

Godfray, H. C. J., Beddington, J. R., Crute, I. R., Haddad, L., Lawrence, D., Muir, J. F., … Toulmin, C. (2010). Food security: the challenge of feeding 9 billion people. *Science*, *327*(5967), 812–818. https://doi.org/10.1126/science.1185383

Gonsamo, A., & Chen, J. M. (2015). Winter teleconnections can predict the ensuing summer European crop productivity. *Proceedings of the National Academy of Sciences*, *112*(18), E2265--E2266. https://doi.org/10.1073/pnas.1503450112

Gonzalez, P. L. M., & Goddard, L. (2016). Long-lead ENSO predictability from CMIP5 decadal hindcasts. *Climate Dynamics*, *46*(9–10), 3127–3147. https://doi.org/10.1007/s00382-015-2757-0

Gouveia, C., & Trigo, R. M. (2008). Influence of climate variability on wheat production in Portugal. In *geoENV VI--Geostatistics for Environmental Applications* (pp. 335–345). Springer.

Gouveia, C., Trigo, R. M., DaCamara, C. C., Libonati, R., & Pereira, J. M. C. (2008). The North Atlantic Oscillation and European vegetation dynamics. *International Journal of Climatology*, *28*(14), 1835–1847. https://doi.org/10.1002/joc.1682

Greatbatch, R. J. (2004). Nonstationary impact of ENSO on Euro-Atlantic winter climate. *Geophysical Research Letters*, *31*(2), 4–7. https://doi.org/10.1029/2003GL018542

Gregersen, I. B., Madsen, H., Rosbjerg, D., & Arnbjerg-Nielsen, K. (2013). A spatial and nonstationary model for the frequency of extreme rainfall events. *Water Resources Research*, *49*(1), 127–136. https://doi.org/10.1029/2012WR012570

Guha-Sapir, D., Vos, F., & Below, R. (2014). EM-DAT: International Disaster Database.

Guimarães Nobre, G., Davenport, F., Bischiniotis, K., Veldkamp, T., Jongman, B., Funk, C. C., … Aerts, J. C. J. H. (2019). Financing agricultural drought risk through ex-ante cash transfers. *Science of the Total Environment*, *653*, 523–535. https://doi.org/https://doi.org/10.1016/j.scitotenv.2018.10.406

Guimarães Nobre, G., Jongman, B., Aerts, J., & Ward, P. J. (2017). The role of climate variability in extreme floods in Europe. *Environmental Research Letters*, *12*(8), 84012. https://doi.org/https://doi.org/10.1088/1748-9326/aa7c22

Haigh, T., Takle, E., Andresen, J., Widhalm, M., Carlton, J. S., & Angel, J. (2015). Climate Risk Management Mapping the decision points and climate information use of agricultural producers across the U . S . Corn Belt. *Climate Risk Management*, *7*, 20–30. https://doi.org/10.1016/j.crm.2015.01.004

Hall, J., Arheimer, B., Borga, M., Brázdil, R., Claps, P., Kiss, A., … Blöschl, G. (2014). Understanding flood regime changes in Europe: A state-of-the-art assessment. *Hydrology and Earth System Sciences*, *18*(7), 2735–2772. https://doi.org/10.5194/hess-18-2735-2014

Hamill, T. M., & Juras, J. (2006). Measuring forecast skill: is it real skill or is it the varying climatology? *Quarterly Journal of the Royal Meteorological Society*, *132*(621C), 2905–2923. https://doi.org/10.1256/qj.06.25

Harvey, C. A., Rakotobe, Z. L., Rao, N. S., Dave, R., Razafimahatratra, H., Rabarijohn, R. H., … MacKinnon, J. L. (2014). Extreme vulnerability of smallholder farmers to agricultural risks and climate change in Madagascar. *Philosophical Transactions of the Royal Society B: Biological Sciences*, *369*(1639), 20130089–20130089. https://doi.org/10.1098/rstb.2013.0089

Harvey, P. (2007). Cash-based responses in emergencies. *IDS Bulletin*, *38*(3), 79–81. https://doi.org/10.1111/j.1759-5436.2007.tb00383.x

Haylock, M., Hofstra, N., Tank, A. K., Klok, L., Jones, P., & New, M. (2008). A

European daily high-resolution gridded dataset of surface temperature and precipitation for 1950-2006. *Journal of Geophysical Research: Atmospheres*, *113*, D20119--D20119. https://doi.org/https://doi.org/10.1029/2008JD010201

Heino, M., Puma, M. J., Ward, P. J., Gerten, D., Heck, V., Siebert, S., & Kummu, M. (2018). Two-thirds of global cropland area impacted by climate oscillations. *Nature Communications*, *9*(1). https://doi.org/10.1038/s41467-017-02071-5

Hernández-Barrera, S., & Rodríguez-Puebla, C. (2017). Wheat yield in Spain and associated solar radiation patterns. *International Journal of Climatology*, *37*, 45–58. https://doi.org/10.1002/joc.4975

Hillier, D., & Magrath, J. (2016). El Niño 2015/6 Briefing: Urgent action now can prevent major suffering and loss. In *Oxfam International*.

Hoeppe, P. (2016). Trends in weather related disasters - Consequences for insurers and society. *Weather and Climate Extremes*, *11*(3), 70–79. https://doi.org/10.1016/j.wace.2015.10.002

Hollinger, S. E. (1991). Incorporating Weather and Climate data into Integrated Crop Management Systems. *Climate, Agriculture and Drought: Miscellaneous Papers*, *1*.

Huang, R., Chen, J., Wang, L., & Lin, Z. (2012). Characteristics, processes, and causes of the spatio-temporal variabilities of the East Asian monsoon system. *Advances in Atmospheric Sciences*, *29*(5), 910–942. https://doi.org/10.1007/s00376-012-2015-x

Huang, Y., Ren, H. L., Chadwick, R., Cheng, Z., & Chen, Q. (2018). Diagnosing changes of winter NAO in response to different climate forcings in a set of atmosphere-only timeslice experiments. *Atmosphere*, *9*(1). https://doi.org/10.3390/atmos9010010

Hurrell, J. W., & Deser, C. (2010). North Atlantic climate variability: The role of the North Atlantic Oscillation. *Journal of Marine Systems*, *79*(3–4), 231–244. https://doi.org/10.1016/j.jmarsys.2009.11.002

Hurrell, J. W., Kushnir, Y., Otterson, G., & Visbeck, M. (2003). An Overview of the North Atlantic Oscillation. In *Wiley Online Library* (Vol. 134). https://doi.org/10.1029/GM134

Iglesias, I., Lorenzo, M. N., & Taboada, J. J. (2014). Seasonal predictability of the east atlantic pattern from sea surface temperatures. *PLoS ONE*, *9*(1), 1–8.

https://doi.org/10.1371/journal.pone.0086439

Iizumi, T., Luo, J.-J., Challinor, A. J., Sakurai, G., Yokozawa, M., Sakuma, H., … Yamagata, T. (2014). Impacts of El Niño Southern Oscillation on the global yields of major crops. *Nature Communications*, *5*, 3712. Retrieved from https://doi.org/10.1038/ncomms4712

Iizumi, T., Yokozawa, M., Sakurai, G., Travasso, M. I., Romanernkov, V., Oettli, P., … Furuya, J. (2014). Historical changes in global yields: Major cereal and legume crops from 1982 to 2006. *Global Ecology and Biogeography*, *23*(3), 346–357. https://doi.org/10.1111/geb.12120

Ionita, M. (2014). The impact of the East Atlantic/Western Russia pattern on the hydroclimatology of Europe from mid-winter to late spring. *Climate*, *2*(4), 296–309. https://doi.org/https://doi.org/10.3390/cli2040296

Ionita, M., Boroneanț, C., & Chelcea, S. (2015). Seasonal modes of dryness and wetness variability over Europe and their connections with large scale atmospheric circulation and global sea surface temperature. *Climate Dynamics*, *45*(9–10), 2803–2829. https://doi.org/10.1007/s00382-015-2508-2

IPCC, C. 5. (2018). IPCC Special Report of Global Warming of 1.5 $^\circ$C Chapter 5 Sustainable Development, Poverty Eradication and Reducing Inequalities. In *IPCC*.

Irannezhad, M., Chen, D., & Kløve, B. (2016). The role of atmospheric circulation patterns in agroclimate variability in finland, 1961--2011. *Geografiska Annaler: Series A, Physical Geography*, *98*(4), 287–301. https://doi.org/10.1111/geoa.12137

IRI. (2019). IRI ENSO Forecast. Retrieved from https://iri.columbia.edu/our-expertise/climate/forecasts/enso/current/?enso_tab=enso-iri_plume

James, G., Witten, D., Hastie, T., & Tibshirani, R. (2013). *An introduction to statistical learning* (Vol. 112). Springer.

Janetos, A., Justice, C., Jahn, M., Obersteiner, M., Glauber, J., & Mulhern, W. (2017). *The risks of multiple breadbasket failures in the 21st century: a science research agenda*. Boston University Frederick S. Pardee Center for the Study of the Longer.

Jeong, J.-H., & Ho, C.-H. (2005). Changes in occurrence of cold surges over East Asia in association with Arctic Oscillation. *Geophysical Research Letters*, *32*(14). https://doi.org/https://doi.org/10.1029/2005GL023024

Johnson, N. C. (2013). How many enso flavors can we distinguish? *Journal of Climate*. https://doi.org/10.1175/JCLI-D-12-00649.1

Jongman, B., Hochrainer-stigler, S., Feyen, L., Aerts, J. C. J. H., Mechler, R., Botzen, W. J. W., … Ward, P. J. (2014). Increasing stress on disaster-risk finance due to large floods. *Nature Climate Change*, *4*(4), 1–5. https://doi.org/10.1038/NCLIMATE2124

Jongman, B., Winsemius, H. C., Aerts, J. C. J. H., de Perez, E. C., van Aalst, M. K., Kron, W., & Ward, P. J. (2015). Declining vulnerability to river floods and the global benefits of adaptation. *Proceedings of the National Academy of Sciences*, *112*(18), E2271--E2280. https://doi.org/https://doi.org/10.1073/pnas.1414439112

JRC MARS Bulletin. (2016). *Crop monitoring in Europe, November 2016: Arrival of the first frosts* (Vol. 24).

Keller, N., Cokely, E. T., Katsikopoulos, K. V., & Wegwarth, O. (2010). Naturalistic Heuristics for Decision Making. *Journal of Cognitive Engineering and Decision Making*, *4*(3), 256–274. https://doi.org/10.1518/155534310X12844000801168

Kellett, J., & Caravani, A. (2013). Financing Disaster Risk Reduction. In *Global Facility for Disaster Reduction and Recovery (GFDRR)*.

Kenter, C., Hoffmann, C. M., & Märländer, B. (2006). Effects of weather variables on sugar beet yield development (Beta vulgaris L.). *European Journal of Agronomy*, *24*(1), 62–69. https://doi.org/10.1016/j.eja.2005.05.001

Kenya Red Cross. (2017). *Drought Emergency Cash Transfer Response 2016-2017 Real Time Evaluation Report*.

Kettlewell, P. S., Easey, J., Stephenson, D. B., & Poulton, P. R. (2006). Soil moisture mediates association between the winter North Atlantic Oscillation and summer growth in the Park Grass Experiment. *Proceedings of the Royal Society B: Biological Sciences*, *273*(1590), 1149–1154. https://doi.org/10.1098/rspb.2005.3428

Kettlewell, P. S., Stephenson, D. B., Atkinson, M. D., & Hollins, P. D. (2003). Summer rainfall and wheat grain quality: relationships with the North Atlantic Oscillation. *Weather*, *58*(4), 155–164. https://doi.org/10.1256/wea.38.02

Kim, M., & Mccarl, B. A. (2005). The Agricultural Value Of Information On The

North Atlantic Oscillation: Yield And Economic Effects. *Climatic Change*, *71*(1–2), 117–139. https://doi.org/http://dx.doi.org/10.1007/s10584-005-5928-x

Kimball, B. A. (2008). Climate Variability and the Global Harvest: Impacts of El Niño and Other Oscillations on Agroecosystems. *Crop Science*. https://doi.org/10.2135/cropsci2008.05.0004br

Kingston, D. G., McGregor, G. R., Hannah, D. M., & Lawler, D. M. (2006). River flow teleconnections across the northern North Atlantic region. *Geophysical Research Letters*, *33*(14). https://doi.org/10.1029/2006GL026574

Kingston, D. G., Stagge, J. H., Tallaksen, L. M., & Hannah, D. M. (2015). European-scale drought: Understanding connections between atmospheric circulation and meteorological drought indices. *Journal of Climate*, *28*(2), 505–516. https://doi.org/10.1175/JCLI-D-14-00001.1

Krichak, S. O., Breitgand, J. S., Gualdi, S., & Feldstein, S. B. (2014). Teleconnection-extreme precipitation relationships over the Mediterranean region. *Theoretical and Applied Climatology*, *117*(3–4), 679–692. https://doi.org/10.1007/s00704-013-1036-4

Krichak, S. O., Kishcha, P., & Alpert, P. (2002). Decadal trends of main Eurasian oscillations and the eastern Mediterranean precipitation. *Theoretical and Applied Climatology*, *72*(3–4), 209–220. https://doi.org/10.1007/s007040200021

Kron, W., Steuer, M., Löw, P., & Wirtz, A. (2012). How to deal properly with a natural catastrophe database - Analysis of flood losses. *Natural Hazards and Earth System Science*, *12*(3), 535–550. https://doi.org/10.5194/nhess-12-535-2012

Kundzewicz, Z. W., Ulbrich, U., Brücher, T., Graczyk, D., Krüger, A., Leckebusch, G. C., … Szwed, M. (2005). Summer floods in Central Europe - Climate change track? *Natural Hazards*, *36*(1–2), 165–189. https://doi.org/10.1007/s11069-004-4547-6

Lagos, P., & Buizer, J. (1992). El niño and Peru: a nation's response to interannual climate variability. In S. K. Majumdar, G. S. Forbers, E. W. Miller, & R. F. Schmalz (Eds.), *Natural and Technological Disaters: Causes, Effects and Preventative Measures* (pp. 223–232). The Pennsylvania Academy of Science.

Lecerf, R., Ceglar, A., López-Lozano, R., Van Der Velde, M., & Baruth, B. (2018). Assessing the information in crop model and meteorological indicators to forecast crop yield over Europe. *Agricultural Systems*, *168*, 191–202. https://doi.org/https://doi.org/10.1016/j.agsy.2018.03.002

Lee, D., Ward, P. J., & Block, P. (2018). Identification of symmetric and asymmetric responses in seasonal streamflow globally to ENSO phase. *Environmental Research Letters*, *13*(4), 044031. https://doi.org/10.1088/1748-9326/aab4ca

Lewis, J. E., Rowland, J., & Nadeau, A. (1998). Estimating maize production in kenya using ndvi: Some statistical considerations. *International Journal of Remote Sensing*, *19*(13), 2609–2617. https://doi.org/10.1080/014311698214677

Li, H. (2010). Predictability and Prediction of the North Atlantic Oscillation. *ECMWF Seminar on Predictability in the European and Atlantic Regions*.

Liang, Y., Chou, C., Yu, J., & Lo, M. (2016). Mapping the locations of asymmetric and symmetric discharge responses in global rivers to the two types of El Niño. *Environmental Research Letters*, *11*(4), 0. https://doi.org/10.1088/1748-9326/11/4/044012

Lindström, G., Pers, C., Rosberg, J., Strömqvist, J., & Arheimer, B. (2010). Development and testing of the HYPE (Hydrological Predictions for the Environment) water quality model for different spatial scales. *Hydrology Research*, *41*(3–4), 295–319. https://doi.org/10.2166/nh.2010.007

Linnerooth-Bayer, J., Warner, K., Bals, C., Höppe, P., Burton, I., Loster, T., & Haas, A. (2009). Insurance, developing countries and climate change. *Geneva Papers on Risk and Insurance: Issues and Practice*, *34*(3), 381–400. https://doi.org/10.1057/gpp.2009.15

Livezey, R. E., & Chen, W. Y. (1983). Statistical Field Significance and its Determination by Monte Carlo Techniques. *Monthly Weather Review*, *111*(1), 46–59. https://doi.org/10.1175/1520-0493(1983)111<0046:SFSAID>2.0.CO;2

Llasat, M. C., López, L., Barnolas, M., & Llasat-Botija, M. (2008). Flash-floods in Catalonia: the social perception in a context of changing vulnerability. *Advances in Geosciences*, *17*(2007), 63–70. https://doi.org/10.5194/adgeo-17-63-2008

Lopez-Bustins, J. A., Martin-Vide, J., & Sanchez-Lorenzo, A. (2008). Iberia winter

rainfall trends based upon changes in teleconnection and circulation patterns. *Global and Planetary Change*, *63*(2–3), 171–176. https://doi.org/10.1016/j.gloplacha.2007.09.002

López-Moreno, J. I., & Vicente-Serrano, S. M. (2008). Positive and negative phases of the wintertime North Atlantic Oscillation and drought occurrence over Europe: A multitemporal-scale approach. *Journal of Climate*, *21*(6), 1220–1243. https://doi.org/10.1175/2007JCLI1739.1

Lorenzo, M. N., Taboada, J. J., & Gimeno, L. (2008). Links between circulation weather types and teleconnection patterns and their influence on precipitation patterns in Galicia (NW Spain). *International Journal of Climatology*, *28*(11), 1493–1505. https://doi.org/https://doi.org/10.1002/joc.1646

Lorenzo, M. N., Taboada, J. J., Lorenzo, J. F., & Ramos, A. M. (2013). Influence of climate on grape production and wine quality in the Rías Baixas , north-western Spain. *Regional Environmental Change*, *13*(4), 887–896. https://doi.org/10.1007/s10113-012-0387-1

Lü, A., Jia, S., Zhu, W., Yan, H., Duan, S., & Yao, Z. (2011). El Niño-southern oscillation and water resources in the headwaters region of the yellow river: Links and potential for forecasting. *Hydrology and Earth System Sciences*, *15*(4), 1273–1281. https://doi.org/10.5194/hess-15-1273-2011

Luan, S., Schooler, L. J., & Gigerenzer, G. (2011). A Signal-Detection Analysis of Fast-and-Frugal Trees. *Psychological Review*, *118*(2), 316–338. https://doi.org/10.1037/a0022684

Lyon, B. (2014). Seasonal drought in the Greater Horn of Africa and its recent increase during the March-May long rains. *Journal of Climate*, *27*(21), 7953–7975. https://doi.org/10.1175/JCLI-D-13-00459.1

Mariotti, A., Zeng, N., & Lau, K.-M. (2002). Euro-Mediterranean rainfall and ENSO-a seasonally varying relationship. *Geophysical Research Letters*, *29*(12), 54–59. https://doi.org/10.1029/2001GL014248

Markovic, D., & Koch, M. (2014). Long-term variations and temporal scaling of hydroclimatic time series with focus on the German part of the Elbe River Basin. *Hydrological Processes*, *28*(4), 2202–2211. https://doi.org/10.1002/hyp.9783

Marta, A. D., Grifoni, D., & Mancini, M. (2011). The influence of climate on durum wheat quality in Tuscany , Central Italy. *International Journal of*

Biometeorology, *55*(1), 87–96. https://doi.org/10.1007/s00484-010-0310-8

Mase, A. S., & Prokopy, L. S. (2014). Unrealized potential: A review of perceptions and use of weather and climate information in agricultural decision making. *Weather, Climate, and Society*, *6*(1), 47–61.

Mathieu, P. P., Sutton, R. T., Dong, B., & Collins, M. (2004). Predictability of winter climate over the North Atlantic European region during ENSO events. *Journal of Climate*, *17*(10), 1953–1974. https://doi.org/10.1175/1520-0442(2004)017<1953:POWCOT>2.0.CO;2

Mati, B. (2000). The influence of climate change on maize production in the semi-humid–semi-arid areas of Kenya. *Journal of Arid Environments*, *46*(4), 333–344. https://doi.org/10.1006/jare.2000.0699

Matyasovszky, I. (2003). The relationship between NAO and temperature in Hungary and its nonlinear connection with ENSO. *Theoretical and Applied Climatology*, *74*(1–2), 69–75. https://doi.org/10.1007/s00704-002-0697-1

Mawejje, J., Mawejje, J., Lwanga, M. M., & Lwanga, M. M. (2016). Inflation dynamics and agricultural supply shocks in Uganda. *African Journal of Economic and Management Studies*, *7*(4), 547–567. https://doi.org/10.1108/AJEMS-07-2015-0079

McPhaden, M. J. (2015). Playing hide and seek with El Niño. *Nature Climate Change*, *5*(9), 791–795. https://doi.org/10.1038/nclimate2775

Mechler, R. (2005). Cost-benefit analysis of natural disaster risk management in developing countries. *Deutsche Gesellschaft Fur Technische Zusammenarbeit*.

Meier, P. (2015). Digital humanitarians: How big data is changing the face of humanitarian response. In *Digital Humanitarians: How Big Data Is Changing the Face of Humanitarian Response*. https://doi.org/10.1201/b18023

Meinke, H., & Stone, R. C. (2005). Seasonal and inter-annual climate forecasting: the new tool for increasing preparedness to climate variability and change in agricultural planning and operations. In J. Salinger, M. Sivakumar, & R. P. Motha (Eds.), *Increasing Climate Variability and Change* (Vol. 70, pp. 221–253). https://doi.org/https://doi.org/10.1007/1-4020-4166-7_11

Merz, B., Aerts, J., Arnbjerg-Nielsen, K., Baldi, M., Becker, A., Bichet, A., … Nied, M. (2014). Floods and climate: Emerging perspectives for flood risk

assessment and management. *Natural Hazards and Earth System Sciences*, *14*(7), 1921–1942. https://doi.org/10.5194/nhess-14-1921-2014

Merz, B., Kundzewicz, Z. W., Delgado, J., Hundecha, Y., & Kreibich, H. (2012). Detection and attribution of changes in flood hazard and risk. In *Changes in flood risk in Europe,Special Pu* (pp. 435–458). https://doi.org/https://doi.org/10.1201/b12348-29

Metz, C. E. (1978). Basic principles of ROC analysis. *Seminars in Nuclear Medicine*, *8*(4), 283–298. https://doi.org/http://dx.doi.org/10.1016/S0001-2998(78)80014-2

Meyer, V., Haase, D., & Scheuer, S. (2009). Flood risk assessment in European river basins-concept, methods, and challenges exemplified at the Mulde river. *Integrated Environmental Assessment and Management*, *5*(1), 17–26. https://doi.org/10.1897/IEAM_2008-031.1

Michel-Kerjan, E., & Kunreuther, H. (2011). Redesigning flood insurance. *Science*, *333*(6041), 408–409. https://doi.org/10.1126/science.1202616

Mitchell, D., Davini, P., Harvey, B., Massey, N., Haustein, K., Woollings, T., … others. (2017). Assessing mid-latitude dynamics in extreme event attribution systems. *Climate Dynamics*, *48*(11–12), 3889–3901. https://doi.org/https://doi.org/10.1007/s00382-016-3308-z

Mohajan, H. K. (2014). Food and Nutrition Scenario of Kenya. *American Journal of Food and Nutrition*, *2*(2), 28–38. https://doi.org/10.12691/ajfn-2-2-3

Motha, R. P., & Baier, W. (2005). Impacts of present and future climate change and climate variability on agriculture in the temperate regions: North America. In *Increasing Climate Variability and Change* (pp. 137–164). Springer.

Mudelsee, M., Börngen, M., Tetzlaff, G., & Grünewald, U. (2004). Extreme floods in central Europe over the past 500 years: Role of cyclone pathway "Zugstrasse Vb." *Journal of Geophysical Research D: Atmospheres*, *109*(23), 1–21. https://doi.org/10.1029/2004JD005034

Muis, S., Haigh, I. D., Guimarães Nobre, G., Aerts, J. C. J. H., & Ward, P. J. (2018). Influence of El Niño-Southern Oscillation on Global Coastal Flooding. *Earth's Future*, *6*(9), 1311–1322.

Muis, S., Verlaan, M., Winsemius, H. C., Aerts, J. C. J. H., & Ward, P. J. (2016). A global reanalysis of storm surges and extreme sea levels. *Nature Communications*, *7*(May), 11969. https://doi.org/10.1038/ncomms11969

Munene, F. M. (2003). Household Population and Housing Characteristics. *Kenya Demographic and Health Survey. KCB o. Statistics. Nairobi, Kenya Central Bureau of Statistics*.

Munich Re. (2016a). *NatCatSERVICE Database (Munich Reinsurance Company, Geo Risks Research, Munich)*. Retrieved from Available at www.munichre.com/natcatservice. Accessed October 12, 2016.

Munich Re. (2016b). *Natural Loss Events Worldwide 1980 - 2015 - Geographical Overview*. (January), 2016.

Myneni, R. B., Hall, F. G., Sellers, P. J., & Marshak, A. L. (1995). Interpretation of spectral vegetation indexes. *IEEE Transactions on Geoscience and Remote Sensing*, *33*(2), 481–486. https://doi.org/10.1109/36.377948

National Drought Management Authority. (2016). *Hunger Safety Net Programme Scalability Policy Paper*.

Nnaji, A. O. (2001). Forecasting seasonal rainfall for agricultural decision-making in northern Nigeria. *Agricultural and Forest Meteorology*, *107*(3), 193–205. https://doi.org/https://doi.org/10.1016/S0168-1923(00)00239-2

NOAA. (2005). The Southern Oscillation Index. Retrieved February 10, 2017, from http://www.cpc.ncep.noaa.gov/products/analysis_monitoring/ensocycle/soi.shtml

NOAA. (2017a). Cold & Warm Episodes by Season. Retrieved April 16, 2018, from http://origin.cpc.ncep.noaa.gov/products/analysis_monitoring/ensostuff/ONI_v5.php

NOAA. (2017b). Northern hemisphere teleconnection patterns. Retrieved March 21, 2016, from http://www.cpc.ncep.noaa.gov/data/teledoc/telecontents.shtml

Ober, E. (2001). The search for drought tolerance in sugar beet. *British Sugar Beet Review*, *69*(1), 40–43.

Omoyo, N. N., Wakhungu, J., & Oteng'i, S. (2015). Effects of climate variability on maize yield in the arid and semi arid lands of lower eastern Kenya. *Agriculture & Food Security*, *4*(1), 8. https://doi.org/10.1186/s40066-015-0028-2

Ossó, A., Sutton, R., Shaffrey, L., & Dong, B. (2017). Observational evidence of

European summer weather patterns predictable from spring. *Proceedings of the National Academy of Sciences*, *115*(1), 59–63. https://doi.org/10.1073/pnas.1713146114

Pacetti, T., Caporali, E., & Cristina, M. (2017). Advances in Water Resources Floods and food security : A method to estimate the effect of inundation on crops availability. *Advances in Water Resources*, *110*, 494–504. https://doi.org/10.1016/j.advwatres.2017.06.019

Paprotny, D., Sebastian, A., Morales-Nápoles, O., & Jonkman, S. N. (2018). Trends in flood losses in Europe over the past 150 years. *Nature Communications*, *9*(1), 1985. https://doi.org/10.1038/s41467-018-04253-1

Petkeviciene, B., & others. (2009). The effects of climate factors on sugar beet early sowing timing. *Agron. Res*, *7*, 436–443.

Phillips, N. D., Woike, J. K., & Gaissmaier, W. (2017). FFTrees : A toolbox to create , visualize , and evaluate fast-and-frugal decision trees. *Judgment and Decision Making*, *12*(4), 344–368.

Pidgeon, J. D., Werker, A. R., Jaggard, K. W., Richter, G. M., Lister, D. H., & Jones, P. D. (2001). Climatic impact on the productivity of sugar beet in Europe, 1961-1995. *Agricultural and Forest Meteorology*, *109*(1), 27–37. https://doi.org/10.1016/S0168-1923(01)00254-4

Pielke Jr, R. A., & Downton, M. W. (2000). Precipitation and damaging floods: Trends in the United States, 1932--97. *Journal of Climate*, *13*(20), 3625–3637.

Pingali, P. (2007). Westernization of Asian diets and the transformation of food systems: Implications for research and policy. *Food Policy*, *32*(3), 281–298. https://doi.org/10.1016/j.foodpol.2006.08.001

Pinto, J. G., Zacharias, S., Fink, A. H., Leckebusch, G. C., & Ulbrich, U. (2009). Factors contributing to the development of extreme North Atlantic cyclones and their relationship with the NAO. *Climate Dynamics*, *32*(5), 711–737. https://doi.org/10.1007/s00382-008-0396-4

Pinzon, Jorge E and Tucker, C. J. (2014). A Non-Stationary 1981–2012 AVHRR NDVI3g Time Series. *Remote Sensing*, *6*(8), 6929–6960. https://doi.org/10.3390/rs6086929

Portmann, F. T., Siebert, S., & Döll, P. (2010). MIRCA2000-Global monthly irrigated and rainfed crop areas around the year 2000: A new high-

resolution data set for agricultural and hydrological modeling. *Global Biogeochemical Cycles*, *24*(1). https://doi.org/10.1029/2008GB003435

Prudhomme, C., & Genevier, M. (2011). Can atmospheric circulation be linked to flooding in Europe? *Hydrological Processes*, *25*(7), 1180–1190. https://doi.org/10.1002/hyp.7879

Pulwarty, R. S., & Sivakumar, M. V. K. (2014). Information systems in a changing climate : Early warnings and drought risk management. *Weather and Climate Extremes*, *3*, 14–21. https://doi.org/10.1016/j.wace.2014.03.005

Quadrelli, R., Pavan, V., & Molteni, F. (2001). Wintertime variability of Mediterranean precipitation and its links with large-scale circulation anomalies. *Climate Dynamics*, *17*(5–6), 457–466. https://doi.org/10.1007/s003820000121

Raab, M., & Gigerenzer, G. (2015). The power of simplicity: A fast-and-frugal heuristics approach to performance science. *Frontiers in Psychology*, *6*, 1672. https://doi.org/10.3389/fpsyg.2015.01672

Ray, D. K., Gerber, J. S., MacDonald, G. K., & West, P. C. (2015). Climate variation explains a third of global crop yield variability. *Nature Communications*, *6*, 5989. https://doi.org/10.1038/ncomms6989

Ray, D. K., Mueller, N. D., West, P. C., & Foley, J. A. (2013). Yield Trends Are Insufficient to Double Global Crop Production by 2050. *PLoS ONE*, *8*(6). https://doi.org/10.1371/journal.pone.0066428

ReliefWeb. (2018). Kenya: Drought - 2014-2018. Retrieved from https://reliefweb.int/disaster/dr-2014-000131-ken

Richard, Y., Fauchereau, N., Poccard, I., Rouault, M., & Trzaska, S. (2001). 20th century droughts in Southern Africa: Spatial and temporal variability, teleconnections with oceanic and atmospheric conditions. *International Journal of Climatology*, *21*(7), 873–885. https://doi.org/10.1002/joc.656

Rios-Cornejo, D., Penas, A., Alvarez-Esteban, R., & del Rio, S. (2015). Links between teleconnection patterns and precipitation in Spain. *Atmospheric Research*, *156*, 14–28. https://doi.org/10.1016/j.atmosres.2014.12.012

Rocha, A. (1999). Low-frequency variability of seasonal rainfall over the Iberian Peninsula and ENSO. *International Journal of Climatology*, *19*(8), 889–901. https://doi.org/10.1002/(SICI)1097-0088(19990630)19:8<889::AID-JOC404>3.0.CO;2-P

Rodó, X., Baert, E., & Comin, F. a. (1997). Climate Dynamics Variations in seasonal rainfall in Southern Europe during the present century : relationships with the North Atlantic Oscillation and the. *Climate Dynamics*, *13*(1997), 275–284. https://doi.org/10.1007/s003820050165

Rodríguez-Fonseca, B., Suárez-Moreno, R., Ayarzagüena, B., López-Parages, J., Gómara, I., Villamayor, J., … Castaño-Tierno, A. (2016). A Review of ENSO Influence on the North Atlantic. A Non-Stationary Signal. *Atmosphere*, *7*(7), 87. https://doi.org/10.3390/atmos7070087

Rojas, O. (2007). Operational maize yield model development and validation based on remote sensing and agro-meteorological data in Kenya. *International Journal of Remote Sensing*, *28*(17), 3775–3793. https://doi.org/10.1080/01431160601075608

Romali, N. S., Sulaiman, M. @ S. A. K., Yusop, Z., & Ismail, Z. (2015). Flood Damage Assessment: A Review of Flood Stage–Damage Function Curve. In S. Abu Bakar, W. Tahir, M. Wahid, S. Mohd Nasir, & H. R. (Eds.), *ISFRAM 2014*. https://doi.org/10.1007/978-981-287-365-1_13

Romano, A., Sorgonà, A., Lupini, A., Araniti, F., Stevanato, P., Cacco, G., & Abenavoli, M. R. (2012). Morpho-physiological responses of sugar beet (Beta vulgaris L.) genotypes to drought stress. *Acta Physiologiae Plantarum*, *35*(3), 853–865. https://doi.org/10.1007/s11738-012-1129-1

Ronghui, H., & Yifang, W. (1989). The influence of ENSO on the summer climate change in China and its mechanism. *Advances in Atmospheric Sciences*, *6*(1), 21–32. https://doi.org/https://doi.org/10.1007/BF02656915

Rowhani, P., Lobell, D. B., Linderman, M., & Ramankutty, N. (2011). Climate variability and crop production in Tanzania. *Agricultural and Forest Meteorology*, *151*(4), 449–460. https://doi.org/10.1016/j.agrformet.2010.12.002

Ryu, J. H., Svoboda, M. D., Lenters, J. D., Tadesse, T., & Knutson, C. L. (2010). Potential extents for ENSO-driven hydrologic drought forecasts in the United States. *Climatic Change*, *101*(3), 575–597. https://doi.org/10.1007/s10584-009-9705-0

Sacks, W. J., Deryng, D., & Foley, J. A. (2010). Crop planting dates : an analysis of global patterns. *Global Ecology and Biogeography*, *19*(5), 607–620. https://doi.org/10.1111/j.1466-8238.2010.00551.x

Santoso, A., Mcphaden, M. J., & Cai, W. (2017). The defining characteristics of

ENSO extremes and the strong 2015/2016 El Niño. *Reviews of Geophysics*, *55*(4), 1079–1129. https://doi.org/https://doi.org/10.1002/2017RG000560

Saunders, M. A., Chandler, R. E., Merchant, C. J., & Roberts, F. P. (2000). Atlantic hurricanes and NW Pacific typhoons: ENSO spatial impacts on occurrence and landfall. *Geophysical Research Letters*, *27*(8), 1147–1150. https://doi.org/10.1029/1999GL010948

Scaife, A. A. (2010). Impact of ENSO on European Climate. *ECMWF Seminar on Predictability in the European and Atlantic Regions*, (September 2010), 83–92.

Scaife, A. A., Arribas, A., Blockey, E., Brookshaw, A., Clark, R. T., Dunstone, N., … Williams, A. (2014). Skillful long range prediction of European and North American winters. *Geophysical Research Letters*, *5*, 2514–2519. https://doi.org/10.1002/2014GL059637.Received

Scaife, A. A., Folland, C. K., Alexander, L. V., Moberg, A., & Knight, J. R. (2008). European climate extremes and the North Atlantic Oscillation. *Journal of Climate*, *21*(1), 72–83. https://doi.org/10.1175/2007JCLI1631.1

Scussolini, P., Aerts, J. C. J. H., Jongman, B., Bouwer, L. M., Winsemius, H. C., de Moel, H., & Ward, P. J. (2015). FLOPROS: an evolving global database of flood protection standards. *Natural Hazards and Earth System Sciences Discussions*, *3*(12), 7275–7309. https://doi.org/10.5194/nhessd-3-7275-2015

Seager, R., Kushnir, Y., Nakamura, J., Ting, M., & Naik, N. (2010). Northern Hemisphere winter snow anomalies: ENSO, NAO and the winter of 2009/10. *Geophysical Research Letters*, *37*(14). https://doi.org/10.1029/2010GL043830

Senay, G. B., & Verdin, J. (2003). Characterization of yield reduction in Ethiopia using a GIS-based crop water balance model. *Canadian Journal of Remote Sensing*, *29*(6), 687–692. https://doi.org/10.5589/m03-039

Shaman, J. (2014). The seasonal effects of ENSO on European precipitation: Observational analysis. *Journal of Climate*, *27*(17), 6423–6438. https://doi.org/10.1175/JCLI-D-14-00008.1

Shaman, J., & Tziperman, E. (2011). An atmospheric teleconnection linking ENSO and Southwestern European precipitation. *Journal of Climate*, *24*(1), 124–139. https://doi.org/10.1175/2010JCLI3590.1

Sheffield, J., Wood, E. F., Chaney, N., Guan, K., Sadri, S., Yuan, X., … Ogallo, L. (2014). A drought monitoring and forecasting system for sub-sahara african water resources and food security. *Bulletin of the American Meteorological Society*, *95*(6), 861–882. https://doi.org/10.1175/BAMS-D-12-00124.1

Shi, W., & Tao, F. (2014). Vulnerability of African maize yield to climate change and variability during 1961-2010. *Food Security*, *6*(4), 471–481. https://doi.org/10.1007/s12571-014-0370-4

Shukla, S., Funk, C., & Hoell, A. (2014). Using constructed analogs to improve the skill of National Multi-Model Ensemble March-April-May precipitation forecasts in equatorial East Africa. *Environmental Research Letters*, *9*(9), 094009. https://doi.org/10.1088/1748-9326/9/9/094009

Smith, D. M., Scaife, A. A., Eade, R., & Knight, J. R. (2016). Seasonal to decadal prediction of the winter North Atlantic Oscillation: Emerging capability and future prospects. *Quarterly Journal of the Royal Meteorological Society*, *142*(695), 611–617. https://doi.org/10.1002/qj.2479

Smith, P. J., Pappenberger, F., Wetterhall, F., Thielen Del Pozo, J., Krzeminski, B., Salamon, P., … Baugh, C. (2016). On the Operational Implementation of the European Flood Awareness System (EFAS). In *Flood Forecasting: A Global Perspective*. https://doi.org/10.1016/B978-0-12-801884-2.00011-6

Snyder, R. L., & de Melo-Abreu, J. P. (2005). *Frost protection: fundamentals, practice and economics*. Food and agriculture organization of the United Nations.

Sousa, P. M., Trigo, R. M., Aizpurua, P., Nieto, R., Gimeno, L., & Garcia-Herrera, R. (2011). Trends and extremes of drought indices throughout the 20th century in the Mediterranean. *Natural Hazards and Earth System Science*, *11*(1), 33–51. https://doi.org/10.5194/nhess-11-33-2011

Steirou, E., Gerlitz, L., Apel, H., Sun, X., & Merz, B. (2019). Climate influences on flood probabilities across Europe. *Hydrology and Earth System Sciences*, *23*(3), 1305–1322. https://doi.org/10.5194/hess-23-1305-2019

Stephens, E., Coughlan de Perez, Erin Kruczkiewicz, A., Boyd, E., & Suarez, P. (2015). Forecast- based action. *Red Cross*, (April), 37.

Stockdale, T. N., Molteni, F., & Ferranti, L. (2015). Atmospheric initial conditions and the predictability of the Arctic Oscillation. *Geophysical Research Letters*, *42*(4), 1173–1179. https://doi.org/10.1002/2014GL062681

Stocker, T. F., Qin, D., Plattner, G. K., Tignor, M. M. B., Allen, S. K., Boschung, J., … Midgley, P. M. (2013). Climate change 2013 the physical science basis: Working Group I contribution to the fifth assessment report of the intergovernmental panel on climate change. In *Climate Change 2013 the Physical Science Basis: Working Group I Contribution to the Fifth Assessment Report of the Intergovernmental Panel on Climate Change*. https://doi.org/10.1017/CBO9781107415324

Struglia, M. V., Mariotti, A., & Filograsso, A. (2004). River discharge into the Mediterranean sea: Climatology and aspects of the observed variability. *Journal of Climate*, *17*(24), 4740–4751. https://doi.org/10.1175/JCLI-3225.1

Suarez, P., & Tall, A. (2010). Towards forecast-based humanitarian decisions: Climate science to get from early warning to early action. *Humanitarian Futures Programme*, 10. Retrieved from http://www.alnap.org/resource/12320

Sun, X., Renard, B., Thyer, M., Westra, S., & Lang, M. (2015). A global analysis of the asymmetric effect of ENSO on extreme precipitation. *Journal of Hydrology*, *530*, 51–65. https://doi.org/10.1016/j.jhydrol.2015.09.016

Sun, X., Thyer, M., Renard, B., & Lang, M. (2014). A general regional frequency analysis framework for quantifying local-scale climate effects: A case study of ENSO effects on Southeast Queensland rainfall. *Journal of Hydrology*, *512*, 53–68. https://doi.org/10.1016/j.jhydrol.2014.02.025

Tabari, H., & Willems, P. (2018). Lagged influence of Atlantic and Pacific climate patterns on European extreme precipitation. *Scientific Reports*, *8*(1), 5748. https://doi.org/10.1038/s41598-018-24069-9

Tall, A., Jay, A., & Hansen, J. (2012). Scaling Up Climate Services for Farmers in Africa and South Asia. In *CCAFS Working Paper*.

The World Bank. (2009). World Development Report 2009 - Reshaping Economic Geography. In *Geography*. https://doi.org/DOI: 10.1596/978-0-8213-7607-2

The World Bank. (2016a). *Disaster risk finance as a tool for development: a summary of findings from the disaster risk finance impact analytics project*.

The World Bank. (2016b). PPP conversion factor. Retrieved from http://data.worldbank.org/indicator/PA.NUS.PPP

Tozier de la Poterie, A. S., Jjemba, W. E., Singh, R., Coughlan de Perez, E.,

Costella, C. V., & Arrighi, J. (2018). Understanding the use of 2015–2016 El Niño forecasts in shaping early humanitarian action in Eastern and Southern Africa. *International Journal of Disaster Risk Reduction*, *30*(81–94). https://doi.org/10.1016/j.ijdrr.2018.02.025

Trenberth, K. E. (1997). The Definition of El Niño. *Bulletin of the American Meteorological Society*, *78*(12), 2771–2778. https://doi.org/10.1175/1520-0477(1997)078<2771:TDOENO>2.0.CO;2

Trenberth, K. E., & Fasullo, J. T. (2012). Climate extremes and climate change: The Russian heat wave and other climate extremes of 2010. *Journal of Geophysical Research Atmospheres*, *117*(17), 1–12. https://doi.org/10.1029/2012JD018020

Trenberth, K. E., & Stepaniak, D. P. (2001). Indices of El Niño evolution. *Journal of Climate*, *30*, 81–94. https://doi.org/10.1175/1520-0442(2001)014<1697:LIOENO>2.0.CO;2

UNDP. (2015). The Impact of Cash Transfers on Local Economies. *Policy in Focus*, *11*(1), 1–28. Retrieved from http://www.ipc-undp.org/pub/eng/PIF31_The_Impact_of_Cash_Transfers_on_Local_Economies.pdf

UNISDR. (2009). UNISDR Terminology on Disaster Risk Reduction.

UNISDR. (2015a). *Americas hit hard by El Niño*. Retrieved from News Archive

UNISDR. (2015b). Sendai framework for disaster risk reduction 2015--2030. *Proceedings of the 3rd United Nations World Conference on DRR, Sendai, Japan*, 14–18.

UNISDR. (2017). Flood Hazard and Risk Assessment. *Words into Action Guidelines: National Disaster Risk Assessment Hazard Specific Risk Assessment*.

United States Department of Agriculture. (2016). National Nutrient Database for Standard Reference Release 28. Retrieved from https://ndb.nal.usda.gov/ndb/foods/show/6595?fg=&manu=&lfacet=&format=&count=&max=50&offset=&sort=default&order=asc&qlookup=20314&ds=&qt=&qp=&qa=&qn=&q=&ing=

UNMGCY. (2017). *Youth Science Policy Interface Publication – Special Edition: Disaster Risk Reduction: A Road of Opportunities*. Retrieved from http://www.preventionweb.net/files/53923_53923unmgcydrreditionmay2017reduced.pdf

UNOCHA. (2016a). Agenda for Humanity. Retrieved August 1, 2018, from https://www.agendaforhumanity.org/

UNOCHA. (2016b). *El nino: overview of impact, projected humanitarian needs and response*.

UNOCHA. (2018). Global Humanitarian Overview. Retrieved April 25, 2019, from https://interactive.unocha.org/publication/globalhumanitarianoverview/

Uvo, C. B. (2003). Analysis and regionalization of northern European winter precipitation based on its relationship with the North Atlantic oscillation. *International Journal of Climatology*, *23*(10), 1185–1194. https://doi.org/10.1002/joc.930

van der Schrier, G., Briffa, K. R., Jones, P. D., & Osborn, T. J. (2006). Summer moisture variability across Europe. *Journal of Climate*. https://doi.org/10.1175/JCLI3734.1

van der Velde, M., Biavetti, I., El-Aydam, M., Niemeyer, S., Santini, F., & van den Berg, M. (2019). Use and relevance of European Union crop monitoring and yield forecasts. *Agricultural Systems*, *168*, 224–230. https://doi.org/https://doi.org/10.1016/j.agsy.2018.05.001

Van Swaaij, A., Heijbroek, W., & Basting, J. L. (2001). Testing and improving seed vigour in sugar beet. *Comptes-Rendus Des Congres de l'Institut International de Recherches Betteravieres (Belgium)*, Vol. 64.

Vandendriessche, J. (1995). Crop Models and Decision Support Systems for Yield Forecasting and Management of the Sugar Beet Crop. *European Journal of Agronomy*, *4*(3), 269–279. https://doi.org/10.1016/S1161-0301(14)80027-0

Veldkamp, T. I. E., Eisner, S., Wada, Y., Aerts, J. C. J. H., & Ward, P. J. (2015). Sensitivity of water scarcity events to ENSO-driven climate variability at the global scale. *Hydrology and Earth System Sciences*, *19*(10), 4081–4098. https://doi.org/10.5194/hess-19-4081-2015

Veldkamp, T. I. E., Wada, Y., Aerts, J. C. J. H., Döll, P., Gosling, S. N., Liu, J., … Ward, P. J. (2017). Water scarcity hotspots travel downstream due to human interventions in the 20th and 21st century. *Nature Communications*, *8*, 15697. https://doi.org/10.1038/ncomms15697

Venton, C. C. (2018). *The economics of resilience to drought*. Retrieved from https://www.usaid.gov/sites/default/files/documents/1867/Kenya_Economics_of_Resilience_Final_Jan_4_2018_-_BRANDED.pdf

Vicente-Serrano, S. M., Beguería, S., & López-Moreno, J. I. (2010). A multiscalar drought index sensitive to global warming: The standardized precipitation evapotranspiration index. *Journal of Climate*, *23*(7), 1696–1718. https://doi.org/10.1175/2009JCLI2909.1

Vicente-Serrano, S. M., Beguería, S., López-Moreno, J. I., El Kenawy, A. M., & Angulo-Martínez, M. (2009). Daily atmospheric circulation events and extreme precipitation risk in northeast Spain: Role of the North Atlantic Oscillation, the Western Mediterranean Oscillation, and the Mediterranean Oscillation. *Journal of Geophysical Research Atmospheres*. https://doi.org/10.1029/2008JD011492

Vicente-Serrano, S. M., García-Herrera, R., Barriopedro, D., Azorin-Molina, C., López-Moreno, J. I., Martín-Hernández, N., … Nieto, R. (2016). The Westerly Index as complementary indicator of the North Atlantic oscillation in explaining drought variability across Europe. *Climate Dynamics*, *47*(3–4), 845–863. https://doi.org/10.1007/s00382-015-2875-8

Vicente-Serrano, S. M., López-Moreno, J. I., Lorenzo-Lacruz, J., Kenawy, A. El, Azorin-Molina, C., Morán-Tejeda, E., … Angulo-Martínez, M. (2011). The NAO Impact on Droughts in the Mediterranean Region. In *Advances in Global Change Research*. https://doi.org/10.1007/978-94-007-1372-7_3

Villafuerte, M. Q., Matsumoto, J., Akasaka, I., Takahashi, H. G., Kubota, H., & Cinco, T. A. (2014). Long-term trends and variability of rainfall extremes in the Philippines. *Atmospheric Research*, *137*, 1–13. https://doi.org/10.1016/j.atmosres.2013.09.021

Vogt, J. V., Naumann, G., Masante, D., Spinoni, J., Cammalleri, C., Erian, W., … Barbosa, P. (2018). *Drought Risk Assessment. A conceptual Framework.* https://doi.org/10.2760/057223, JRC113937

Wake, B. (2013). Flooding costs. *Nature Climate Change*, *3*(9), 778. https://doi.org/10.1038/nclimate1997

Wang, G., Dolman, A. J., & Alessandri, A. (2011). A summer climate regime over Europe modulated by the North Atlantic Oscillation. *Hydrology and Earth System Sciences*, *15*, 57–64. https://doi.org/10.5194/hess-15-57-2011

Wang, L., & Gu, W. (2016). The Eastern China flood of June 2015 and its causes. *Science Bulletin*, *61*(2), 178–184. https://doi.org/10.1007/s11434-015-0967-9

Ward, P. J., Beets, W., Bouwer, L. M., Aerts, J. C. J. H., & Renssen, H. (2010).

Sensitivity of river discharge to ENSO. *Geophysical Research Letters*, *37*(12), 1–6. https://doi.org/10.1029/2010GL043215

Ward, P. J., De Moel, H., & Aerts, J. C. J. H. (2011). How are flood risk estimates affected by the choice of return-periods? *Natural Hazards and Earth System Science*, *11*, 3181–3195. https://doi.org/10.5194/nhess-11-3181-2011

Ward, P. J., Eisner, S., Flörke, M., Dettinger, M. D., & Kummu, M. (2014). Annual flood sensitivities to El Niño–Southern Oscillation at the global scale. *Hydrology and Earth System Sciences*, *18*(1), 47–66. https://doi.org/10.5194/hess-18-47-2014

Ward, P. J., Jongman, B., Kummu, M., Dettinger, M. D., Sperna Weiland, F. C., & Winsemius, H. C. (2014). Strong influence of El Nino Southern Oscillation on flood risk around the world. *Proceedings of the National Academy of Sciences*, *111*(44), 15659–15664. https://doi.org/10.1073/pnas.1409822111

Ward, P. J., Jongman, B., Salamon, P., Simpson, A., Bates, P., De Groeve, T., … Winsemius, H. C. (2015). Usefulness and limitations of global flood risk models. *Nature Climate Change*, *5*(8), 712–715. https://doi.org/10.1038/nclimate2742

Ward, P. J., Kummu, M., & Lall, U. (2016). Flood frequencies and durations and their response to El Niño Southern Oscillation: Global analysis. *Journal of Hydrology*, *539*, 358–378. https://doi.org/10.1016/j.jhydrol.2016.05.045

Wens, M., Johnson, J. M., Zagaria, C., & Veldkamp, T. I. E. (2019). Integrating human behavior dynamics into drought risk assessment—A sociohydrologic, agent-based approach. *Wiley Interdisciplinary Reviews: Water*. https://doi.org/10.1002/wat2.1345

Wilhite, D. A., & Glantz, M. H. (1985). Understanding: The drought phenomenon: The role of definitions. *Water International*, *10*(3), 111–120. https://doi.org/10.1080/02508068508686328

Wilkinson, E., Weingärtner, L., Choularton, R., Bailey, M., Todd, M., & Kniveton, D. (2018). *Forecasting hazards, averting disasters: Implementing forecast-based early action at scale*.

WMO. (2015). *WMO Guidelines on Multi-hazard Impact-based Forecast and Warning Services*. Retrieved from https://www.wmo.int/pages/prog/www/DPFS/Meetings/ET-

OWFPS_Montreal2016/documents/WMOGuidelinesonMulti-hazardImpact-basedForecastandWarningServices.pdf

World Bank. (2015). *Kenya Toward a National Crop and Livestock Insurance Program : Background Report*. Retrieved from https://openknowledge.worldbank.org/handle/10986/24444

World Food Programme. (2016). *FoodSECuRE - Food Security Climate Resilience Facility Supporting community resilience-building before and after climatic shocks*. Retrieved from http://documents.wfp.org/stellent/groups/public/documents/communications/wfp279583.pdf?_ga=2.214535189.368957664.1513674688-1083946025.1513674688

World Health Organization. (2004). *Human energy requirements: Report of a Joint FAO/WHO/UNU Expert Consultation, Rome 17-24 October 2001*. Rome: Food and Agriculture Organization of the United Nations.

Wulff, C. O., Greatbatch, R. J., Domeisen, D. I. V., Gollan, G., & Hansen, F. (2017). Tropical Forcing of the Summer East Atlantic Pattern. *Geophysical Research Letters*, *44*(21). https://doi.org/10.1002/2017GL075493

Yeh, S. W., Cai, W., Min, S. K., McPhaden, M. J., Dommenget, D., Dewitte, B., … Kug, J. S. (2018). ENSO Atmospheric Teleconnections and Their Response to Greenhouse Gas Forcing. *Reviews of Geophysics*, *56*(1), 185–206. https://doi.org/10.1002/2017RG000568

Zanardo, S., Nicotina, L., Hilberts, A. G. J., & Jewson, S. P. (2019). Modulation of Economic Losses From European Floods by the North Atlantic Oscillation. *Geophysical Research Letters*, *46*(5), 2563–2572. https://doi.org/10.1029/2019GL081956

Zhang, R., Sumi, A., & Kimoto, M. (1999). A Diagnostic Study of the Impact of El Nino on the Precipitation in China. *Advances in Atmospheric Sciences*, *16*(2), 229–241. https://doi.org/10.1007/BF02973084

Zweig, M. H., & Campbell, G. (1993). Receiver-operating characteristic (ROC) plots: A fundamental evaluation tool in clinical medicine. *Clinical Chemistry*. https://doi.org/ROC; Receiver-Operating Characteristic; SDT; Signal Detection Theory

Summary in Portuguese (Resumo)

A variabilidade climática, como por exemplo o fenômeno El Niño-Oscilação Sul, desencadeia oscilações anuais de extremos hidrometeorológicos e climatológicos, por exemplo, inundações e secas. Todos os anos, esses extremos resultam em importantes perdas econômicas em todo o mundo. Alguns estudos sugerem progressos na redução da vulnerabilidade social e das perdas econômicas decorrentes de inundações nas últimas décadas. No entanto, para um efetivo gerenciamento de riscos, uma mudança substancial na gestão de desastres é necessária para a redução do risco de desastres (RRD). Portanto, um passo importante para alcançar a redução do risco está na compreensão de como a variabilidade climática pode resultar em impactos de enchentes e secas.

O impacto de desastres pode ser reduzido quando informações confiáveis sobre a previsão de riscos estão disponíveis. Nos últimos anos, sistemas que guiam medidas para redução de risco foram criados. Esses sistemas aperfeiçoaram a capacidade de previsão de variáveis hidrometeorológicas e climatológicas, produzindo previsões de inundação e seca com maior precisão e em prazos mais longos. No entanto, ainda existe uma lacuna entre a identificação de eventos de risco e informações de impacto, como danos econômicos causados por eventos climáticos. Assim, um dos maiores desafios de pesquisa atualmente é a transição de "qual é a previsão do tempo?" para "o que o tempo fará?". Informações de previsão que são projetadas para expressar os impactos esperados são conhecidas como "previsão baseada em impacto". Recentemente, muitos estudos têm sido publicados descrevendo maneiras de adotar automaticamente ações preventivas para reduzir os impactos de eventos climáticos com base em sistemas de alerta antecipados. Nesses sistemas, as ações preventivas podem ser acionadas quando uma variável ultrapassa um certo limite. Por exemplo, os agricultores podem receber compensação monetária quando um sistema de alerta antecipado prevê déficits de precipitação abaixo de um certo limite crítico, usando índice de anomalia de chuvas. No entanto, informações de previsão de enchentes e secas permanecem incertas.Do mesmo modo, evidências científicas para os impactos benéficos da atuação antecipada com base nas informações de previsão ainda são limitadas. Assim, não é sabido como riscos hidrometeorológicos podem impactar a os meios de subsistência individuais e a economia. Além disso, as diversas partes interessadas muitas vezes não tomam as medidas apropriadas. Em conseqüência, grande maioria das informações procedentes de sistemas de alerta antecipado não são rotineiramente usadas como base para o

financiamento e desencadeamento de ações preventivas contra eventos climáticos.

O principal objetivo desta tese é aprimorar o conhecimento sobre conexões entre a variabilidade climática e os impactos decorrentes de inundações e secas. Essa associação é investigada em escalas globais a regionais, e em diferentes intervalos de tempo, com o objetivo de alcançar uma previsão baseada em impacto que possa orientar a implementação de ações antecipadas de forma eficaz antes que uma possível seca ou inundação se materialize.

Em primeiro lugar, usando uma escala pan-Europeia, analisa-se a influência espacial e temporal da variabilidade climática em eventos meteorológicos e inundações extremas. Isso é realizado investigando a El Niño-Oscilação Sul (ENOS), a Oscilação do Atlântico Norte (OAN) e o padrão Atlântico Leste (EA) durante suas fases neutras, positivas e negativas, para entender suas relações com quatro indicadores de inundação: Ocorrência de Precipitação Extrema, Intensidade de Precipitação Extrema, Ocorrência de Inundações e Dano de Inundações. Os resultados mostram que os quatro indicadores de inundação são fortemente associados com a variabilidade climática. Ambas as fases positiva e negativa da OAN e do EA estão associadas a precipitações extremas mais frequentes e intensas em grandes áreas da Europa, enquanto o efeito do ENOS na intensidade e frequência de precipitações extremas na Europa é muito menor. É demonstrado pela primeira vez que tanto as ocorrência de inundações como os danos causados por elas na Europa estão fortemente associados à variabilidade climática, especialmente no sul e no leste da Europa, sendo a associação mais forte observada para a OAN.

Posteriormente, examinam-se as associações entre os índices de variabilidade climática em escalas sazonais (com defasamento e síncronos) e as perdas econômicas por inundações em sub-regiões europeias. É dada especial atenção à investigação da probabilidade de perdas econômicas decorrentes de cheias sazonais com base em índices de variabilidade climática, e à detecção destas perdas em escalas sazonais. Os resultados mostram que os índices de variabilidade climática podem ser usados para prever as classes de eventos de inundação (Danos, Baixo Danos e Médio Danos), principalmente em pelo menos 2 de 4 estações em todas as sub-regiões da Europa. Além disso, demonstra-se que algumas das classes de danos por inundações podem ser previstas com antecedência de uma estação de tempo. Isso explica-se pelo fato de poder existir uma relação defasada entre os índices de variabilidade climática e os danos por inundação em todas as sub-regiões europeias. Observa-se que a probabilidade de ocorrência de danos por inundações pode aumentar ou diminuir em até ± 100% em comparação com probabilidades históricas. Os

resultados possibilitam uma melhor compreensão do efeito combinado da variabilidade climática sobre danos por inundações e refletem sobre como essas informações baseadas em impacto podem ser usadas para aperfeiçoar as práticas de gestão de risco de inundação.

Além disso, esta tese identifica regiões onde anomalias na produção agrícola na Europa podem ser previstas com base nos índices de variabilidade climática usando uma técnica de *Machine Learning* chamada "*Fast-and-Frugal trees*". Os resultados mostram que, aplicando a técnica de *Fast-and-Frugal trees*, pode-se prever altas/ baixas classes de produção de beterraba em 77% das regiões investigadas, correspondendo a 81% da produção total de beterraba na Europa. Para quase metade destas regiões, essas informações baseadas no impacto estão disponíveis seis ou cinco meses antes do início da colheita da beterraba, onde aproximadamente 44% da beterraba média anual é produzida. Com base nessas constatações, esta tese discute como as informações de previsão baseadas no impacto podem melhorar amplamente a gestão do setor agrícola na Europa. Para fornecer mais informações sobre o vigor e as limitações da abordagem, o método proposto é posteriormente testado em outro banco de dados de produção de culturas e tipo de cultura.

A técnica de *Fast-and-Frugal trees* também é aplicada a um estudo no Quênia (baseado em índices de variabilidade climática e cobertura de vegetação) para prever a produção de milho. Esta informação de alerta antecipado de baixa produção de milho é utilizada para avaliar a relação custo-eficácia de fornecer aos agricultores transferências de recursos antecipados, ao invés de compensar as perdas de rendimento após uma seca. Os resultados mostram que os modelos *Fast-and-Frugal Trees* têm habilidade para prever a baixa produção de milho nos cinco distritos quenianos. Na maioria dos casos, os modelos possuem capacidade de previsão seis meses antes do início da época de colheita. Embora não seja perfeito, o modelo prevê corretamente 85% das vezes os diferentes percentuais de baixa produção do milho nos distritos testados e nos diversos períodos de tempo. O desempenho dos modelos melhora no final do ciclo de crescimento, impulsionado por uma diminuição de 29% na probabilidade de alarmes falsos. Ao assumir uma previsão perfeita (sucesso = 100% e alarmes falsos = 0%), as transferências em recursos ex-ante podem ser mais custo-eficaz com 6 meses de antecedência. Além disso, ao usar as previsões reais com base em previsões de modelos de *Fast-and-Frugal trees*, os resultados demonstram que as transferências monetárias ex-ante podem ser mais eficazes em termos de custo do que as transferências tardias, especialmente para os déficits mais extremos. Múltiplos desafios para operacionalizar transferências de renda baseadas em indicadores de secas são identificados. Por exemplo, tomar ações

adequadas em resposta a alertas antecipado de riscos de seca baseados em índices de variabilidade climática requer uma compreensão profunda do impacto e do momento de risco.

Apesar desses desafios, ao fornecer uma melhor compreensão dos riscos associados com a variabilidade climática, esta tese apresenta recomendações de políticas que mostram oportunidades para reduzir o risco de desastres. Esta tese apresenta exemplos de instituições que já utilizam as previsões do ENOS para reduzir riscos, mas também reconhece que ainda existem algumas restrições à ação antecipada para responder às previsões do ENOS. Portanto, conclui-se que informações antecipadas sobre configurações espaciais do risco de desastres, alavancadas por previsões baseadas no impacto e com longos prazos de precauções, podem servir de base para uma mudança na gestão de risco que tenha um foco antecipado e preventivo.

Esta tese destaca alguns dos principais desafios e tópicos que requerem mais investigação em futuras pesquisas. Por exemplo, sugere-se que, para melhorar a compreensão dos impactos, é necessária uma pesquisa sobre a dinâmica da variabilidade climáticadesses eventos. Também propõe-se que, para melhorar a compreensão sobre os impactos da variabilidade climática, faz-se necessário melhores dados e uma investigação sobre as relações humanas e naturais. Além disso, esta tese indica que estudos futuros podem melhorar a previsão baseada no impacto, melhorando a habilidade de previsão com longos prazo de índices de variabilidade climática, e combinando a previsão de índices de variabilidade climática com impactos socioeconômicos de inundações e secas. Por fim, mais pesquisas podem ser realizadas para identificar os interesses e incentivos subjacentes que são relevantes para as partes interessadas na integração da redução de risco de desastres na gestão e políticas de risco de inundações e secas, em associação com a exploração dos benefícios das ações preventivas. Esta tese contribui para o avanço do entendimento sobre relações entre a variabilidade climática e os impactos relacionados ao clima, tanto de inundações quanto de secas. Resultados desta tese podem ser utilizados para gerar previsões baseadas em impactos e ações preventivas.

Summary in Dutch (Samenvatting)

Klimaatvariabiliteit, zoals de El Niño-Southern Oscillation, zorgt voor jaarlijkse fluctuaties in hydro-meteorologische en klimatologische extremen. Elk jaar veroorzaken zulke extremen, zoals overstromingen of droogtes, wereldwijd voor hoge economische schades. Ondanks dat een aantal studies suggereren dat de kwetsbaarheid en financiële verliezen van overstromingen de laatste paar decennia afnemen, vergt rampenrisicovermindering (disaster risk reduction; DRR) nog steeds een substantiële verandering van het managen van rampen naar het managen van risico's. Om DRR te bereiken is het daarom belangrijk om te begrijpen hoe klimaatvariabiliteit kan resulteren in impacts van overstromingen en droogtes.

De impact van rampen kan worden verminderd wanneer betrouwbare, voorspelde risico informatie beschikbaar is om preventieve risicoverminderingsmaatregelen aan te sturen. De afgelopen jaren hebben deze systemen de kwaliteit van voorspellingen over hydro-meteorologische en klimatologische variabelen verbeterd, door voorspellingen over de omvang van overstromingen en droogtes met hogere precisie op langere tijdschalen dan voorheen te produceren. Er is echter nog steeds een gat in het vertalen van extreme gebeurtenissen naar impact informatie, zoals de schade van weer-gerelateerde gebeurtenissen. Eén van de grootste uitdagingen is daarom de overgang van "wat voor een weer wordt het?" naar "wat zal het weer doen?". Voorspellingen die zijn ontworpen om de verwachte impact uit te drukken, worden "impact-based forecasting" genoemd. Recente literatuur beschrijft manieren om automatisch preventieve maatregelen, gebaseerd op vroege waarschuwingssystemen, te activeren om zo de impact van weer-gerelateerde gebeurtenissen te verminderen. In zulke systemen kunnen vroege acties worden geactiveerd wanneer een voorspelling een bepaalde drempelwaarde overstijgt. Boeren kunnen bijvoorbeeld van tevoren financieel gecompenseerd worden wanneer neerslagtekorten onder een bepaalde drempelwaarde voorspeld worden, gebruik makende van indicatoren van neerslaganomalieën. Echter, ondanks vooruitgang in overstromings- en droogtevoorspellingen, blijven bijbehorende onzekerheden van de voorspellingsinformatie groot, en is wetenschappelijk bewijs voor de gunstige impact van vroeg handelen gebaseerd op voorspellingen nog beperkt. Doordat men niet precies weet hoe hydro-meteorologische gebeurtenissen een impact kunnen hebben op mens hun leven, levensonderhoud en op de economie, treffen stakeholders vaak niet de juiste maatregelen. Als gevolg hiervan wordt het grote deel van vroege waarschuwingen niet routinematig gebruikt als een basis voor het financieren

en activeren van preventieve maatregelen tegen weer-gerelateerde gebeurtenissen.

Het hoofddoel van deze scriptie is om het begrip van de verbanden tussen klimaatvariabiliteit en weer-gerelateerde impacts van zowel overstromingen als droogtes te verbeteren. Dit verband wordt onderzocht van globale tot regionale schaal en op verschillende tijdschalen, met als doel om een impact-based forecast te bereiken die effectief de implementatie van vroege handelingen kan leiden voordat een potentiele droogte of overstroming plaatsvindt.

Als eerste worden de ruimtelijke en temporele invloeden van klimaatvariabiliteit op extreme meteorologische- en overstromingsgebeurtenissen op pan-Europese schaal geanalyseerd. Dit wordt gedaan door de El Niño Southern Oscillation (ENSO), de North Atlantic Oscillation (NAO) en de East Atlantic pattern (EA) te onderzoeken tijdens hun neutrale, positieve en negatieve fases, om zo hun relatie tot vier overstromingsindicatoren te begrijpen: het voorkomen van extreme neerslag, de intensiteit van extreme neerslag, het voorkomen van overstromingen en schade van overstromingen. Resultaten laten zien dat klimaatvariabiliteit sterke connecties heeft met de vier overstromingsindicatoren. Zowel de positieve als de negatieve fase van de NAO en EA worden in verband gebracht met meer frequente en intensere extreme neerslag over grote gebieden in Europa, terwijl de effecten van ENSO op de intensiteit en frequentie van extreme neerslag in Europa veel kleiner is. Voor de eerste keer wordt aangetoond dat de schade van overstromingen en het voorkomen van overstromingen in Europa sterk geassocieerd worden met klimaatvariabiliteit, met name in Zuid- en Oost-Europa, waarbij de sterkste link geobserveerd wordt voor de NAO.

Vervolgens wordt de rol van seizoensgebonden vertragingen en gelijktijdige indices van klimaatvariabiliteit op overstromingsverliezen op sub-regionale Europese schaal onderzocht. Speciale aandacht wordt gegeven aan het onderzoeken van de waarschijnlijkheid van seizoensgebonden overstromingsverliezen gebaseerd op indices van klimaatvariabiliteit, en om te detecteren of sommige van deze verliezen een seizoen eerder voorspeld kunnen worden. Resultaten laten zien dat de indices van klimaatvariabiliteit gebruikt kunnen worden om classificaties van schadelijke, laag schadelijke en medium schadelijke overstromingsgebeurtenissen te voorspelling, veelal in op zijn minst twee van de vier seizoenen in alle Europese deelregio's. Bovendien wordt aangetoond dat de classificaties van overstromingsverliezen een seizoen eerder voorspeld kunnen worden omdat er een vertraagde relatie kan bestaan tussen de indices van klimaatvariabiliteit en de overstromingsverliezen in alle Europese deelregio's. We zien dat de waarschijnlijkheid van het voorkomen van

overstromingsverliezen kan toe- of afnemen met tot wel ±100% in vergelijking met historische kansen. De resultaten bieden een beter begrip van het gecombineerde effect van klimaatvariabiliteit op overstromingsverliezen, en reflecteren op hoe zulke op impact gebaseerde informatie kan worden gebruikt om overstromingsrisicomanagement te verbeteren.

Bovendien identificeert deze scriptie regio's waarin anomalieën in Europese gewassenproductie kunnen worden voorspeld aan de hand van de indices van klimaatvariabiliteit, gebruik makend van een Machine Learning techniek genaamd "Fast-and-Frugal Trees". Resultaten laten zien dat door Fast-and-Frugal Trees toe te passen, hoge/lage klassen van suikerbietenproductie in 77% van de onderzochte regio's kunnen worden voorspeld, overeenkomend met 81% van de totale Europese suikerbietenproductie. Voor bijna de helft van deze regio's is zulke op impact gebaseerde informatie zes of vijf maanden voor het begin van het suikerbietenoogst beschikbaar, wanneer ongeveer 44% van de gemiddelde jaarlijkse suikerbieten worden geproduceerd. Gebruikmakend van deze resultaten bediscussieert deze scriptie hoe impact-based forecasting het management van de agrarische sector in Europa sterk kan verbeteren. Om verdere inzichten in de sterke en zwakke punten van deze aanpak te verschaffen, wordt de voorgestelde methode vervolgens getest op andere datasets van gewassenproducties en typen gewassen.

De Fast-and-Frugal Trees aanpak wordt ook toegepast op een case in Kenia (gebaseerd op indices van klimaatvariabiliteit en vegetatie dekking) om maïsoogsten te voorspellen. Dit vroege waarschuwingssysteem van lage maïsoogsten wordt gebruikt om de kostenefficiëntie te analyseren van het van tevoren uitbetalen van boeren in plaats van het compenseren van gederfde inkomsten na een droogte. Resultaten laten zien dat de Fast-and-Frugal Trees modellen vaardig zijn in het voorspellen van lage maïsoogsten in alle vijf Keniaanse districten. In de meeste gevallen hebben de modellen al zes maanden voor het begin van het oogstseizoen een voorspellende vaardigheid. Ondanks dat het niet perfect is, voorspelt het model 85% van de tijd correct de "lagere oogst drempelwaarde", over verschillende percentielen, districten en looptijden van de opbrengsten. De modelprestaties verbeteren richting het einde van het groeiseizoen, gedreven door een afname van 29% in de kans op een False Alarm. Wanneer we een perfecte voorspelling aannemen (Hits=100% en False Alarms=0%), zijn geldtransacties zes maanden van tevoren het meest kosteneffectief. Bovenal, wanneer gebruik gemaakt wordt van de daadwerkelijke voorspellingen gebaseerd op de Fast-and-Frugal Trees voorspellingen, laten resultaten zien dat geldtransacties vooraf vaak meer kosteneffectief zijn dan geldtransacties achteraf, in het bijzonder voor de meer

extreme oogsttekorten. Meerdere uitdagingen voor het operationaliseren van geldtransacties gebaseerd op indicatoren van droogtes worden geïdentificeerd. Zo heeft het ondernemen van gepaste maatregelen naar aanleiding van vroege waarschuwingen van droogte-risico's gebaseerd op indices van klimaatvariabiliteit bijvoorbeeld een diepgaand begrip nodig van de potentiele impact en timing van een extreme gebeurtenis.

Ondanks zulke uitdagingen, biedt deze scriptie beleidsaanbevelingen waarin we kansen laten zien om het risico op rampen te verminderen, door te reageren op voorspellingen van klimaatvariabiliteit, en door het bijbehorende risico beter te begrijpen. Het laat voorbeelden zien van organisaties die al gebruik maken van ENSO-voorspellingen om risico's te verminderen, maar erkent ook dat een aantal beperkingen voor vroeg handelen met betrekking tot de ENSO-voorspellingen nog bestaan. Ondanks dit concluderen we dat vooraf bekende informatie over de ruimtelijke configuratie van risico, bevorderd door impact-based forecasting met lange looptijden zoals degene ontworpen in deze scriptie, een verschuiving richting een meer anticiperende en preventieve risicomanagement kan ondersteunen.

Deze scriptie laat een aantal belangrijke uitdagingen en onderwerpen zien die in de toekomst verder onderzocht moeten worden. Zo wordt gesuggereerd dat onderzoek naar de dynamiek van klimaatvariabiliteit nodig is om het begrip van de impacts van klimaatvariabiliteit te verbeteren. Verder wordt ook voorgesteld om dit begrip van de impacts van klimaatvariabiliteit te verbeteren, betere data en een onderzoek naar de relatie tussen mensen en natuurlijke systemen nodig is. Bovendien laat deze scriptie zien dat toekomstig onderzoek naar impact-based forecasting verbeterd kan worden door de voorspellingsvaardigheden en looptijden van indices van klimaatvariabiliteit te verbeteren, en door de voorspelling van de indices van klimaatvariabiliteit met de socio-economische impact van overstromingen en droogtes te combineren. Als laatste kan toekomstig onderzoek worden uitgevoerd om de onderliggende interesses en motieven die belangrijk zijn voor stakeholders om DRR te integreren in overstromings- en droogterisicomanagement te identificeren, in combinatie met het verkennen van de voordelen van vroeg handelen. Deze scriptie biedt vooruitgang in het begrip van de connecties van klimaatvariabiliteit en weer-gerelateerde impacts van zowel overstromingen als droogtes, die gebruikt kunnen worden om impact-based forecasts te maken en vroegtijdige handelingen te activeren.

People don't do it alone
(Acknowledgment)

Supposing that everything goes well during my Ph.D. defense, I will be 31 years old by the time I close my student's life cycle. 28 out of 31 years were within some sort of educational institution, of which 9 were spent abroad (Ireland, Germany, Denmark and the Netherlands). In these past 9 years, everyone who I've met, whether it was a friend, a colleague, a child has had a great influence in my life. On the other hand, 21 out 31 years, I spent in Brazil, and the person who supported me the most back then was my mom. Therefore, I would like to dedicate the first lines of this acknowledgement to thank her, the person behind this achievement. Before my brothers and me, my mom was the first from our family to attend university. My dream of pursuing this journey was also born due to the importance that she gave to academic studies, and I'm glad that she will be here to see me finishing my doctorate.

Mãe, sei que você não entende bem o que aconteceu durante esses quatro anos, mas sim, o "curso" (ou doutorado) encerrou-se e devo isso principalmente a você. Através do seu esforço diário, você pode me proporcionar uma educação de qualidade mesmo tendo que colocar em segundo plano seus próprios interesses. Você é uma peça-chave nesse processo, e estou muito feliz em compartilhar deste momento com você.

My deep gratitude to those who gave me the chance to start a Ph.D.: my supervisors Professor Philip Ward and Professor Jeroen Aerts. You chose me among 150 candidates, and even though we will never know whether I was the best candidate for this position, I sincerely think that we were a good match. I never thought that four years into investigating disasters would bring me so much "joy". Philip, I look up to you in many levels: you are a respected researcher, a dedicated professor and an excellent beer drinker. I really appreciate your positive attitude, openness for new ideas and loud laughs. Jeroen, I can't thank you enough for all of your support, guidance and leadership through these four years. Big thanks for inviting me to visit you in Santa Barbara during your sabbatical. I feel that this trip was a milestone in my Ph.D. studies. Philip and Jeroen, I could not have made a better choice.

Special appreciation goes to the seven members of my promotion committee: Associate Professor Kees Boersma, Associate Professor Liz Stephens, Associate Professor Micha Werner, Dr. Peter Salamon, Professor Bart van den Hurk, Professor Maarten van Aalst and Associate Professor Dim Coumou. Your comments and feedback helped me shape this book. I highly value your efforts

to attend the ceremony, and the time taken to assess my dissertation. I look forward to future opportunities for collaboration.

Throughout these four years, I had the pleasure of collaborating further with great institutions and researches. Many thanks to my external co-authors Bettina Baruth (EU Joint Research Centre), Brenden Jongman (World Bank), Matteo Giuliani (Politecnico di Milano), Johannes Hunink (FutureWater), Frank Davenport (UC Santa Barbara), Chris Funk (UC Santa Barbara) and Greg Husak (UC Santa Barbara). Without the experiences, encouragement and support from these peers, this book would not exist.

I cannot imagine a better place for doing a Ph.D. than the IVM. Everybody knows that the research is great, but for me what makes a place really special is the people. I believe that the best part of working with such nice people like these fellows at IVM is that I didn't feel like I was working at all. To the (former) IVM's support staff - Marjolijn, Corry, Rita and the cleaning team - thank you for your wonderful care and your big smiles. To the (former) IVM's research staff - Anaïs, Andres, Efi, Elco, Eric, Fei, Hannah, Hans, Hiroaki, Iris, James, Jens, Johanna, Job, Lars, Lisellote, Marleen, Max, Marthe, Niels, Paolo, Pete, Sadhana, Sam, Sanne (thank you for saving me from all lizards in Jamaica), Shija, Oscar, Tadzio, Ted (Challenge Fund 5?), Toon - you have all truly inspired me. To the IVM's beach volleyball crew - Dirk, Jantsje and Lisa - we are surely the best volleyball players that IVM has ever had. To the (former) members of coolest office in town (C-553) - Flavio, Kostas, Giorgia, Kris, Fidel, Yus, Maria, Nadia, Douwe, Petra, Timothy - you're the best! I want to thank EVERYONE from the IVM who I haven't explicitly mentioned. I'm very lucky to have nice colleagues like you. Obrigada! Tak! Merci! Grazie! Spasibo! Gracias! Efharisto! Danke! Bedankt!

All my gratitude to Gabi and Kostas, my neighbours and paranymphs, who have been with me in this journey since day 1. Gabi, a nossa amizade é fruto de uma coincidência absurda. Não bastasse termos o mesmo nome e semelhança física, quem imaginaria que começaríamos um doutorado no mesmo dia, universidade e que ainda seriamos vizinhas de porta? Ter te conhecido e vivido essa jornada junto com você foi uns dos acontecimentos mais especiais da minha vida.

Obrigada por estar sempre presente. Kostas, my neighbour next desk and #4everyoung friend. Many people say that our friendship seems like an old couple that has never divorced, but I believe that we made an excellent duo –as you would say "not bad, not bad". Looking back at these four years, I can only remember all the (very loud) laughs we shared together with loads of coffees, raki, random conversations and sarcasms. Gabi and Kostas, our friendship is beyond words, distance and time.

In 2016 I first came in contact with two (extremely talented) youth-led organizations that helped me to develop myself in many ways: the UN Major Group for Children and Youth and the Water Youth Network. Since then, we have collaborated and worked hard during the weekends/late nights for a cause that we believe in. Donovan, Annisa, Robert (when is our next trip to Mexico?), Moa, Sara, Lydia, Miguel, Nhilce, Javed and all members of the DRR team –You fellows are super stars! If the world becomes a better place tomorrow, it will happen because of people like you.

As a result of my engagement with UNMGCY, in 2018 I was invited to serve as a young scientist representative for the Global Risk Assessment Framework expert group convened by the UN office for Disaster Risk Reduction (DRR). Since then, I have been couple of times in the UN headquarters in Geneva, and I have got to know a number of experts in the field of DRR. Special appreciation goes to Adam Fysh, Chiara Menchise, Costis Toregas, David Green, Finn Løvholt, Jasmina Karba, John Rees, John Schneider, Lisa Robinson, Mami Mizutori, Marc Gordon, Ricardo Mena, Rhea Katsanakis, Scott Williams, Tom de Groeve, and all others that have contributed to the foundations of the GRAF. It was an unforgettable experience to moderate the GRAF Working Session, and feel extremely honoured, inspired and rewarded to have worked with you over the past two years.

My previous staying in Ireland, Germany and Denmark gave me basis for a smooth sail through the Ph.D. All my thankfulness goes to the O'Mullane family, Professor Nassos Vafeidis and the Coastal Risks and Sea-Level Rise Research Group, my dearests friends Mayra and Julia, Professor Karsten Arnbjerg-Nielsen, Professor Dan Rosbjerg, Dr. Henrik Madsen, the DTU Department of Environmental Engineering, and the Roulund family.

This moment is extra special because I have some very charming people to share it with. Big thank you to Juliano, Tay, Luiz, Gabi, Chrats, Laura, Kostas, Marianna, Julia, Ivan, Claudia, Lenny, Federica, Venetia, Fabio, Flavinha and Sanne: there are >7 billion people in the world, and the fact that we have met makes me feel as the luckiest person alive.

Aos que seguramente compartilham esse momento com tanta felicidade como eu, à minha família, meu muito obrigada. Acredito que pessoas não se fazem sozinhas, por isso, vocês são fundamentais nessa jornada. Minha gratidão: ao meu padrasto "tio" Wellington, ao meu pai e Silvana, às minhas avós Carminha (RIP) e Onete, aos meus irmãos, cunhadas, sobrinhos, tios e tias, primos e primas (Nay, que bom compartilhar esse momento com você em Amsterdam!). Estendo esse agradecimento aos meus queridos amigo(a)s no Brasil. Obrigada pelo carinho e pela amizade ao longo dos anos. Nada é melhor que voltar para casa e reencontrar todos vocês. An die Lochocki's, meine ewige Dankbarkeit für die jahrelange Unterstützung und dass ich ein Teil Eurer Familie sein darf.

Ben, du bist in allen Zeilen dieser Dissertation, in denen die vorher geschrieben wurden und jenen die noch kommen werden. Es gibt viele Dinge für die ich in meinem Leben dankbar bin und du stehst ganz oben auf der Liste.

"I like to travel, but I hate to arrive". Well… it feels that now I arrived. If you have ever crossed my path, thank you.

Publication list

Guimarães Nobre, G., Jongman, B., Aerts, J.C.J.H. and Ward, P.J., 2017. The role of climate variability in extreme floods in Europe. Environmental Research Letters, 12(8), p.084012.

Muis, S., Haigh, I. D., **Guimarães Nobre, G.**, Aerts, J. C., & Ward, P. J. 2018. Influence of El Niño-Southern Oscillation on Global Coastal Flooding. Earth's Future, 6(9), 1311-1322.

Guimarães Nobre, G., Hunink, J.E., Baruth, B., Aerts, J.C. and Ward, P.J., 2019. Translating large-scale climate variability into crop production forecast in Europe. Scientific reports, 9(1), p.1277.

Guimarães Nobre, G., Davenport, F., Bischiniotis, K., Veldkamp, T., Jongman, B., Funk, C.C., Husak, G., Ward, P.J. and Aerts, J.C., 2019. Financing agricultural drought risk through ex-ante cash transfers. Science of the Total Environment, 653, pp.523-535.

Guimarães Nobre, G., Muis, S., Veldkamp, T.I. and Ward, P.J., 2019. Achieving the reduction of disaster risk by better predicting impacts of El Niño and La Niña. Progress in Disaster Science, p.100022.

Guimarães Nobre, G., Peters, K., Mayhew, L., Šakić Trogrlić, R., Guttieres, D., Ixel Cruz, J., Saccoccia, L., Kerins P., Kuzma, S., 2019. Migration and displacement risks: connecting dots, understanding trends. Contributing Paper to GAR 2019.

Guimarães Nobre, G., de Moel, H., Giuliani, M., Bischiniotis, K., Aerts, J.C.J.H. and Ward, P.J., 2019. What will the weather do? forecasting flood losses based on oscillation indices. *In review.*

Bischiniotis, K., Coughlan de Perez, E., Veldkamp, T., van den Hurk, B. **Guimarães Nobre, G.,** Aerts, J.C. 2019. Assessing time, cost and quality trade-offs in forecast-based action for floods. International Journal of Disaster Risk Reduction, p.101252.

About the author

I was born in Recife, Brazil, on November 2nd 1988. In 2012, I obtained a Bachelor's degree in Business Administration with an specialization in Financial Management at the University of Pernambuco (Brazil). In paralell to my undergraduate studies, I worked for two years in the field of Business and Finance Management in the private sector in Brazil. In 2015, I obtained a Master's degree in Environmental Management from the Christian-Albrechts-Universität zu Kiel, Germany. During my studies, I was a junior researcher at the Coastal Risk and Sea-level Rise Research Group (Kiel, Germany), and a guest researcher at the Technical University of Denmark.

I joined the Institute for Environmental Studies at the Vrije Universiteit Amsterdam in 2015, as part of the IMPREX project. My research investigated how climate variability can be used as early warning predictors of flood and agricultural drought impacts, and as drivers of risk financing mechanisms. Over the course of my PhD, I collaborated closely with several institutes including the Climate Hazard Group at the University of California, Santa Barbara, and the Joint Research Center of the European Commission. In the past 4 years, I (co-) authored 8 papers in international peer-reviewed journals, and presented my work at several conferences and institutes including the World Bank and the World Meteorological Organisation. As part of my teaching responsibilities, I supervised BSc and MSc theses, and assisted as a lecturer in the BSc Earth & Economics and the MSc in Hydrology.

I developed a passion for science and policy while volunteering in two youth-led organisations: Water Youth Network and United Nations Major Group for Children and Youth. Through these organisations, I participated in global consultations for the implementation of the Sendai Framework, and organized numerous networking and capacity building events. Currently, I represent young scientists at the Global Risk Assessment Framework expert group of the UN office for Disaster Risk Reduction.

Currently, I am working as a postdoctoral researcher at the Institute for Environmental Studies as part of the Forecast-based Financing for Food Security project.

Netherlands Research School for the
Socio-Economic and Natural Sciences of the Environment

D I P L O M A

for specialised PhD training
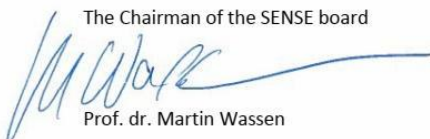
The Netherlands research school for the
Socio-Economic and Natural Sciences of the Environment
(SENSE) declares that

Gabriela Guimarães Nobre

born on 2 November 1988 in Recife, Brazil

has successfully fulfilled all requirements of the
educational PhD programme of SENSE.

Amsterdam, 15 November 2019

The Chairman of the SENSE board

Prof. dr. Martin Wassen

the SENSE Director of Education

Dr. Ad van Dommelen

The SENSE Research School declares that Gabriela Guimarães Nobre has successfully fulfilled all requirements of the educational PhD programme of SENSE with a work load of 41 EC, including the following activities:

SENSE PhD Courses

o   Environmental research in context (2016)
o   Research in context activity: 'Initiating, developing and implementing successful App and Website EQA Green Scholar: http://greenscholar.eu/' (2016-2017)

Other PhD and Advanced MSc Courses

o   Bayesian statistics, Wageningen University (2016)
o   Writing a scientific article, VU Amsterdam (2017)
o   RISC-KIT Summer School, University of the Algarve (2017)
o   Workshop in Decision Making Under Deep Uncertainty, University of Oxford (2017)
o   CNDS Summer School 'Natural Hazards in the Anthropocene', Uppsala University (2018)

External training at a foreign research institute

o   Research visit to the University of California, Santa Barbara, United States of America (2017)

Management and Didactic Skills Training

o   Supervising MSc student with thesis entitled 'Monitoring Drought in Europe: Developing a Methodology' (2016)
o   Supervising BSc student with thesis entitled 'Which climate variables are most valuable for predicting the variability of maize yields in Kenya, using the decision tree method?' (2018)
o   Teaching assistant at the MSc courses 'Water Risk' (2017-2019), the MSc course 'Integrated Modelling' (2018-2019) and the BSc course 'Inleiding Wiskunde' (2016-2018)
o   Co-organizing Pressure cooker event: 'Risk communication', Understanding Risk Forum (2018)
o   Co-convener of EGU session 'Operational forecasting and warning systems for natural hazards: challenges and innovation' (2018-2019)

Selection of Oral Presentations

o   *Drought and food security: from early warning to early action.* The Second Multi-Hazard Early Warning Conference, 13-14 May 2019, Geneva, Switzerland
o   *Drought: from early warning to early action.* Understanding Risk Forum, 14 -18 May 2018, Mexico City, Mexico

SENSE coordinator PhD education

Dr. ir. Peter Vermeulen

Appendix A

Appendix A1 Indices of climate variability

Negative (positive) ENSO phases are classified when the threshold of – (+) 0.5°C is met for a minimum of five consecutive overlapping 3-month periods. The "Neutral" phase is obtained for periods when these thresholds are not reached. Both the NAO and EA were classified using a ± 1σ.
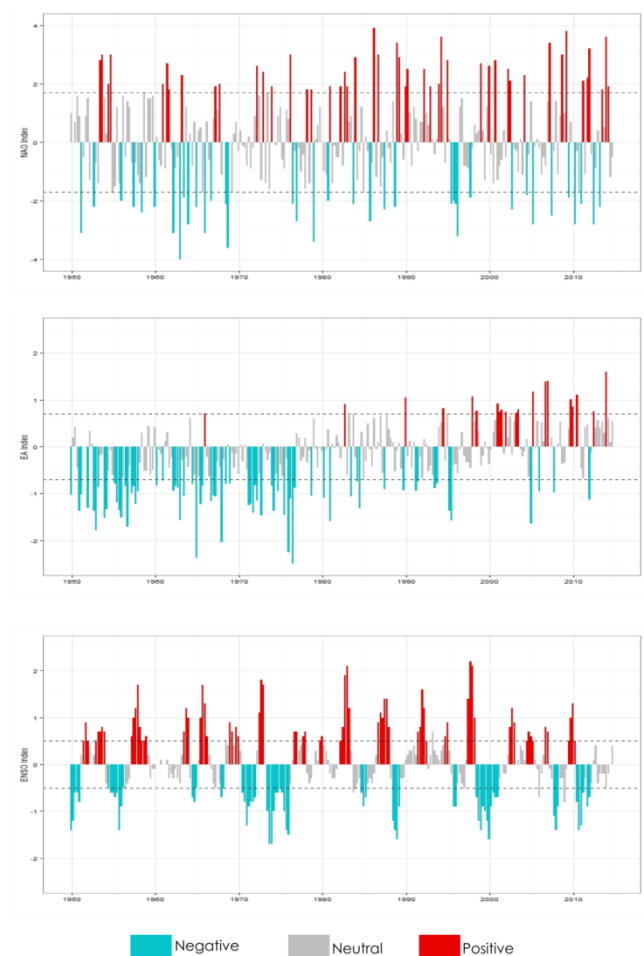
Figure A1 Identification of positive, negative and neutral phases of the indices of climate variability from 1950-2014. Dashed line illustrates the threshold level used to derive the classes.

Appendix A2 European sub-regions

European sub-regions were defined using the classification of the United Nations Statistics Division. Countries following such categorization, but not displayed in the map, were excluded from the analysis because flood events were not registered there by the NatCatSERVICE database of Munich Re.
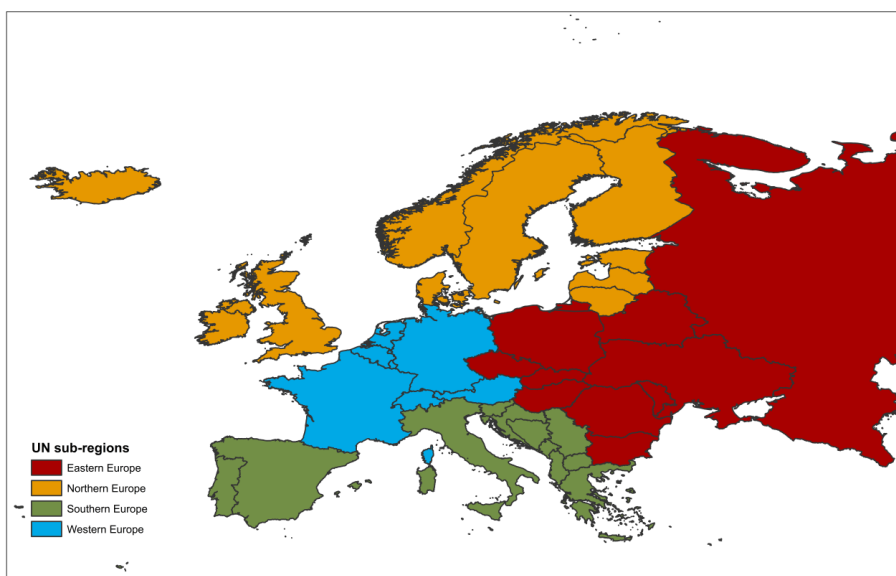
Figure A2 European sub-regions classification by the United Nations Statistics Division. Classification available at: http://unstats.un.org/unsd/methods/m49/m49regin.htm

Appendix A3 Distribution of reported Flood Occurrence and Flood Damage

To calculate Flood Damage we deflated the nominal flood damage recorded from 1980-2012 into 2010 US$ values, and converted these into Purchasing Power Parity (PPP) equivalent. PPP "represents the number of units of a country's currency required to buy the same amount of goods and services in the domestic market as U.S. dollar would buy in the United State" (The World Bank, 2016b). This index simply compares prices in different countries to detect which countries currency are currently under- or overvalued. Therefore, for comparison purpose, flood damage figures in this study are in 2010 international US dollars on PPP basis.

In Figure A3.A we show the reported flood events and damage recorded in the Munich Re database per sub-region and season. For the 22 years' time-series, 1227 flood events were reported in total. Between 1980 and 2012, western Europe was the sub-region with the highest number of (reported) flood events. For eastern Europe, approximately 90% (235 out of 289) of the floods occurred in spring and summer, while events in southern Europe occurred mostly during autumn and winter. Northern and western Europe often experience floods during summer and autumn, reaching up to 64% and 65% of the total events, respectively.

In terms of reported flood damage, southern and eastern Europe show the highest values. In southern Europe, most of the total reported damage occurs during autumn (Figure A3.B). Summer floods in eastern, western and northern Europe cause the highest economic damage there.
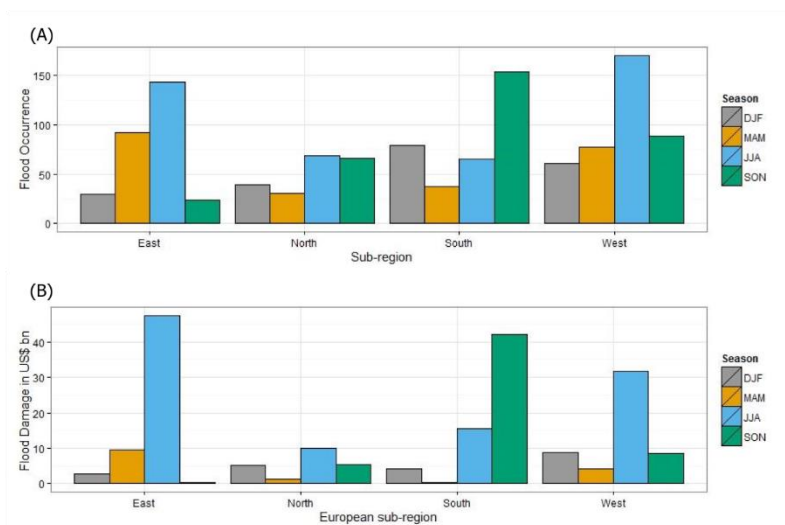
Figure A3 Distribution of (a) Flood Occurrence and (b) Flood Damage registered by the Munich Re database between 1980 and 2012 for each European sub-region and season. To calculate Flood Damage we deflated the flood damage recorded from 1980 to 2012 into 2010 US$ values, and converted them into Purchasing Power Parity (PPP), as described in section 2.2.2.2.

Appendix A4 Stablishing a normal value for Flood Occurrence and Flood Damage
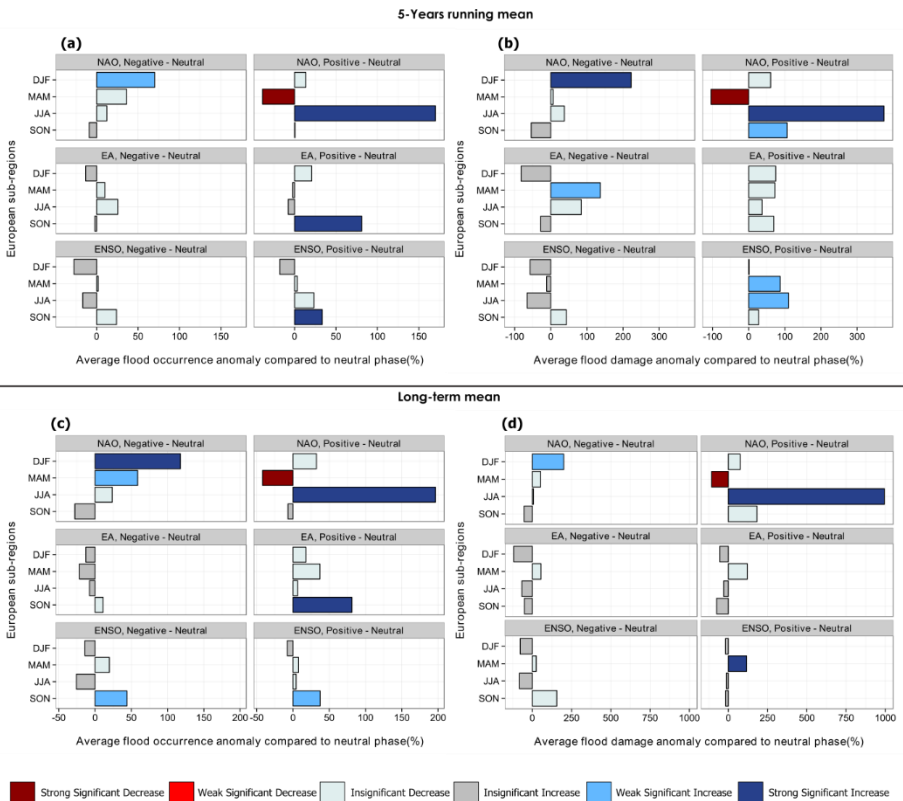
Figure A4.1 Comparison of methodologies to analyse the pan-European average percentage anomalies in Flood Occurrence and Flood Damage per season, during the positive and negatives phases of the different climate indices (compared to neutral). Results in (a) and (b) used a 5-years running mean, and in (c) to (d) the 32-years average.
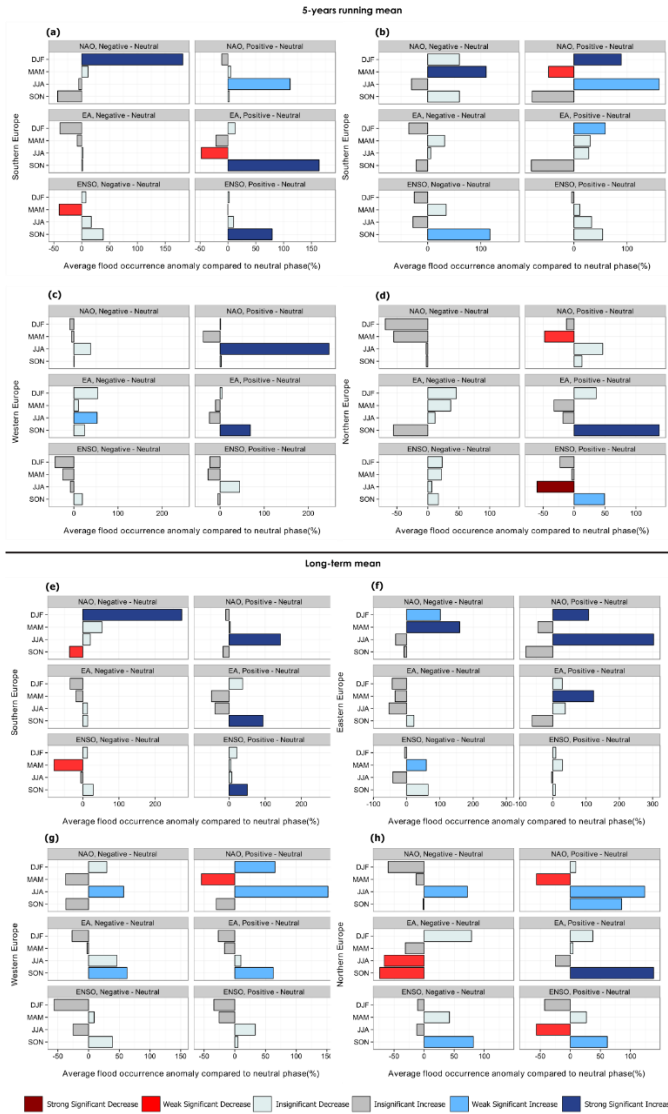
Figure A4.2 Comparison of methodologies to analyse the average percentage anomalies in flood occurrence per season and sub-region within the positive and negative phases of the different climate indices (compared to neutral). Results in (a) - (d) used a 5-years running mean, and in (e) - (h) the 32-years average.
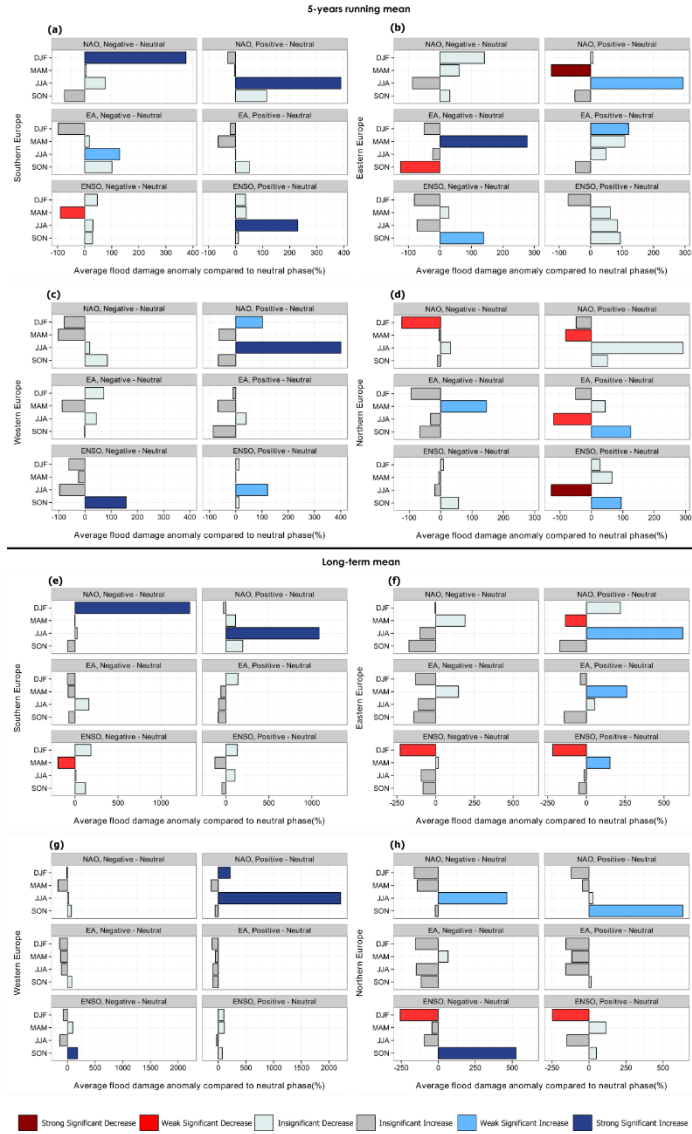
Figure A4.3 Comparison of methodologies to analyse the average percentage anomalies in flood damage per season and sub-region within the positive and negative phases of the different climate indices (compared to neutral). Results from (a) to (d) used a 5-years running mean, and from (e) to (h) the 32-years average.

Appendix A5 Bootstrapping the percentage flood anomaly

We tested the significance of the percentage anomalies using bootstrapping, which we describe it in five steps. For simplification, we give an example of how the bootstrap was applied to ENSO phases, however the same methodology was repeated for the NAO and EA:

(1)   From the 29 samples (from 1982 to 2010), we calculated the average anomaly in Flood Occurrence and Flood Damage between El Niño and neutral years and between La Niña and neutral years;

(2)   Then, we applied bootstrapping with replacement to obtain 10,000 samples of length referent to the number of years of each phase in the original series. For example, for ENSO$^+$ we randomly selected 9 values 10,000 times as there are 9 ENSO$^+$ years in the 29 years;

(3)   For each ENSO phase, we calculated the average anomalies in Flood Occurrence and Flood Damage of these random series obtained in step 2. Therefore we extracted 10,000 random average anomalies per ENSO phase;

(4)   Next, we calculated the difference for each of the 10,000 samples between ENSO$^-$ and ENSO neutral, and ENSO$^+$ and ENSO neutral;

(5)   Lastly, we obtained values for the 5% and 95% (for the "Strong" class) and 10% and 90% (for the "Weak" class) percentiles from the distribution of 10,000 random samples, and compared these to the averages obtained in step 1.

Appendix A6 Mean OER and IER per season and phase of the indices of climate variability
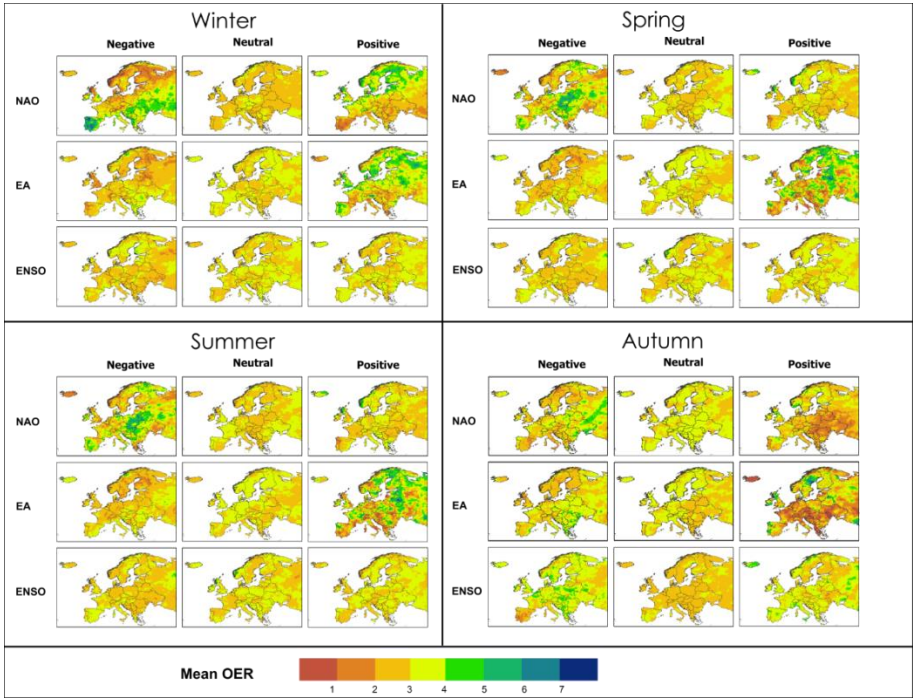
Figure A6.1 Mean occurrence of extreme rainfall per season and phase of the indices of climate variability.
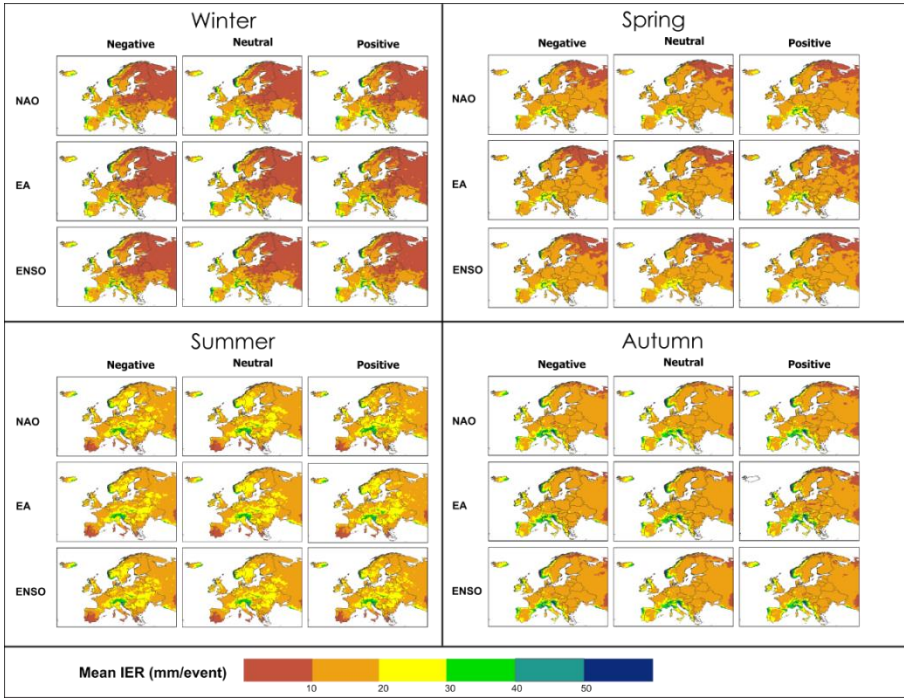
Figure A6.2 Mean intensity of extreme rainfall per season and phase of the indices of climate variability.

Appendix A7 Comparing the significance of the indicators

Table A7 Qualitative summary of the effects of NAO, EA and ENSO on Flood Damage and Flood Occurrence. Arrows show the effect of NAO, EA and ENSO on Flood Damage where a significant effect is found on Flood Occurrence. " ⇑ " describes significant high anomalies, while " ⇓ " describes significant low anomalies (compared to neutral phases). Colours characterize the phases of the indices of climate variability. Blank spaces mean that no significant effect was found on the Flood Occurrence indicator for the specific season.

Appendix A8 Comparison to previous research

In this section, we compare in more detail the findings of our research for each European sub-region with past studies. We particularly highlight past researches that dealt with the challenges of observing ENSO's influence in Europe.

A8.1 Southern Europe

NAO during winter has a north–south dipole, and NAO negative phases are related to a higher intensity and recurrence of winter extreme rainfall in parts of southern Europe, which is in agreement with other studies (Casanueva et al., 2014; Lopez-Bustins et al., 2008; Quadrelli et al., 2001; Rios-Cornejo et al., 2015; Rodó et al., 1997). During spring, we found that the relationship with NAO and the occurrence and intensity of extreme rainfall is less strong, and EA^+ (EA^-) is linked to less (more) frequent and intense extreme rainfall over sparse areas in southern Europe, which agrees with previous research (Casanueva et al., 2014). In summer, we observed that the overall NAO pattern weakens comparatively with the winter season, since the NAO's action centres tend to retreat northward, which is also reported by others (Rios-Cornejo et al. 2015; Barnston & Livezey 1987). Positive phases of NAO and EA during summer are linked to less frequent and intense extreme rainfall in vast area of southern Europe. In autumn, we observe that during EA^+ extremes are, in parts of Spain and Italy, significantly more intense, while more frequent in south-eastern Europe during both phases of ENSO.

Southern Europe, especially the Iberian Peninsula, is especially susceptible to ocean-atmospheric oscillations that can lead to anomalies in flood occurrence. On the one hand, that is due to its geographical position, located between the tropical and middle latitudes (Casanueva et al., 2014). Additionally, southern countries such as Italy, Croatia, Bosnia and Herzegovina, Albania, Slovenia and Greece have some of the lowest protection standards against flooding in Europe. According to a modelling study by Scussolini et al. (2015), large portions of many of these countries have flood protection structures that are only capable of coping with flood events of up to a 20-year return period. Consequently, many locations in southern Europe are not well adapted to deal with extreme flood events of low probability and high impact; this has been the case in Italy and Spain, which have previously suffered major flash floods and river flood disasters (Barredo, 2007).

A8.2 Eastern Europe

For winter, past studies suggested that the NAO$^+$ and EA$^+$ phases are linked to heavier precipitation over North-eastern areas, and a higher number of consecutive wet days (Casanueva et al., 2014; Krichak et al., 2014). The authors also pointed that the NAO$^-$ causes a reverse pattern, which is also in line with the results of our study. In spring, NAO$^-$ phases are linked to more frequent extreme rainfall, also observed by others (Krichak et al., 2014). In summer, NAO$^-$ is related to drier conditions in the Balkans. In addition, in autumn we observed less intense and frequent extreme rainfalls during both phases of NAO and EA$^+$, which are also in line with past research (Simon O. Krichak et al., 2014). Drier conditions over this region during this phase is also highlighted by others (Casanueva et al., 2014; López-Moreno & Vicente-Serrano, 2008).

Eastern European countries compose one of the sub-regions with the lowest standards for flood protection in the continent, and the FLOPROS database by Scussolini et al. (2015) suggests that countries such as Romania, Moldova, Ukraine, Belarus and Hungary have an average protection level of 1/20-years (Scussolini et al., 2015). Such factors should be taken into account when analysing the positive anomalies associated with the different phases of the indices of climate variability in registered floods events and their respective damages. It suggests that eastern Europe is influenced by climate variability in terms of flood occurrence and flood damage.

A8.3 Western Europe

In western Europe, in terms of peak discharge, several previous studies have found low sensitivity of west and central European rivers to NAO. Previous investigation emphasize that these regions comprise a transition zone of the NAO effect, and consequently, precipitation and river discharge only correlate weakly to the NAO index, which is line with our findings (Bouwer et al., 2006). In addition, other research indicate that NAO$^+$ (NAO$^-$) are associated with higher winter precipitation over northern (southern) Europe, while anomalies in rainfall in large western areas may be connected to other atmospheric indices such as the frequency of west circulation (FWC), and the north to south sea level pressure difference across the European continent (SLPD) (Bouwer et al., 2008). In complement, authors indicated that winter floods on the Elbe and Oder river have no significant correlation with the NAO index (Mudelsee et al., 2004). However, more recent studies point that NAO and EA positive phases are strongly related to a higher intensity and recurrence of winter extreme rainfall in the Atlantic Basin of western Europe, which is also highlighted by our findings (Casanueva et al., 2014; Simon O. Krichak et al., 2014). In summer and autumn NAO$^+$ phases are related to drier conditions in large areas of western Europe (Casanueva et al., 2014).

A8.4 Northern Europe

Winter precipitation extremes in northern Europe are greatly connected to NAO[+] and EA[+]. Such climatic variations bring more frequent extremes and intense heavy rainfall in the Atlantic Basin of northern Europe for the season compared to the neutral phase (Casanueva et al., 2014), especially over areas of the Norwegian coast, which is in agreement with past research (Uvo, 2003). Other studies also highlighted that NAO[+] phases cause heavier winter precipitation (Scaife et al., 2008) and increased consecutive wet days in the north of Europe (Casanueva et al., 2014). NAO[+], EA[+], and ENSO[+] phases are related with more intense and frequent extremes during spring in Sweden. However, extreme precipitation during summer is mostly related to NAO[-] phases. This could be the result of changes in the spatial configuration of the NAO influence in summer compared to winter, as in summer the positive centre of the NAO index moves towards north-eastern areas (Bladé et al., 2012; Casanueva et al., 2014).

Northern areas are under strong influence of climate oscillations, especially during winter and spring. However, higher anomalies of flood occurrence and flood damage are little perceived. The high levels of flood protection in northern Europe, as modelled and observed by Scussolini et al. (2015), may reduce the influence of climate variability in terms of flood occurrence and flood damage.

A8.5 ENSO's influence in Europe

ENSO is the most important mode of global climate variability, and has been linked with interannual changes in rainfall in many parts of the world, especially in the tropics. ENSO has a strong signal in rainfall at extratropical regions of North America and Australia, however ENSO's influence in the Atlantic and Europe is not clear yet, and several past studies attempted to identify ENSO teleconnections in these regions (Scaife, 2010).

The ENSO signal in Europe is not strong but may still be important under certain conditions, depending on how particularly strong is the ENSO event (Brönnimann, 2007). Past researches identified ENSO's signal in rainfall in southern Europe (Frias et al., 2010; Rocha, 1999; Rodó et al., 1997). For instance, a recent study found that ENSO influences rainfall in the Iberian Peninsula mostly during spring and autumn seasons with opposite sign (Casanueva et al., 2014); others suggest that some of the effects undergo a seasonal modulation or are nonlinear or asymmetric (Brönnimann, 2007). Previous research linked ENSO[+] to changes in the intensity of extreme rainfall in the Southern Europe (Casanueva et al., 2014; Mariotti et al., 2002; Shaman &

Tziperman, 2011; Sun et al., 2015), which is in agreement with our results. In our findings, the changes in the intensity of extreme rainfall linked to ENSO$^+$ is mostly limited to Spain.

During spring and autumn, ENSO is linked with a dipole of vorticity anomalies in the exit region of the North Atlantic jet along the European coast, whose anomalies extend to the surface and alter onshore winds and moisture fluxes (Shaman, 2014). Consequently, onshore moisture advection appears to be a main driver of ENSO-related mean precipitation changes over western Europe (Shaman, 2014). However, in terms of ENSO's influence on the intensity of extreme precipitation over western Europe, we observe only minor significant differences, which is in line with the results of a recent investigation (Sun et al., 2015). In addition, ENSO also affects northern Europe during winter asymmetrically for both positive and negative phases.

Furthermore, impacts of ENSO on climate may vary throughout the developing, mature or decaying its phases (Huang et al., 2012; Ronghui & Yifang, 1989; Wang & Gu, 2016; Zhang et al., 1999). Developing and decaying stages of El Niño and La Niña events show some common features (e.g., over eastern North America), but also significant differences in the pattern of observed and simulated anomalies, suggesting that the impacts of ENSO on the North Atlantic-European climate vary significantly between individual events (Mathieu et al., 2004). However, recent study suggests that discharges in the Danube River in Central Europe demonstrate same-signal response pattern throughout the developing, mature and decaying El Niño phases (Liang et al., 2016). Therefore, it is plausible that the results related to ENSO shown in Figures 2.2-2.3 may differ if the developing/decaying phase of ENSO is considered for the seasons.

Appendix B

Appendix B1 Seasonal distribution of flood losses

In the appendix Figure B1, we illustrate the seasonal distribution of flood events recorded in the 37 years' time series per country, and the adopted UN sub-regional division. The largest share of the total seasonal losses is attributed to southern Europe, where floods in fall account for 21% of all losses (appendix Figure B2). However, flood losses in western Europe account for 41% of all losses recorded between 1980 and 2016 (approximately 185 billion US$ 2016). In terms of annual distribution, summer is the season with the highest share of losses (37% of total), while in total winter is the season with the lowest share of losses (25 % of total).
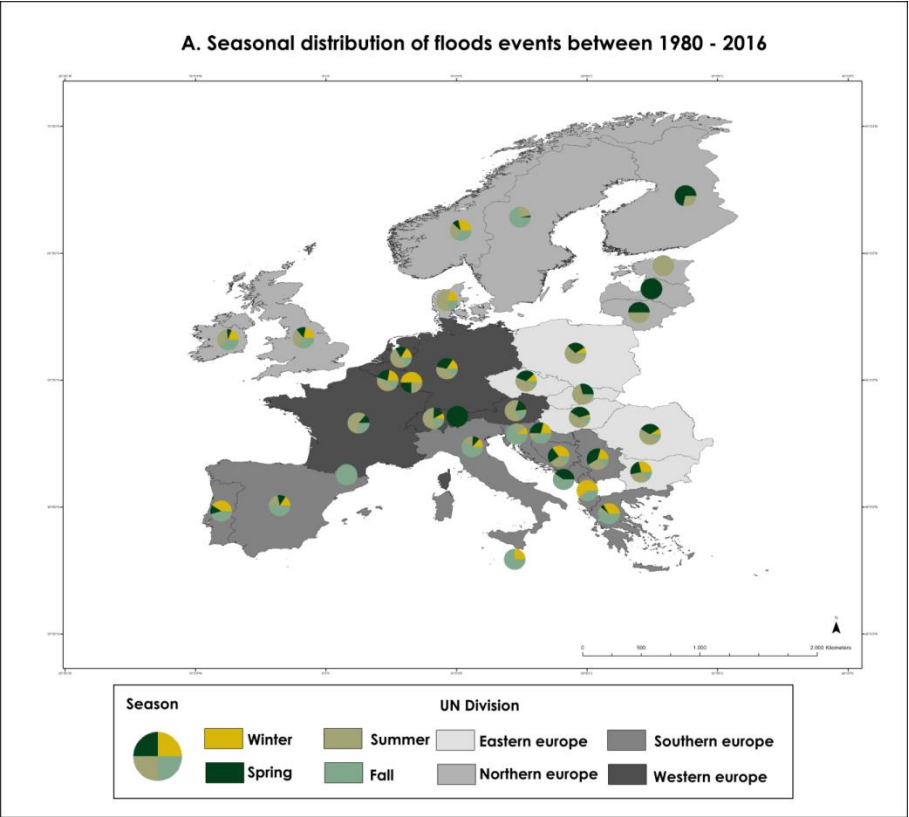
Figure B1 Flood events recorded during the period of 1980 - 2016 per season and sub-region.

Appendix B2 Distribution of flood losses 2016 per season and sub-region
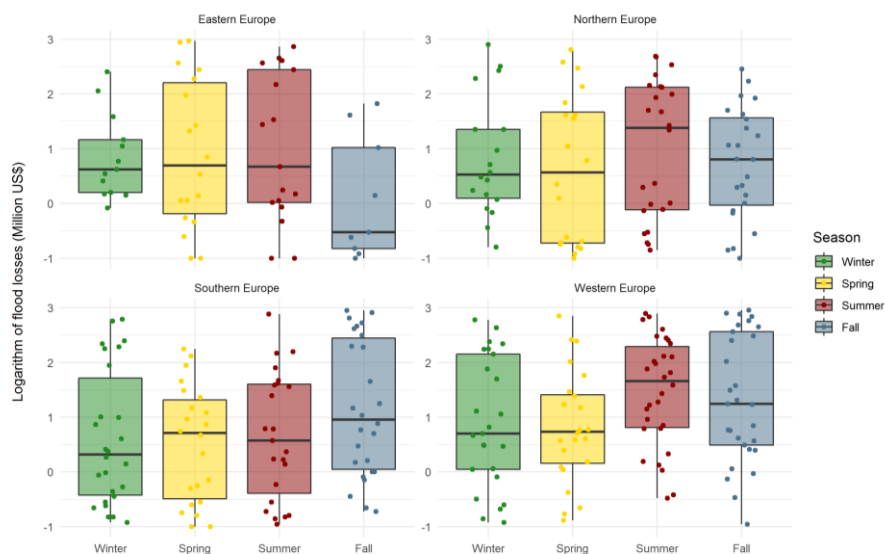
Figure B2 Distribution of flood losses recorded during the period of 1980 - 2016 per season and sub-region.

Appendix B3 Indices of atmospheric oscillations
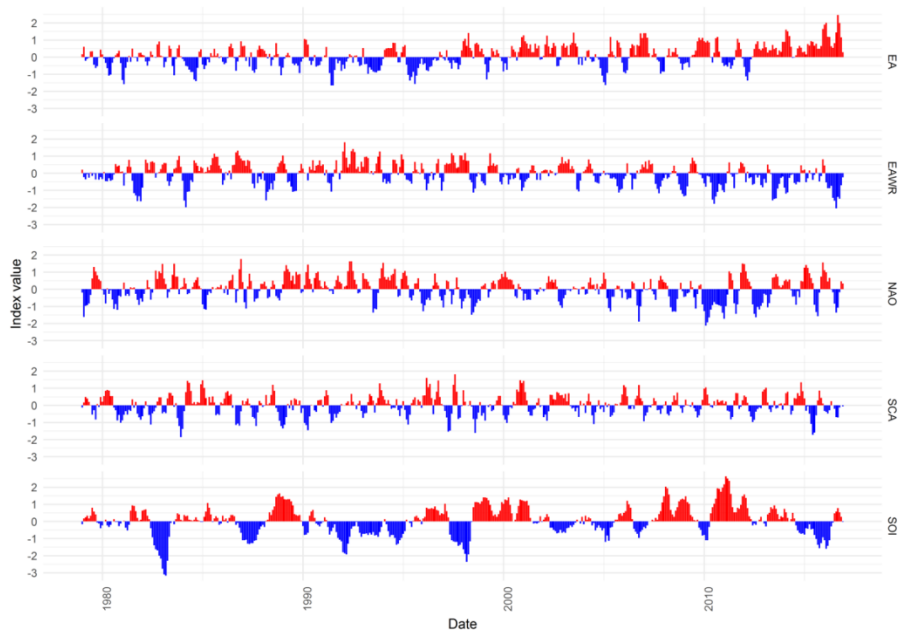
Figure B3 Time series of the 3-month average values of the five indices of atmospheric oscillations

Appendix B4 Measuring similarities among indices of atmospheric oscillations.

In the appendix Figure B4 and B5, we display the measured auto- and cross-correlation of the indices of atmospheric oscillations. We observe in Figure B4 that at lag 3 (seasonal lag), the autocorrelation is positive and below 0.25 for the four northern atmospheric oscillations. For the SOI index, we use an average over NDJ months, and the SOI's autocorrelation at lag 12 (one year) is slightly below zero. All the considered indices of atmospheric oscillations thus appear weakly auto correlated. In Figure B5, we show that the cross-correlation between the indices using a 3-month average at lag 0 is mostly low. Consequently, the low level of auto and cross-correlation between the indices of atmospheric oscillation should not negatively affect the performance of the logistic regressions.
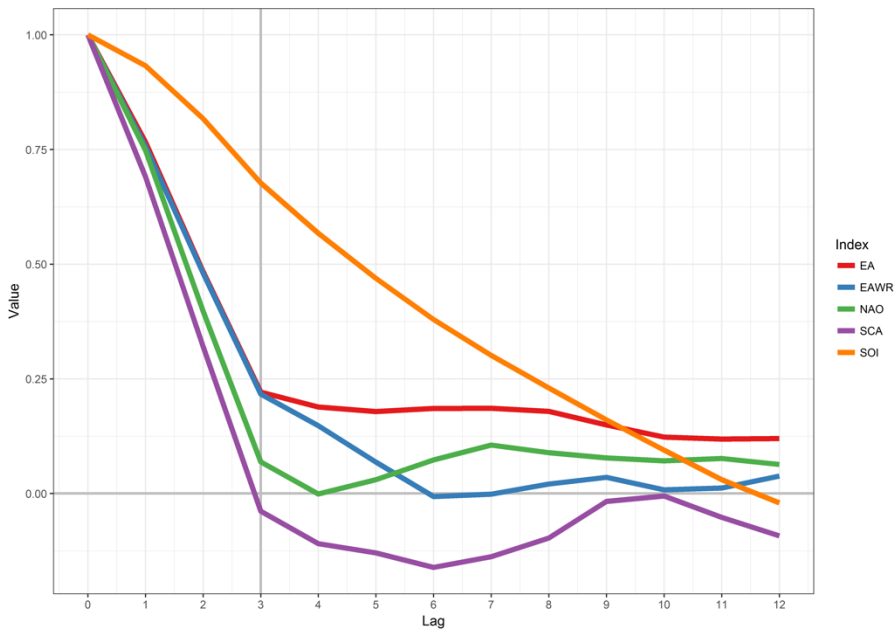
Figure B4 Autocorrelation coefficient of the five indices of atmospheric oscillations using a 3-month average at different lags.

Appendix B5 Cross-correlation coefficient
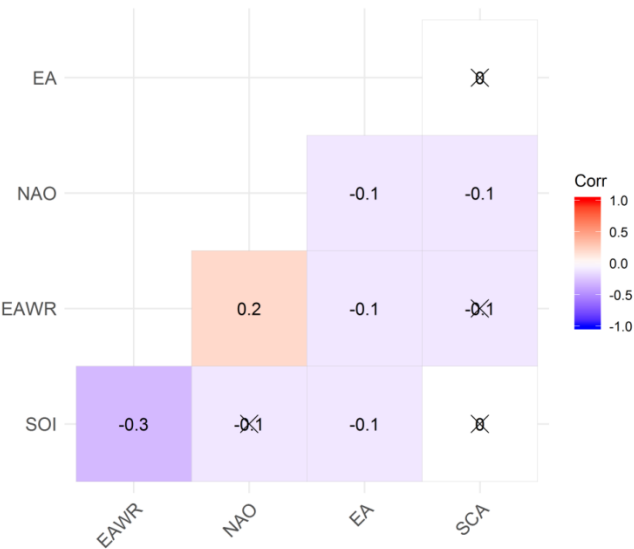
Figure B5 Cross-correlation coefficient of the five indices of atmospheric oscillations at lag 0 using a 3-month average. Insignificant cross-correlations are shown with an 'X' through the value (p-value < 0.1)

Appendix B6 Probability of Damaging flood events based on synchronous oscillations
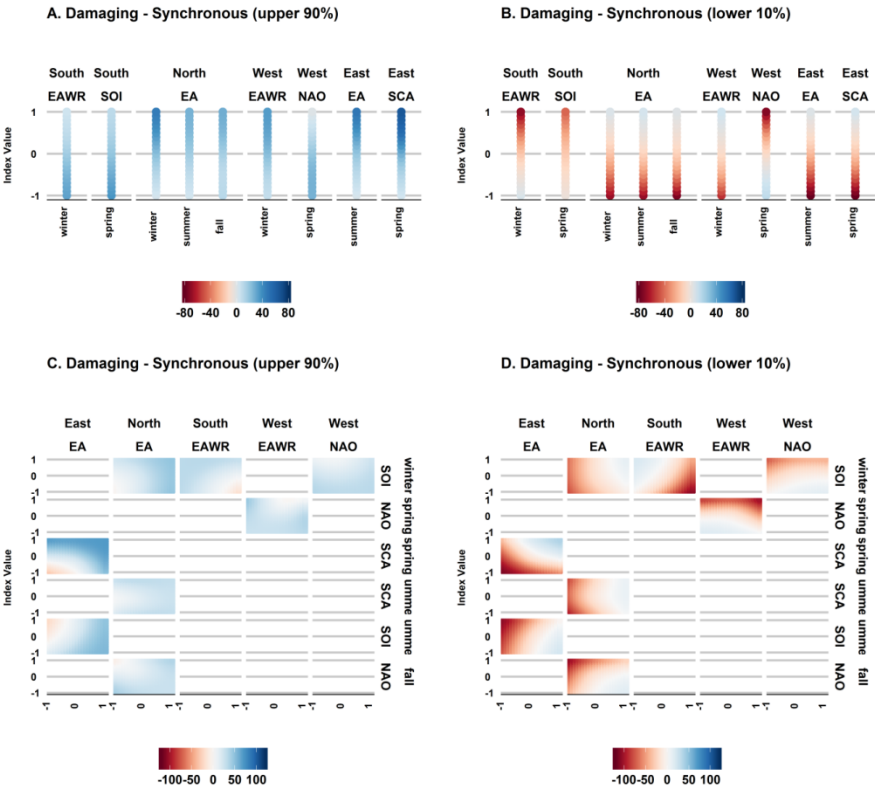
Figure B6 Confidence interval of the percentage increase and decrease in the probability of Damaging flood events based on synchronous oscillations.

Appendix B7 Probability of Damaging flood events based on seasonally lagged oscillations.
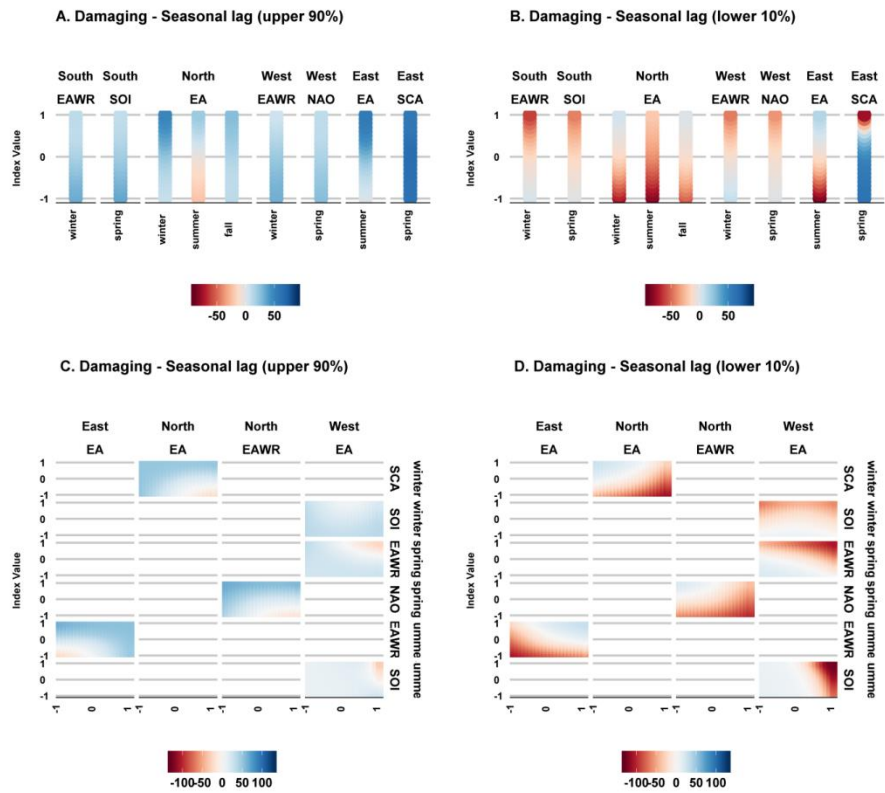
Figure B7 Confidence interval of the percentage increase and decrease in the probability of Damaging flood events based on seasonally lagged oscillations.

Appendix B8 Probability of Low Damaging flood events based on synchronous oscillations
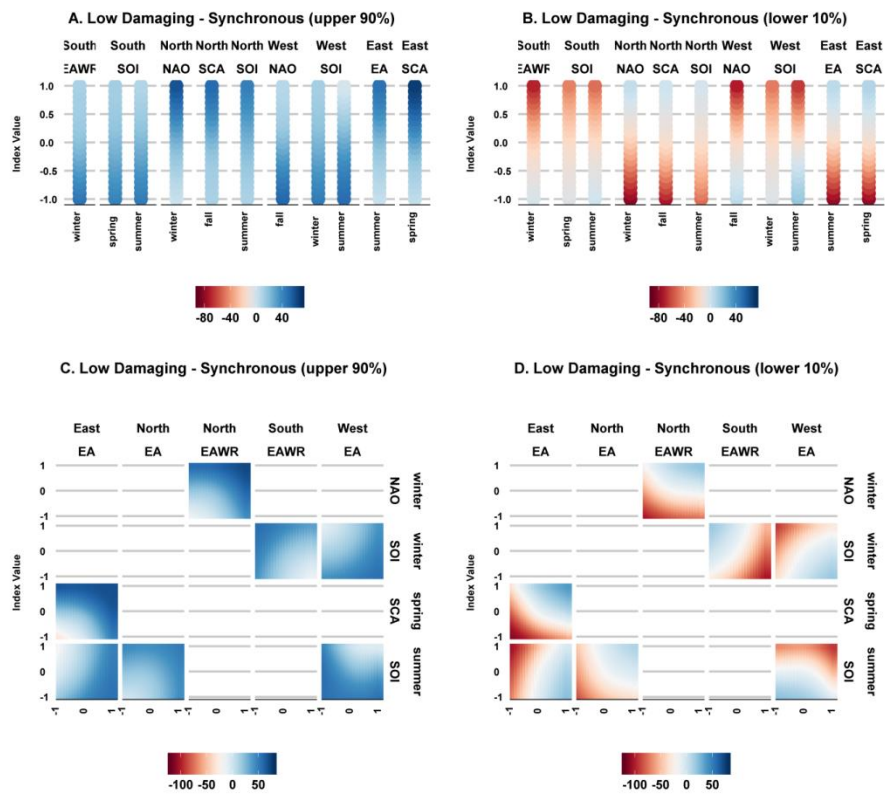
Figure B8 Confidence interval of the percentage increase and decrease in the probability of Low Damaging flood events based on synchronous oscillations.

Appendix B9 Probability of Low Damaging flood events based on seasonally lagged oscillations
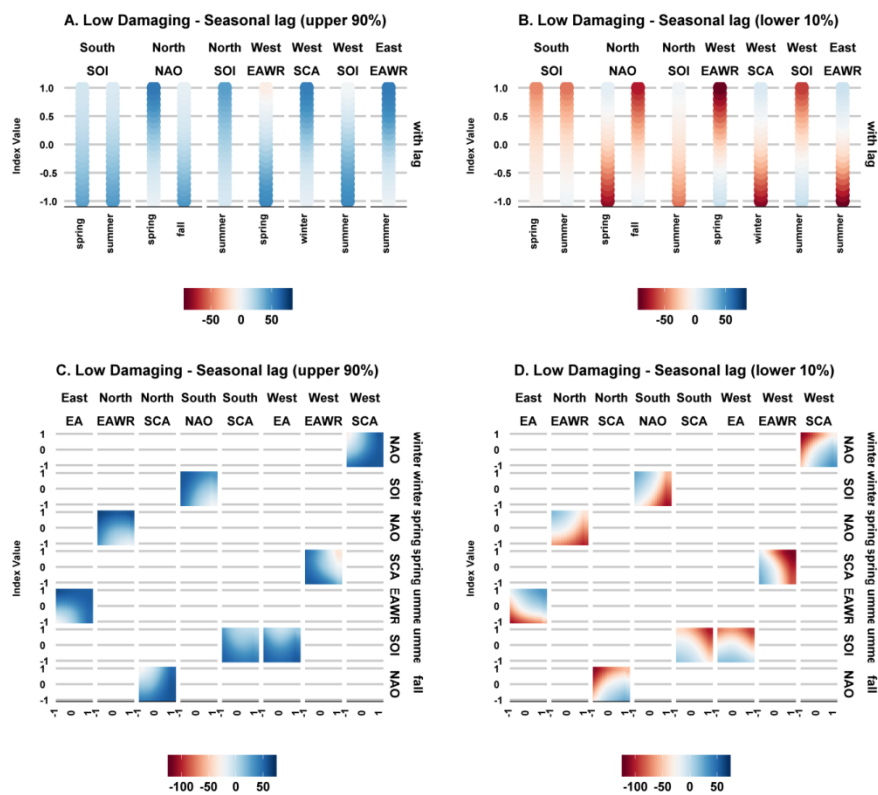
Figure B9 Confidence interval of the percentage increase and decrease in the probability of Low Damaging flood events based on seasonally lagged oscillations.

Appendix B10 Probability of Medium Damaging flood events based on synchronous oscillations
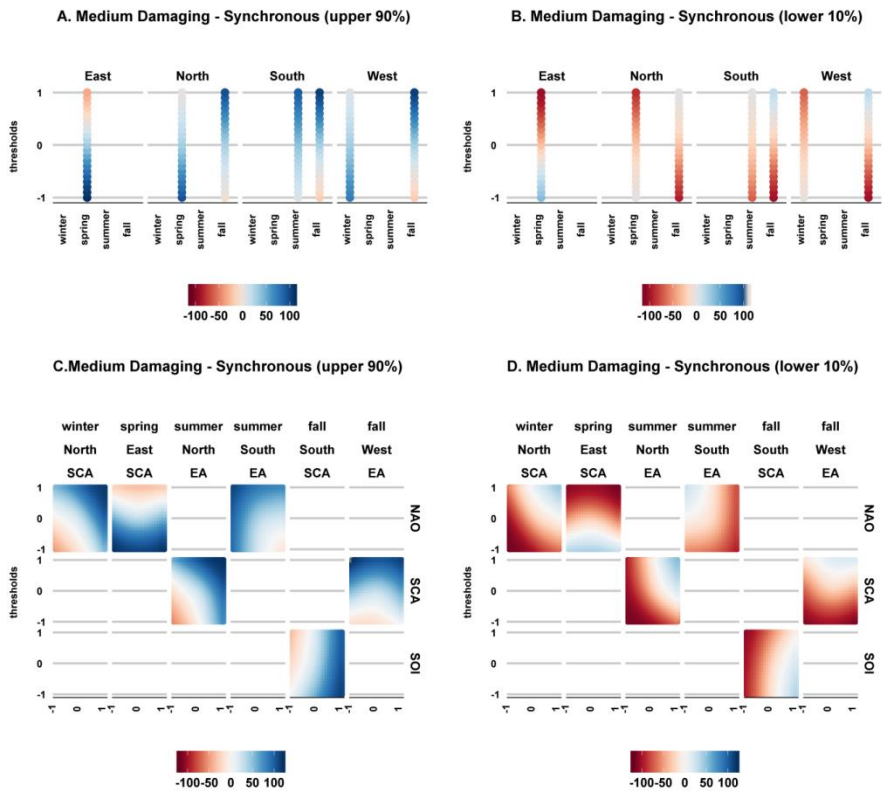
Figure B10 Confidence interval of the percentage increase and decrease in the probability of Medium Damaging flood events based on synchronous oscillations.

Appendix B11 Probability of Medium Damaging flood events based on seasonally lagged oscillations
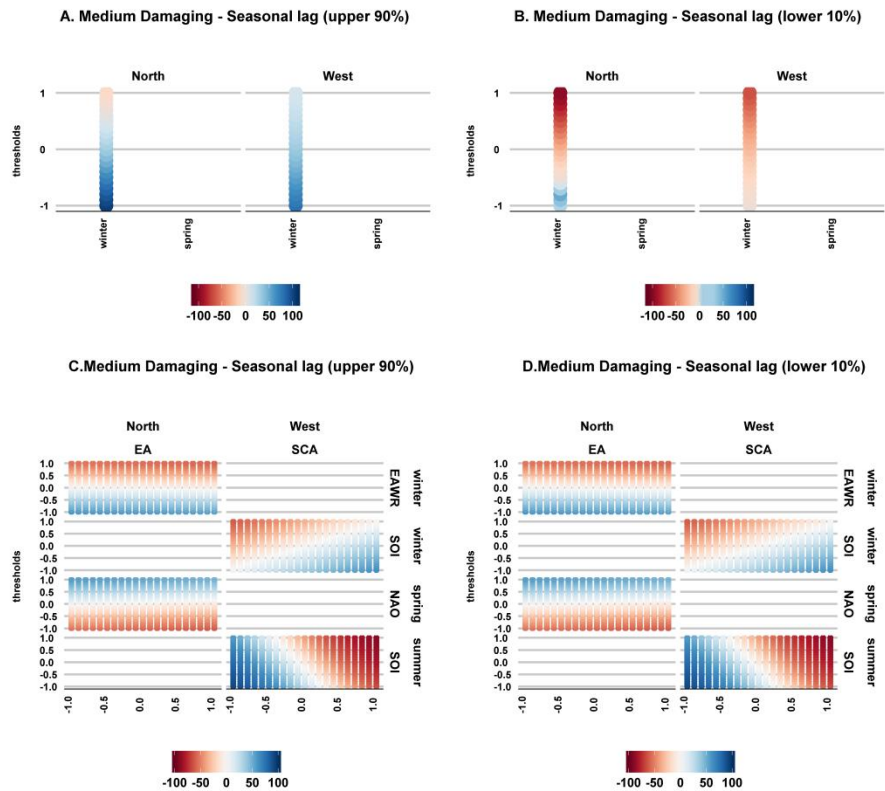
Figure B11 Confidence interval of the percentage increase and decrease in the probability of Medium Damaging flood events based on seasonally lagged oscillations.

Appendix C

Appendix C1 Estimate of the sugar beet harvest area
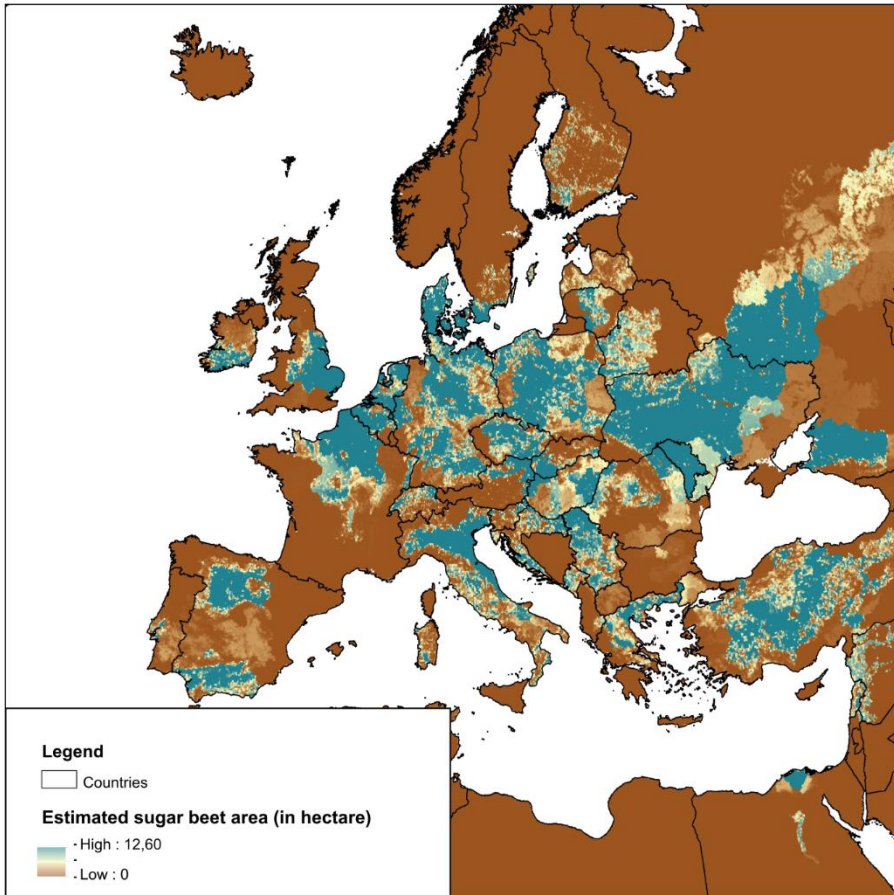
Figure C1 Estimated sugar beet area (in hectare) per grid cell (0.08° x 0.08°) obtained from the MIRCA 2000 project. For further description of dataset refer to previous studies (Portmann, Siebert, & Döll, 2010; Sacks et al., 2010). Dataset is available online at http://www.uni-frankfurt.de/45218023/MIRCA?legacy_request=1

Appendix C2 Study case regions

Figure C2 NUTS2 regions investigated in this study.

Appendix C3 Summary of statistics

Table C3 Summary of statistics presenting mean, standard deviation and length of sugar beet production dataset for 207 NUTS2 regions investigated in this study from 1975-2013.

NUTS2	Mean Value Sugar Beet Production (in 1000 tons)	Standard Deviation of Sugar Beet Production (in 1000 tons)	Length of data	NUTS2	Mean Value Sugar Beet Production (in 1000 tons)	Standard Deviation of Sugar Beet Production (in 1000 tons)	Length of data
AT11	276,28	276,28	39	FR91	600,65	600,65	37
AT12	2047,30	2047,3	39	FR92	182,16	182,16	37
AT13	22,47	22,47	39	FR93	4,85	4,85	37
AT21	0,98	0,98	39	FR94	1621,94	1621,94	37
AT22	14,26	14,26	39	HU10	98,99	98,99	27
AT31	383,26	383,26	39	HU21	274,40	274,4	27
BE10	2,77	2,77	39	HU22	600,86	600,86	27
BE21	36,89	36,89	39	HU23	315,51	315,51	27
BE22	394,58	394,58	39	HU31	151,64	151,64	27
BE23	338,40	338,4	39	HU32	922,16	922,16	27
BE24	507,99	507,99	39	HU33	489,58	489,58	27
BE25	795,36	795,36	39	IE01	91,71	91,71	39
BE33	756,37	756,37	39	IE02	1079,85	1079,85	39
BE34	8,46	8,46	39	ITC1	349,30	349,3	39
BE35	670,75	670,75	39	ITC4	1027,49	1027,49	39
BG31	31,33	31,33	27	ITF1	253,15	253,15	39
BG32	78,70	78,7	27	ITF2	112,30	112,3	39
BG33	21,90	21,9	27	ITF3	61,68	61,68	39
CZ01	23,99	23,99	27	ITF4	643,52	643,52	39
CZ02	1020,14	1020,14	27	ITF5	114,44	114,44	39
CZ03	237,45	237,45	27	ITF6	110,80	110,8	39
CZ04	251,88	251,88	27	ITH1	1,62	1,62	39

CZ05	773,31	773,31	27	ITH2	7,08	7,08	39
CZ06	795,80	795,8	27	ITH3	1817,47	1817,47	39
CZ07	344,02	344,02	27	ITH4	200,11	200,11	39
CZ08	179,23	179,23	27	ITH5	4073,35	4073,35	39
DE11	755,29	755,29	39	ITI1	271,24	271,24	39
DE12	277,68	277,68	39	ITI2	142,78	142,78	39
DE13	28,01	28,01	39	ITI3	1139,66	1139,66	39
DE14	63,45	63,45	39	ITI4	220,10	220,1	39
DE21	531,53	531,53	39	LT00	840,75	840,75	27
DE22	1197,99	1197,99	39	LV00	315,42	315,42	27
DE23	330,27	330,27	39	NL11	798,15	798,15	39
DE24	93,61	93,61	39	NL12	246,91	246,91	39
DE25	355,81	355,81	39	NL13	751,28	751,28	39
DE26	1083,94	1083,94	39	NL21	125,71	125,71	39
DE27	451,22	451,22	39	NL22	243,42	243,42	39
DE30	0,64	0,64	39	NL31	15,29	15,29	39
DE40	702,26	702,26	39	NL32	450,96	450,96	39
DE50	0,70	0,7	39	NL33	486,50	486,5	39
DE60	2,20	2,2	39	NL34	939,97	939,97	39
DE71	553,28	553,28	39	NL41	765,20	765,2	39
DE72	79,93	79,93	39	NL42	646,99	646,99	39
DE73	315,70	315,7	39	PL11	519,81	519,81	27
DE80	1274,25	1274,25	39	PL12	1022,96	1022,96	27
DE91	2360,38	2360,38	39	PL21	92,80	92,8	27
DE92	1921,12	1921,12	39	PL22	159,68	159,68	27
DE93	1373,65	1373,65	39	PL32	298,47	298,47	27
DE94	154,78	154,78	39	PL33	421,40	421,4	27
DEA1	1022,11	1022,11	39	PL34	214,15	214,15	27
DEA2	2067,79	2067,79	39	PL41	2478,34	2478,34	27
DEA3	85,05	85,05	39	PL42	646,76	646,76	27

DEA4	361,25	361,25	39	PL43	129,82	129,82	27
DEA5	155,91	155,91	39	PL51	1311,76	1311,76	27
DEB1	138,06	138,06	39	PL52	1001,29	1001,29	27
DEB2	31,45	31,45	39	PL61	2293,47	2293,47	27
DEB3	1012,11	1012,11	39	PL62	240,94	240,94	27
DEC0	5,85	5,85	39	PL63	599,05	599,05	27
DED2	302,06	302,06	39	PT16	9,91	9,91	37
DED4	169,39	169,39	39	PT17	14,74	14,74	37
DED5	404,66	404,66	39	PT18	111,06	111,06	37
DEE0	2558,20	2558,2	39	PT20	16,50	16,5	39
DEF0	753,51	753,51	39	RO12	422,81	422,81	27
DEG0	623,89	623,89	39	RO21	673,22	673,22	27
DK01	91,57	91,57	39	RO22	177,39	177,39	27
DK02	872,27	872,27	39	RO31	117,94	117,94	27
DK03	855,21	855,21	39	RO32	1,11	1,11	27
DK04	814,13	814,13	39	RO41	37,41	37,41	27
DK05	386,18	386,18	39	RO42	220,47	220,47	27
EE00	1,54	1,54	26	SE21	206,24	206,24	30
EL11	717,67	717,67	39	SE22	2102,53	2102,53	30
EL12	767,65	767,65	39	SE23	53,02	53,02	30
EL13	182,59	182,59	39	SK01	53,24	53,24	27
EL14	427,69	427,69	39	SK02	1127,16	1127,16	27
EL24	93,00	93	39	SK03	53,35	53,35	27
ES21	144,25	144,25	39	SK04	71,69	71,69	27
ES22	26,39	26,39	39	UKD1	9,82	9,82	39
ES23	156,48	156,48	39	UKD3	3,57	3,57	39
ES24	63,63	63,63	39	UKD4	12,41	12,41	39
ES30	3,04	3,04	39	UKD6	6,46	6,46	39
ES41	3749,21	3749,21	39	UKD7	1,26	1,26	39
ES42	555,70	555,7	39	UKE1	276,69	276,69	39

ES43	99,26	99,26	39	UKE2	391,99	391,99	39
ES61	1973,30	1973,3	39	UKE3	66,02	66,02	39
ES62	62,04	62,04	39	UKE4	70,45	70,45	39
FI19	290,77	290,77	30	UKF1	325,78	325,78	39
FI1B	0,90	0,9	30	UKF2	533,68	533,68	39
FI1C	289,65	289,65	30	UKF3	648,75	648,75	39
FI1D	290,80	290,8	30	UKG1	380,14	380,14	39
FI20	17,36	17,36	30	UKG2	243,24	243,24	39
FR10	3001,08	3001,08	39	UKG3	24,30	24,3	39
FR21	6641,02	6641,02	39	UKH1	3906,58	3906,58	39
FR22	10810,33	10810,33	39	UKH2	364,88	364,88	39
FR23	1717,46	1717,46	39	UKH3	663,21	663,21	39
FR24	1953,61	1953,61	39	UKJ1	300,71	300,71	39
FR25	546,24	546,24	39	UKJ3	6,89	6,89	39
FR26	442,75	442,75	39	UKK1	42,98	42,98	39
FR30	4378,33	4378,33	39	UKK2	8,63	8,63	39
FR41	20,35	20,35	39	UKK3	3,69	3,69	39
FR42	360,29	360,29	39	UKK4	6,87	6,87	39
FR43	60,59	60,59	39	UKL1	2,27	2,27	39
FR51	41,51	41,51	39	UKL2	11,21	11,21	39
FR71	14,00	14	39	UKN0	0,62	0,62	39
FR72	251,10	251,1	39				

Appendix C4 Train-test split method

We cross-validated and pruned the FFTs models using the train-test split method, which we describe below in five steps. Pruning is a technique in machine learning that reduces the size of decision trees by removing predictors that provide little decision power to the model.

1. Set the maximum number of predictors levels equal to 5, and train the FFTs models in 70% of all data.
2. Test the model in the other 30% remaining;
3. Calculate the balanced accuracy of the tested model;
4. Repeat step 1-3 four times adopting a maximum predictors levels equal to 4, 3, 2 and 1, subsequently;
5. Select the model and the pruning parameter (predictor's levels) that maximizes the balanced accuracy of the FFTs models.

Appendix C5 The AUC index
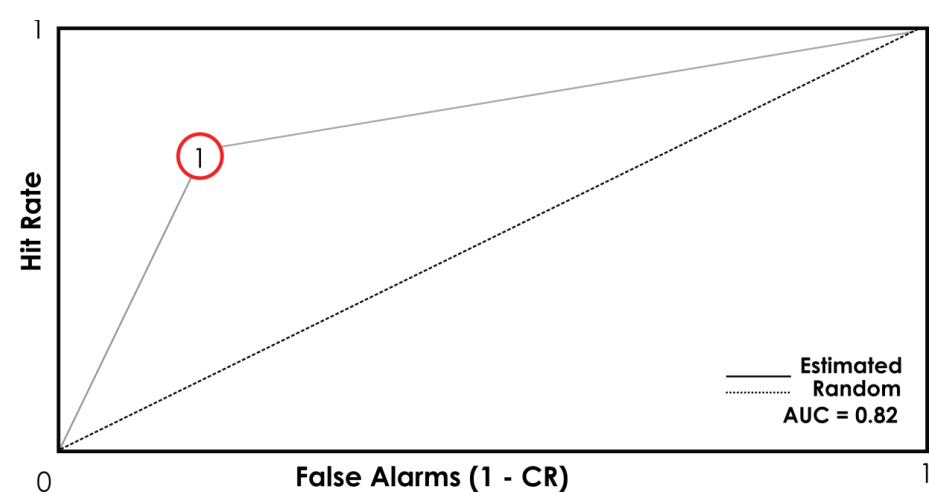
Figure C5 Representation of the AUC index calculated using the trapezoidal rule. The AUC index measures how well the FFT model can distinguish between two classes (low/high). A random classification migrates towards the diagonal dashed line.

Appendix C6 Bootstrapping and assessing the significance of the AUC index

We tested the significance of the AUC index at the NUTS2 level using a bootstrapping method, which we describe in 5 steps. The bootstrapping method is applied after we obtain the FFT model and the pruning parameter (described in appendix C8) that maximizes the balanced accuracy. We apply bootstrapping to test whether the AUC index of a random series is higher than AUC index obtained from the original series. Lastly, we assess the spatial significance of the results by applying a Field Significance test using the binomial distribution (Livezey & Chen, 1983). This test addresses the null hypothesis that the number of significant regions is different to the number of regions that one would expect by chance.

1. First, we bootstrap with replacement to obtain 1,000 samples of binary high and low sugar beet production events of length referent to the number of years of each NUTS2 region. For example, for the NUTS2 region AT11 and each lead time, we randomly selected 39 values 1,000 times as there are 39 years of sugar beet production available;

2. Second, we split the random series into training (70%) and testing (30%) data, similarly as applied in the original series. For example, for NUTS2 region AT11 the 1,000 training data each have a length of 27 values, while the 1,000 testing data have each a length of 12 values;

3. Third, for each NUTS2 region, lead time and testing data, we fitted our best performing FFT model. Next, we calculate for each NUTS2 region and lead time, 1,000 AUC indices of the tested models;

4. Fourth, for each NUTS2 region and lead time, we ranked the 1,000 AUC indices, and obtained the 90% percentile value ($\alpha=10$ %) from the distribution of 1,000 AUC indices. Lastly, we compared this value to the one obtained in the original series;

5. Fifth, we assessed the large-scale significance of the results by applying a Field Significance test using the binomial distribution. The results that were found not to be highly significant ($P<0.001$) are indicated in Figure 3.1 with an asterisk. In other words, regions that were found to be significant only due bootstrap test are indicated with an asterisk in Figure 3.1.

Appendix C7 Standard classification statistics for areas with predictive skill (AUC>0.7)

Table C7.1 Standard classification statistics for best performing FFT at lead time 6.

NUTS 2 ID	AUC	FAR (%)	MS (%)	CR (%)	HR (%)	NPV (%)	PPV (%)	Cues	Predictors	NA Values
AT13	0,75	33	17	67	83	71	80	NAO; SOI;EA	3	0
AT21	0,80	0	40	100	60	100	78	SOI;EA;NAO;EAWR;SCA	5	0
AT22	0,75	50	0	50	100	67	100	EA;SCA;NAO	3	0
AT31	0,73	40	14	60	86	75	75	EA	1	0
BE22	0,70	60	0	40	100	70	100	SCA;EA;EAWR	3	0
BE34	1,00	0	0	100	100	100	100	EAWR;NAO;SOI;EA	4	0
CZ01	0,80	0	40	100	60	100	60	EAWR	1	39
CZ02	0,80	0	40	100	60	100	60	EAWR	1	39
CZ03	0,80	0	40	100	60	100	60	EAWR	1	39
CZ04	0,80	0	40	100	60	100	60	EAWR	1	39
CZ05	0,80	0	40	100	60	100	60	EAWR	1	39

CZ06	0,80	0	40	100	60	100	60	EAWR	1	39
CZ07	0,80	0	40	100	60	100	60	EAWR	1	39
CZ08	0,80	0	40	100	60	100	60	EAWR	1	39
DE14	0,80	0	40	100	60	100	78	NAO; SCA	2	31
DE22	0,71	0	57	100	43	100	56	SCA;E AWR; SOI;N AO	4	31
DE24	0,80	0	40	100	60	100	78	NAO; SCA	2	31
DE27	0,71	0	57	100	43	100	56	SCA;E AWR; SOI;N AO	4	31
DE50	0,78	11	33	89	67	67	89	EAWR ;SCA; NAO	3	18
DE72	0,75	0	50	100	50	100	50	SCA;N AO;EA WR	3	33
DE94	0,70	0	60	100	40	100	70	NAO	1	32
DEB2	0,70	0	60	100	40	100	70	NAO	1	31
DEF0	0,70	60	0	40	100	70	100	EAWR ;NAO; EA	3	9
DEG0	0,76	20	29	80	71	83	67	EA	1	24
FR23	0,86	0	29	100	71	100	71	NAO; SCA;E AWR; EA	4	2
FR25	0,75	0	50	100	50	100	67	EA;EA WR;S OI;NA	4	2

							O		
FR26	0,70	0	60	100	40	100	70	SOI;EA;SCA;EAWR;NAO	5	2
HU23	0,75	25	25	75	75	75	75	NAO;SCA;SOI;EA;EAWR	5	20
HU31	0,75	25	25	75	75	75	75	EA;NAO;SCA	3	20
HU32	0,75	50	0	50	100	86	100	NAO;SOI;EA	3	20
IE01	0,81	25	12	75	88	88	75	NAO;SCA;EA;EAWR;SOI	5	38
IE02	0,81	25	12	75	88	88	75	NAO;SCA;EA;EAWR;SOI	5	38
ITC4	0,70	50	10	50	90	90	50	NAO;SCA;SOI	3	6
ITF1	0,83	20	14	80	86	86	80	EAWR;SCA	2	6
ITH1	0,83	20	14	80	86	86	80	NAO;SCA;EA;EAWR	4	32
ITH2	0,83	20	14	80	86	86	80	NAO;SCA;EA;EAWR	4	32
ITI1	0,80	0	40	100	60	100	33	EAWR;NAO;SCA	3	6

ITl4	0,70	50	10	50	90	90	50	NAO;SCA;SOI	3	6
NL22	0,81	25	12	75	88	88	75	EA;NAO	2	6
NL33	0,75	50	0	50	100	80	100	NAO;EA;EAWR	3	1
NL41	0,70	50	10	50	90	90	50	EAWR;NAO	2	1
NL42	0,86	0	29	100	71	100	71	NAO;EAWR;SCA;EA	4	1
PL33	1,00	0	0	100	100	100	100	EAWR;NAO;SCA;EA	4	20
PL34	0,75	50	0	50	100	86	100	EA;SCA	2	20
PL43	0,75	50	0	50	100	86	100	EA	1	20
PL63	0,90	0	20	100	80	100	75	SOI;EAWR;EA;NAO	4	20
PT20	0,81	25	12	75	88	88	75	EA;EAWR;SOI	3	6
RO21	0,79	43	0	57	100	25	100	EAWR;NAO;SCA;SOI;EA	5	20
RO32	0,75	0	50	100	50	100	86	SCA;SOI	2	25
RO41	0,75	0	50	100	50	100	86	EA;SCA	2	24
SE22	0,86	0	29	100	71	100	50	NAO;SCA;SOI	3	18

NUTS 2 ID	AUC	FAR (%)	MS (%)	CR (%)	HR (%)	NPV (%)	PPV (%)	Cues	Predictors	NA Values
SK02	0,90	0	20	100	80	100	75	EAWR ;NAO	2	20
SK03	0,75	50	0	50	100	86	100	SOI;E AWR; NAO; EA;	4	20
SK04	0,70	0	60	100	40	100	50	SOI	1	22

Table C7.2 Standard classification statistics for best performing FFT at lead time 5.

NUTS 2 ID	AUC	FAR (%)	MS (%)	CR (%)	HR (%)	NPV (%)	PPV (%)	Cues	Predictors	NA Values
AT22	0,75	50	0	50	100	100	67	EA	1	0
AT31	0,80	40	0	60	100	100	78	EA	1	0
BE34	0,75	17	33	83	67	71	80	SOI;EA	2	0
DE13	0,75	50	0	50	100	100	67	NAO	1	31
DE14	0,83	14	20	86	80	86	80	EA;SOI;NAO	3	31
DE21	0,88	25	0	75	100	100	89	SCA;NAO	2	31
DE24	0,83	14	20	86	80	86	80	EA;SOI;NAO	3	31
DE25	0,75	50	0	50	100	100	67	NAO	1	31
DE40	0,81	0	38	100	62	57	100	EA;SOI;NAO	3	39
DE50	0,72	22	33	78	67	88	50	NAO; EA;EAWR;S	4	18

								OI		
DE71	0,72	33	22	67	78	50	88	NAO; SOI;EAWR	3	33
DE73	0,72	33	22	67	78	50	88	NAO; EAWR	2	33
DE80	0,83	20	14	80	86	80	86	NAO; EA	2	24
DE91	0,81	25	12	75	88	75	88	NAO; EAWR	2	32
DE93	0,88	25	0	75	100	100	89	NAO	1	32
DE94	0,83	14	20	86	80	86	80	EA;SOI;NAO	3	32
DEA3	0,75	50	0	50	100	100	67	NAO	1	31
DEA4	0,88	25	0	75	100	100	89	SCA;NAO	2	31
DEA5	0,75	17	33	83	67	71	80	EAWR;SOI;SCA;NAO	4	31
DEB1	0,71	57	0	43	100	100	56	SCA;NAO	2	31
DEC0	0,81	0	38	100	62	57	100	EA;SOI;NAO	3	39
DED4	0,81	0	38	100	62	57	100	EA;SOI;NAO	3	39
DED5	0,81	0	38	100	62	57	100	EA;SOI;NAO	3	39
DEE0	0,81	0	38	100	62	57	100	EA;SOI;NAO	3	39
DEF0	0,73	40	14	60	86	75	75	EA	1	9

DEG0	0,80	40	0	60	100	100	78	EA;SCA;NAO	3	24
FR10	0,75	50	0	50	100	100	67	EA	1	2
FR22	0,75	50	0	50	100	100	67	EA	1	2
FR23	0,79	0	43	100	57	62	100	NAO	1	2
FR25	0,75	50	0	50	100	100	67	EA	1	2
FR30	0,94	0	12	100	88	80	100	NAO;EA;EAWR;SCA;SOI	5	2
FR51	0,75	50	0	50	100	100	67	EA	1	2
HU33	0,75	50	0	50	100	100	86	EAWR	1	20
IE01	0,75	25	25	75	75	60	86	NAO;EA	2	38
IE02	0,75	25	25	75	75	60	86	NAO;EA	2	38
ITF1	0,70	60	0	40	100	100	70	SOI	1	6
ITF6	0,75	50	0	50	100	100	91	SCA	1	6
ITH1	0,76	20	29	80	71	67	83	NAO;EA;EAWR	3	32
ITH2	0,76	20	29	80	71	67	83	NAO;EA;EAWR;;	3	32
NL22	0,94	0	12	100	88	80	100	EA;NAO;EAWR;SOI;SCA	5	6

NUTS2 ID	AUC	FAR (%)	MS (%)	CR (%)	HR (%)	NPV (%)	PPV (%)	Cues	Predictors	NA Values
NL42	0,73	40	14	60	86	75	75	NAO;EAWR	2	1
PL32	0,83	0	33	100	67	83	100	EAWR;SOI;EA	3	20
PL33	0,80	0	40	100	60	60	100	EAWR	1	20
PL43	0,83	0	33	100	67	50	100	EA;EAWR	2	20
PL61	0,75	50	0	50	100	100	67	SOI;NAO	2	20
SK02	0,80	0	40	100	60	60	100	EA;EAWR;SOI	3	20
SK04	0,83	33	0	67	100	100	83	SOI;EA;SCA	3	22

Table C7.3 Standard classification statistics for best performing FFT at lead time 4.

NUTS2 ID	AUC	FAR (%)	MS (%)	CR (%)	HR (%)	NPV (%)	PPV (%)	Cues	Predictors	NA Values
AT12	0,76	29	20	71	80	83	67	EA;NAO	2	0
AT22	0,75	50	0	50	100	100	67	EAWR;EA	2	0
AT31	0,76	20	29	80	71	67	83	EA;EAWR;SOI;SCA	4	0
DE13	0,92	0	17	100	83	86	100	EAWR;SCA;SOI;NAO	4	31
DE25	0,92	0	17	100	83	86	100	SCA;EA;EAWR;SOI;NAO	5	31

DE80	0,76	20	29	80	71	67	83	EA;SOI;EAWR;SCA;NAO	5	24
FI20	0,75	33	17	67	83	67	83	NAO;EAWR	2	20
FR10	0,83	0	33	100	67	75	100	EA	1	2
FR21	0,75	25	25	75	75	60	86	SCA;EAWR;EA	3	2
FR23	0,73	40	14	60	86	75	75	EA;EAWR;SOI;SCA	4	2
FR30	0,81	0	38	100	62	57	100	EAWR;SCA;EA	3	2
FR41	0,78	33	11	67	89	67	89	EAWR;NAO	2	2
FR92	0,75	50	0	50	100	100	78	EAWR;SOI;NAO;EA	4	5
HU21	0,83	0	33	100	67	83	100	EAWR;SCA	2	20
HU23	0,75	50	0	50	100	100	67	SCA;EA;EAWR	3	20
HU32	0,83	0	33	100	67	50	100	SCA;SOI	2	20
ITF4	0,75	17	33	83	67	71	80	SCA;EAWR;EA;NAO	4	6
ITI1	0,70	50	10	50	90	50	90	EAWR;SCA;SOI	3	6
NL11	0,80	0	40	100	60	33	100	SCA;NAO	2	1

NUTS2 ID	AUC	FAR (%)	MS (%)	CR (%)	HR (%)	NPV (%)	PPV (%)	Cues	Predictors	NA Values
NL13	0,73	14	40	86	60	75	75	NAO	1	1
NL34	0,83	17	17	83	83	83	83	SCA;NAO	2	1
NL41	0,75	0	50	100	50	29	100	NAO	1	1
PL32	0,83	0	33	100	67	83	100	EAWR;SOI;EA	3	20
PL51	0,83	33	0	67	100	100	83	EA;SCA	2	20
RO31	0,70	60	0	40	100	100	50	EA;EAWR	2	21

Table C7.4 Standard classification statistics for best performing FFT at lead time 3.

NUTS2 ID	AUC	FAR (%)	MS (%)	CR (%)	HR (%)	NPV (%)	PPV (%)	Cues	Predictors	NA Values
BE21	0,75	17	33	83	67	71	80	SCA;EAWR;EA;NAO	4	0
BE22	0,76	20	29	80	71	67	83	EAWR	1	0
BE23	0,75	17	33	83	67	71	80	SCA;EAWR;EA;NAO	4	0
BE25	0,75	0	50	100	50	67	100	EA;NAO;SCA;SOI;EAWR	5	0
BE34	0,75	50	0	50	100	100	67	EA;NAO;EAWR;SCA;SOI	5	0
DE13	0,75	0	50	100	50	67	100	EAWR;SCA	2	31

DE14	0,73	14	40	86	60	75	75	EAWR	1	31
DE22	0,73	40	14	60	86	75	75	SCA;NAO;SOI	3	31
DE23	0,73	40	14	60	86	75	75	SCA;SOI	2	31
DE24	0,73	14	40	86	60	75	75	EAWR	1	31
DE25	0,75	33	17	67	83	80	71	SCA	1	31
DE27	0,73	40	14	60	86	75	75	SCA;NAO;SOI	3	31
DE50	0,89	22	0	78	100	100	60	SOI	1	18
DE91	0,75	50	0	50	100	100	80	SCA;EAWR	2	32
DE92	0,75	50	0	50	100	100	80	SCA;EAWR	2	32
DE94	0,73	14	40	86	60	75	75	EAWR	1	32
DEA1	0,70	60	0	40	100	100	70	SCA;SOI;EAWR	3	31
DEA2	0,70	60	0	40	100	100	70	SCA;SOI;EAWR	3	31
DEA5	0,75	33	17	67	83	80	71	SOI	1	31
DEB1	0,80	0	40	100	60	78	100	SCA;EAWR	2	31
DEB2	0,73	14	40	86	60	75	75	EAWR	1	31
DEG0	0,70	60	0	40	100	100	70	SCA;EA	2	24

EL11	0,75	25	25	75	75	60	86	SCA	1	16
EL14	0,75	0	50	100	50	50	100	SOI;EA WR;E A;NAO ;SCA	5	11
EL24	0,75	17	33	83	67	71	80	SOI;EA WR;E A	3	16
ES22	0,81	38	0	62	100	100	57	EA;SC A;NAO ;SOI	4	3
FR24	0,71	0	57	100	43	56	100	SOI;EA	2	2
FR71	0,70	50	10	50	90	50	90	SOI;N AO	2	2
FR92	0,88	25	0	75	100	100	88	SOI;EA ;EAW R	3	5
FR93	0,75	50	0	50	100	100	78	EA;EA WR;N AO;SC A	4	5
HU21	1,00	0	0	100	100	100	100	EA;EA WR	2	20
HU23	0,75	50	0	50	100	100	67	NAO;E A;EA WR	3	20
IE01	0,94	0	12	100	88	80	100	SOI	1	38
IE02	0,94	0	12	100	88	80	100	SOI	1	38
ITF6	0,90	0	20	100	80	50	100	SOI	1	6
ITH1	0,70	60	0	40	100	100	70	NAO;E A;EA WR;SC A;SOI	5	32
ITH2	0,70	60	0	40	100	100	70	NAO;E A;EA WR;SC	5	32

								A;SOI		
ITH5	0,72	33	22	67	78	50	88	EA;NAO;SCA;EAWR	4	39
ITI3	0,72	33	22	67	78	50	88	EA;NAO;SCA;EAWR	4	39
NL12	0,81	25	12	75	88	75	88	EAWR;SCA	2	1
NL13	0,79	43	0	57	100	100	62	NAO;EA;SCA;SOI	4	1
NL21	0,75	25	25	75	75	86	60	NAO	1	6
NL34	0,75	17	33	83	67	71	80	NAO	1	1
PT18	0,70	60	0	40	100	100	67	EA;SCA;EAWR	3	25
RO12	0,79	43	0	57	100	100	25	EAWR;SOI	2	20
RO21	0,86	29	0	71	100	100	33	EAWR;SOI;EA;SCA;NAO	5	20
RO41	0,83	33	0	67	100	100	50	EAWR	1	24
UKD1	0,88	25	0	75	100	100	89	SOI	1	39
UKD3	0,88	25	0	75	100	100	89	SOI	1	39
UKD4	0,88	25	0	75	100	100	89	SOI	1	39
UKD6	0,88	25	0	75	100	100	89	SOI	1	39

UKD7	0,88	25	0	75	100	100	89	SOI	1	39
UKE1	0,88	25	0	75	100	100	89	SOI	1	39
UKE2	0,88	25	0	75	100	100	89	SOI	1	39
UKE3	0,88	25	0	75	100	100	89	SOI	1	39
UKE4	0,88	25	0	75	100	100	89	SOI	1	39
UKF1	0,88	25	0	75	100	100	89	SOI	1	39
UKF2	0,88	25	0	75	100	100	89	SOI	1	39
UKF3	0,88	25	0	75	100	100	89	SOI	1	39
UKG1	0,88	25	0	75	100	100	89	SOI	1	39
UKG2	0,88	25	0	75	100	100	89	SOI	1	39
UKG3	0,88	25	0	75	100	100	89	SOI	1	39
UKH1	0,88	25	0	75	100	100	89	SOI	1	39
UKH2	0,88	25	0	75	100	100	89	SOI	1	39
UKH3	0,88	25	0	75	100	100	89	SOI	1	39
UKJ1	0,88	25	0	75	100	100	89	SOI	1	39
UKJ3	0,88	25	0	75	100	100	89	SOI	1	39
UKK1	0,88	25	0	75	100	100	89	SOI	1	39

UKK2	0,88	25	0	75	100	100	89	SOI	1	39
UKK3	0,88	25	0	75	100	100	89	SOI	1	39
UKK4	0,88	25	0	75	100	100	89	SOI	1	39
UKL1	0,88	25	0	75	100	100	89	SOI	1	39
UKL2	0,88	25	0	75	100	100	89	SOI	1	39
UKN0	0,88	25	0	75	100	100	89	SOI	1	39

Table C7.5 Standard classification statistics for best performing FFT at lead time 2.

NUTS2 ID	AUC	FAR (%)	MS (%)	CR (%)	HR (%)	NPV (%)	PPV (%)	Cues	Predictors	NA Values
AT12	0,80	0	40	100	60	78	100	NAO;EA;SCA	3	0
AT31	0,76	20	29	80	71	67	83	EA;NAO	2	0
BE21	0,75	0	50	100	50	67	100	SOI;SCA;EA;NAO	4	0
BE22	0,79	0	43	100	57	62	100	EA;EAWR	2	0
BE23	0,92	0	17	100	83	86	100	EAWR;SOI;SCA;EA;NAO	5	0
BE25	0,75	50	0	50	100	100	67	SCA;NAO;EA;EAWR	4	0
BE33	0,76	20	29	80	71	67	83	EA;EAWR	2	0

DE13	0,75	17	33	83	67	71	80	EA;SOI;EAWR;NAO;SCA	5	31
DE50	0,78	11	33	89	67	89	67	SOI	1	18
DE60	0,80	0	40	100	60	78	100	SOI	1	17
DE72	0,75	50	0	50	100	100	80	SCA;NAO;EAWR;EA;SOI	5	33
DE80	0,93	0	14	100	86	83	100	EA;SOI;EAWR;SCA	4	24
DEF0	0,83	20	14	80	86	80	86	EAWR;SOI;SCA;NAO	4	9
DEG0	0,70	60	0	40	100	100	70	EA;SOI;SCA	3	24
DK02	0,75	25	25	75	75	86	60	SCA;EA;SOI;EAWR;NAO	5	31
EL13	0,83	0	33	100	67	75	100	EAWR	1	16
EL24	0,83	0	33	100	67	75	100	EAWR	1	16
ES22	0,75	25	25	75	75	86	60	SOI;SCA;EA;EAWR;NAO	5	3
ES42	0,81	25	12	75	88	75	88	SCA	1	3
ES43	0,72	0	56	100	44	38	100	EA;SOI;SCA	3	3
ES61	0,80	40	0	60	100	100	78	SCA;SOI;NAO	3	3

ES62	0,78	33	11	67	89	67	89	SCA	1	4
FI20	0,75	33	17	67	83	67	83	EA;NAO;SCA;EAWR	4	20
FR25	0,75	17	33	83	67	71	80	EAWR;SCA;EA;SOI;NAO	5	2
FR26	0,70	0	60	100	40	70	100	EA;SOI	2	2
FR43	0,71	57	0	43	100	100	56	SCA;EA;EAWR	3	2
FR51	0,75	17	33	83	67	71	80	SCA;EA;SOI;EAWR;NAO	5	2
FR92	0,75	50	0	50	100	100	78	EAWR;SOI	2	5
FR94	0,93	0	14	100	86	80	100	SCA;SOI	2	5
HU10	0,80	0	40	100	60	60	100	SCA;SOI;EAWR;NAO	4	20
HU21	0,80	40	0	60	100	100	60	EA;SOI;EAWR	3	20
HU23	0,75	50	0	50	100	100	67	EA;SCA	2	20
HU33	0,75	50	0	50	100	100	86	EA;NAO;SOI;SCA	4	20
ITF5	0,76	29	20	71	80	83	67	SOI;EAWR	2	6
ITF6	0,70	50	10	50	90	50	90	EAWR;SOI;EA;NAO	4	6

LV00	1,00	0	0	100	100	100	100	EA;EAWR;SOI	3	22
NL22	0,94	0	12	100	88	80	100	EAWR;SOI	2	6
NL41	0,75	50	0	50	100	100	91	SCA;EA;NAO	3	1
PL42	1,00	0	0	100	100	100	100	SOI;EAWR;EA;SCA;NAO	5	20
PL61	0,75	0	50	100	50	67	100	EA;EAWR	2	20
PL63	0,73	33	20	67	80	67	80	SOI	1	20
RO12	0,79	43	0	57	100	100	25	EAWR	1	20
RO21	0,79	43	0	57	100	100	25	EAWR	1	20
RO22	0,75	0	50	100	50	86	100	EAWR;EA;SOI;SCA;NAO	5	22
RO31	0,90	20	0	80	100	100	75	EAWR	1	21
RO32	0,83	33	0	67	100	100	50	EA;EAWR	2	25
RO41	0,92	17	0	83	100	100	67	EAWR	1	24
RO42	0,90	20	0	80	100	100	75	EAWR	1	20
SK02	0,73	33	20	67	80	67	80	EA;SOI;SCA;EAWR	4	20

Table C7.6 Standard classification statistics for best performing FFT at lead time 1.

NUTS2 ID	AUC	FAR (%)	MS (%)	CR (%)	HR (%)	NPV (%)	PPV (%)	Cues	Predictors	NA Values
AT31	0,71	0	57	100	43	56	100	EA;EAWR;SOI;SCA;NAO	5	0
BE10	0,70	50	10	50	90	50	90	EAWR;EA;NAO;SCA;SOI	5	3
BE21	0,83	0	33	100	67	75	100	NAO;EA;SOI	3	0
BE23	0,83	0	33	100	67	75	100	EA;SOI	2	0
BE25	0,92	17	0	83	100	100	86	NAO;SOI;EA;SCA;EAWR	5	0
DE13	0,75	50	0	50	100	100	67	EA;NAO;SCA	3	31
DE21	0,75	50	0	50	100	100	80	EA;EAWR;NAO;SCA	4	31
DE50	0,72	22	33	78	67	88	50	SOI	1	18
DE80	0,76	20	29	80	71	67	83	NAO;EA	2	24
DE93	0,75	50	0	50	100	100	80	SCA;EA;EAWR;NAO	4	32
DEA3	0,75	50	0	50	100	100	67	EA;NAO;SCA	3	31
DEA4	0,75	50	0	50	100	100	80	EA;SCA;EAWR;N	5	31

							AO;SOI		
ES22	0,81	38	0	62	100	100	57	SCA;EA;EAWR;SOI;NAO	5	3
ES61	0,79	0	43	100	57	62	100	EA;EAWR;NAO;SCA;SOI	5	3
FI1B	0,86	0	29	100	71	50	100	EA;EAWR;NAO	3	39
FI1C	0,86	0	29	100	71	50	100	EA;EAWR;NAO	3	39
FI1D	0,86	0	29	100	71	50	100	EA;EAWR;NAO	3	39
FR43	0,90	0	20	100	80	88	100	NAO;EA;SCA;SOI;EAWR	5	2
IE01	0,88	0	25	100	75	67	100	SCA;SOI;EAWR;EA;NAO	5	38
IE02	0,88	0	25	100	75	67	100	SCA;SOI;EAWR;EA;NAO	5	38
NL22	0,75	50	0	50	100	100	80	EA;EAWR;SOI;NAO	4	6
PL22	0,75	50	0	50	100	100	67	NAO;SCA;SOI	3	20
PL34	0,92	0	17	100	83	67	100	EA;SCA;SOI;EAWR	4	20
PL62	0,70	60	0	40	100	100	50	NAO	1	20

RO21	0,86	29	0	71	100	100	33	EA;SCA;SOI;EAWR;NAO	5	20
RO22	1,00	0	0	100	100	100	100	EA;SCA;EAWR;SOI;NAO	5	22
RO42	0,83	0	33	100	67	83	100	SOI;EA;EAWR;SCA;NAO	5	20

Appendix C8 Spatial distribution of the sugar beet production predictors
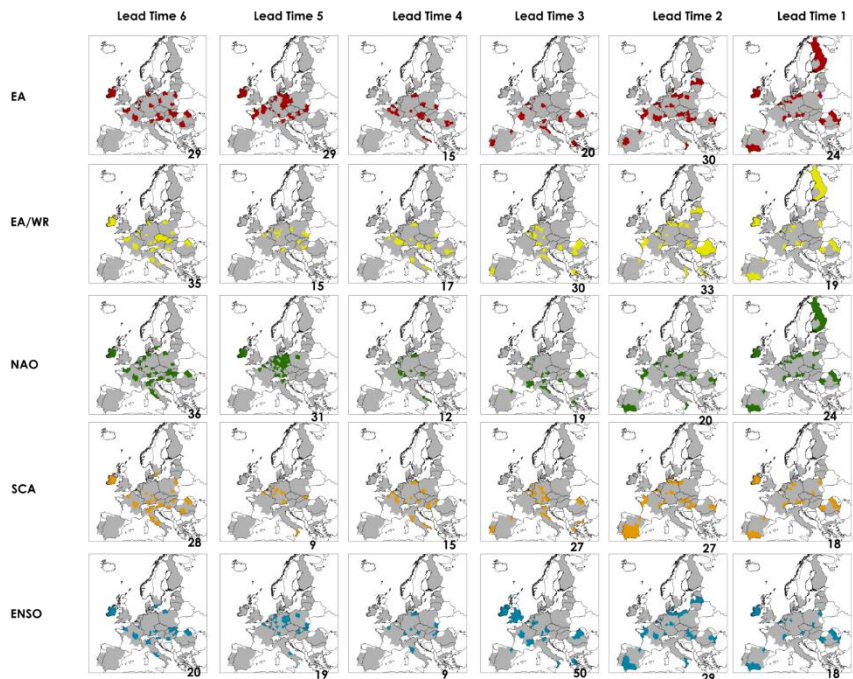
Figure C8 Spatial distribution of the indices of climate variability that were used as predictors by the FFT model for regions with significant AUC>0.7 at six lead times. Regions without predictive skill (AUC<0.7) are shown in grey, and the number at the bottom of each map the amount of times that each index was used as predictors.

Appendix C9 Spatial distribution of the sugar beet production
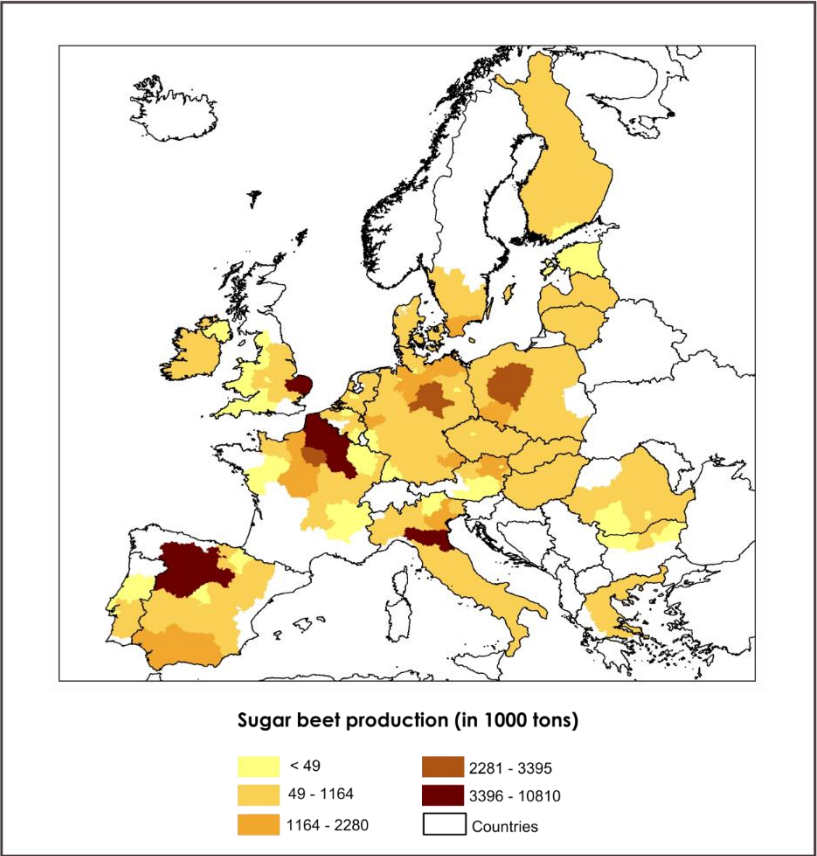
Figure C9 Distribution of the mean sugar beet production (in 1000 tons) per NUTS2 region in the investigated areas.

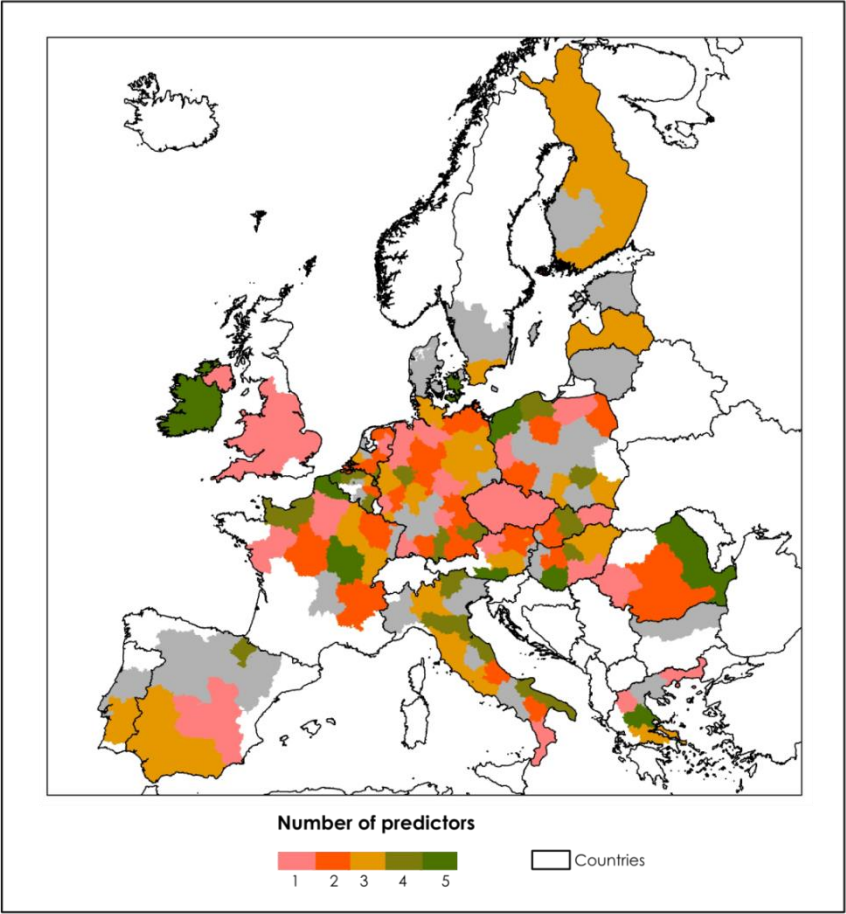# Appendix C10 Spatial distribution of number of predictors

Figure C10 Spatial distribution of number of indices of climate variability that were used as predictors by the FFT model for regions with significant AUC>0.7 at six lead times. NUTS2 regions in grey represent the areas investigated. The maps were overlaid in descending order from longest to shortest lead time.

Appendix D

Appendix D1 Maize yield and respective percentiles per district
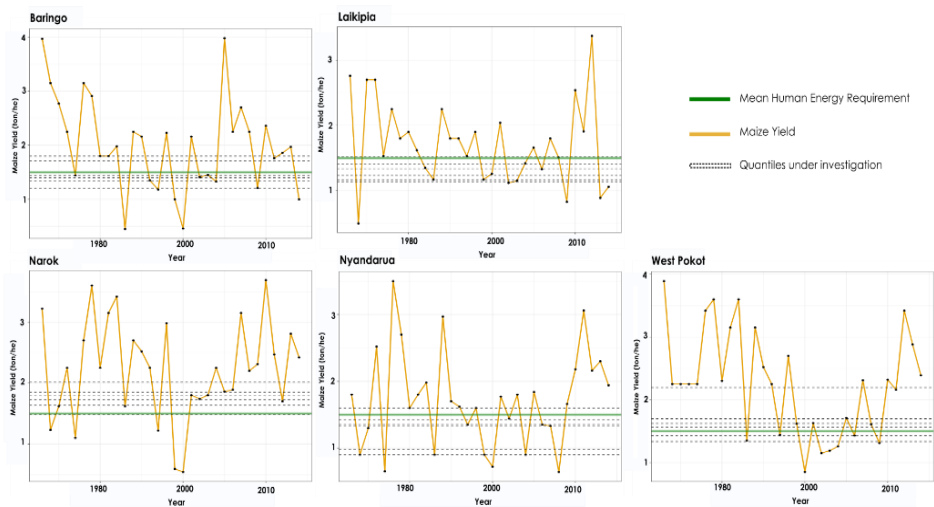
Figure D1 Time series of Maize yield per district. From bottom-up in the plots, dashed lines represent maize yields percentiles 15% or $Y_{15\%}$, 20% or $Y_{20\%}$, 25% or $Y_{25\%}$, 30% or $Y_{30\%}$, 35% or $Y_{35\%}$ and 40% or $Y_{40\%}$, respectively. Green line represents the mean Human Energy Requirement threshold (3,000 kcal/cap/day ≈ 1.5 ton/he/household/year).

Appendix D2 Example of a Fast-and-Frugal Tree (FFT) model for maize yield Y$_{15\%}$.
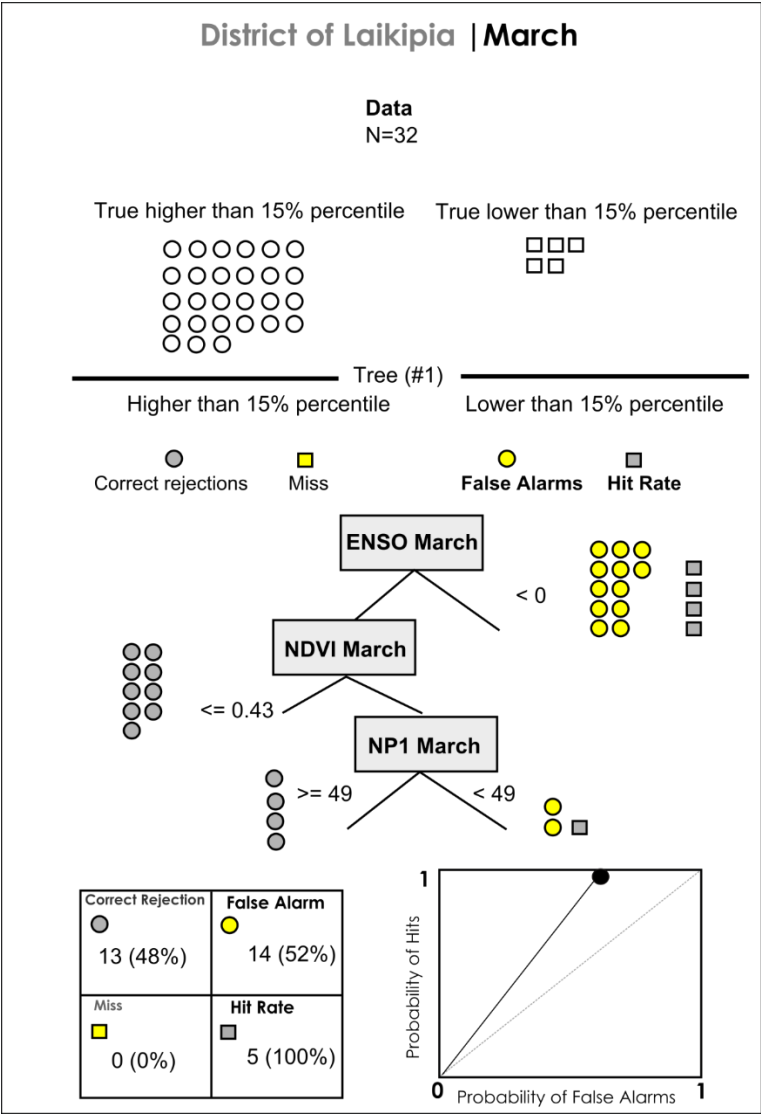
Figure D2 Example of an FFT model at Lead Time 6 that predicts maize yield percentile Y$_{15\%}$ in Laikipia. This output shows standard classification statistics, chosen predictors and their thresholds.

Appendix D3 The ROC index
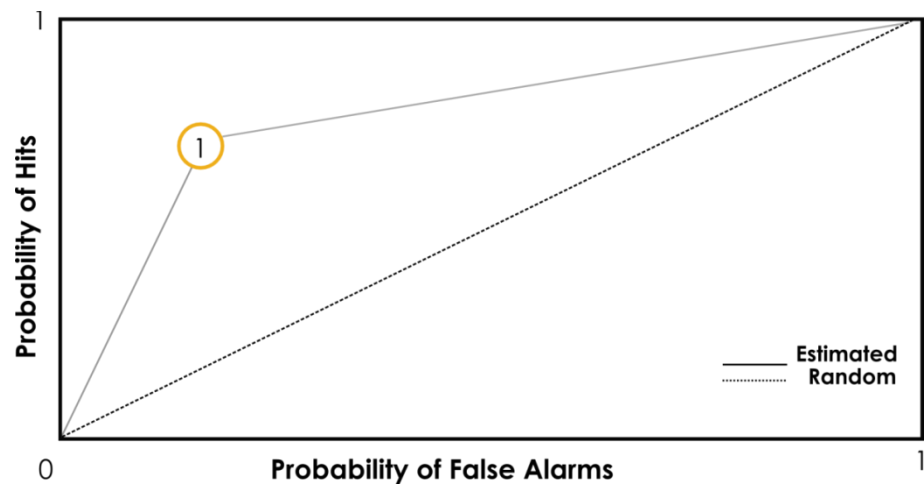
Figure D3 Representation of the Receiver operating characteristic (ROC) curve calculated using the trapezoidal rule. The ROC curve is a graphical plot that illustrates the performance of a binary classifier system, and the area under the curve of the ROC index measures how well the FFT model can distinguish between two classes (low/high). A random classification migrates towards the diagonal dashed line.

Appendix D4 Leave-one-out cross validation

We cross-validated and pruned the FFT models using the Leave-one-out cross validation method, which we describe below in five steps. Pruning is a technique in machine learning that reduces the size of decision trees by removing predictors that provide little decision power to the model.

1. Set the maximum number of predictors levels equal to 5, and train the FFT model using N-1 samples, leaving one out.
2. Test the model in the sample left out;
3. Repeat this N times and calculate the weighted accuracy of the tested model;
4. Repeat step 1-3 four times adopting a predictors level equal to 4, 3, 2 and 1, subsequently;
5. Select the model and the pruning parameter (predictor's level) that maximizes the weighted accuracy of the FFT model.

Appendix D5 Descriptive statistics

Table D5 Definition of standard classification statistics

Standard Classification Statistics	Definition	Abbreviation	Formula
Hits	Probability of a "True Yield Below Threshold" (TB) over the total samples of "Yield Below Threshold" (YB)	H	$\left(\dfrac{TB}{YB}\right) \times 100$
Correct Rejections	Probability of a "True Yield Above Threshold" (TA) over the total samples of "Yield Above Threshold" (YA)	CR	$\left(\dfrac{TA}{YA}\right) \times 100$
False Alarms	Probability of a false "Yield Below Threshold"	FA	1 - CR
Misses	Probability of a false "Yield Above Threshold"	MS	1 - HR
Weighted Accuracy	Weighted average of hit rate and correct rejection dictated by a sensitivity weighting parameter w	WACC	$\dfrac{H}{H + MS} \times w +$ $\dfrac{CR}{CR + FA} \times (1 - w)$

Appendix D6 Maize price averages: observed and assumed linear models

A) Price model in Baringo

$Ps = -3.9*Y + 30.4$

B) Price model in Narok

$Ps = -3.6*Y + 31.1$
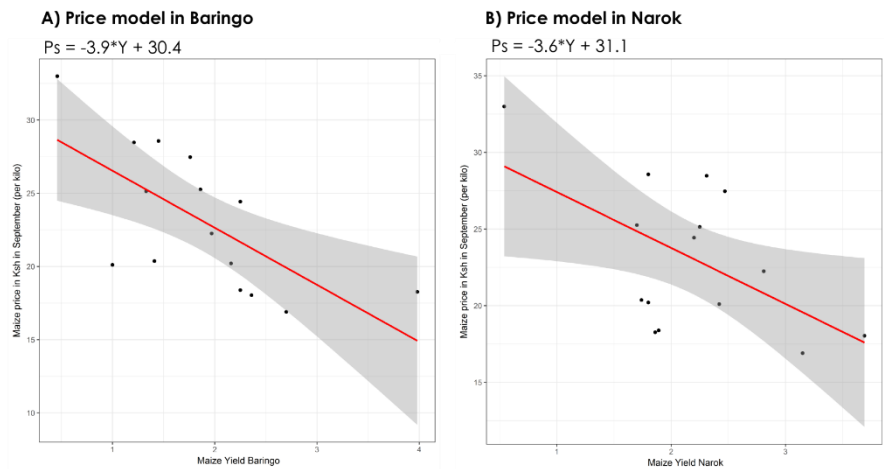
Figure D6.1 Linear model representing a significant (p-value < 0.05) relationship between deflated Nairobi prices in September and observed annual maize yields in a) Baringo and b) Narok.
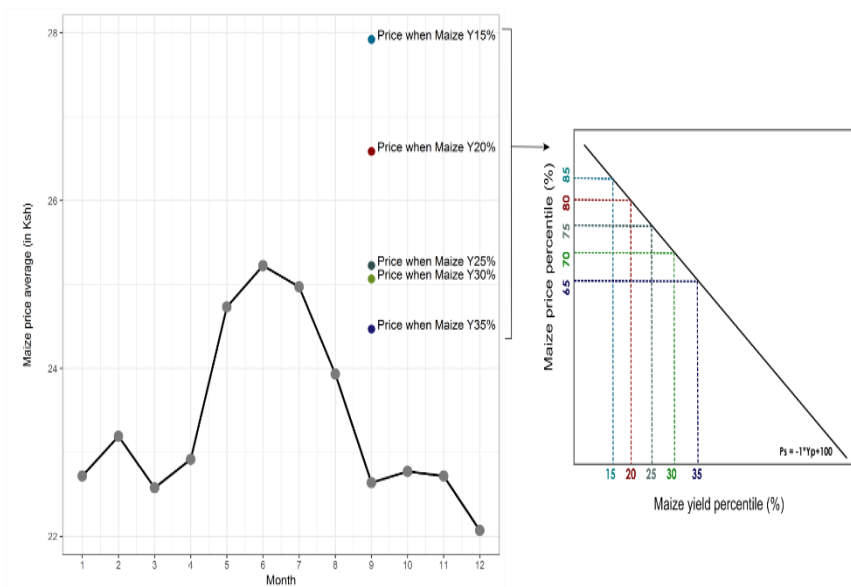
Figure D6.2 Time series of deflated monthly maize price average in Nairobi. In this study for the districts of Laikipia, Nyandarua and West Pokot. We consider prices and yield to have negative relationship, therefore, when one increases the other decreases, and vice-versa. In September, which represents the starting of the harvesting season, we consider prices (P_s) to vary relative to the maize yield being investigated (Y_p) . For instance, when maize yield $Y_{15\%}$, price is at its 85th percentile observed in September, therefore relationship follows $P_s = -1\ Y_p + 100$. Such assumption was adopted due to insignificant linear relationship (p-value > 0.05) between deflated Nairobi prices in September and observed maize yield in Laikipia, Nyandaura and West Pokot.

Appendix D7 Sensitivity analysis of maize price variations for districts of Laikipia, Nyandarua and West Pokot
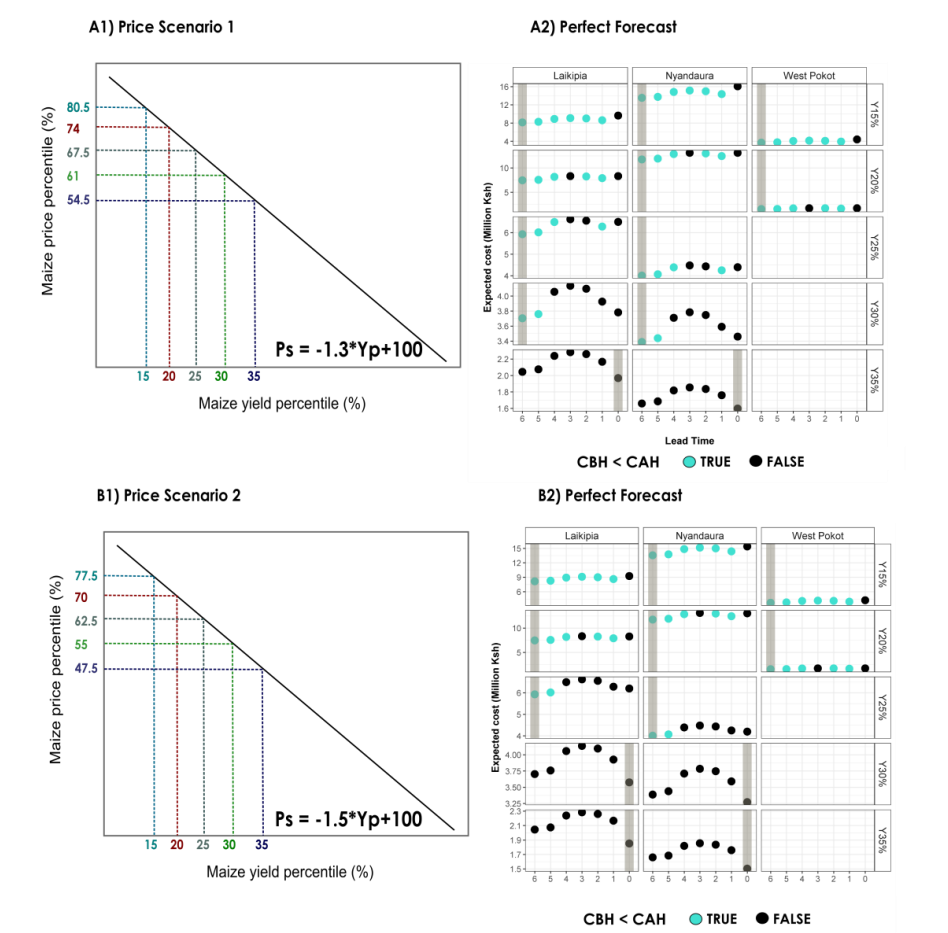
Figure D7.1 Sensitivity analysis of maize price variations testing two moderate (A1 and B1) rates of change in P_s (price) as Y_p (maize yield percentile) changes. Additionally, we display the results of the total expected cost of cash transfer per district, lead time and maize yield percentile simulating a perfect forecast.
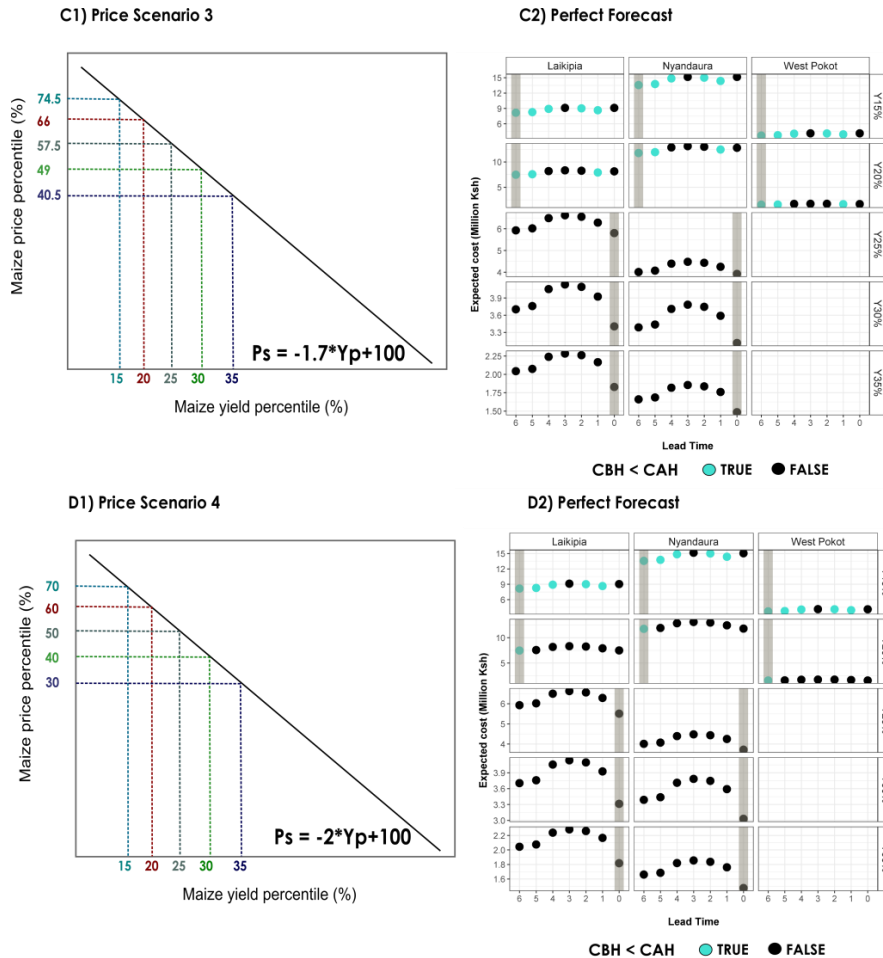
Figure D7.2 Sensitivity analysis of maize price variations testing two conservative rates of change in P_s (price) as Y_p (maize yield percentile) changes. Additionally, we display the results of the total expected cost of cash transfer per district, lead time and maize yield percentile simulating a perfect forecast.

Appendix D8 Spatial distribution of the probabilities of Hits and False Alarms
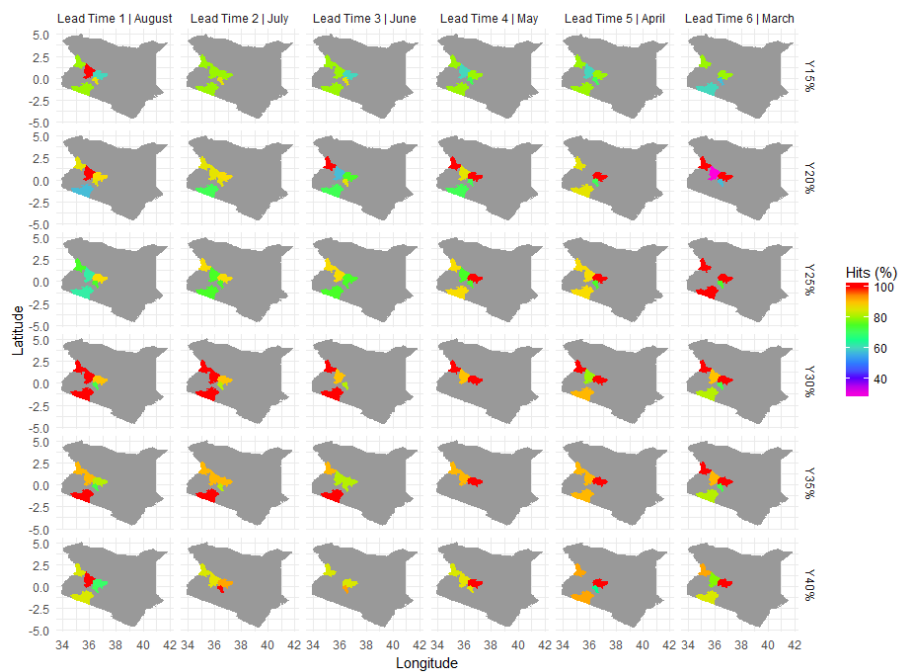
Figure D8.1 Performance of the tested FFT models in predicting true low maize yield events (Hits), for different maize yield percentiles and lead times. Sensitivity weighting parameter is w=0.75.
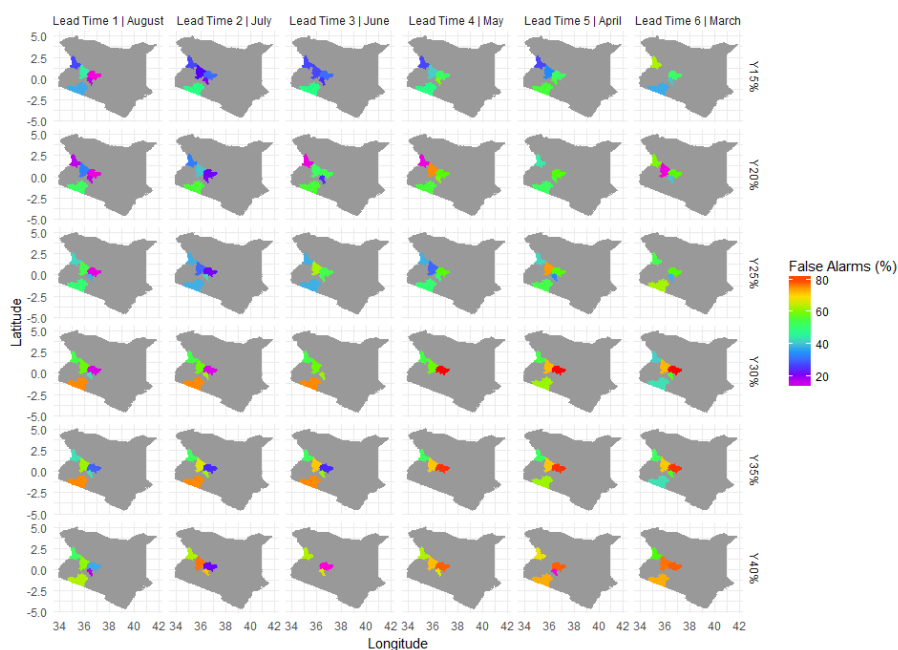
Figure D8.2 Performance of the tested FFT models in predicting false low maize yield events (False Alarms), for different maize yield percentiles and lead times. Sensitivity weighting parameter is w=0.75.

Appendix D9 Overview of Weighted Accuracy (WACC) and Receiver operating characteristic (ROC) indices
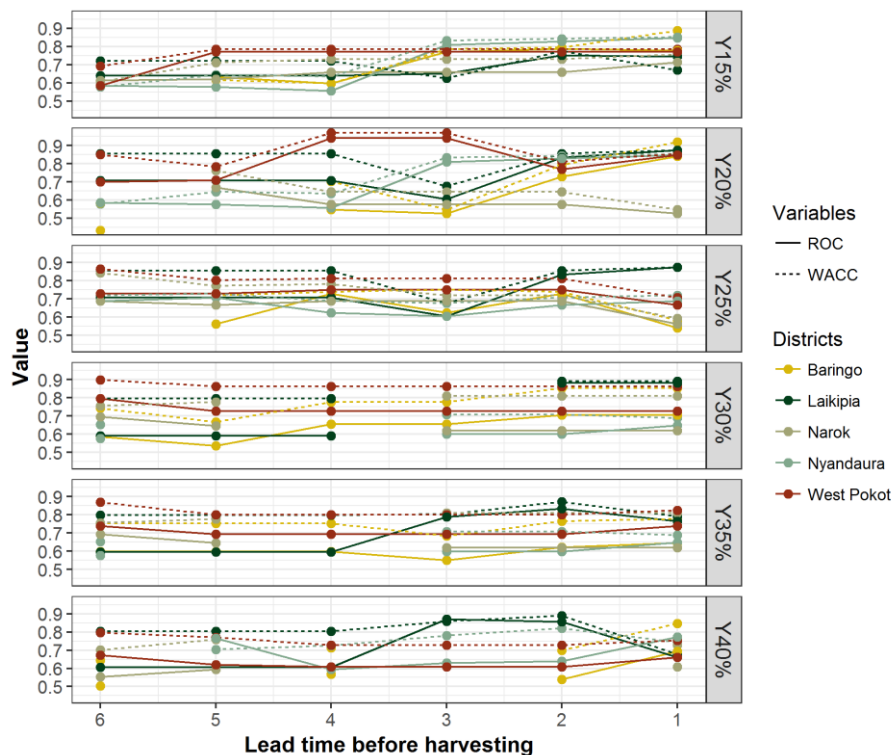
Figure D9 Representation of the performance of the ROC and WACC indicators for each district, lead time and maize yield percentile level. FFT model sensitivity weighting parameter equals w=0.75.

Appendix D10 Sensitivity analysis of FFT model and maize price variations
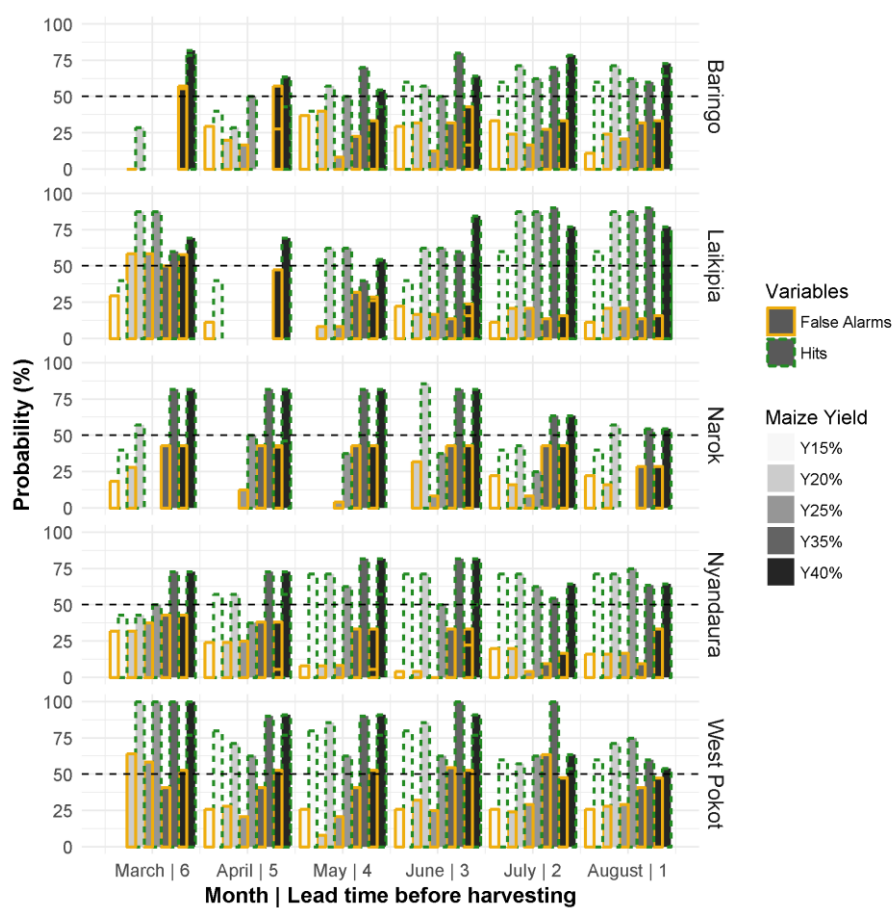
Figure D10.1 Performance of the tested FFT models in predicting true maize low yield events (Hits), and false maize low yield events (False Alarms) per district, percentile and lead time. Yellow bars represent the probabilities of False Alarms, and green dashed lines the probabilities of Hits. Different levels of low maize yields are highlighted in shades of grey. Dashed black line is drawn at the 50% probability. Sensitivity weighting parameter w=0.50.
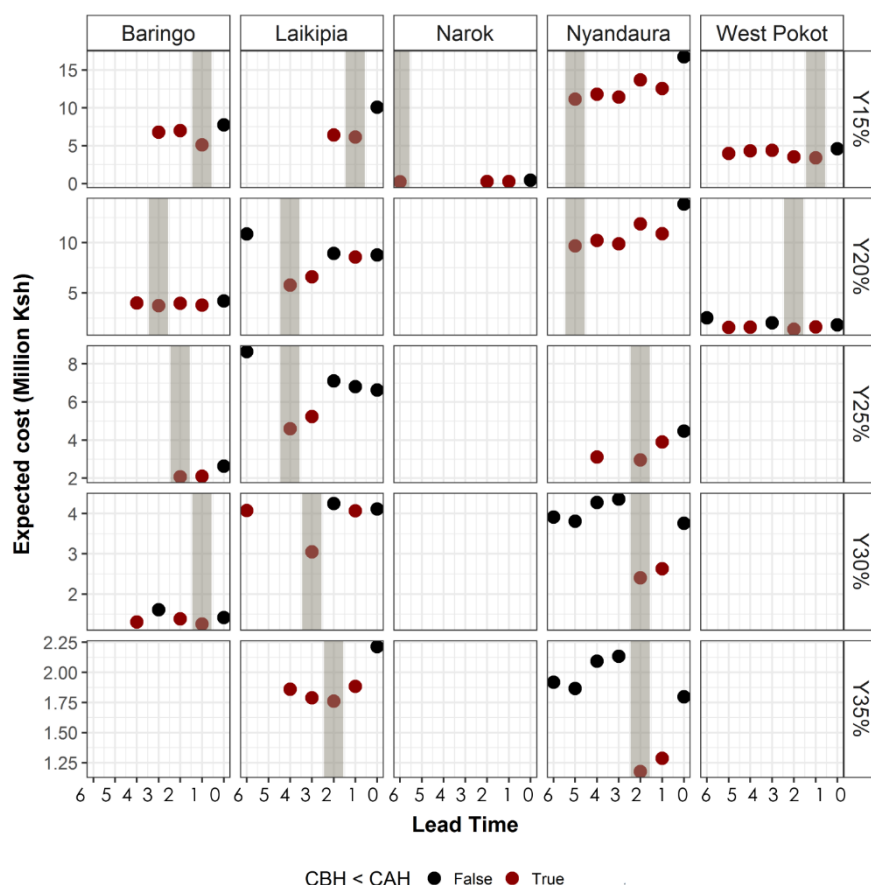
Figure D10.2 Total expected cost of cash transfer per district, lead time and maize yield percentile calculated based on FFT model results (using a weighting parameter of w=0.50). Red dots show all lead times before harvesting (starts in September) for which expected cost of cash transfer is lower than the expected cost of cash transfer after harvesting ($CBH_m < CAH$); black dots show the opposite. The most cost effective lead time is highlighted in grey. Boxes are blank when the maize yield percentile for the specific district is higher than the mean human energy requirement (3,000 kcal/day/person), and therefore no cash transfer is required.
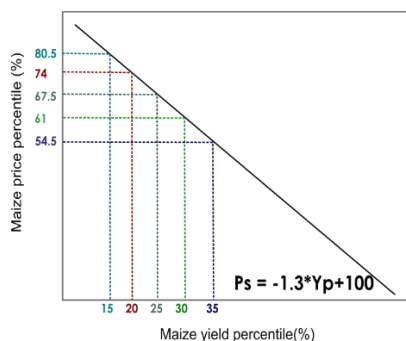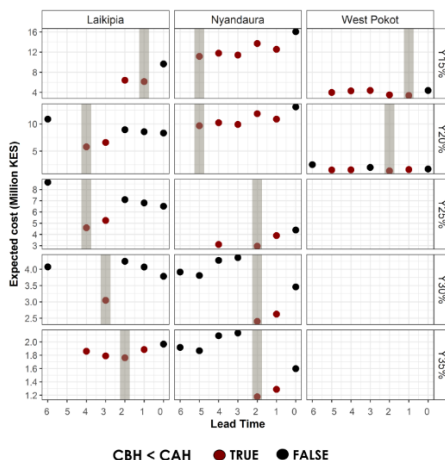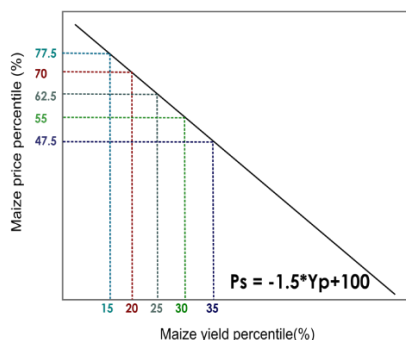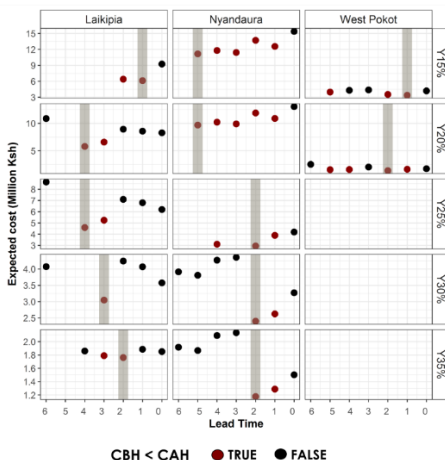
Figure D10.3 Sensitivity analysis of total expected cost of cash transfer testing moderate rates (A.1 and B.1) of change in Ps (price) for change in Yp (maize yield), per district, lead time, and maize yield percentile. Red dots in A.2 and B.2 highlight all lead times before harvesting when expected ex-ante costs of cash transfer are lower than the expected ex-post costs of cash transfer (CBHm < CAH); black dots show the opposite. The most cost effective lead time is highlighted in grey. Boxes are blank when the maize yield percentile for the specific district is higher than the mean human energy requirement, and therefore cash transfer is not triggered. Results are shown only for models with ROC>0.5. FFT model sensitivity weight equals 0.5

C1) Price Scenario 3

C2) FFT Models Forecast

$Ps = -1.7*Yp+100$

D1) Price Scenario 4

D2) FFT Models Forecast

$Ps = -2*Yp+100$

CBH < CAH ● TRUE ● FALSE
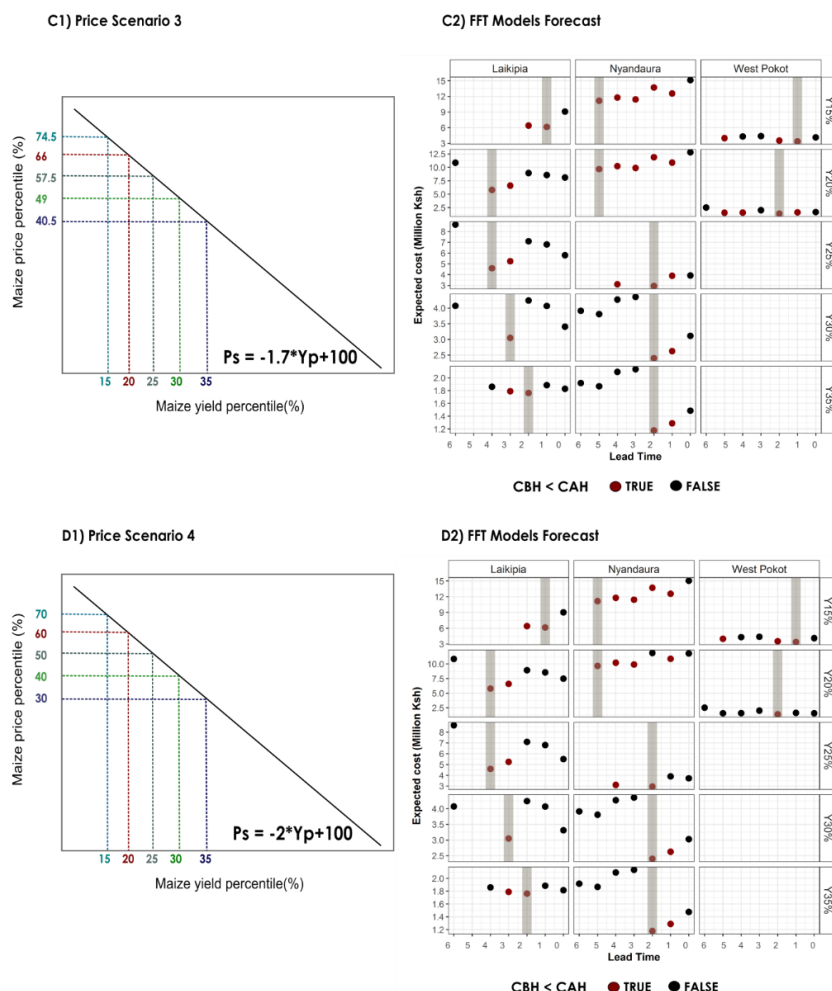
Figure D10.4 Sensitivity analysis of total expected cost of cash transfer testing conservative rates (C1 and D1) of change in Ps (price) for change in Yp (maize yield), per district, lead time, and maize yield percentile. Red dots in C2 and D2 highlight all lead times before harvesting when expected ex-ante costs of cash transfer are lower than the expected ex-post costs of cash transfer (CBHm < CAH); black dots show the opposite. The most cost effective lead time is highlighted in grey. Boxes are blank when the maize yield percentile for the specific district is higher than the mean human energy requirement, and therefore cash transfer is not triggered. Results are shown only for models with ROC>0.5. FFT model sensitivity weight equals 0.5

Appendix D11 Best performing predictors of maize yields

Table D11 Definition of thresholds per district, maize yield percentile level and lead time

District	Maize Yield Percentile (%)	Lead Time	Number of predictors	Predictors	Threshold	WACC	AUC
Baringo	15	1	1	NP4August	369,83	0,89	0,78
Baringo	15	2	5	NDVIJune;NP3July;NP5May;NP6May;NP1June	0,51;295,49;335,46;355,91;84,69	0,79	0,79
Baringo	15	3	5	NDVIJune;NP5May;NP6May;NP6June;NP1June	0,51;335,46;355,91;285,34;84,69	0,79	0,77
Baringo	15	4	4	NP1May;NP4May;NP5May;NP6May	77,39;234,72;335,46;355,91	0,60	0,60
Baringo	15	5	1	NDVI3April	1,3	0,62	0,63
Baringo	20	1	2	NP4August;NP3July	369,83;295,49	0,92	0,84
Baringo	20	2	4	NP2July;NP3July;NP1June;NP2June	154,08;295,49;62,02;150,46	0,79	0,73
Baringo	20	3	2	NP1June;NP2June	62,02;150,46	0,55	0,53
Baringo	20	4	4	NP4May;NP3May;NP6May;NDVI4May	252,47;247,48;355,91;1,99	0,70	0,55
Baringo	25	6	1	NDVI3March	1,18	0,43	0,58
Baringo	25	1	5	NP6July;NP5June;NP4May;NP2June;NP6June	389,19;357,15;252,47;150,46;285,34	0,58	0,54

Baringo	25	2	3	NP6July;NP5June;NP4May	389,19;357,15;252,47	0,74	0,73
Baringo	25	3	4	NP5June;NP4May;NDVIJune;NP2June	357,15;252,47;0,51;150,46	0,75	0,63
Baringo	25	4	2	NP4May;NP3May	252,47;247,48	0,74	0,73
Baringo	25	5	2	NP6April;NDVI4April	284,33;1,89	0,72	0,56
Baringo	30	1	1	NP6June	453,14	0,85	0,70
Baringo	30	2	2	NP6June;NP4May	453,14;343,93	0,85	0,70
Baringo	30	3	1	NP6June	453,14	0,78	0,65
Baringo	30	4	1	NP4May	343,93	0,78	0,65
Baringo	30	5	2	NP6April;NDVI4April	356,05;1,89	0,67	0,54
Baringo	30	6	2	NDVI4March;NDVI3March	1,83;1,31	0,74	0,59
Baringo	35	1	2	NDVI6May;NDVI4May	2,82;1,99	0,78	0,65
Baringo	35	2	2	NDVI6May;NDVI4May	2,82;1,99	0,77	0,62
Baringo	35	3	1	NDVI6May	2,82	0,69	0,55
Baringo	35	4	1	NDVI6May	2,82	0,75	0,60
Baringo	35	5	1	NDVI4April	1,89	0,75	0,60
Baringo	35	6	1	NDVI4March	1,83	0,75	0,60
Baringo	40	1	4	NP5July;NP6July;NDVI6J	577,42;574,55;2,99;	0,85	0,69

				uly;NDVI5June	2,5		
Baringo	40	2	3	NP5July;NP6July;NDVI6July	577,42;574,55;2,99	0,70	0,54
Baringo	40	4	2	NDVI6May;NP3May	2,82;247,48	0,71	0,57
Baringo	40	6	2	NDVI2March;NP5March	0,89;228,17	0,64	0,50
Laikipia	15	1	4	ONIMarch;NP3July;ONIApril;NDVI6March	0,2;119,83;0,3;2,53	0,67	0,74
Laikipia	15	2	4	ONIMarch;NP3July;ONIApril;NDVI6March	0,2;119,83;0,3;2,53	0,78	0,75
Laikipia	15	3	4	ONIMarch;NP1June;ONIApril;NDVI6March	0,2;28,67;0,3;2,53	0,63	0,65
Laikipia	15	4	1	ONIMarch	0,2	0,72	0,64
Laikipia	15	5	1	ONIMarch	0,2	0,72	0,64
Laikipia	15	6	1	ONIMarch	0,2	0,72	0,64
Laikipia	20	1	2	NP2July;NDVI6March	75,54;2,53	0,88	0,88
Laikipia	20	2	1	NP2July	75,54	0,85	0,83
Laikipia	20	3	4	NDVI6March;NP1June;NDVI5March;NP5March	2,53;28,67;2,1;174,58	0,68	0,60
Laikipia	20	4	1	NDVI6March	2,53	0,85	0,71
Laikipia	20	5	1	NDVI6March	2,53	0,85	0,71

Laikipia	20	6	1	NDVI6March	2,53	0,85	0,71
Laikipia	25	1	2	NP2July;NDVI6March	75,54;2,53	0,88	0,88
Laikipia	25	2	1	NP2July	75,54	0,85	0,83
Laikipia	25	3	4	NDVI6March;NP1June;NDVI5March;NP5March	2,53;28,67;2,1;174,58	0,68	0,60
Laikipia	25	4	1	NDVI6March	2,53	0,85	0,71
Laikipia	25	5	1	NDVI6March	2,53	0,85	0,71
Laikipia	25	6	1	NDVI6March	2,53	0,85	0,71
Laikipia	30	1	1	NP2July	75,54	0,89	0,88
Laikipia	30	2	1	NP2July	75,54	0,89	0,88
Laikipia	30	4	1	NP5March	279,72	0,80	0,59
Laikipia	30	5	1	NP5March	279,72	0,80	0,59
Laikipia	30	6	3	ONIMarch;NP5March;NDVI5March	282,03	0,80	0,59
Laikipia	35	1	2	NP2July;NP1June	75,54;28,67	0,79	0,77
Laikipia	35	2	2	NP2July;NP3July	75,54;140,83	0,87	0,84
Laikipia	35	3	1	NP1June	28,67	0,80	0,79
Laikipia	35	4	1	NP5March	279,72	0,80	0,60
Laikipia	35	5	1	NP5March	279,72	0,80	0,60

Laikipia	35	6	1	NP5March	279,72	0,80	0,60
Laikipia	40	1	2	NP2July;NP1June	78,94;28,67	0,68	0,66
Laikipia	40	2	2	NP2July;NP1June	78,94;28,67	0,89	0,86
Laikipia	40	3	2	NP1June;NP5March	28,67;279,72	0,86	0,87
Laikipia	40	4	1	NP5March	279,72	0,80	0,61
Laikipia	40	5	1	NP5March	279,72	0,80	0,61
Laikipia	40	6	1	NP5March	279,72	0,80	0,61
Narok	15	1	5	NP6April;NP6June;NP5May;NP6May;NP6July	480,78;567,76;498,72;569,76;538,26	0,85	0,85
Narok	15	2	5	NP6April;NP6June;NP5May;NP6May;NP6July	480,78;567,76;498,72;569,76;538,26	0,84	0,83
Narok	15	3	2	NP6April;NP6June	480,78;567,76	0,83	0,81
Narok	15	4	2	NP6April;NP5May	480,78;498,72	0,64	0,56
Narok	15	5	5	NP6April;NP5March;NP5April;NP4April;NDVI2April	480,78;350,64;428,67;423,86;1,2	0,65	0,58
Narok	15	6	3	NP5March;NP4March;NDVIMarch	350,64;220,04;0,52	0,58	0,59
Narok	20	1	2	NDVI5June;NDVI3May	2,93;1,83	0,85	0,85
Narok	20	2	2	NDVI5June;NDVI3May	2,93;1,83	0,84	0,83

Narok	20	3	2	NDVI5June; NDVI3May	2,93;1,83	0,83	0,81
Narok	20	4	1	NDVI3May	1,83	0,64	0,56
Narok	20	5	2	NDVI4April; NDVI6April	2,39;3,4	0,65	0,58
Narok	25	1	2	NDVI5June; NDVI3May	2,93;1,83	0,58	0,59
Narok	25	2	1	NDVI5June	2,93	0,72	0,69
Narok	25	3	1	NDVI5June	2,93	0,71	0,67
Narok	25	4	2	NDVI3May; NDVI4May	1,83;2,41	0,68	0,60
Narok	25	5	2	NDVI4April; NDVI3March	2,39;1,79	0,69	0,63
Narok	25	6	2	NDVI3March;NP5March	1,79;454,3	0,73	0,71
Narok	30	1	1	NDVI3June	1,88	0,72	0,69
Narok	30	2	1	NDVI3June	1,88	0,69	0,65
Narok	30	3	1	NDVI3June	1,88	0,71	0,60
Narok	30	5	2	NP2March; ONIApril	162;-0,3	0,71	0,60
Narok	30	6	1	NP2March	162	0,65	0,58
Narok	35	1	1	NDVI3June	1,88	0,69	0,65
Narok	35	2	1	NDVI3June	1,88	0,71	0,60
Narok	35	3	1	NDVI3June	1,88	0,71	0,60
Narok	35	5	2	NP2March; ONIApril	162;-0,3	0,65	0,58

Narok	35	6	1	NP2March	162	0,74	0,77
Narok	40	1	5	NP6May;NP6April;NP4March;NDVI4June;NP5April	478,26;567,36;370,14;2,5;640,31	0,82	0,64
Narok	40	5	4	NP2March;ONIApril;NP6April;NP4March	162;-0,2;567,36;370,14	0,78	0,63
Narok	40	6	3	NP2March;NP5March;ONIMarch	162;454,3;-0,2	0,73	0,60
Nyandaura	15	1	2	NP6August;NP5July	591,36;510,26	0,70	0,77
Nyandaura	15	2	2	NP5July;NP6July	510,26;513,87	0,76	0,71
Nyandaura	15	3	5	NP5June;NP4June;NP6April;NDVI5June;NDVIJune	426,17;375,57;488,46;3,07;0,65	0,73	0,66
Nyandaura	15	4	5	NP4May;NP1May;NP3May;NP6April;NDVI5May	365,04;107,32;341,38;488,46;3,07	0,73	0,66
Nyandaura	15	5	3	NP1April;NP6April;NP3April	124,93;488,46;223,7	0,73	0,66
Nyandaura	15	6	2	NP5March;NP6March	280,67;364,17	0,71	0,62
Nyandaura	20	1	2	NP6August;NP5July	591,36;510,26	0,61	0,61
Nyandaura	20	2	2	NP5July;NP6July	510,26;513,87	0,55	0,53
Nyandaura	20	3	5	NP5June;NP4June;NP6April;NDVI5June;NDVIJun	426,17;375,57;488,46;3,07;0,65	0,65	0,58

				e			
Nyanda ura	20	4	5	NP4May;NP 1May;NP3M ay;NP6April; NDVI5May	365,04;10 7,32;341,3 8;488,46; 3,07	0,65	0,58
Nyanda ura	20	5	3	NP1April;NP 6April;NP3A pril	124,93;48 8,46;223,7	0,65	0,58
Nyanda ura	20	6	2	NP5March; NP6March	280,67;36 4,17	0,76	0,67
Nyanda ura	25	1	1	NP2August	174,97	0,59	0,56
Nyanda ura	25	2	4	NP5July;ND VI5June;ND VI5May;ND VI6June	510,26;3,0 7;3,07;3,7 3	0,72	0,69
Nyanda ura	25	3	1	NDVI5June	3,07	0,72	0,69
Nyanda ura	25	4	5	NP2May;ND VI5May;NP3 May;NDVI4 May;NDVI3 May	180,86;3,0 7;256,72; 2,44;1,84	0,78	0,69
Nyanda ura	25	5	2	NP1April;NP 6April	124,93;48 8,46	0,77	0,67
Nyanda ura	25	6	2	NDVI3Marc h;NDVI2Mar ch	1,86;1,21	0,84	0,69
Nyanda ura	30	1	4	NP2August; NDVI5June; NP1May;NP 5May	176,11;3,1 1;137,12; 490,61	0,81	0,62
Nyanda ura	30	2	1	NDVI5June	3,11	0,81	0,62
Nyanda ura	30	3	1	NDVI5June	3,11	0,81	0,62
Nyanda ura	30	6	1	NDVI5Marc h	3,12	0,78	0,65

Nyanda ura	35	1	4	NP2August; NDVI5June; NP1May;NP5May	176,11;3,11;137,12; 490,61	0,76	0,69
Nyanda ura	35	2	1	NDVI5June	3,11	0,81	0,62
Nyanda ura	35	3	1	NDVI5June	3,11	0,81	0,62
Nyanda ura	35	6	1	NDVI5March	3,12	0,81	0,62
Nyanda ura	40	1	2	NP1August; NP2August	97,51;176,11	0,78	0,65
Nyanda ura	40	2	3	NP1July;NDVI3April;NP5July	70,6;1,71;526,31	0,76	0,69
Nyanda ura	40	3	3	NDVI3April; NDVI2April; NP4June	1,71;1,1;375,57	0,73	0,61
Nyanda ura	40	4	2	NDVI3April; NDVI3May	1,71;1,77	0,76	0,59
Nyanda ura	40	5	4	NDVI4April; NDVI3April; NDVI2April; ONIApril	2,42;1,71;1,1;-0,6	0,70	0,55
West Pokot	15	1	1	NDVI2April	0,87	0,79	0,77
West Pokot	15	2	1	NDVI2April	0,87	0,79	0,77
West Pokot	15	3	1	NDVI2April	0,87	0,79	0,77
West Pokot	15	4	1	NDVI2April	0,87	0,79	0,77
West Pokot	15	5	1	NDVI2April	0,87	0,79	0,77
West Pokot	15	6	4	NP3March; NDVIMarch; NP5March; NDVI2Marc	85,96;0,41;164,43;0,86	0,69	0,59

				h			
West Pokot	20	1	5	NDVI6August;NP2July;NDVI3May;NDVI5July;NDVI5April	2,91;125,17;1,44;2,46;2,26	0,85	0,85
West Pokot	20	2	5	NP2July;NDVI3May;NDVI5July;NDVI5April;NP5March	125,17;1,44;2,46;2,26;164,43	0,81	0,77
West Pokot	20	3	5	NDVI3May;NDVI5April;NP5March;NP1May;NDVI6May	1,44;2,26;164,43;68,58;2,78	0,97	0,94
West Pokot	20	4	5	NDVI3May;NDVI5April;NP5March;NP1May;NDVI6May	1,44;2,26;164,43;68,58;2,78	0,97	0,94
West Pokot	20	5	3	NDVI5April;NP5March;NDVI4April	2,26;164,43;1,81	0,78	0,71
West Pokot	20	6	2	NP5March;NP6March	164,43;260,4	0,85	0,70
West Pokot	25	1	4	ONIAugust;NDVI5April;NP5March;NDVI6May	0,1;2,26;164,43;2,78	0,71	0,67
West Pokot	25	2	5	NDVI5April;NP5March;NDVI6May;NDVI4April;NDVI5June	2,26;164,43;2,78;1,81;2,4	0,81	0,75
West Pokot	25	3	5	NDVI5April;NP5March;NDVI6May;NDVI4April;NDVI5June	2,26;164,43;2,78;1,81;2,4	0,81	0,75

West Pokot	25	4	5	NDVI5April; NP5March; NDVI6May; NDVI4April; NDVI4May	2,26;164,43;2,78;1,81;1,88	0,81	0,75
West Pokot	25	5	3	NDVI5April; NP5March; NDVI4April	2,26;164,43;1,81	0,80	0,73
West Pokot	25	6	2	NP5March; NP6March	164,43;260,4	0,86	0,73
West Pokot	30	1	1	NP5March	164,43	0,86	0,73
West Pokot	30	2	1	NP5March	164,43	0,86	0,73
West Pokot	30	3	1	NP5March	164,43	0,86	0,73
West Pokot	30	4	1	NP5March	164,43	0,86	0,73
West Pokot	30	5	1	NP5March	164,43	0,86	0,73
West Pokot	30	6	4	NP5March; NP6March; NDVI3March;NDVI4March	164,43;260,4;1,39;1,92	0,90	0,80
West Pokot	35	1	2	NP5March; NDVI5April	172,09;2,26	0,82	0,74
West Pokot	35	2	1	NP5March	172,09	0,80	0,69
West Pokot	35	3	1	NP5March	172,09	0,80	0,69
West Pokot	35	4	1	NP5March	172,09	0,80	0,69
West Pokot	35	5	1	NP5March	172,09	0,80	0,69
West Pokot	35	6	1	NP5March	172,09	0,87	0,74

West Pokot	40	1	3	NDVI5April; NP5March; NDVI6May	2,26;189,67;2,78	0,75	0,66
West Pokot	40	2	2	NDVI5April; NP5March	2,26;189,67	0,73	0,61
West Pokot	40	3	2	NDVI5April; NP5March	2,26;189,67	0,73	0,61
West Pokot	40	4	2	NDVI5April; NP5March	2,26;189,67	0,73	0,61
West Pokot	40	5	3	NDVI5April; NP5March; NDVI4April	2,26;189,67;1,81	0,77	0,62
West Pokot	40	6	4	NP5March; NDVI3March;NP6March;NDVI4March	189,67;1,3;268,12;1,92	0,80	0,67